Investigating Mechanisms of Salt-Sensitive Hypertension in 11β-HSD2 Heterozygote Mice

Eilidh Craigie

Doctor of Philosophy

Department of Molecular Physiology

The University of Edinburgh

2010

I declare that all work presented in this thesis is my own except where stated otherwise, and that it has been entirely composed by myself.

Eilidh Craigie

Acknowledgements

Firstly I would like to thank my supervisor Dr Matthew Bailey for his constant and unfaltering support and encouragement throughout my PhD studies and beyond. I would also like to thank my other supervisor Professor John Mullins for giving me the opportunity to carry out my PhD work in his laboratory, and for all of his help and advice throughout. Additional thanks go to Dr Chris Kenyon for his invaluable contributions to my work, and to Dr Janet Paterson for passing on her molecular biology wisdom. The financial support of my MRC studentship is gratefully acknowledged, as is the generous award of a small project grant from the University of Edinburgh.

Thank you to my fiancé Scott and to my friends and family for always being there and supporting me no matter what.

Individual thanks must go to Audrey Peter, Gillian Brooker and Nina Kotelevtseva for their excellent technical assistance; this would not have been possible without you. Thank you to Dr Matthew Sharp for helpful discussions regarding the floxed construct, and to Dr Yuri Kotelevtsev for providing the pS141 plasmid construct. Thanks to Dr Dawn Livingston for expertise (and the early morning starts) with the HPA axis work and to Dr Emad Al-Dujaili for help with urinary steroid analysis. Big thanks to all of the BRR/BRF staff for all their help with my mouse colonies and experiments. Thank you to Dr David Brownstein for performing necropsies at short notice and to Dr Caitlin Wyroll for assistance with LacZ staining protocol optimisation. Finally, thank you to Ali Ashek, Carl Tucker and Louise Evans for keeping my "chin up" in the lab and office.

Dedication

In memory of

My Grandfather David Lowson

For his encouragement of intellectual pursuits and always believing in me.

Abbreviation List

	11β-HSD1 -	11β-hydroxysteroid dehydrogenase type 1
	11β-HSD2 -	11β-hydroxysteroid dehydrogenase type 2
	3′ -	3 prime
	5′ -	5 prime
	8-iso-PGF2α -	8-isoprostane
A	ACE -	Angiotensin Converting Enzyme
	ACTH -	Adrenal Corticotrophic Hormone
	ADH -	Antidiuretic Hormone
	AGT -	Angiotensinogen
	AngI -	Angiotensin I
	AngII -	Angiotensin II
	ANOVA -	Analysis of Variants
	ASDN -	Aldosterone Sensitive Distal Nephron
	AT_1 -	Angiotensin Type I Receptor
	AT_2 -	Angiotensin Type II Receptor
	AR -	Androgen Receptor
	AUC -	Area Under the Curve
	AQP -	Aquaporin
B	BAC -	Bacterial Artificial Chromosome
	BHT -	Butylated Hydroxyl-Tolulene
	BP -	Blood Pressure
	BSA -	Bovine Serum Albumin
C	cAMP -	Cyclic Adenosine Monophosphate
	CAT -	Catalyse
	CCD -	Cortical Collecting Duct

CD - Collecting Duct

C_{IN} - Clearance of Inulin

CNS - Central Nervous System

CNT - Connecting Tubule

CRH - Corticotropin-Releasing Hormone

CtBP - Carboxyl-terminal Binding Protein

D

DCT - Distal Convoluted Tubule

DMSO - Dimethyl Sulfoxide

DOC - 11-deoxycortisol

DOCA - Deoxycorticosterone Acetate

DRA - Downstream Recombination Arm

DRC - Dose Response Curve

E

E - Embryonic day

ECF - Extracellular Fluid

ECV - Extracellular Volume

ELISA - Enzyme-Linked Immunosorbent Assay

E_{Na} - Sodium Excretion

ENaC - Epithelial Sodium Channel

EP - External Probe

ES - Embryonic Stem

F

FCS - Foetal Calf Serum

FE_{Na} - Fractional Sodium Excretion

FF - Filtration Fraction

G

GFR - Glomerular Filtration Rate

GPX - Glutathione Peroxidase

GR - Glucocorticoid Receptor

GRA - Glucocorticoid-Remediable Aldosteronism

H	H_2O_2 -	Hydrogen Peroxide
	HCL -	Hydrochloric Acid
	HPA -	Hypothalamic-Pituitary-Adrenal
	HSD11B2 -	11β-HSD2 human gene
	Hsd11b2 -	11β-HSD2 mouse gene
	Hsd11b2$^{-/-}$ -	*Hsd11b2* transgenic null mouse
	Hsd11b2$^{+/-}$ -	*Hsd11b2* transgenic heterozygote mouse
	Hsd11b2$^{+/+}$ -	Wild type mouse
	Hox -	Homeobox gene
	Hoxb7$^{+/-}$ -	*Hoxb7* transgenic heterozygote mouse
	Hoxb7$^{+/+}$ -	Wild type mouse
	HR -	Heart Rate
	HREs -	Hormone Response Elements
	HSP -	Heat Shock Protein
	HUVECs -	Human Umbilical Vein Endothelial Cells
I	ICM -	Inner Cell Mass
	ICF -	Intracellular Fluid
	IMCD -	Inner Medullary Collecting Duct
	IHA -	Idiopathic Hyperaldosteronism Aldosteronism
	I.P. -	Intraperitoneal
	IP_3 -	Inositol triphosphate
	I.V. -	Intravenous
K	Kb -	Kilobases
L	LacZ -	β-galactosidase
	LB -	Liquid Broth
	LC -	Liquid Chromotography
M	MABP -	Mean Arterial Blood Pressure

MBPR - Maximal Blood Pressure Response

MR - Mineralocorticoid Receptor

MS - Mass Spectrometry

N NAD^+ - Nicotinamide Adenine Dinucleotide

NADP - Nicotinamide Adenine Dinucleotide Phosphate

NADH - Reduced NAD^+

NADPH - Reduced NADP

Na-K-ATPase - Sodium Potassium Pump

NCC - Sodium Chloride Symporter

Nedd - Neuronal precursor cell Expressed Developmentally Down-regulated

NKCC - Sodium Potassium Chloride Symporter

NO - Nitric Oxide

O O_{2^-} - superoxide radial

OMCD - Outer Medullary Collecting Duct

P PA - Primary Aldosteronism

PAH - p-Aminohippuric Acid

PBS - Phosphate Buffered Saline

PCR - Polymerase Chain Reaction

PDTC - Pyrrolidinedithiocarbamate

P_{IN} - Plasma concentration of Inulin

PMSF - Phenylmethylsulfonyl Fluoride monohydrate

P_{Na} - Plasma Sodium Concentration

ppm - parts per million

PR - Progesterone Receptor

PRA - Plasma Renin Activity

PVN - Paraventricular Nucleus

R	R2F -	Region to Flox
	RAAS -	Renin Angiotensin Aldosterone System
	RAS -	Renin Angiotensin System
	RBP -	Renal Blood Flow
	REDOX -	Reduction-Oxidation reaction
	RIA -	Radio Immunoassay
	ROMK -	Renal Outer Medullary Potassium (K) channel
	ROS -	Reactive Oxygen Species
	RPF -	Renal Plasma Flow
	RVR -	Renal Vascular Resistance
S	SAME -	Syndrome of Apparent Mineralocorticoid Excess
	SE -	Standard Error
	SBP -	Systolic Blood Pressure
	SGK-	Serum- and Glucocorticoid-inducible protein Kinase
	SHR -	Spontaneously Hypertensive Rat
	SOD -	Superoxide Dismutase
	SPA -	Scintillation Proximity Assay
	SR -	Salt Resistant
	SS -	Salt Sensitive
	StAR -	Steroidgenic acute regulatory protein
T	TASK -	TWIK-related acid sensitive potassium
	TCA -	Trichloroacetic Acid
	TEMPOL -	4-Hydroxy-2,2,6,6-tetramethylpiperidine-N-oxyl
	THE -	Tetrahydrocortisol
	THF -	Tetrahydrocortisone
	TLC -	Thin Layer Chromotography
U	UFR -	Urine Flow Rate

	U_{IN} -	Urinary Inulin concentration
	URA -	Upstream Recombination Arm
V	VSMC -	Vascular Smooth Muscle Cell
	VSV -	Vascular System Volume
W	WNK -	With no lysine (K)

Table of Contents

Abstract

The mineralocorticoid hormone, aldosterone, classically acts via the Mineralocorticoid Receptor (MR) to promote sodium transport in aldosterone target tissues, such as the kidney, thereby controlling long-term electrolyte homeostasis and blood pressure (BP). Aldosterone biosynthesis by the adrenal gland is regulated by a negative feedback loop called the Renin Angiotensin Aldosterone System (RAAS). The glucocorticoid cortisol (corticosterone in rodents), which has a very similar structure to aldosterone, shares with aldosterone an equal affinity for the MR. Typically, plasma cortisol levels are approximately 1000-fold higher than plasma aldosterone, and so the ligand specificity for aldosterone must be imposed on MR by other, non-structural, means. This specificity is important in order to retain electrolyte and BP balance within the control of the RAAS.

The co-localisation of the enzyme 11β-Hydroxysteroid Dehydrogenase Type 2 (11β-HSD2) with the MR in aldosterone target tissues provides the MR with the aldosterone specificity it inherently lacks. 11β-HSD2 achieves this by converting active cortisol to its inactive 11-keto metabolite, cortisone (dehydrocorticosterone in rodents). In humans with the monogenetic Syndrome of Apparent Mineralocorticoid Excess (SAME), inactivating mutations in the HSD11B2 gene allows cortisol unregulated access to the MR. Resultant symptoms include severe hypertension and life-threatening hypokalemia. Individuals heterozygous for SAME display no overt phenotypes. However, some studies have associated SAME heterozygosity and loss-of-function polymorphisms within the HSD11B2 gene with essential and/or salt-sensitive hypertension in the general population.

Targeted disruption of the *Hsd11b2* gene in mice (*Hsd11b2*$^{-/-}$) faithfully reproduces with all the major phenotypes of SAME patients. Mice

heterozygote for the targeted gene (*Hsd11b2*$^{+/-}$) have no phenotype and display a normal BP. In the present study, *Hsd11b2*$^{+/-}$ mice were used to explore the relationship between reduced 11β-HSD2 enzyme activity and salt-sensitive hypertension. On a high salt diet, *Hsd11b2*$^{+/-}$ mice were found to have increased BP and impaired natriuresis, compared to wild-type controls (*Hsd11b2*$^{+/+}$). Further studies used pharmacological blockade of the Epithelial Sodium Channel (ENaC) and MR to ascertain the contributions of these pathways towards the observed phenotypes. These identified a deregulation of ENaC activity pertaining to an inability to regulate sodium appropriately.

Investigations into the contributions of the RAAS and the Hypothalamus Pituitary Adrenal (HPA) axis have revealed valuable insights into their roles in this model. There is an implication that the RAAS has increased sensitivity in *Hsd11b2*$^{+/-}$, further exacerbated by increased dietary sodium, and that the regulation of corticosteroids may also be altered. Novel observations have suggested that oxidative stress in response to a high salt diet could also be involved, as a study administering an antioxidant drug in conjunction with a high salt diet prevented the manifestation of a phenotype in *Hsd11b2*$^{+/-}$.

Finally, the generation of a floxed *Hsd11b2* targeting construct for tissue-specific deletion of 11β-HSD2 will allow future studies into the contributions of specific 11β-HSD2 expression sites (such as the kidney) towards the phenotypes of both homozygous and heterozygous mice

.

Chapter 1

Introduction

1.1 Hypertension

Hypertension is a complex disorder that affects approximately one quarter of the Western population and is a major risk factor for many different causes of mortality and morbidity, such as myocardial infarction, stroke, and renal failure (Kannel, 2000). Hypertension is defined as an abnormally high blood pressure (BP) that is sustained over a long period of time; a systolic and/or diastolic pressure taken at rest that averages 140/90 mmHg or above. In some cases, a hypertensive phenotype can be attributed to a heritable genetic condition (Mendelian hypertension) (Lifton et al., 2001). However, in the vast majority of patients diagnosed with hypertension no single underlying cause can be identified; this is termed essential hypertension. Although essential hypertension has no single identifiable cause, lifestyle factors such as obesity, lack of exercise, and a high dietary salt intake can all contribute towards the condition (Kunes and Zicha, 2009).

1.1.1 Salt-Sensitive Hypertension

In general, the underlying causes of essential hypertension can be difficult to elucidate. However, numerous studies into human hypertension have found a positive correlation between hypertensive populations and a diet high in salt content (Elliott and Stamler, 2002; Group, 1988; Khaw et al., 2004; Page et al., 1981). Current epidemiological evidence shows that the relationship between dietary salt and BP varies between the absence of hypertension in populations whose intake is less than 3g per day of salt, to the high incidence of hypertension in populations that consume more than 15g of salt per day (Meneton et al., 2005). For example, the Yanomamo Indians of Brazil consume a diet very low in salt content (typically 0.46g per day; equivalent to

20mmol of sodium) and have no incidences of age-related increases in BP, whereas populations in Northern Japan consume in excess of 13.8g of salt per day (equivalent to 600mmol sodium) and have the highest rate of age-related hypertension in the world (Franco and Oparil, 2006). In support of these observations, reductions of dietary salt intake during controlled studies involving hypertensive populations has consistently resulted in reductions in BP (Forte et al., 1989; Sacks et al., 2001; Swift et al., 2005; Tian et al., 1995). Salt-sensitivity is defined as the response of BP to an acute change in salt intake; some individuals can effectively excrete an increased salt load without an associated increase in BP, whereas those deemed to be SS cannot (Cowley, 1997). A seminal study by Weinberger and colleagues demonstrated a SS BP response (defined as a 10 mmHg change in BP) to a four hour infusion of saline, when compared to BP measured after one day on a 10 mmol diet plus furosemide administration, in 51% of hypertensive and 26% of normotensive study participants, thus highlighting the prevelnce of SS BP in humans (Weinberger et al., 1986).The observations made in humans highlighting a link between high salt intake and hypertension has been further corroborated by studies investigating SS hypertension in animal models. One such example is the Dahl SS rat (Dahl et al., 1962), and extensive studies on the mechanism underlying the SS BP of this strain has culminated in thorough genetic analysis in attempts to identify candidate genes for essential hypertension (Deng, 1998; Kato, 1999). It must be pointed out that salt excess is not the cause of all essential hypertension, as the BP response of individuals to dietary salt content is heterogeneous.

1.1.1.1 The Kidney and Salt-Sensitive Hypertension

Epidemiological, migration, medical intervention, and genetic studies in humans and animals have provided insights into the relationships that exist

between dietary salt, renal salt handling, and BP, and they highlight an important link between high salt intake and hypertension (Meneton et al., 2005). The evidence suggests that salt handling by the kidneys is an important mechanism for the regulation of BP, and that genetic mutations affecting this can account for at least some of the molecular causes of essential hypertension.

This theory is further verified by investigations into the molecular mechanisms of SS hypertension. The pathophysiological link between salt intake and BP is predictable from the relationship between salt and vascular volume homeostasis (Lifton et al., 2001). Experimental evidence reinforcing this link comes from kidney cross transplantations carried out between Dahl SS and salt-resistant (SR) rats (Churchill et al., 1992; Dahl and Heine, 1975). Dahl *et al* found that renal homografts from SR rats to hypertensive SS rats led to a sharp fall in the recipients BP. The reverse happened when the transplant was in the opposite direction, so that the SS recipient rats became uncharacteristically hypertensive. Churchill *et al* built upon this further by conducting a study into kidney transplants where SR and SS rats had both a native kidney and a transplanted kidney of the opposite genotype. Renal clearance studies showed differences between the two different kidneys in the same rat, thus concluding that the differences were determined by the kidneys genotype, and not the recipients.

1.1.2 Renal Sodium and Water Handling

In order to maintain BP homeostasis the body must be able to appropriately match the intake of water and electrolytes (including sodium) with their excretion. This requires the kidneys to be able to respond to fluctuating dietary intakes of both and adapt excretion appropriately. The kidneys

achieve this by balancing water and sodium excretion in response to hormonal signals such as Anti diuretic hormone (ADH; also known as vasopressin) and aldosterone. This involves a fine balance of reabsorption and excretion of the luminal fluid along the nephron (Figure 1.1), and de-regulation of this system can result in a sustained elevation in BP.

1.1.2.1 Long-term BP Regulation by the Kidney – Guyton's Model

Guyton and Coleman's computer model of circulatory control was fundamental in demonstrating that cardiac output and the peripheral resistance of the vasculature have a combined effect upon BP regulation via pressure natriuresis (Guyton et al., 1972). An imbalance between sodium intake and sodium excretion can lead to an increase in vascular system volume (VSV), thus causing parallel increases in arterial BP (Bongartz et al., 2005). In turn, these changes in BP can directly alter sodium excretion so as to normalise VSV and BP via pressure natriuresis; this demonstrates the overriding importance of renal sodium handling in long-term BP regulation (Figure 1.2). Guyton explains this as a "kidney-fluid mechanism for controlling arterial BP involving an infinite feedback gain property"; that is, the kidneys adjust to an elevated BP by increasing their excretion of sodium and water so as to reduce VSV, and will decrease sodium and water excretion in response to a BP fall to increase VSV and BP (Guyton, 1990). Thus, the renal excretion of both sodium and water is carefully regulated so as to maintain a balance for regulation of an appropriate BP.

1.1.2.2 Sodium Reabsorption

Urinary excretion of any given substance is the determined by the balance between filtration at the glomerulus and tubular handling (either

Renal Tubular Reabsorption and Excretion of Sodium and Water

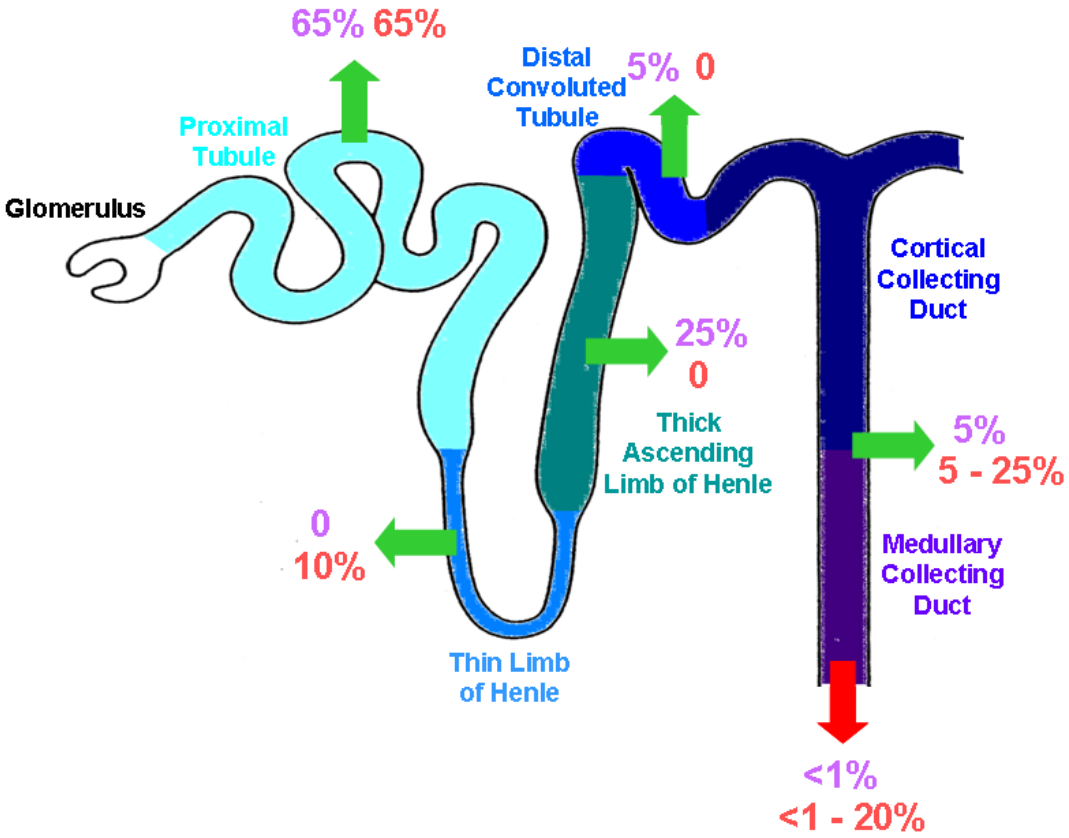

Figure 1.1. Representation of sodium and water reabsorbed in different segments of the nephron as a % of the total amount entering the tubule by filtration at the glomerulus. Sodium is represented by purple text, water by pink text, reabsorption by green arrows and final excretion by a red arrow.

reabsorption or secretion) (Guyton, 1990). Varying amounts of sodium are filtered from circulating plasma at the glomerulus (depending upon dietary intake), with the vast majority being reabsorbed back into the circulation, and generally a fraction of less than 1% excreted in the urine (see Figure 1.1). The final urinary excretion of sodium can be increased or decreased depending upon dietary load. The reabsorption of sodium is mainly an active transcellular process driven by the sodium-potassium

Guyton's Model of Blood Pressure Regulation

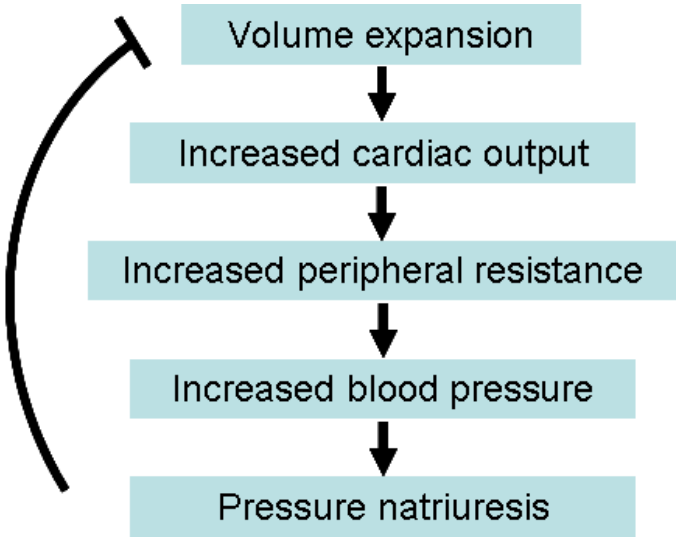

Figure 1.2 Guyton's model of long-term blood pressure regulation by the kidney. An increase in extracellular fluid volume causes a volume expansion, which in turn leads to an increased cardiac output. This results in an increase in peripheral resistance, causing a rise in mean arterial blood pressure. The kidney adapts to this by increasing its excretion of sodium (known as pressure natriuresis), acting to reduce extracellular volume, and this ultimately causes a reduction in mean arterial blood pressure. Adapted from (Bongartz et al., 2005).

ATPase (Na-K-ATPase) pump. The Na-K-ATPase pump is an example of primary active transport, as it moves sodium against its electrochemical gradient across the basolateral membrane of tubular lumen cells and into the interstitial fluid; the energy for this process comes from the hydrolysis of ATP.

The Na-K-ATPase is responsible for the active reabsorption of sodium into the interstitial fluid in most parts of the nephron. However, this can only occur if sodium is reabsorbed from the tubular lumen into cells of the nephron at their apical membrane. This is regulated differently in separate segments of the nephron. In the proximal tubule (the major site of sodium reabsorption in the nephron), sodium entry is coupled with hydrogen

secretion via the NHE-3 antiporter, or in symport with glucose, amino acids and/or phosphate; there is also additional sodium transport across the basolateral membrane in symport with bicarbonate (Figure 1.3a). No sodium is reabsorbed in the thin limbs of Henle. The thick ascending limb of Henle reabsorbs sodium via the sodium-potassium-chloride symporter (NKCC) as well as paracellularly due to a favourable electrochemical gradient between the lumen and the interstitium (Figure 1.3b). In the distal convoluted tubule, sodium crosses the apical membrane either by the sodium-chloride symporter (NCC) or via the epithelial sodium channel (ENaC) (Figure 1.3c). The last point of sodium reabsorption in the nephron occurs in the principal cells of the cortical collecting duct via ENaC (Figure 1.3d). Although the amount of sodium reabsorbed in the collecting duct is relatively small compared to other nephron segments, it has been shown that this final "fine tuning" of sodium reabsorption is paramount in sodium balance homeostasis, and is actively regulated by the renin angiotensin aldosterone system (RAAS) via mineralocorticoid receptor (MR) regulation of ENaC (discussed in more detail later in this chapter).

Overall, the reabsorption of sodium from the tubular lumen back into blood involves movement across the apical membrane of nephron cells from the lumen (by the variety of processes described above), followed by active transport out across the basolateral membrane into interstitial fluid by the Na-K-ATPase, and finally reabsorbtion from interstitial fluid into peritubular capillaries, which occurs passively due to osmotic pressure gradients.

a) Proximal Tubule

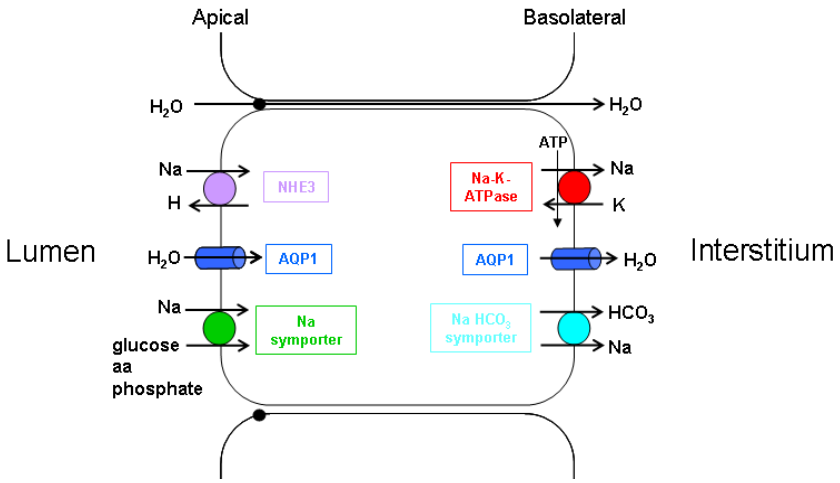

b) Thick Ascending Limb

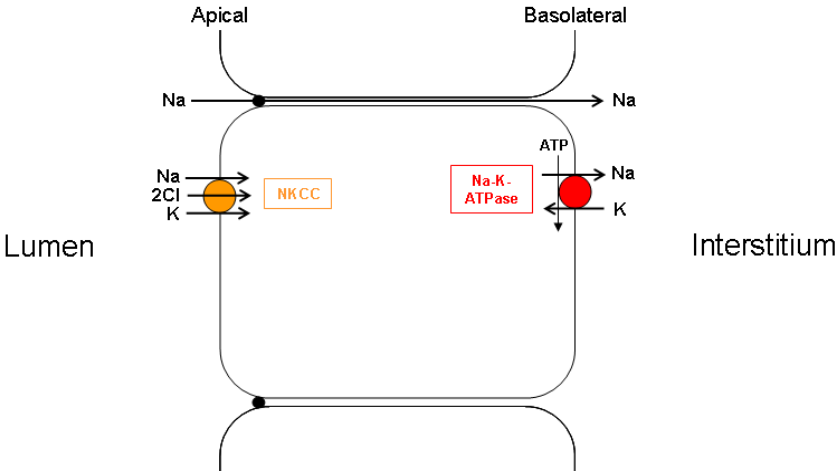

c) Distal Convoluted Tubule

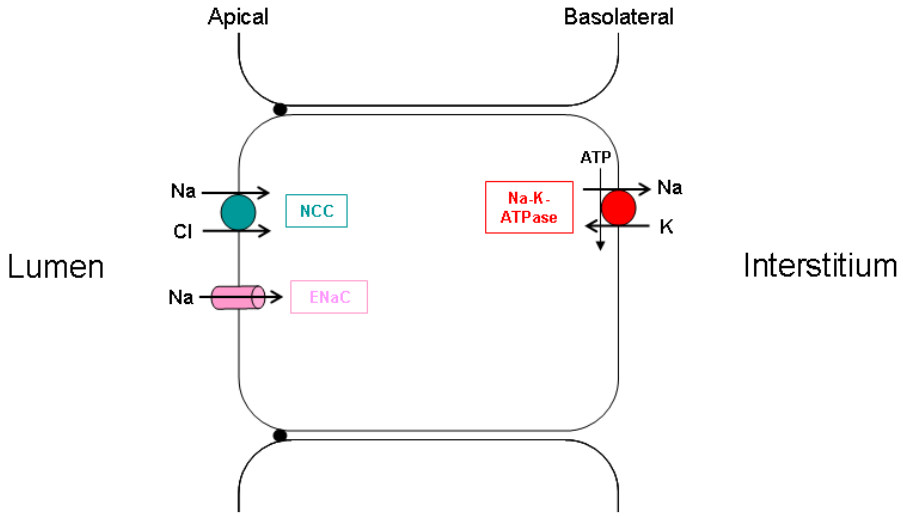

d) Collecting Duct: Principal Cell

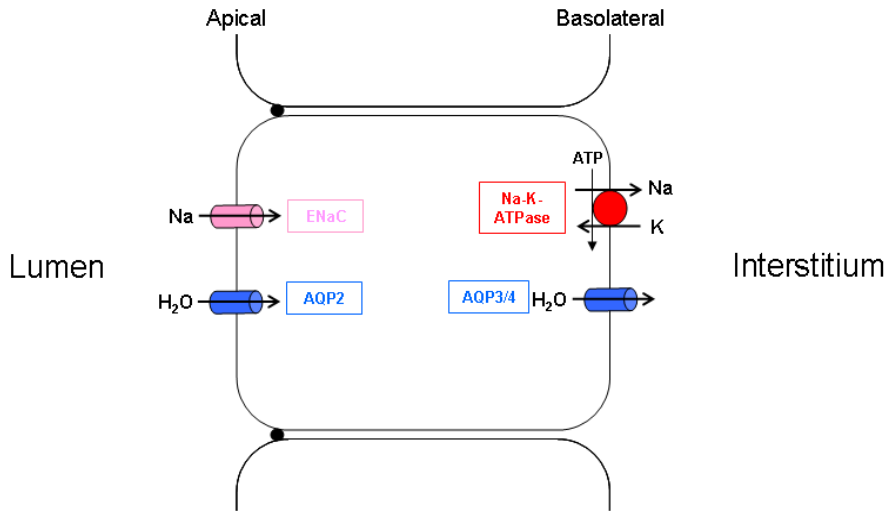

Figure 1.3. Mechanisms of transport for sodium and water reabsorption in different segments of the nephron. **a)** In the proximal tubule sodium can be moved across the apical membrane by the sodium-hydrogen exchanger (NHE3, purple) or the sodium symporter (green). Sodium is transported across the basolateral membrane by the sodium-potassium-ATPase (Na-K-ATPase; red; main source of sodium movement across the basolateral membrane in all nephron cell-types) or the sodium-bicarbonate symporter (Na HCO_3; aqua blue). Water is moved across both membranes by the water channel aquaporin 1 (AQP1; blue), and can also move paracellularly through leaky tight junctions. **b)** In the thick ascending limb sodium is moved across the apical membrane by the sodium-chloride-potassium co-transporter (NKCC; orange); sodium can also move paracellularly. The thick ascending limb is impermeable to water. **c)** Sodium moves across the apical membrane of the distal convoluted tubule by either the sodium-chloride co-transporter (NCC; teal) or the epithelial sodium channel (ENaC; pink); this segment is impermeable to water. **d)** In the principal cells of the collecting duct sodium is moved across the apical membrane by ENaC, and water is transported via AQP2. At the basolateral membrane, water moves via AQP3 and 4.

1.1.2.3 Water Reabsorption

The water content of urine in relation to other solutes can be varied by the kidneys according to the volume of water intake; dilute urine will be produced during large intakes of water, and concentrated urine during

periods of reduced water ingestion. The kidney reabsorbs water by osmosis only, never active transport, and this is secondary to the reabsorption of solutes, principally sodium. Different parts of the nephron are responsible for the reabsorption of different volumes of water (see Figure 1.1 for overview).

Water can be reabsorbed from tubular cells in several different ways including diffusion through the lipid bilayer of the cell membrane, in-between the tight junctions between cells, and across the cell membrane via specialised water channels called aquaporins (AQPs). The presence of AQP3 and 4 in the basolateral membranes of renal cells ensures that the cytosolic osmolality is similar to that of the interstitium. Although the basolateral membranes are always water permeable, the permeability of the apical membranes and the tight junctions vary depending upon nephron section.

As with sodium reabsorption, water is reabsorbed in different quantities along the nephron. In the proximal tubule, water is reabsorbed to the same extent as sodium (Figure 1.3a). The proximal tubule is the major site of water reabsorption, and this occurs both paracellularly (by osmotic gradient between leaky tight junctions) and transcellularly (via AQP1 expression in the apical membrane). The descending limb of Henle reabsorbs water as it is relatively water permeable (Figure 1.3b). No water is reabsorbed in the thin and thick ascending limbs, as their apical membranes are impermeable to water (Figure 1.3c). As a result of this, the nephron will always reabsorb more solute than water before tubular fluid reaches the cortical collecting duct, resulting in the tubular fluid entering the collecting duct being relatively dilute. The distal convoluted tubule can alter its water permeability to produce either concentrated or dilute urine, depending upon hormonal signals. ADH is secreted by the pituitary gland in response to

water homeostasis and acts to promote AQP2 insertion at the apical cell membrane of collecting duct principal cells (Figure 1.3d). This permits the collecting duct to vary its reabsorption of water by AQP2; AQP2 is the only AQP regulated in this way (for review of AQP2 regulation, see (Noda and Sasaki, 2006).

Overall, the final dilution of urine depends upon both the medullary osmotic gradient produced by the impermeability of the loop of Henle to water compared to solute reabsorption, and to the variable water permeability of the collecting duct due to hormonal regulation.

1.1.3 Monogenic Hypertension

Essential hypertension accounts for over 90% of all clinical cases of hypertension and it is likely that multiple genes with different degrees of functional polymorphisms are involved (McBride et al., 2006). The exact causes of essential hypertension are difficult to identify, as there are many different genes involved in the homeostatic control of BP. It is likely that multiple genes with slight functional mutations contribute towards the total phenotype of essential hypertension. However, molecular genetic studies into monogenic forms hypertension (and hypotension) in humans have been vital in improving the understanding of the molecular and physiological mechanisms underlying essential hypertension within the general population.

Eight genes have been identified as causing monogenic hypertension, and nine that cause monogenic hypotension (Lifton et al., 2001). A crucial observation from both hyper- and hypotension monogenic conditions is that in all cases the single gene identified as responsible for the phenotype exert their BP effects via renal sodium handling pathways (Figure 1.4). Mutations

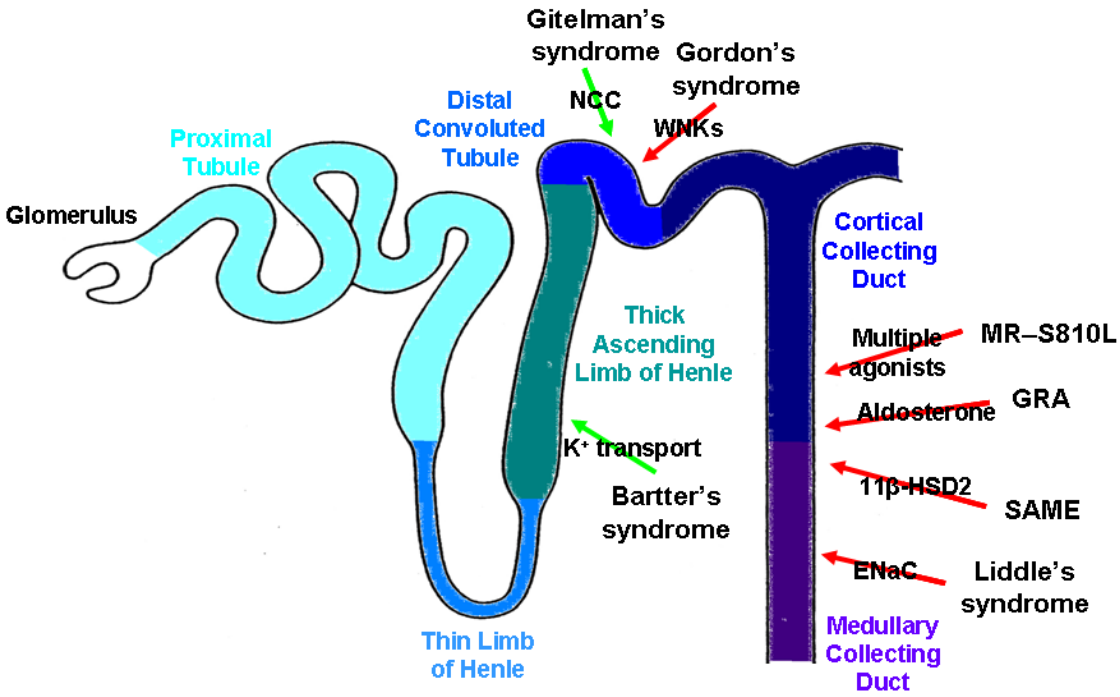

Figure 1.4. Monogenic mutations that have been identified as the molecular cause(s) of Mendelian hypo- and hypertension in humans (black text). Green arrows indicate hypotensive disorders, red arrows indicate hypertensive disorders, and black text across arrows highlights molecular mechanisms causing the disorders. Adapted from Meneton, Jeunemaitre et al. 2005.

that increase sodium reabsorption cause hypertension and those that impair it lead to hypotension.

1.1.3.1 Hormones and Hormone Receptors

Glucocorticoid-remediable aldosteronism (GRA) and the syndrome of apparent mineralocorticoid excess (SAME) are both examples of monogenic hypertension where the mutation affects hormonal regulation of renal sodium handling. Ultimately, these mutations cause an over activation of the MR, resulting in inappropriate up regulation of ENaC-mediated sodium reabsorption out with the control of the RAAS. Both of these conditions will

be discussed in more detail in context to their disruption of hormonal regulation later in this chapter.

A mutation in the MR receptor itself that permits compounds that would not normally activate it to behave as potent agonists has also been identified as a cause of Mendelian hypertension. The MR-S810L mutation allows both endogenous hormones, such as progesterone, and pharmacological antagonists, such as spironolactone, to activate the MR; the hypertensive phenotype becomes particularly prominent during pregnancy, when endogenous progesterone levels can increase 100-fold (Geller et al., 2000).

1.1.3.2 Renal Ion Channels and Transporters

Monogenic mutations in renal ion channels and transporters have also been identified as causes of Mendelian hypertension. The importance of ENaC in sodium homeostasis and BP control has been underlined by the direct genetic linkage of its genes to genetic hypertension, namely Liddle's syndrome (also known as pseudohyperaldosteronism) (Warnock, 2001). Functional ENaC is comprised of three different subunits; α, β, and γ (Rossier et al., 1994). Liddle's syndrome is caused by a mutation in the PY motif of either the β or γ ENaC subunits; the PY motif is recognised by the neural precursor cell-expressed developmentally down-regulated (Nedd) type 4 ubiquitin-protein ligase that is responsible for the ubiquitination and degradation of ENaC subunits (Staub et al., 2000). Mutations in the PY motif prevent Nedd4-mediated retrieval from the apical membrane and consequent degradation of ENaC, and as a result the channel remains constitutively active in the distal nephron. This results in a hypertensive phenotype due to excess salt retention and hypokalemia. A transgenic mouse that was generated using Cre/*lox*P-mediated recombination (see Chapter 6 for details on technique) to delete the c-terminus of the ENaC-β

subunit displays Liddle's syndrome-like phenotypes when exposed to a high sodium diet (Pradervand et al., 1999).

Recent advances in molecular biology of another form of monogenic hypertension, Gordon's syndrome (also known as pseudohypoaldosteronism type II), has revealed regulatory elements involved in nephron sodium reabsorbtion that were previously unknown. The molecular etiology of the disease is attributed to mutations in either with-no-K (lysine) (WNK) 1 or 4 (Kahle et al., 2004). WNKs are members of the serine-threonine kinase family and are expressed in the kidney (Yang et al., 2003). WNK4 normally reduces NCC activity by phosphorylating NCC; this phosphorylation acts as a molecular tag for degradation. This results in a reduced abundance of NCC at the apical membrane, where it is normally responsible for sodium reabsorption (see Figure 1.3c for demonstration of normal NCC role). Inactivating mutations in WNK4 result in increased NCC activity as it becomes over expressed at the apical membrane; consequently excess sodium is reabsorbed (Glover and O'Shaughnessy, 2010). In contrast, WNK1 has no direct effects upon NCC per se, but can act as an inhibitory regulator of WNK4 action. Two isoforms of WNK1 have been identified; a *WNK1* transcript that contains a kinase domain, known as the long isoform (L-WNK1), and a shorter isoform that lacks the kinase domain, know as the kidney-specific isoform (KS-WNK1). L-WNK1 is expressed in many different tissues, including along the entire nephron at low levels, whereas KS-WNK1 is highly expressed in the aldosterone-sensitive distal nephron (ASDN) (O'Reilly et al., 2006). Studies have shown that in the presence of L-WNK1 WNK4 no longer inhibits NCC, suggesting that L-WNK1 is an upstream inhibitor of WNK4 action upon NCC (Yang et al., 2005). KS-WNK1 is a dominant-negative regulator of L-WNK1; KS-WNK1 inhibits

NCC activity indirectly by inhibiting L-WNK1, which will consequently increase WNK4 activity (Kahle et al., 2008). Therefore, mutations that result in a gain-of-function for L-WNK1 or a loss-of-function for KS-WNK1 can both cause increased NCC activity and lead to an excess of sodium reabsorption. A transgenic mouse generated using a WNK4 mutation known to cause Gordon's syndrome displayed hypertension, hypokalemia and hyperplasia of the distal nephron (Lalioti et al., 2006). Interestingly, cross-breeding of this transgenic mouse with another transgenic mouse with a targeted NCC deficiency rescued the phenotype, further proving that molecular cause of Gordon's syndrome is via WNK effects upon NCC function in the distal nephron.

Overall, characterisations of monogenic forms of hypertension have provided important insights into the molecular mechanisms that may contribute towards essential hypertension in the general population. This is also true of monogenic hypotension, although it has not been discussed here (for review see(Rosskopf et al., 2007)). The observation that all forms of Mendelian hyper- and hypotension have a renal origin demonstrates the paramount importance of the kidney in normal BP regulation.

1.2 Glucocorticoids and Mineralocorticoids

Glucocorticoids and mineralocorticoids are members of the corticosteroid hormone family and are synthesised in the adrenal gland from the common precursor cholesterol via the intermediate pregnenolone (Figure 1.5). The principal glucocorticoid in humans is cortisol (corticosterone in rodents) and the principal mineralocorticoid is aldosterone. Sharing a common synthesis pathway, cortisol and aldosterone are also structurally similar and exhibit a degree of cross-receptor affinity and function. Nevertheless, small differences in structure permit important differences in physiological function. Aldosterone classically acts via the MR to promote sodium transport in the kidney and gut, thereby regulating long-term electrolyte homeostasis and BP control. Cortisol, by comparison, exhibits a wide range of metabolic and stress-related response effects. This section will highlight the significance of aldosterone and cortisol regulation in BP homeostasis and cardiovascular disease, discussing examples of human disease and animal models.

1.2.1 Corticosteroid Synthesis

Corticosteroid synthesis occurs principally in the adrenal gland. The biosynthetic pathways of cortisol and aldosterone share a number of common intermediates and enzymes, and only become fully exclusive at 11-deoxycortisol (DOC; cortisol pathway) and 11-deoxycorticoisterone (aldosterone pathway) (Figure 1.5a). In rodents, exclusivity occurs at 11-deoxycorticoisterone (Figure 1.5b). The reason for the difference between the primary glucocorticoid in humans and rodents (cortisol and corticosterone,

a) Aldosterone and Cortisol Synthesis (Humans)

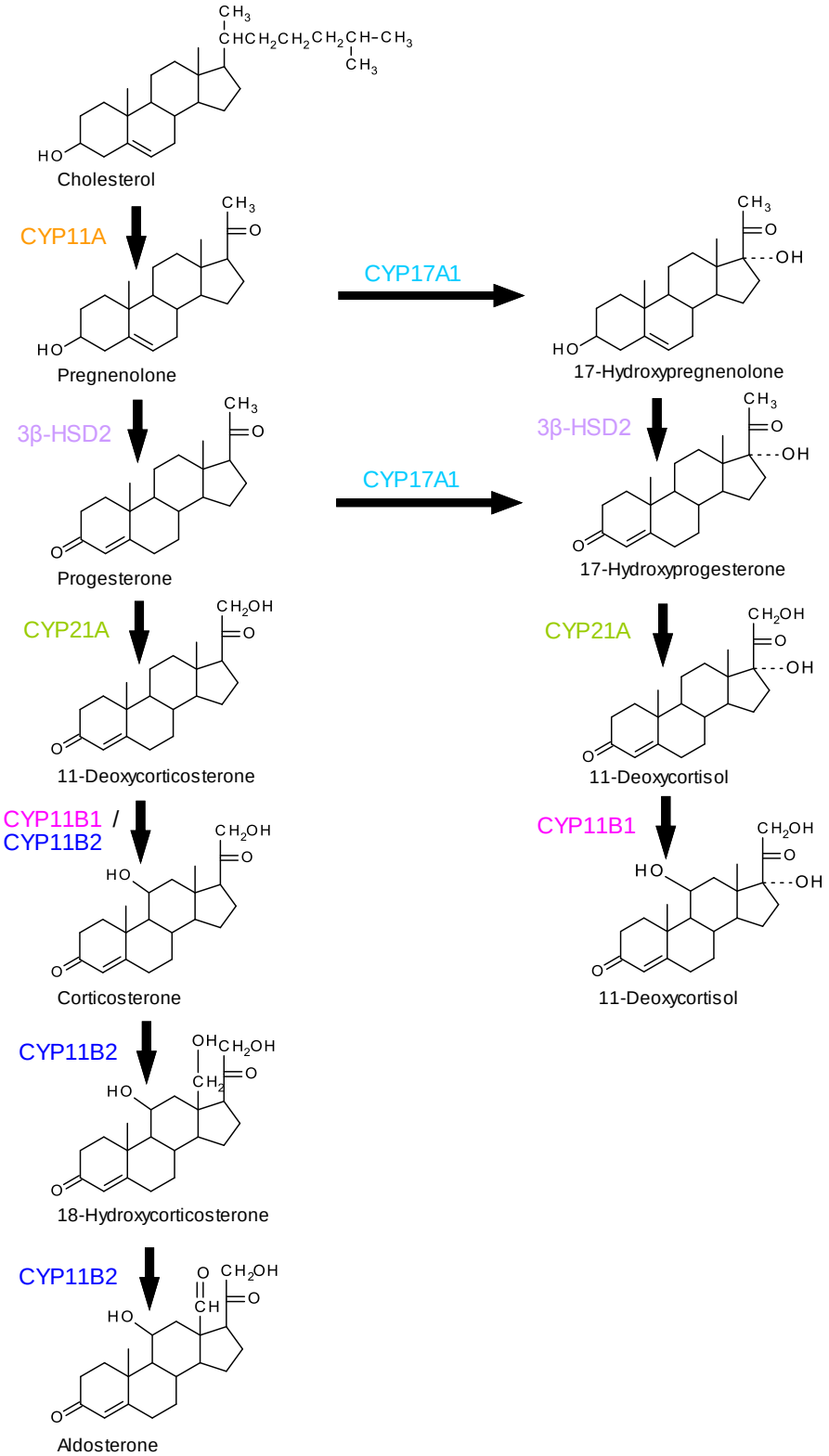

b) Aldosterone and Corticosterone Synthesis (Rodents)

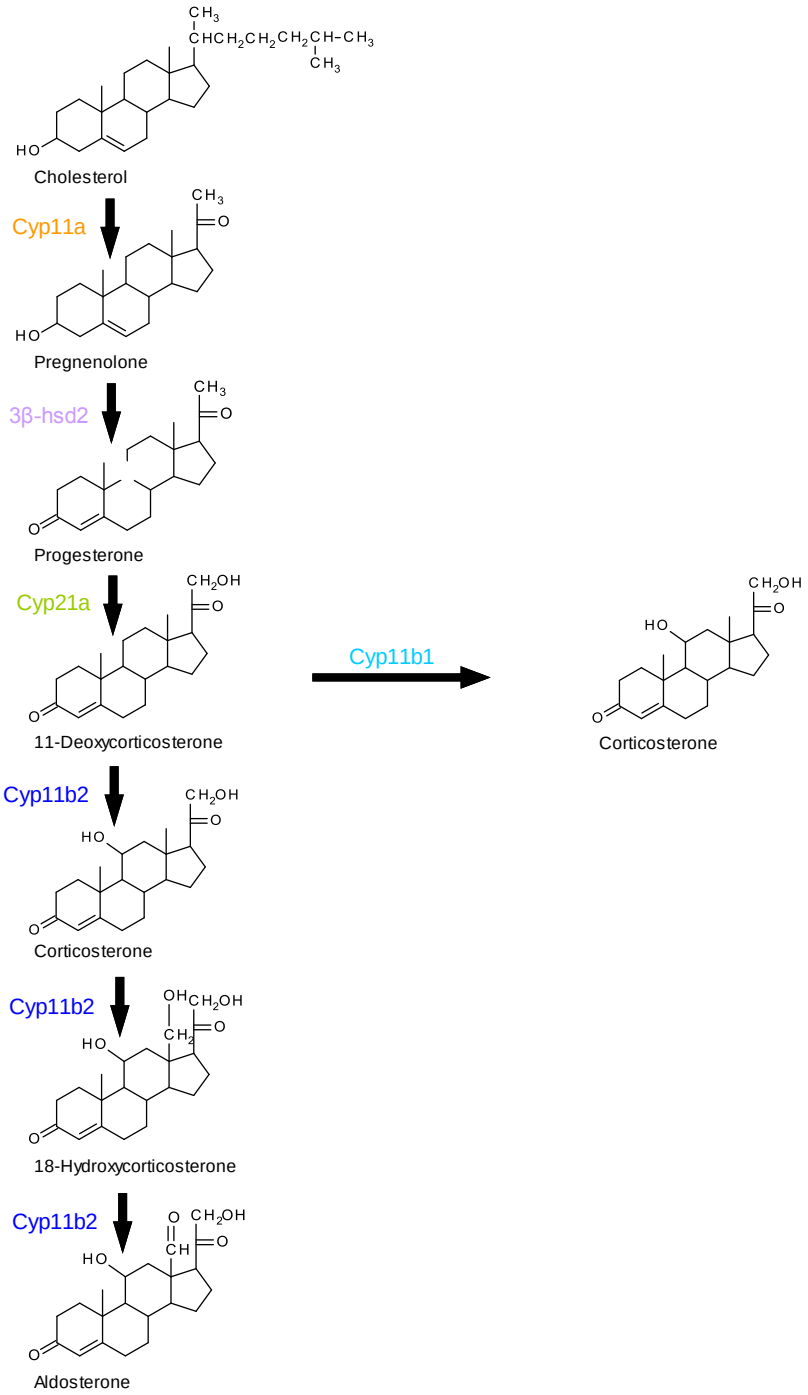

Figure 1.5. The biosynthesis pathways of aldosterone and cortisol/corticosterone. In **a)** humans the synthesis pathways become exclusive at 11-deoxycortisol and 11-deoxycorticoisteroid (cortisol and aldosterone, respectively). In **b)** rodents, the pathways diverge at 11-deoxycorticoisteroid.

respectively) is expression of the *CYP171A* gene product, CYP17. CYP17 is the enzyme responsible for the production of the 11-deoxycortisol precursors; 17-OH-pregnenolone and 17-OH-progesterone (see blue text in Figure 1.5a). 11-deoxycortisol is then converted to cortisol by *CYP11B1*. DNA methylation of *Cyp17a* prevents CYP17 production in the adrenal gland of rodents (thus they cannot synthesis the cortisol precursor 11-Deoxycortisol), and instead they utilise corticosterone as their primary glucocorticoid (Martinez-Arguelles and Papadopoulos). This epigenetic regulation of CYP17 in rodents can be chemically reversed, thus permitting rodents to express CYP17 and synthesise cortisol (Missaghian et al., 2009).

The final step in cortisol synthesis, the conversion of 11-deoxycortisol to cortisol, is catalysed by the enzyme 11β-hydroxylase (CYP11B1), while the final three stages of aldosterone synthesis are catalysed by aldosterone synthase (CYP11B2). There is a differential spatial expression of these two enzymes in the cortex of the adrenal gland which is divided into three distinct zones: zona glomerulosa, zona fasciculata, and zona reticularis. Cortisol is synthesised primarily in the zona fasciculata, with a small amount being produced by neighbouring cells in the zona reticularis. 11β-hydroxylase is present in both these zones. Aldosterone is produced in the zona glomerulosa, where aldosterone synthase is exclusively expressed. The final step in cortisol synthesis, the conversion of 11-deoxycortisol to cortisol, is catalysed by the enzyme 11β-hydroxylase (CYP11B1), while the final three stages of aldosterone synthesis are catalysed by aldosterone synthase (CYP11B2).

There is a differential spatial expression of these two enzymes in the cortex of the adrenal gland which is divided into three distinct zones: zona glomerulosa, zona fasciculata, and zona reticularis. Cortisol is synthesised

primarily in the zona fasciculata, with a small amount being produced by neighbouring cells in the zona reticularis. 11β-hydroxylase is present in both these zones. Aldosterone is produced in the zona glomerulosa, where aldosterone synthase is exclusively expressed.

1.2.2 Corticosteroid Regulation

1.2.2.1 Glucocorticoids

Glucocorticoid synthesis is regulated by the hypothalamic-pituitary-adrenal (HPA) axis (Figure 1.6). Adrenocorticotropic hormone (ACTH) is synthesised by the posterior pituitary mainly in response to two synergistic factors – Corticotropin-Releasing Hormone (CRH) and ADH, both of which are produced in the paraventricular nucleus (PVN) of the hypothalamus in response to a physiological stress. ACTH then acts to stimulate the synthesis and release of cortisol from the adrenal gland. Cortisol itself exerts negative feedback on the HPA axis by inhibiting both the release and the actions of CRH. ACTH also exerts a short-loop negative feedback by inhibiting its own secretion. Plasma cortisol levels fluctuate throughout the day as release follows a circadian rhythm. Most secretion occurs from the third hour of sleep to the early hours of wakefulness, and plasma cortisol is lower during the rest of the day. The rhythm synchronizes, to an extent, with plasma ACTH concentration and there is a peak in CRH preceding that of cortisol by 4-5 hours. There is a well-established circadian variation in cardiovascular risk events, with an increase in events in the morning compared to other times of day (Giles, 2006), coinciding with elevated glucocorticoid and aldosterone levels.

Hypothalamus Pituitary Adrenal Axis

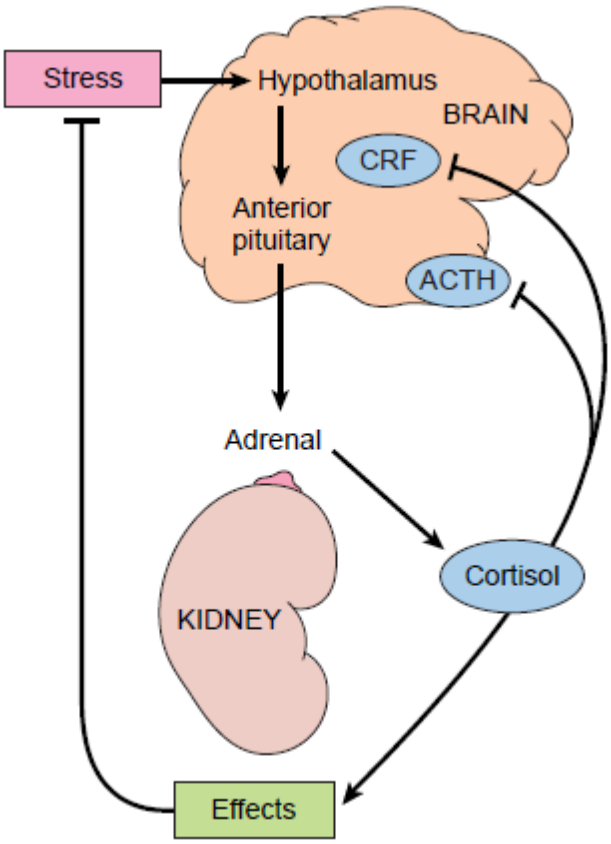

Figure 1.6. Hypothalamus Pituitary Adrenal (HPA) axis and regulation of cortisol release. Stress causes a release of corticotrophin release factor (CRF) from the hypothalamus, which in turn promotes the release of adrenocorticotropic hormone (ACTH) from the pituitary gland. ACTH then acts upon the adrenal gland to increase the synthesis and release of cortisol (corticosterone in rodents), which itself acts as a regulator of the HPA axis by inhibiting CRF and ACTH release.

1.2.2.2 Aldosterone

The production of aldosterone from the zona glomerulosa is controlled by the RAAS (Figure 1.7) and plasma potassium concentration. Angiotensin II (AngII) and potassium have been shown to exert trophic effect on adrenal gland structure, promoting both hypertrophy of the zona glomerulosa and increased sensitivity of aldosterone secretion (Quinn and Williams, 1988).

Renin Angiotensin Aldosterone System

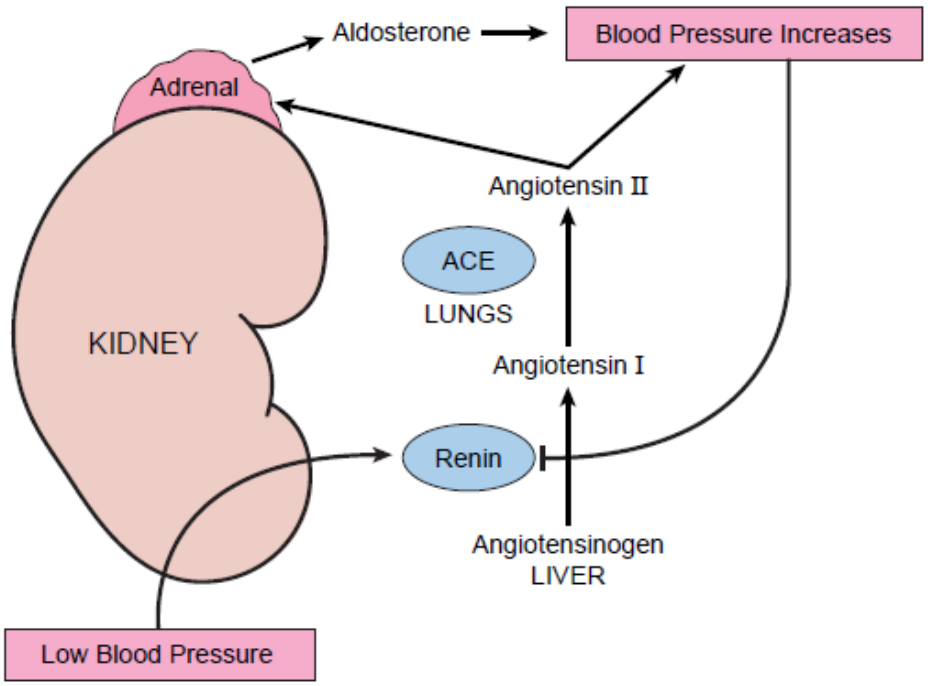

Figure 1.7. Renin angiotensin aldosterone system (RAAS) in the control of blood pressure. Signals that indicate reductions in blood pressure and/or the sodium concentration of renal filtrate promote the release of renin from granular cells of the juxtaglomerular apparatus. Renin cleaves inert angiotensinogen to produce angiotensin I, which is in turn cleaved by angiotensin converting enzyme (ACE) into angiotensin II. Angiotensin II acts to increase blood pressure either directly (vasoconstrictive actions) or by promoting the synthesis and release of aldosterone from the adrenal gland. Aldosterone then exerts genomic effects to increase sodium reabsorption and blood pressure.

Overall, the net secretion of aldosterone normally results from the integration of both of these signals.

The RAAS begins with the cleavage of the inert peptide angiotensinogen (AGT) (which is primarily synthesized in the liver) by the aspartyl protease renin to produce angiotensin I (AngI). This is further cleaved by angiotensin converting enzyme (ACE) to yield the octapeptide, AngII. AngII acts via angiotensin type 1 and 2 receptors (AT_1 and AT_2, respectively) to increase BP

by increasing vascular resistance and renal sodium reabsorption. Due to its effects upon the vasculature, AngII can be considered as an important cardiovascular hormone in its own right, separately from its effects on aldosterone synthesis. AngII also stimulates aldosterone production by activation of both early and late stages of steroid biosynthesis (Kramer et al., 1980), thus completing the RAAS-induced synthesis of aldosterone. Classically, the RAAS operates at a systemic level. Recent evidence, however, demonstrates that the RAAS can operate independently at the level of the tissue and exert powerful cardiovascular effects quite independently of the systemic system (Lazartigues et al., 2007).

The observation that aldosterone synthesis can occur even when the RAAS is suppressed highlights the important regulatory role of plasma potassium concentration. The regulation of aldosterone synthesis by potassium is very sensitive, and changes of ± 0.1mM can alter the rate of production independently of either AngII or plasma sodium (Quinn and Williams, 1988). This sensitivity is due to the high expression of specific potassium channels in the glomerulosa cells of the adrenal; namely TWIK-related acid sensitive potassium channels 1 and 3 (TASK1 and 3) (Bandulik et al., 2010). These channels are active at negative membrane potentials, and as a result relatively small changes in extracellular potassium concentration can activate voltage-activated calcium channels leading to a calcium influx in these cells (Lotshaw, 2001). This calcium influx, in turn, can induce and activate CYP11B2 (see figure 1.5), as well as steroidogenic acute regulatory protein (StAR), which is the transport protein that regulates cholesterol transfer within mitochondria (the rate limiting step in the production of steroid hormones, such as aldosterone) (Spat, 2004). This provides a feedback loop of potassium plasma concentration whereby if plasma potassium rises, the

increase in aldosterone synthesis promotes kaliuresis and a redistribution of potassium from the extracellular fluid into the cytosol, thereby returning plasma potassium levels to normal (Young, 1985). This feedback loop can uncouple the secretion of aldosterone from control by AngII under conditions of sodium depletion (Cowley and McCaa, 1976). The binding of AngII to its type 1 receptor (AT_1) also stimulates a variety of signalling cascades that lead to an increase in intracellular calcium that increases CYP11B2 and StAR expression (Nogueira et al., 2010)

Abnormal regulation of the RAAS is regularly implicated in hypertension (Campese and Park, 2006; Mullins et al., 2006) and the beneficial effects of ACE inhibitors and AT_1 receptor blockers in patients with cardiovascular disease have been demonstrated many times in large scale clinical trials (Stojiljkovic and Behnia, 2007). Similarly, the renin inhibitor, Aliskiren, is effective in the treatment of moderate hypertension, although long-term outcome data are not yet available (Van Tassell and Munger, 2007). In addition, the use of transgenic animals has clearly demonstrated the major role of the RAAS in cardiovascular homeostasis; for a detailed review of this subject, see (Mullins et al., 2006).

1.2.3 Corticosteroid Receptors and Control of Ligand Access

1.2.3.1 Steroid Receptors

The glucocorticoid receptor (GR) and the MR are the intracellular hormone receptors responsible for binding and mediating the "classic" effects of cortisol and aldosterone, respectively. They belong to subfamily 3C of a large and diverse family of transcription factors known as the nuclear receptor family. Other members of subfamily 3C include the progesterone

receptor (PR) and the androgen receptor (AR). GR and MR share a high degree of structural homology, reflecting the structural similarities between their corticosteroid ligands. The structural homology is highest at the DNA-binding domains at 94%, and is 56% between the ligand-binding domains (Lu et al., 2006). This high degree of homology suggests that the two receptors are closely associated in evolutionary terms, and are most likely descended from a common ancestral receptor (Baker et al., 2007). A polar surface within the ligand-binding pocket of MR, absent in GR and other receptors of the family, permits preferential binding of aldosterone. Nevertheless, the cloning and expression of MR (Arriza et al., 1987) revealed considerable ligand-promiscuity with receptor specificity being governed by ligand access (to be discussed in more detail later in chapter).

Un-activated, GR and MR are sequestered in the cytoplasm by a heat shock protein (HSP) complex which prevents the receptors entering the nucleus in the absence of an appropriate activation signal. Cortisol and aldosterone circulate in plasma bound to plasma proteins, and can easily diffuse through the cell membrane into the cytoplasm. Here they displace the HSP from their receptor to allow the formation of a hormone-receptor complex. This changes the conformation of the receptor, allowing it to form a homodimer, which can now readily enter the nucleus where it will recognise specific hormone response elements (HREs) associated with target genes, and act as a ligand-dependent transcription factor (Figure 1.8). A recent study has shown that GR and MR can form heterodimers that successfully translocate into the nucleus; however the downstream effects on DNA transcription of this complex are as yet unknown (Nishi and Kawata, 2007). HREs are typically located within a gene enhancer, which can be several kilobases (Kbs) away from the gene promoter. GR and MR, along with PR and AR, recognise

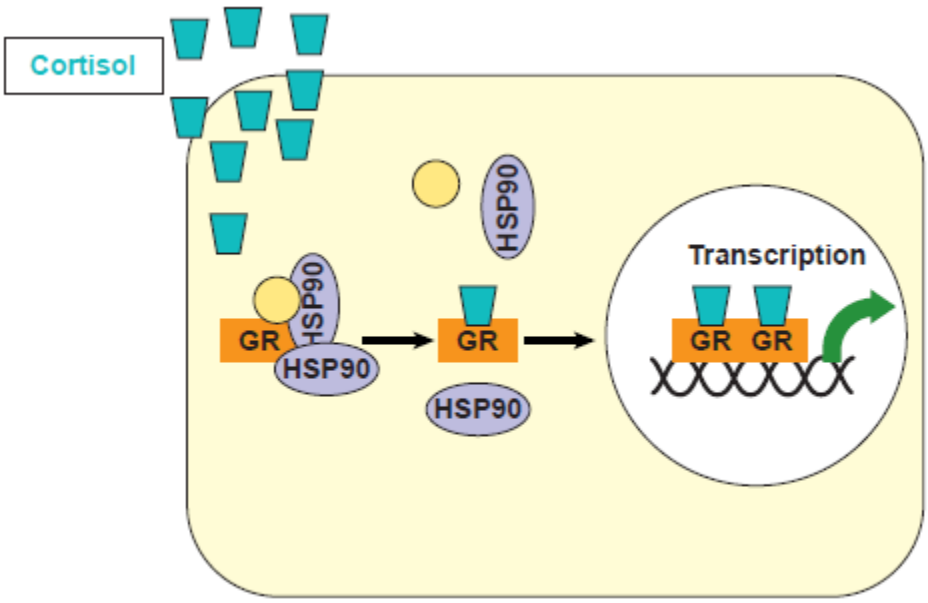

Figure 1.8. Schematic representation of the transcriptional activation of a sequestered GR monomer. Upon ligand binding, the GR monomer is released from its associated heat-shock protein inhibitory complex and forms a homodimer, which then translocates into the nucleus where it instigates transcription of GR-target genes. MR monomers are regulated in a similar manner, and there are recent reports in the literature of GR-MR heterodimers.

response elements whose HRE sequence consists of two hexameric half-sites (TGTTCT). This allows the transcription of genes that mediate GR- and MR-induced responses to be tightly regulated by appropriate ligand binding and hormone-receptor complex conformation.

1.2.3.2 Control of Ligand Access

The enzymes 11β-hydroxysteroid dehydrogenase type 1 and 2 (11β-HSD1 and 2) are key determinants of ligand access to the GR and MR, respectively. The enzymes interconvert between cortisol (active) and cortisone (inactive),

thereby controlling the local concentrations of active glucocorticoids (Figure 1.9).

Post-Synthesis Glucocorticoid Regulation

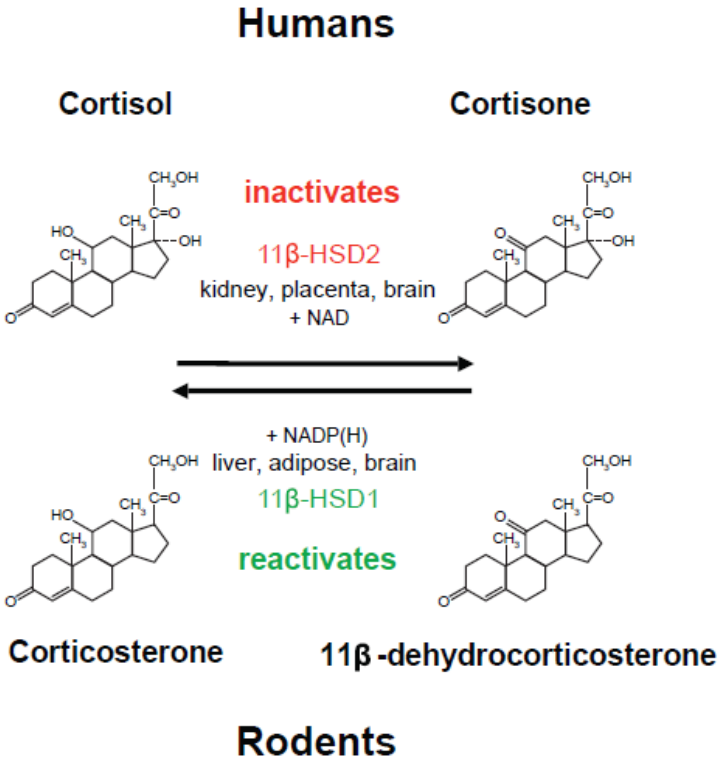

Figure 1.9. Diagrammatic representation of the *in vivo* interconversion between active (cortisol/corticosterone) and inactive (cortisone/11β-dehydrocorticosterone) glucocorticoids by the enzymes 11β-HSD1 and 2, in humans and rodents. 11β-HSD1 and 2 have different expression patterns that complement their physiologic roles, and require either NADP(H) or NAD(H) co-factor for their enzymatic activity, respectively.

11β-HSD1 has a wide distribution, but its main areas of action, in terms of both transcript expression and activity, are the liver, adipose tissue and brain (Seckl and Walker, 2004). 11β-HSD1 can control the concentration of available glucocorticoids at a more local, tissue-specific level, and an up-regulation of 11β-HSD1 can result in increased generation of cortisone to

cortisol at a local level. *in vivo,* 11β-HSD1 governs the extent to which the GR is activated by up-regulating active glucocorticoid signalling at a local level (Paterson et al., 2005). Due to its widespread distribution and the lack of specific inhibitors, functional dissection of the role of the enzyme in specific tissues is difficult. However, significant advances in the understanding of this have come from the generation of genetically modified mice.

11β-HSD2 has a more limited distribution, and is expressed predominantly in aldosterone target tissues such as the distal nephron and colon (Brown et al., 1996). 11β-HSD2 is also found in non-epithelial cell types such as the placenta (Thompson et al., 2002; 2004), the vascular endothelium (Christy et al., 2003) and specific regions of the brain (Holmes and Seckl, 2006). *In vitro*, MR can be activated with equal potency by both aldosterone and cortisol (Arriza et al., 1987). *In vivo*, ligand access to MR is determined by co-localization with 11β-HSD2 (Figure 1.10). By catalysing the rapid conversion of cortisol into cortisone (which does not activate MR) 11β-HSD2 confers aldosterone specificity upon the MR (Funder et al., 1988; Stewart et al., 1987). MR and 11β-HSD2 have overlapping distributions in those tissues classically held to be aldosterone selective, such as kidney and colon epithelia (Brown et al., 1996).

Human 11β-HSD1 was originally cloned from the liver (Agarwal et al., 1989) and human 11β-HSD2 from the kidney (Agarwal et al., 1995). Although both enzymes belong to the same super family of short-chain alcohol dehydrogenase reductases, comparison reveals little sequence identity with the exception of the regions encompassing cofactor binding (nicotinamide adenine dinucleotide (NAD^+(P)) or nicotinamide adenine dinucleotide phosphate (NAD(P)H)) and the active site (Paterson et al., 2005). In cell culture systems, both enzymes are single chain polypeptides localized to the

11β-HSD2 Protection of MR Specificity

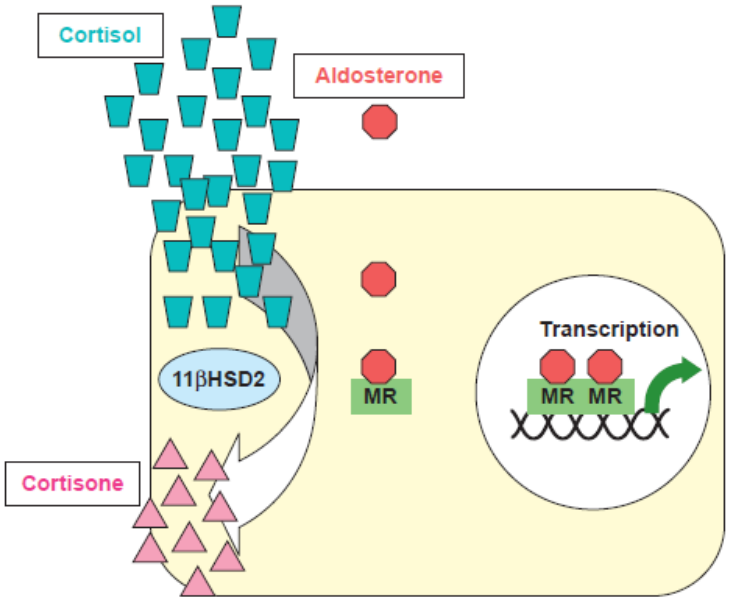

Figure 1.10. Schematic representation of 11β-HSD2 conferring aldosterone specificity upon the MR. 11β-HSD2 is co-expressed with MR in principal cells of the collecting duct, where it prevents cortisol from binding and activating the MR by converting it into inactive cortisone. This maintains MR transcriptional regulation under the control of the RAAS homeostatic feedback loop.

membrane of the endoplasmic reticulum, with opposing orientations of their catalytic sites (Naray-Fejes-Toth and Fejes-Toth, 1996; Odermatt et al., 1999). *In vivo*, however, homo-dimerisation may provide additional regulation of enzyme activity; dimerisation supports full activity of 11β-HSD1 (Maser et al., 2002) but inactivates 11β-HSD2 (Gomez-Sanchez et al., 2001).

1.2.4 Glucocorticoids - Cardiovascular Effects

Glucocorticoids are responsible for a wide range of physiological effects, the majority of which are united under the common sub-heading of stress responses (Figure 1.11). The release of glucocorticoids, following stress-

Glucocorticoid Actions

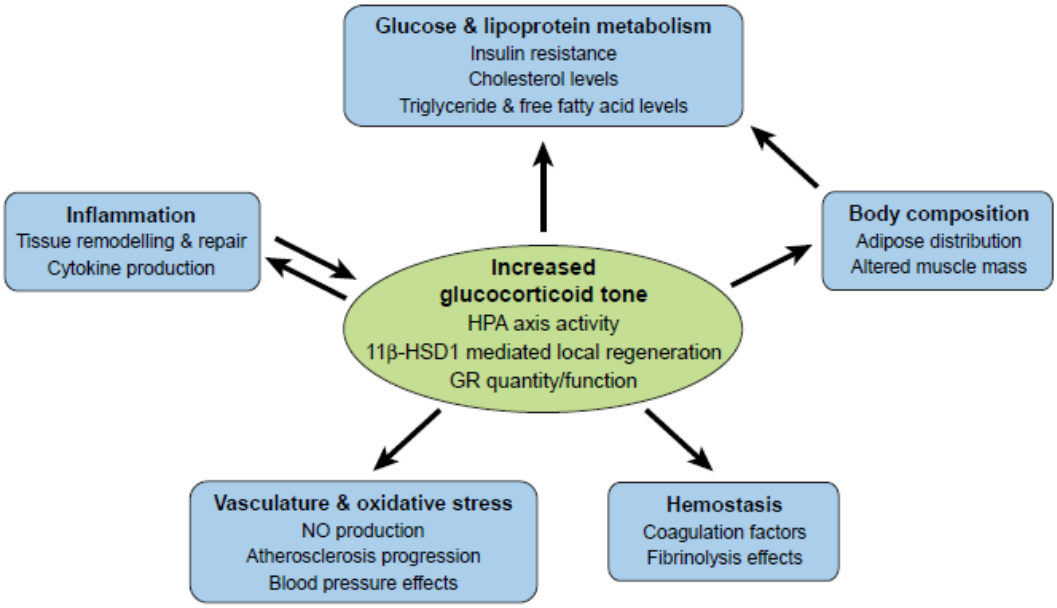

Figure 1.11. The many effects of glucocorticoids upon various cardiovascular risk factors.

induced stimulation of the HPA axis, promotes the coordination of endocrine, immune and nervous system responses to the initial stimuli. Examples of this include inducing the mobilisation of energy resources in response to physical stresses, such as starvation and the "fight or flight" response, by stimulating gluconeogenesis and lipolysis, and by inhibiting glucose uptake by peripheral tissues. Glucocorticoids also act to suppress inflammatory responses, cellular proliferation, and tissue repair, suggesting a regulatory role that acts to prevent these responses becoming undisciplined and destructive. Several clinical disorders associated with cortisol deregulation - whether a consequence of altered synthesis, HPA axis deregulation or GR-mediated effects - have been associated with an increased risk of cardiovascular events, which in turn is linked with an

increased rate of morbidity and mortality (for review see (Girod and Brotman, 2004)).

Due to the widespread distribution of GR, it is difficult to separate the direct primary effects of glucocorticoids upon the heart and vasculature from secondary changes arising from activation of GR in other systems (see Figure 1.11). However, evidence from human patients and transgenic mice has helped to establish the nature of these primary responses. That glucocorticoids are important cardiovascular hormones is illustrated through the extremes of altered glucocorticoid secretion in human conditions.

1.2.4.1 Cushing's Syndrome

Cushing's syndrome is the result of prolonged exposure to excessive cortisol; this can be due to an unregulated hyper-secretion of endogenous cortisol, or as a result of intensive exposure in the form of exogenous steroid treatment. Cardiovascular disease is the main cause of death and disease in Cushing's syndrome patients, and an elevated risk remains even after successful treatment of other symptoms (Whitworth et al., 2005); epidemiological studies of Cushing's syndrome show patients have a mortality rate 4 times higher than average due to cardiovascular complications (Etxabe and Vazquez, 1994). Hypertension is one of the major cardiovascular risk factors associated with Cushing's syndrome, being present in ~80% of adult patients (Arnaldi et al., 2004). The key underlying mechanism of hypertension is glucocorticoid excess; this can in part be attributed to illicit MR occupation, but this is not the only cause as MR antagonists do not fully alleviate the hypertension (Whitworth et al., 2005). A recent study investigating the contributions of MR and GR towards Cushing's phenotypes in a mouse model of the disease demonstrated that blockade of both receptors was

required to fully alleviate the phenotypes, suggesting that both are involved in Cushing's disease (Bailey et al., 2009). Other BP effects are mediated by excessive activation of the RAAS, potentiation of vasoactive substances, and/or suppression of vasodilators (for review, see (Magiakou et al., 2006)). Hypertension is generally resolved in patients after successful treatment, but in a few cases the hypertension persists, suggesting permanent damage to, and remodelling of, the renal and cardiovascular systems.

1.2.4.2 Metabolic Syndrome

The metabolic syndrome is defined as the clustering of a plethora of metabolic and cardiovascular phenotypes, including hypertension, hyperglycaemia (type 2 diabetes), dyslipidemia, and abdominal obesity (Aizawa et al., 2006). The metabolic syndrome has been shown to be a major cardiovascular risk factor, and its prevalence in modern society may be related to relatively recent lifestyle changes, such as dramatic increases in calorie and salt intake coupled with a rise in sedentary lifestyle habits (Chew et al., 2006). However, the metabolic interactions leading to the clustering of metabolic syndrome phenotypes are not completely understood (Grundy, 2007). A similarity between the phenotypes of metabolic syndrome and Cushing's disease cannot help but to be noticed, and glucocorticoids excess/resistance is a possible underlying cause of metabolic syndrome (Walker, 2006). As GR are ubiquitously expressed throughout all tissues, the effects of a global increase in plasma glucocorticoids levels can have many varied physiological effects (refer back to Figure 1.11).

1.2.4.3 Glucocorticoid Receptor Polymorphisms

GR variation exists in the general population, and several GR polymorphisms have been identified that seem to be associated with altered

glucocorticoid sensitivity and metabolic parameters (for review see (van Rossum and Lamberts, 2004)). The N363S variant is associated with hypertension, obesity, angina and coronary artery disease, suggesting a role for altered GR variation in these conditions (Lin et al., 2003). Conversely, the ER22/23EK polymorphism is associated with glucocorticoid resistant phenotypes (Koper et al., 1997), and carriers tend to be protected from cardiovascular damage (van Rossum et al., 2004).

That no complete loss-of-function mutations in the GR are present in the human population indicates that glucocorticoid activity is essential for life. Transgenic mice with GR gene mutations, leading to partial or complete ablation of GR function support this hypothesis (for review see (Wintermantel et al., 2005)) and have not been particularly informative due to high levels of neonatal mortality; GR null mice die a few hours after birth due to respiratory failure as glucocorticoids are critical in foetal lung maturation (Cole et al., 1995). Studies in GR null heterozygote mice have revealed a hypertensive phenotype that is caused by an activated RAAS, further highlighting a potential role for GR function in cardiovascular disease (Michailidou et al., 2008).

1.2.4.4 11β-hydroxysteroid dehydrogenase type 1

Due to 11β-HSD1s widespread distribution and lack of specific inhibitors, functional dissection of the role of the enzyme in specific tissues is difficult. However, significant advances in the understanding of this have come from the generation of genetically modified mice. The 11β-HSD1 null mouse has elucidated major functions for the enzyme in the response to stress and in regulation of the HPA axis (Paterson et al., 2005); for the latter, regeneration of glucocorticoids by the liver appears to be particularly important (Paterson

et al., 2007). In addition, 11β-HSD1 null mice are resistant to age-related cognitive impairment (Yau et al., 2001), indicating roles in the brain. These studies have important implications for human disease, and studies to identify 11β-HSD1 specific inhibitors for clinical use are currently underway (Webster et al., 2007).

11β-HSD1 null mice have improved glucose tolerance, a favorable lipoprotein profile, and increased sensitivity of their liver and fat stores to insulin (Morton et al., 2001). Moreover, on the obese-prone C57BL6/J strain background, mice carrying the null mutation were resistant to the weight gain induced by high-fat feeding (Morton et al., 2004). That loss of 11β-HSD1 confers a cardio-protective metabolic profile is intriguing and most probably results from a lack of glucocorticoid regeneration in adipocytes (Wolf, 2002). However, these mice also had an increase calorific intake, suggesting that energy expenditure was also stimulated (Morton et al., 2004).

The generation of a mouse that over-expresses 11β-HSD1 under the control of an adipocyte-specific promoter further highlights the role of the enzyme in metabolic function (Masuzaki et al., 2001). The amplification of glucocorticoids was relatively modest, and was confined to the adipocyte with plasma corticosterone concentrations being normal. Nevertheless, these transgenic mice developed central obesity, insulin resistance and glucose intolerance. In addition, the animals were hypertensive due to a chronic activation of the RAAS (Masuzaki et al., 2003). This clustering of metabolic and cardiovascular phenotypes is characteristic of the metabolic syndrome, as discussed earlier.

1.2.5 Aldosterone - Cardiovascular Effects

The classical action of aldosterone is as a major regulator of body fluid and electrolyte homeostasis. These effects are exerted by MR expressed in the distal nephron to induce sodium and water reabsorption, as well as potassium excretion, and contribute towards the regulation of BP homeostasis (Booth et al., 2002; Good, 2007). Aldosterone can also exert non-classical effects in the heart (Young et al., 2007), vasculature and brain (Gomez-Sanchez, 1997) that can also influence BP homeostasis and cardiovascular regulation. Both classical and non-classical actions of aldosterone can instigate inflammation and fibrosis that can ultimately lead to cardiac, vascular, and renal damage. Indeed, the Framingham Heart Study reports a complex, but positive correlation between serum aldosterone in the physiological range and cardiovascular risk (Kathiresan et al., 2005).

In addition, there is a growing body of evidence to suggest that some physiological responses to aldosterone are initiated within too short a time frame (seconds to minutes) to be the result of a genomic mechanism. Membrane transporters have been shown to be activated rapidly by aldosterone, such as NHE1, potassium channels NaKATPase and ENaC, and increased intracellular concentrations of electrolytes are frequently cited as a rapid effect of aldosterone (see review (Harvey et al., 2008)). There is some suggestion that non-genomic effects of aldosterone may be mediated via a distinct membrane-associated receptor, and this is supported by the observation that rapid responses to aldosterone can be detected in MR knockout mice (Haseroth et al., 1999). In addition, many rapid aldosterone actions are not blocked by MR antagonists, such as the kinase-dependent activation of NHE1 (Markos et al., 2005). Others suggest that the rapid effects may be mediated via MR either directly, or by induction of

intracellular second messengers such as cyclic monophosphate (cAMP) and inositol triphosphate (IP_3) (for review see (Losel et al., 2004)).

1.2.5.1 Primary Aldosteronism

Primary Aldosteronism (PA) is disorder characterised by a high aldosterone production out with the control of the RAAS, and extracellular fluid volume expansion. Clinical effects include hypertension, cardiovascular damage, sodium retention and hypokalemia (Funder et al., 2008). Causes of PA include adrenal adenoma, unilateral and bilateral adrenal hyperplasia (idiopathic hyperaldosteronism (IHA)), and the monogenetic disorder, GRA. GRA is an autosomal dominant trait that results in an aldosterone synthase gene whose expression is under the control of ACTH instead of AngII i.e. expressional control is now out with the RAAS (Lifton et al., 1992). This causes ectopic secretion of aldosterone, leading to increased renal salt reabsorption, and hypertension.

It is estimated that between 5 – 13% of clinical hypertensive cases and up to 20% of drug-resistant hypertension are due to PA (Carey 2010). That such a significant percentage of hypertensive cases can be directly linked to an excess of circulating aldosterone emphasises how important this hormone, and its subsequent regulation by the RAAS, is in BP homeostasis. In addition, the high incidence of proteinuria in PA patients (85%) suggests that renal damage is a prominent consequence of chronically elevated aldosterone (Conn et al., 1964).

1.2.5.2 Mineralocorticoid Receptor Activation and Cardiovascular Disease

A seminal a study by Brilla and Weber investigated the effects of mineralocorticoid excess with relation to cardiovascular function, and demonstrated that rats exposed to high levels of both aldosterone and salt

developed hypertension and cardiac fibrosis (Brilla and Weber, 1992). This discovery triggered a resurgence in the clinical interest of pathological MR activation (Williams and Williams, 2003), with data suggesting that mineralocorticoid excess was associated with cardiac abnormalities (Sato and Saruta, 2004).

The potential benefits of MR blockade in treating cardiovascular disease was potentiated by the positive outcomes of two major clinical trials; RALES and EPHESUS (Pitt et al., 2003; Pitt et al., 1999). In the RALES study, patients with severe heart failure were administered the MR antagonist spironolactone, alongside their continuing conventional medication. This produced a 30% reduction in mortality and a 35% lower-frequency of hospitalization versus placebo-treated patients. Further verification of the beneficial effects of MR blockade and aldosterone antagonism was provided by the EPHESUS study in which eplerenone, an antagonist at MR more selective than spironolactone, was administered to patients who had suffered an acute myocardial infarction. Again, the results of the MR blockade were particularly positive in terms of patient morbidity and mortality.

These trials showed MR blockade to be beneficial in the treatment of cardiovascular disease; however, the underlying mechanisms of action were not clear. An obvious explanation is that MR blockade was inhibiting the effects of aldosterone in the heart, and was therefore cardio-protective. Indeed, it has been shown experimentally that increased aldosterone levels coupled with increased salt levels instigates deleterious cardiac and vascular pathologic responses (Rocha and Funder, 2002) and aldosterone levels are often raised in congestive heart failure (Swedberg et al., 1990). However, plasma aldosterone levels were not raised in patients in either the RALES or the EPHESUS studies (Pitt et al., 2003; Pitt et al., 1999). Similarly, in Dahl SS

rats fed a high salt diet, MR blockade prevented the development of cardiac hypertrophy and the onset of chronic heart failure, despite the fact that aldosterone was lower in this group than for controls to begin with (Nagata et al., 2006). In this case, the cardio-protective effects of eplerenone were independent of the antihypertensive effect of MR blockade, as has been reported elsewhere (Levy et al., 2004). Together these data indicate that MR activation per se, rather than excess of agonist, is critical to the developing pathology of hypertension and cardiovascular disease.

In contrast to classical aldosterone target tissues, occupancy of cardiac MR by glucocorticoids is the physiological norm, as 11β-HSD2 is not expressed in cardiomyocytes at physiologically relevant levels (Funder, 2004). This indicates that the benefits of MR blockade could be attributed to relief from stimulation by glucocorticoids. However, the mode of glucocorticoid action at cardiac MR is not clear. Experiments designed to test this hypothesis followed the generation of a mouse over-expressing 11β-HSD2 selectively in cardiomyocytes (Qin et al., 2003). Surprisingly, these mice developed severe cardiac hypertrophy and fibrosis, and died from accelerated heart failure. Moreover, an MR antagonist rescued the cardio-pathology, whereas a GR antagonist did not. These data indicate that glucocorticoids that normally occupy the cardiac MR are acting as agonists rather than antagonists, and that aldosterone activation of MR (only observed when 11β-HSD2 prevents glucocorticoid occupancy) is detrimental to heart function.

Targeted disruption in mice of the gene encoding MR has not been particularly informative in terms of the role of aldosterone in cardiovascular function. Mice over-expressing human MR display only mild cardiomyopathy (Le Menuet et al., 2001), and MR null mice die within 8 days of birth due to uncorrected salt-wasting (Berger et al., 1998). Mice in which

MR has been knocked down via an inducible antisense transgene have severe heart failure (Beggah et al., 2002). These experiments not only indicate the critical role for renal MR in the long term regulation of BP, but also demonstrate that activation of the GR does not compensate for loss of MR. Studies using a conditional knockout MR mouse model have allowed for the dissection of MR function in different tissues and cell-type. In collecting duct-specific knock out mice, ENaC trafficking to the membrane is abolished in targeted cells, and affected mice display unregulated sodium and water excretion on a low sodium diet accompanied by dramatic weight loss; on a standard sodium diet, this can be compensated for by ENaC expression in the connecting tubule and the late distal convoluted tubule (Ronzaud et al., 2007).

1.2.5.3 Aldosterone Effects upon the Vasculature

MR have been located in freshly isolated vascular tissue and in both cultured vascular smooth muscle cells (VSMC) and the vascular endothelium (Duprez, 2007). 11β-HSD2 is also present in human VSMC, adventitial fibroblasts and endothelial cells (Cai et al., 2001; Hatakeyama et al., 1999; Hatakeyama et al., 2000). Physiologically, both aldosterone and glucocorticoids potentiate the action of vasoconstrictors. This effect was first described in the 1950s for catecholamines, but is also true for other vasoactive agents, notably AngII (Ullian, 1999). There is some evidence to suggest that the potentiating effect of corticosteroids differs throughout the vasculature. For example, in the DOCA-salt hypertensive rat model, the pressor effects of AngII are exacerbated, indicating an increased sensitivity of the resistance vasculature to vasoconstrictors (Couture and Regoli, 1980). The mechanisms of potentiation have focused on increased receptor density, since both aldosterone and glucocorticoids greatly enhance AT_1 receptor

density (Ullian, 1999); these effects are exclusive to the AT_1 receptor (Schelling et al., 1994), consistent with the fact that the promoter region for the gene contains several steroid response elements (Uno et al., 1994).

Aldosterone also exerts profound pathological effects in the vasculature. The accumulative and slowly-developing disease atherosclerosis is a major cause of heart disease. Disruption of vascular homeostasis predisposes the endothelial vessel wall to vasoconstriction, inflammation, and atherosclerosis, all of which contribute towards cardiac disease onset. The development and progression of atherosclerosis is largely associated with endothelial dysfunction (reviewed (Landmesser et al., 2004)), and it has been suggested that the positive clinical outcomes of the RALES and EPHESUS studies may be in part due alleviation of vascular endothelial aldosterone and/or MR antagonism. Using cultured human umbilical vein endothelial cells (HUVECs), Oberleithner *et al* demonstrated that aldosterone promotes remodelling of the endothelium *in vitro* (Oberleithner, 2005). They observed that aldosterone administration caused the cells to increase in both size and stiffness, which, *in vivo*, could lead to endothelial dysfunction and associated pathogenesis. Endothelial dysfunction can be rescued in the stroke-prone spontaneously hypertensive rat by administration of eplerenone (Endemann et al., 2004), and aldosterone has also been shown to play a major role in AngII-induced vascular inflammation in the setting of high salt intake (Rocha and Funder, 2002).

These findings, together with the positive outcomes of clinical trials, would advocate the use of MR antagonists in hypertension and cardiovascular disease.

1.2.5.4 11β-hydroxysteroid dehydrogenase type 2

Inactivating mutations in *HSD11B2* cause the clinical disorder SAME. In this setting cortisol causes unregulated activation of the MR resulting in severe hypertension thought to arise from volume expansion secondary to renal sodium retention (Dave-Sharma et al., 1998; Monder et al., 1986; New and Wilson, 1999). Dexamethasone, a synthetic glucocorticoid, can be therapeutically effective as it will suppress endogenous glucocorticoids due its affinity for GR, and does not activate MR (Stewart et al., 1988). In addition, dexamethasone may act as a chaperone and stabilize mutant enzyme (Atanasov et al., 2007). Nevertheless, neither synthetic glucocorticoid nor MR blockade produce a consistent antihypertensive effect (Milford, 1999).

SAME has been modeled by targeted disruption of the 11β-HSD2 locus, producing a mouse in which the cardinal features of the disorder were preserved (Kotelevtsev et al., 1999). Although animals were born in normal Mendelian ratios, there was high neonatal mortality in the homozygote null animals, and the survivors were hypertensive and severely hypokalemic. The RAAS was show to be suppressed and plasma aldosterone was low (Bailey et al., 2008; Kotelevtsev et al., 1999). In one patient with SAME, the disorder was fully corrected by kidney transplant (Palermo et al., 2000), indicating the disease is of renal origin. In support of this, 11β-HSD2 null mice have excess renal sodium reabsorption due to activation of ENaC (Bailey et al., 2008).

11β-HSD2 is also expressed in the nucleus of the solitary tract and the amygdala of the mouse brain which are regions important to the central regulation of BP (Robson et al., 1998; Roland et al., 1995). Thus, SAME may reflect over-activation of MR in regions other than the kidney. This is

supported by experiments showing that central administration of either aldosterone (Gomez-Sanchez, 1986) or 11β-HSD2 inhibitors (Gomez-Sanchez and Gomez-Sanchez, 1992) have a sustained hypertensive effect. In addition, inhibition (pharmacological or antisense) of 11β-HSD2 sensitizes the vasculature to the vasoconstrictive actions of both AngII (Hatakeyama et al., 2000) and catecholamines (Souness et al., 2002). Vascular reactivity to noradrenalin was enhanced in a patient with SAME (Walker et al., 1992) and 11β-HSD2 null mice have demonstrated endothelial dysfunction, with enhanced sensitivity to vasoactive agents being underpinned by a reduction in nitric oxide production (Christy et al., 2003; Hadoke et al., 2001). However, the extent of the endothelial dysfunction following targeted disruption of 11β-HSD2 is dependent on the underlying background strain of the mouse and may not, therefore, contribute in a major way to altered BP homeostasis (Bailey et al., 2008). The enzyme is also expressed in the placenta where it serves to prevent maternal-fetal transfer of high levels of glucocorticoid. The deleterious effects on fetal development of *in utero* exposure to high levels of glucocorticoid are well documented and such programming is associated with low birth weight and adverse cardiovascular risk. This subject has recently been reviewed (Seckl and Holmes, 2007).

Although SAME is an extreme phenotype and very rare within the general human population, it illustrates the role that 11β-HSD2 in the kidney, brain and vasculature has in the regulation of cardiovascular homeostasis. Indeed, it is possible that mild mutations are prevalent in the essential hypertensive population (Bocchi et al., 2004), particularly in those individuals with low-renin or SS hypertension. Human molecular genetic studies in hypertensive populations have sought associations between BP and loss-of function-polymorphisms in 11β-HSD2, with conflicting results (Melander et al., 2003;

Poch et al., 2001; Williams et al., 2005). A more direct relationship between 11β-HSD2 and BP was obtained in non-hypertensive individuals subject to salt-loading. For those individuals with a SS BP, the extent of the rise in BP following salt load was indirectly related to 11β-HSD2 enzyme activity. That is, the lower the activity, the more exaggerated the response to salt-loading.

1.3 Aim of PhD:

Investigating Mechanisms of Salt-Sensitive Hypertension in *Hsd11b2* Heterozygote Mice

The aim of my PhD was to further investigate the proposal from human hypertensive populations that a link exists between SS BP and HSD11B2 polymorphisms that impair 11β-HSD2 enzyme activity (Ferrari et al., 2000). This association between SS BP and reduced 11β-HSD2 activity has been observed by association studies only and direct *in vivo* evidence is so far lacking. An 11β-HSD2 null transgenic mouse model previously generated within our laboratory provides an excellent opportunity for studying this association directly. Mice homozygous for the null *Hsd11b2* transgene faithfully reproduce the major phenotypes of SAME patients (Kotelevtsev et al., 1999). Heterozygous mice (who presumably express 50% 11β-HSD2 enzyme activity compared to wild type mice) do not present with a phenotype on a standard diet. Our hypothesis was to challenge the *Hsd1b2* heterozygous mice with a high sodium diet to investigate if they have a SS phenotype. Due to a successful kidney transplant in a notable case of SAME (Palermo et al., 2000), and evidence obtained in our laboratory that *Hsd11b2* null mice have impaired renal sodium excretion due to unregulated ENaC activity (Bailey et al., 2008), the renal origins of any observed phenotypes were of a particular interest. The presence of 11β-HSD2 within the vasculature could also affect the sensitivity of these mice to vasoconstrictors, such as AngII, and a high sodium diet may exacerbate this; this theory was tested in this model. In addition, mechanisms underlying the cause of a high salt diet to effect steroid receptor activation under conditions of reduced 11β-HSD2 activity were also begun.

The expression of 11β-HSD2 in multiple sites throughout the body that are important for BP homeostasis (kidney, vasculature, brain, and placenta) whether it be via sodium and water balance regulation, altered sensitivity to vasoconstrictors, or prenatal programming, ultimately makes the dissection of the contribution of individual expression sites towards any phenotype complicated and incomplete. The generation of a tissue-specific *Hsd11b2* null mouse model would be invaluable towards further research within this field. In the hope to achieve this, the construction of an *Hsd11b2* floxed targeting allele with the aim of generating a kidney-specific *Hsd11b2* null mouse model was undertaken during my PhD studies.

Chapter 2

Materials and Methods

2.1 Animal Breeding and Husbandry

All animal experiments described in this work were performed in accordance with the UK Home Office (Scientific Procedures) Act 1986.

2.1.1 *Hsd11b2* Heterozygote Line

Mice homozygous for a null mutation in *Hsd11b2* (*Hsd11b2*$^{-/-}$) were previously generated on a mixed background as described (Kotelevtsev et al., 1999). These mice were then crossed for more than 12 generations onto a C57Bl6/J background (Bailey et al., 2008). The male mice used in the described studies were obtained from heterozygote (*Hsd11b2*$^{+/-}$) crosses of the congenic *Hsd11b2*-C57BL6/J line. Mice were genotyped by Southern hybridization, as described (Kotelevtsev et al., 1999) and heterozygote (*Hsd11b2*$^{+/-}$) mice were compared with wild-type (*Hsd11b2*$^{+/+}$) animals. All *Hsd11b2* mouse genotyping was carried out by Mrs. Nina Kotelevtseva, senior laboratory technician. All experimental mice were used between 120-200 days of age.

2.1.2 *Hoxb7* Cre Line

The *Hoxb7* Cre line was purchased from Jackson Laboratories (JAX Mice and Services, Bar Harbour, Maine, USA) as two breeding pairs. Homozygous mice are not viable, so the line was maintained on the hemizygous background (*Hoxb7*$^{+/-}$). *Hoxb7*$^{+/-}$ mice were crossed with C57Bl6/J (background strain) mice and subsequent offspring screened for *Hoxb7*$^{+/-}$ genotype by polymerase chain reaction (PCR).

Primers for genotyping were as follows: wild-type Forward primer 5′-CTAGGCCACCGAATTGAAAGATCT-3′; wild-type Reverse primer 5′-GTAGGTGGAAATTCTAGCATCATCC-3′; transgene Forward primer 5′-GGTCACGTGGTCAGAAGAGG-3′; transgene Reverse primer 5′-CTCATCACTCGTTGCATCGA-3′ (all primers synthesised by MWG Biotech, Ebersberg, Germany). PCR cycle conditions were 94°C 3 minutes, 94°C 30 seconds, 60°C 45 seconds, 72°C 45 seconds (repeat cycle 35 cycles), 72°C 2 minutes using Thermo Taq DNA Polymerase (Thermo Scientific Inc., Waltham, MA, USA).

2.1.3 ROSA26 Cre Reporter Line

Hoxb7$^{+/-}$ mice were crossed with a ROSA26 Cre reporter strain (breeding female generously donated by the Vascular Biology Group, University of Edinburgh). The ROSA26 mouse colony was maintained as a homozygous line. Genotyping for ROSA26 allele was carried out by PCR as follows: transgene Forward primer 5′-GCGAAGAGTTTGTCCTCAACC-3′; wild-type Forward primer 5′-GGAGCGGGAGAAATGGATATG-3′; common Reverse primer 5′-AAAGTCGCTCTGAGTTGTTAT-3′. PCR Cycle conditions were 94°C 90 seconds, 94°C 20 seconds, 67°C 45 seconds, 72°C 1 minute (repeat cycle 39 cycles), 72°C 10 minutes using Thermo Taq DNA Polymerase.

2.2 Metabolic Cage Studies

2.2.1 Metabolic Cage Experiment

Cohorts of *Hsd11b2*$^{+/+}$ and *Hsd11b2*$^{+/-}$ mice were housed in metabolic cages (Tecniplast, Italy) and allowed free access to water and powdered rodent

chow (rat and mouse maintenance (RM1) diet (0.25% sodium and 0.67% potassium content), Special Diet Services Ltd., Essex, UK). After an acclimatisation period (at least five days (Gomez-Sanchez and Gomez-Sanchez, 1991; Hoppe et al., 2009)), experimental collections of faeces and urine were made. Food and water intake and body weight was also recorded daily. Following three days of control measurements, the animals were moved onto a high sodium diet (2.5% sodium and 0.5% potassium content, Special Diet Services Ltd.) and daily collections and recordings continued for three weeks. All urine and faeces collections were stored at -20°C, with additional aliquots for certain assays stored to specification (detailed in assay methods to follow). At the end of the study, animals were sacrificed by cervical dislocation, and kidneys removed and stored at -80°C, unless otherwise stated.

2.2.2 Metabolic Cage Sample Analysis

2.2.2.1 Urine and Faecal Electrolytes

Urine samples collected during the metabolic cage studies described above were analysed for sodium and potassium concentrations. Measurements were made using a flame photometer (BWB-1 Performance Plus Model, BWB Technologies UK Ltd, Essex, UK) at a 1 in 100 dilution (diluted 1 in 1000 from diluent concentrate blanking solution, 1% w/v Brij 35, BWB Technologies). Results (in parts per million (ppm)) were then converted to molar values and multiplied by urinary flow rate to give the excretion in μmol per 24 hours. These values were then normalised for body weight in grams.

Following extraction in nitric acid (as detailed in (Thiesson et al., 2007)) faecal sodium content was also measured by flame photometry.

2.2.2.2 Sodium and Water Balance

Values for individual daily sodium balance were calculated by subtracting the urinary sodium values (as calculated above) from the amount of dietary sodium consumed; final balance values presented as μmol corrected for body weight in grams.

Water balance was calculated by subtracting the volume of urine produced in mls added to faecal water content (calculated by weighing faeces before and after drying out at 100°C for 24 hours) from the volume of drinking water consumed per day. Final value given as μl per gram body weight.

2.2.2.3 Urinary Steroid Extractions

Aldosterone, corticosterone and deoxycorticosterone (DOC) were extracted from urine and measured by ELISA analysis as described (Al-Dujaili et al., 2009a; Al-Dujaili et al., 2009b). Samples from standard sodium diet days were reconstituted in a volume equal to the samples initial volume. In the instance of the high sodium diet urine samples, the urine volume is very large, thus diluting the steroids. To ensure concentrations were on the standard curve, samples were reconstituted in a lower volume of assay buffer so as to make them 4 times more concentrated. All dilution factors were accounted for in subsequent calculations.

2.2.2.4 Urinary Isoprostane Assay

Urine sample aliquots for isoprostane measurement were collected in 0.005% butylated hydroxyl-toluene (BHT) and stored at -80°C as detailed in (Yoshida et al., 2009). The assay was carried out using defrosted samples according to manufactures protocol (8-Isoprostane EIA Kit, Cayman Chemicals, Michigan, USA).

2.3 BP Measurements in Conscious Animals

Systolic BP (SBP) was recorded in conscious and restrained mice using tail plethysmography (tail cuff). Mice were warmed in a heat box at 30°C for 5 - 10 minutes in order to optimise the signal from the tail vein. The tail cuff measures changes in blood flow in the mouse's tail via an optical transducer inside the cuff. As the cuff inflates, the optical transducer measures the pressure at which the blood vessel is occluded and blood flow stopped i.e. the SBP in mmHg. The data measured were amplified, and viewed on a PC via a serial link, from where the data was recorded. A total of eight recordings were made for each measurement – four on the cuff inflation, and four on the cuff deflation. A record was made of the four deflation values, and the mean of these calculated as the SBP. The inflate values were rejected as they were usually inaccurate due to the mouse reacting with movement at the cuff tightening around its tail.

Animals were trained to have their SBP recorded using the tail cuff technique over a number of weeks until the recordings became stable. A study analysing how significant the effects of training can be towards obtaining stable SBP results using the tail cuff technique demonstrates the need for this training (Figure 2.1). This involved firstly training the animals to enter the restraint tube repeatedly until this could be achieved with minimum stress. They were then left inside the restraint tube for increasing lengths of time, before finally attaching the measuring cuff to their tail. Repeated measurements were then made over a number sessions until the BP recordings reached a stable level (Lorenz, 2002; Meneton et al., 2000).

Once stable recordings for SBP were achieved, the trained mice were placed on a high sodium diet for 3 weeks. During the diet regime, additional SBP measurements were made after weeks 1 and 2 under exactly the same

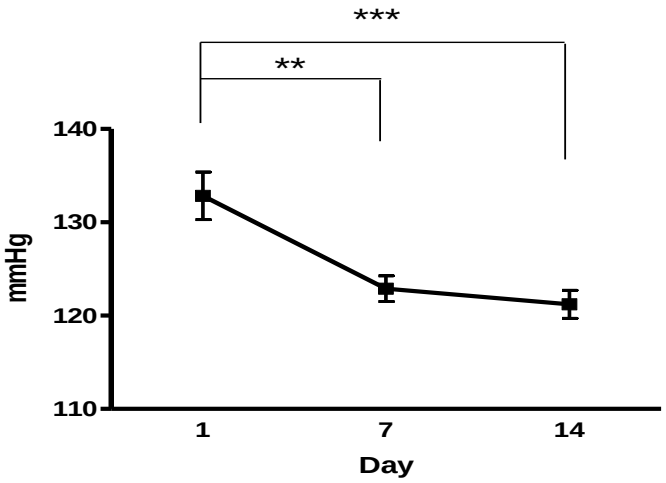

Figure 2.1. Systolic blood pressure measurements by tail plethysmography over a two week training period in wild type mice (n = 6). ** P < 0.01; *** P < 0.001. Data are means ± SEM.

experimental conditions. All experimental measurements were made under randomised blinded conditions.

2.4 Renal Clearance Experiments

Renal clearance methods were adapted from (Lorenz, 2002).

2.4.1 Surgical Protocol

Animals were anesthetised with an intraperitoneal (I.P.) injection of Inactin (100mg/Kg, IP; Thiobutabarbital Sodium; Sigma). The jugular vein and carotid artery were cannulated using PE10 tubing (Jencons). The cannulae were then connected to a 1ml syringe containing 0.9% saline and 0.9% saline plus heparin at 20 units per ml, respectively. A tracheotomy was performed

to maintain a clear airway. The bladder was cannulated using a 1cm length of PE50 tubing (Jencons) into which a length of PE10 tubing was inserted to minimise dead space during urine collections. Surgical suture used in surgery was Deknatel silk 5.0 (Teleflex Medical, NC, USA). The vein cannulae was subsequently linked to an infusion pump (AL2000 model, World Precision Instruments, Sarasota, FL, USA) permitting continuous infusion of a saline infusion solution containing 120mM NaCl, 10mM $NaHCO_3$, 5mM KCl, 15mM LiCl, 0.5% Inulin-FITC (Fluorescein Isothiocyanate; Sigma) plus 2% p-Aminohippuric Acid (PAH; Sigma) at a rate of 0.2µl/min/g body weight. The carotid artery cannula was connected to a MLT0699 disposable BP transducer (ADInstruments Ltd, Chalgrove Oxfordshire, UK) attached to a ML224 Quad Bridge Amp (ADInstruments Ltd) to allow for the conversion of the BP signal to be measured using a PowerLab 4/30 data acquisition system (Powerlab, ADInstruments Ltd). This setup allowed for continuous mean arterial BP (MABP) recording (2 Hertz sampling rate). The BP transducer was regularly subjected to a 2-point calibration curve (once a week during experimental cohorts) by attaching it to a sphygmomanometer and checking that pressure exerted to 50 and 100 mmHg gave an accurate signal on the PowerLab software. Any discrepancies were rectified by changing the unit conversion for BP within the software to match what the sphygmomanometer read. See Figure 2.2 for a photograph of a completed surgery.

Post-surgery there was a 40 minute equilibration period after which a small sample of arterial blood (approximately 20µl) was collected into a heparinised capillary tube (Hawksley, Lancing, Sussex, UK) and centrifuged for 3 minutes in a Haematospin 1400 centrifuge (Hawksley). The hematocrit value was obtained and plasma was stored at -20°C for subsequent analysis.

Photograph of Renal Clearance Surgery

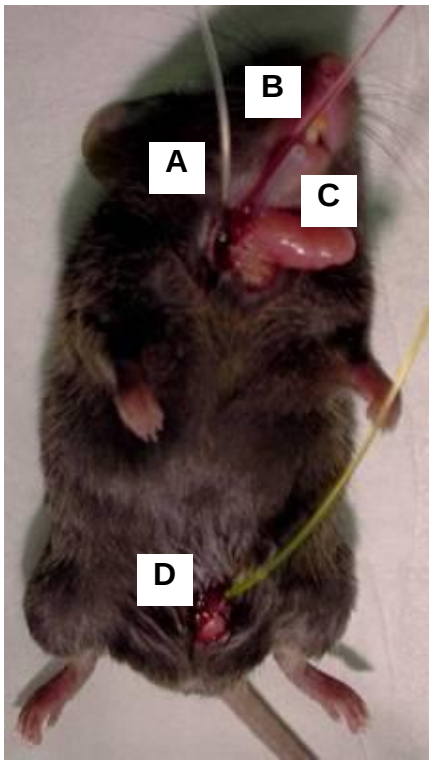

Figure 2.2. A mouse undergoing renal clearance protocol after surgery. **A**, Jugular vein cannulae; **B**, Carotid artery Cannulae; **C**, tracheotomy; **D**, bladder cannulae.

For the next 40 minute period, urine was collected into a pre-weighed tube containing water-saturated mineral oil to prevent sample evaporation. After the 40 minute period, a second arterial blood sample was taken. Next, a bolus injection of amiloride (Sigma) was given intravenously (I.V.) at a dose of 0.1mg/g body weight. After 10 minutes, a second urine collection is made. After the third arterial blood sample is taken, Evans blue dye (0.5% in 0.9% saline; Sigma) was injected intravenously (I.V.) at a dose of 1µl/g body weight and allowed to circulate systemically for approximately 10 minutes. After this period, a terminal blood collection was made from the artery cannulae into heparinised tubes (Sarstedt AG and Co., Nümbrecht, Germany) and centrifuged for 5 minutes at 10 000 rpm to separate plasma.

The animal was then sacrificed by I.V. anaesthetic overdose, and the kidneys were removed and weighed.

2.4.2 Sample Analysis

2.4.2.1 Glomerular Filtration Rate Measurements

Glomerular filtration rate (GFR) was calculated as the clearance of FITC-labelled inulin, as detailed in (Lorenz, 2002). FITC fluorescence was measured in plasma and urine samples using a Wallac multilabel counter (model 1420; Perkin Elmer, Waltham, Massachusetts, USA). Urine samples were diluted 1:10000 and plasma 1:100 in HEPES buffer (pH 7.4) in a black 96 well plate (Mircofluor Solid Microplate, Nunc, Thermo Scientific). HEPES buffer was used in order to normalise the pH of the samples, as the fluorescence reaction is pH dependent. Samples were excited at 485 nm wavelength, and results read at 538 nm.

GFR was then calculated in mls per minute using the formula $C_{IN} = (U_{IN} \times V)/ P_{IN}$; where C_{IN} = clearance of inulin, U_{IN} = urinary inulin concentration, V = urine flow rate, and P_{IN} = plasma inulin concentration.

2.4.2.2 Renal Plasma Flow

Effective renal plasma flow (RPF) was calculated using the standard equation, as with inulin clearance, as outlined in (Agarwal, 2002). Briefly, urine and plasma samples were diluted in 3.2% trichloro acetic acid (TCA). They were then mixed with a solution of 2 parts 0.2% HCL and 1 part 0.1% $NaNO_2$. 0.5% $NH_2SO_3NH_4$ was then added and incubated for 3 minutes at room temperature. Next, 0.1% N-(1-napthyl)-ethylenediamine dihydrochloride was added, and the samples were incubated at room temperature for 45 minutes. All samples were then transferred in duplicate

to a 96 well plate (IWAKI), and PAH concentrations were measured colourimetrically on a spectrophotometer at excitation wave length 450 nm (Wallac multilabel counter). Renal blood flow (RBF) was then calculated in mls per minutes using the following equation: RBF = RPF/1-hematocrit value. Filtration fraction (FF) was calculated as GFR / RPF, and renal vascular resistance (RVR) was calculated as MABP / RBF.

2.4.2.3 Plasma and Urine Measurements

Plasma and urine sodium and potassium levels were measured using an ISE electrolyte analyzer (Electrolyte analyzer 9180, Roche, UK). Plasma and urine osmolarities were measured using an osmometer (OMS01 model, Vogel, Giessen, Germany).

Fractional excretion of electrolytes was calculated using the equation $FE_{Na} = E_{Na} / ((P_{Na} \times GFR) \times 100)$; where FE_{Na} = fractional sodium excretion, E_{Na} = urinary sodium excretion and P_{Na} = Plasma sodium concentration.

2.5 Chronic Inhibitor Studies

To identify processes contributing towards the salt-sensitive phenotypes, *Hsd11b2*$^{+/+}$ and *Hsd11b2*$^{+/-}$ mice received one of three treatments alongside the high sodium diet. In each set of experiments, mice were housed in metabolic cages (see section 2.2) for collections, as described. After one to two weeks of experimental collections, the mice were moved to normal cages, and the experiment continued so that in all cases the mice were fed the high sodium diet for a total of three weeks. Mice were then anaesthetised and prepared for renal clearance experiments as described previously (section 2.4).

2.5.1 Benzamil

To assess the role of the epithelial sodium channel (ENaC) in the observed phenotypes, the ENaC-specific inhibitor benzamil (Sigma) was administered via an osmotic minipump (model 2004, Alzet, Cupertino, CA, USA). Benzamil was dissolved in a propanediol solution (Sigma) at a concentration of 3.35mg/ml to deliver the dose at a rate of 0.7μg/g body weight/day (administration protocol modified from (Sepehrdad et al., 2004)) for up to 4 weeks. Minipumps were primed in a 0.9% saline solution at 37°C for 40 hours, and then implanted subcutaneously under Isoflurane gas anaesthesia and I.V. buprenorphine as an analgesic (Vetergesic, Pfizer, at 0.01ml/g body weight). Minipumps were subcutaneously implanted between the shoulder blades, and surgical wounds were closed with auto-wound clips (Clay Adams, BD, NJ, USA). The animals were placed into a heated recovery box until consciousness regained, when they were then placed back into their individual metabolic cages. The mice were allowed three days to recover from surgery before experimental measurements commenced.

2.5.2 Spironolactone

To assess the role of the mineralocorticoid receptor (MR) in the observed phenotypes, the MR inhibitor spironolactone (Sigma) was administered via an osmotic mini-pump, as with benzamil. Spironolactone was dissolved in a 50:50 dimethyl sulfoxide (DMSO) and propylene glycol solution (both Sigma) so as to deliver 20 mg/kg per day to the animals, as detailed in (MacDonald et al., 2000). Minipumps were primed and implanted subcutaneously, as with benzamil.

2.5.2.1 Mass Spectrometry Measurement of Canrenone

Analysis was carried out to ensure that the delivery of spironolactone by the minipumps was at sufficient levels to elicit a physiological effect. This is done by measuring the levels of the spironolactone active metabolite, canrenone, in terminal plasma samples of mice from this study. Briefly, 100µl of plasma was diluted with 90µl of HPLC grade water and 10µl of an internal standard (100ng Alfaxalone (Steraloids Inc., Newport, RI, USA). A 10 times volume of ethyl acetate was then added and samples were vortexed to mix. Samples were then centrifuged at 3000 x g for 5 minutes; the resulting top layer was transferred to a 5 ml glass vial and dried down under oxygen-free nitrogen at 60°C. The plasma sample was then re-extracted by repeating from the ethyl acetate step. Once dried down, samples were reconstituted in 100µl of mass spectrometry (MS) mobile phase solution (50:50 5 mM ammonium acetate:MeOH) and transferred to 1.5 ml glass autosampler vials with 200µl glass inserts (both from Agilent Technologies UK). Samples were then analysed by liquid chromatography (LC)-MS/MS (model Thermo TSQ Quantum Discovery Instrument, Thermo Scientific) by the Edinburgh University Wellcome Trust Clinical Research Facility MS Core (senior technician Mr. Scott Denham).

2.5.3 TEMPOL

To assess the role of the oxidative stress in the observed phenotypes, the antioxidant 4-Hydroxy-2,2,6,6-tetramethylpiperidine-N-oxyl (TEMPOL; Sigma) was diluted in drinking water at a concentration of 2mmol/litre (administration dose obtained from personal communication with Professor Christopher Wilcox). The TEMPOL drinking solution is light-sensitive, and so was protected by wrapping the drinking bottle in silver foil, and fresh

solution was made every day. The experiment then continued as above, without the need for the surgery recovery period.

2.6 Renal 11β-HSD2 Enzyme Activity

11β-HSD2 enzyme activity was measured in homogenised kidney extracts by calculating the conversion rate of titrated (^{3}H) labelled corticosterone to dehydrocorticosterone.

2.6.1 Kidney Homogenate Preparation

Kidneys were dissected from *Hsd11b2*$^{+/+}$ and *Hsd11b2*$^{+/-}$ mice and stored at -80°C until required. They were then individually homogenised in 1ml per 100mg tissue of Krebs Buffer (118mM NaCl, 3.8mM KCl, 1.19mM KH_2PO_4, 2.5mM $CaCl_3$, 1.19mM $MgSO_4$ and 25mM $NaHCO_3$, 0.2% glucose, pH 7.4) using a small metallic bead at the rate of 2 times 30 seconds at 30 times per second (Mixer Mill 301 model, Retsch, Haan, Germany), taking care to keep the kidney homogenate cold at all times. The homogenate was then centrifuged at 2000 rpm for 5 minutes at 4°C. The top layer was transferred into a clean tube and the remainder discarded. Total protein concentration of the kidney homogenates was measured using a Bradford-base protein assay (Bio-Rad Protein Assay, Bio-Rad Laboratories, Hercules, California, USA). These values were then used to calculate the protein concentration required for the enzyme activity assay.

2.6.2 11β-HSD2 Enzyme Activity Assay

The homogenised kidneys were then used immediately as the source of 11β-

HSD2 for an enzyme activity assay (concentration of 0.1 mg/ml). NAD^+ (Sigma) was used at a final assay concentration of 100μM as the assay co-factor (required for 11β-HSD2 enzyme activity). The substrate ^{3}H-corticosterone (1,2,6,7-^{3}H-corticosterone, GE Healthcare Life Sciences, Anachem, Bucks, UK) was used at a 100nM final assay concentration. The activity assay mix consisted of 180μl homogenated kidney, 50μl cofactor and 20μl substrate mix to give a final assay volume of 250μl. Controls for the assay included reactions with no protein added and with no co-factor added, as well as including an *Hsd11b2*$^{-/-}$ kidney homogenate. The assay minus the enzyme (i.e. the kidney homogenate) was pre-warmed to 37^{0}C in a water bath for 15 minutes, with tubes covered with parafilm to prevent evaporation (Laboratory film, Pechiney Plastic Packaging, Chicago, IL, UK) to prevent evaporation. Upon addition of kidney homogenate to the assay, the reaction was allowed to proceed for 3 minutes before being stopped by the addition of 10 volumes of HPLC grade ethyl acetate, removed from the water bath and vortexed hard to mix. The assay tubes were then left to settle and separate, and the top aqueous phase was transferred into clean tubes; the remaining organic phase was discarded. Samples were dried down under Oxygen-free Nitrogen at 37°C until all liquid had evaporated, and a dry precipitate remained at the bottom of the tubes.

2.6.3 Thin Layer Chromatography Assay

The dried down enzyme assay samples were re-constituted 30μl of absolute ethanol and vortexed to mix. Thin Layer Chromatography (TLC) plates (Alugram Silicon G/UV$_{254}$ TLC plates, Macherey-Nagel, GmbH and Co., Straubenhardt, Germany) were prepared by drawing a pencil line 2cm from the bottom of the plate and lightly marking along the line evenly spaced

positions where the samples were to be spotted. 3µl of each sample was spotted at a time, allowing sample spots to dry completely before re-spotting; this was continued until the entire sample had been applied to the plate. Once the samples had all dried completely, the TLC plates were run in a glass tank covered with glass lid for approximately 1 hour (until the solvent has run about 2cm from the top of the plate) in a solvent mix (92mls chloroform + 8mls 95% ethanol). Once finished, the TLC plates were allowed to air dry, and then placed in a light-proof cassette (BAS cassette 2040, Fuji Photofilm Co. Ltd., Japan) for exposure against a tritium-sensitive screen (Fuji Imaging plate, BAS-TR2040, Fuji) for 72 hours. The tritium screen was then processed using a Fujifilm FLA-2000 plate reader (Fuji) and the AIDA Imageanalyzer 344.exe program to analyse densitometry (Raytest, GmbH and Co.)

2.7 Renin-Angiotensin-System Measurements

2.7.1 Angiotensin Dose Response Experiments

2.7.1.1 Surgery

Cohorts of *Hsd11b2*$^{+/+}$ and *Hsd11b2*$^{+/-}$ mice were fed either standard or a high sodium diet (as described previously) in normal cages with free access to drinking water for a period of 3 weeks. The animals then underwent surgery to cannulate the carotid artery and the jugular vein under Inactin anaesthesia, as described in part 2.5.1. No Bladder cannulation was required for this procedure.

2.7.1.2 Dose Response Administration

MABP was monitored as before for renal clearance surgery. Bolus

administrations of either Angiotensin I or Angiotensin II (Sigma) were I.V. injected into the jugular vein at increasing concentrations (Liu et al., 2009). Concentrations injected were 0.625, 1.25, 2.5, 5 and 10ng, for both drugs. Responses to the injections measured as delta MABP. MABP was allowed to return to baseline measurements and the jugular vein catheter flushed with 0.9% saline before the next bolus dose was administered to minimise carry over effects.

2.7.2 Measurements of RAAS Components

2.7.2.1 Sodium Diet Trunk Blood Culls

Cohorts of *Hsd11b2* $^{+/+}$ and *Hsd11b2*$^{+/-}$ mice were fed a standard or high sodium diet (as before) in normal cages with free access to drinking water for a period of 3 weeks. The animals were culled by decapitation. Trunk blood was collected in a 0.5M EDTA in heparinised tubes and centrifuged for 5 minutes at 10 000 rpm to separate plasma and stored immediately on ice. Half of the plasma collected (approximately 200µl) was added to 0.1 volume of inhibitor cocktail (4mM PMSF (Phenylmethylsulfonyl Fluoride monohydrate), 2.5µg/µl o-phenanthroline, 0.16mg/ml captopril, 40µg/ml pepstatin, and 4% β-mercaptoethanol, all reagents from Sigma (Kantachuvesiri et al., 2001)), and both stored at -80°C until required. Kidneys and adrenals were removed from sacrificed animals, and also stored at -80°C.

2.7.2.2 Angiotensinogen and Renin Concentration

Plasma angiotensinogen and renin concentrations were measured via the generation of angiotensin I, as detected by radioimmunoassay (RIA). For the angiotensinogen concentrations, plasma was incubated in an excess of renin in order to generate maximal angiotensin I levels from existing angiotensinogen. For the renin concentrations, this was reversed and the plasma was incubated with an excess of the renin substrate angiotensinogen. Plasma was diluted appropriately with Tris assay buffer (Tris 50 mM, pH 7.4; 0.175% neomycin sulphate (Sigma), 0.0875% BSA) in quadruplet, and incubated with either excess angiotensinogen (previously purified from the plasma of a binephrectomised rat; donated by Dr Chris Kenyon) or excess renin (previously purified from mouse submaxillary glands; donated by Dr Chris Kenyon) in RIA cups (Sarstedt). This mixture (constantly kept on wet ice) was incubated with an in-house available angiotensin I antibody (donated by Dr Chris Kenyon); one set of duplicates was incubated at 4°C and the other set at 37°C, both for 30 minutes. Iodine-125 (^{125}I)-labelled angiotensin I (Amersham) was then added, and the assay was incubated for a further 18 hours at 4°C. The bound and unbound ^{125}I angiotensin I was then separated by adding a charcoal suspension to the assay (0.01% 5M HCl, 0.2% neomycin sulphate, 0.185% EDTA, 0.5% BSA, 0.3 % Dextran T70 (Sigma), 6% Norit activated charcoal (Sigma)) and centrifuging at 3000 rpm for 15 minutes. Supernatant was removed, and the remaining charcoal pellet was counted for emissions on a Wizard 1470 gamma-counter (Wallac).

2.7.2.3 Angiotensinogen and Renin Enzyme Activity

Plasma angiotensinogen and renin enzyme activity was measured as the total angiotensin I generated from endogenous renin and endogenous angiotensinogen. Undiluted plasma was assayed with a small amount of

either angiotensinogen or renin in order to determine the enzyme activity of endogenous renin and angiotensinogen, respectively. The assay then continued as before for the concentration assays (section 2.7.2.2).

2.7.2.4 Plasma Aldosterone Assay

Plasma samples taken from carotid artery during surgery experiments described in section 2.4.1 were analysed for aldosterone concentration. Aldosterone concentrations were measured in 100µl of plasma by radioimmunoassay, according to manufactures protocol (Coat-A-Count, DPC, Los Angeles, California, USA).

2.8 Stress Testing

2.8.1 Restraint Stress Test

Cohorts of *Hsd11b2*$^{+/+}$ and *Hsd11b2*$^{+/-}$ mice (nine per genotype) were single-housed in normal cages with free access to standard chow and water for one week. These mice were then transferred one at a time to a procedure room for blood collection by tail nick technique in order to measure baseline corticosteroid plasma levels. The samples were taken between 7 - 8am, as this is when the circadian rhythm of mice determines that their corticosterone levels will be at their lowest. Blood collections were made directly into a heparinised tube (Sarstedt) within one minute of disturbing each individual mouse's cage in order to obtain corticosterone levels as close to baseline levels as possible. After a baseline blood sample was collected, the mice were transferred to a restraint tube where they were held for 15 minutes. After 15 minutes, another blood sample was taken using the same tail nick wound in order to measure stress levels of plasma corticosterone.

The mice were then returned to their individual cages and allowed to recover for 90 minutes, after which a further blood sample was taken, as described before. The mice were then moved on to a high sodium diet for three weeks, after which the stress test experiments were repeated exactly as before. See Figure 2.3 for an overview of the HPA testing design. All blood samples were stored immediately on wet ice, centrifuged at 13 000 rpm for 10 minutes, plasma removed and stored on dry ice temporally; -80°C for long-term storage.

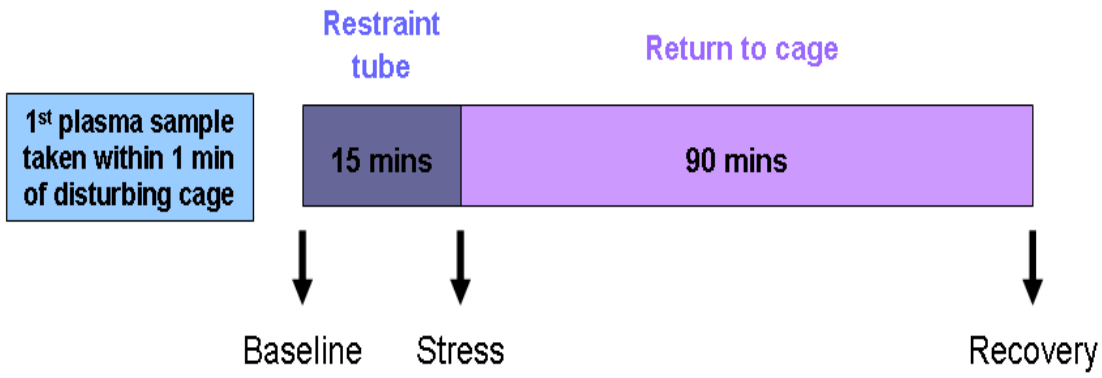

Figure 2.3. Baseline plasma measurements were obtained using the tail nick technique within 1 minute of disturbing individual cages from *Hsd11b2*$^{+/+}$ and *Hsd11b2*$^{+/-}$ mice on a standard sodium diet. Mice were then placed in individual restraint tubes for 15 minutes, after which a second plasma sample was taken; the stress sample. Mice were then returned to their individual cages and allowed to recover for 90 minutes after which the third and final plasma sample was obtained; the recovery sample. The same mice were then placed on a high sodium diet for three weeks and the experiment was repeated. Black arrows represent when plasma samples were taken during the experiment.

2.8.2 Plasma Corticosterone Assay

Plasma samples obtained from the stress test experiments were analysed by RIA for corticosterone concentration. Briefly, plasma samples were diluted 1 in 10 in borate buffer (0.133 M boric acid, 67.5 mM NaOH, 0.5% BSA, 1% methanol, 0.1% ethylene glycol, pH7.4 with HCl). Diluted plasmas were then incubated at 80°C for 30 minutes. Aliquots of the diluted plasma were mixed in duplicate in a 96 well plate (BD Falcon, 96 well flexible plate) with 1:4000 dilution of sheep antibody to corticosterone (Micropharm Ltd., Newcastle Emlyn, Carmarthenshire, UK), 1.5 M ^{3}H-labelled corticosterone, and anti sheep scintillation proximity assay (SPA) reagent (1:4 dilution; GE Healthcare). This mixture was incubated overnight at room temperature, and then sample wells were counted in a liquid scintillation counter (1450 Microbeta Plus model, Wallac).

2.9 Generating a Floxed *Hsd11b2* Mouse

2.9.1 Construct Design

The *Hsd11b2* floxed construct was designed and built using a clone derived from the HSD2 B6 BAC RP23-410B24. The clone pS141 was used in a previous gene targeting experiment (Kotelevtsev et al., 1999), and was available within the laboratory. pS141 spans 15Kb of the mouse strain 129Sv *Hsd11b2* gene, which incorporates all 5 exons of the gene, and exons 4-8 of the neighbouring downstream ATP6V0D1 gene. The polyA sites for both genes were included. The clone had been previously ligated into the pBluescript II SK phagemid vector (Stratagene, La Jolla, California, USA). 20 Kb of the RP23-410B24 BAC was analysed by a web tool

(http://tools.neb.com/NEB_cutter2) to generate a map of restriction enzyme sites. This was used to generate a step-by-step plan for building the *Hsd11b2* floxed construct.

The pL451 plasmid was used to provide the upstream *lox*P element and a neomycin selection cassette, flanked by two FRT sites, that were used in the final construct. pL451 had been previously obtained by the laboratory with permission to use from Professor Neal Copeland, National Cancer Institute, Frederick, Maryland, USA (Liu et al., 2003).

2.9.2 Construct Building

For a schematic representation of the construction of the *Hsd11b2* floxed targeting construct, see Chapter 6 Part 1, Figure 1a and b. A BamHI digest separated the pS141 clone into the main sub-clones for building the construct (all restriction enzymes supplied by New England BioLabs, Ipswich, Massachusetts, USA; or Roche Diagnostics GmbH, Manheim, Germany; or Promega, Madison, Wisconsin, USA). The digested pS141 DNA was separated by gel electrophoresis on an agarose gel (SeaKem LE agarose, Lonza Group Ltd, Basel, Switzerland). The DNA fragments were then excised from the gel, purified using GeneClean Turbo kit (QBiogene, Cambridge, UK)) and sub-cloned into the pBluescript II vector. These sub-clones were manipulated to become the upstream recombination arm (URA), the floxed region of the *Hsd11b2* gene (exons 2-5), and the downstream recombination arm (DRA), as well as separating both the 5 prime (5′) and 3 (3′) prime external probes (EP) (used for homologous recombination screening).

2.9.2.1 Recombination Arm Generation

The URA was engineered to incorporate the upstream *lox*P element with the neomycin cassette flanked by two FRT sites isolated from the pL451 plasmid (Figure 2.4) by ligation. A HindIII restriction site from within the cloning site

pL451 Plasmid

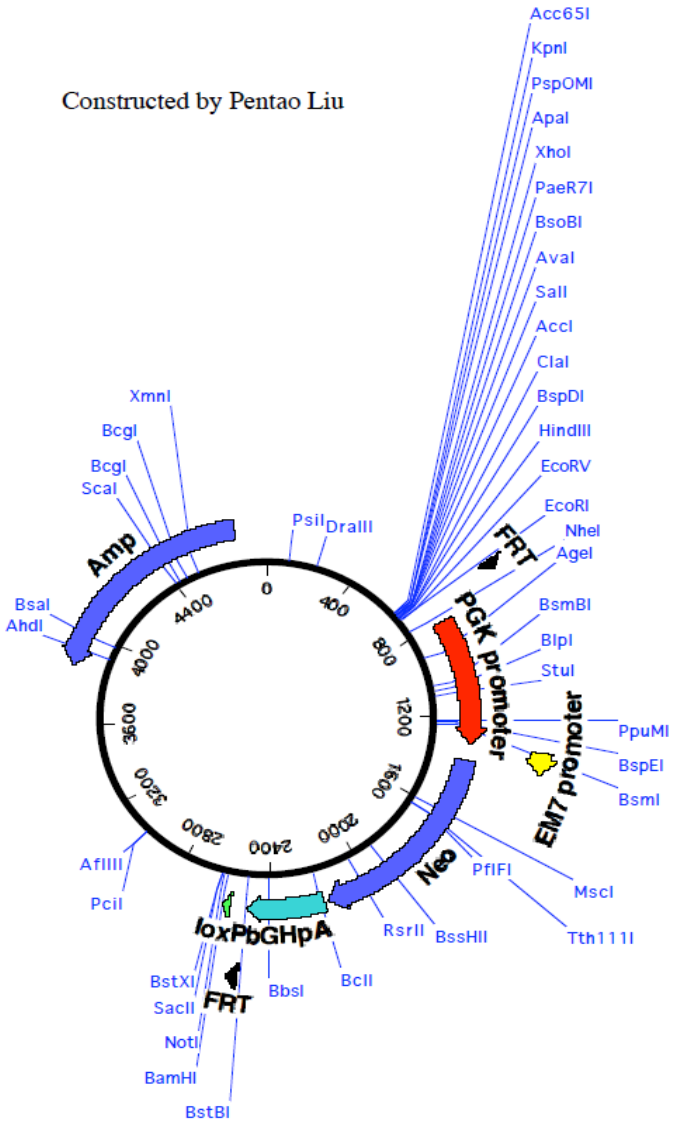

Figure 2.4. pL451 Plasmid Map (Courtesy of Dr. Pentao Liu).

of pL451 was deliberately included in the ligated fragment so as to introduce a novel site for subsequent homologous recombination screening requirements. The DRA required no further manipulation.

2.9.2.2 Region to Flox Generation

The sub-clone containing the region to be floxed (*Hsd11b2* exons 2-5) had the 34-base pair downstream *lox*P site plus a novel BamHI restriction site incorporated for subsequent homologous recombination screening. These elements were introduced to the sub-clone using the Linker Tailing method (Lathe et al., 1984). Briefly, oligonucleotides were designed (Forward 5'-GATCCATAACTTCGTATAATGTATGCTATACGAAGTTATAAGGATCCC -3'; Reverse 5'-GATCGGGATCCTTATAACTTCGTATAGCTACATTATA CGAAGT TATG-3'; synthesised by Invitrogen, Paisley, UK) and introduced into an open BglII restriction site (oligonucleotides were designed to subsequently destroy the opened BglII site). 5µg of each oligonucleotide was mixed, heated to 65°C for 20 minutes, and slowly cooled down to 4°C. 0.5µg of the oligonucleotide mix was then combined with 0.1µg BglII linearised plasmid, 5 x ligation salts (150mM NaCl, 150mM Tris, pH7.5, 38mM $MgCl_2$), 10 x ligation mixture (2.5mM ATP, 20mM DTT, 2mM Na_2EDTA, pH8.0, 10mM spermidine, 1mg/ml bovine serum albumin (BSA; BDH Lab Supplies, VWR, Lutterworth, Leicestershire, UK), 2µl T4 DNA ligase (Invitrogen) and PCR-grade water (Invitrogen) to a final volume of 20µl. After overnight incubation at 4°C, 360µl 1xTE buffer (10mM Tris, 1mM Na_2EDTA), 40µl DMSO (Sigma-Aldrich Co., St Louis, Missouri, USA) and 10µl spermine.HCl (100mM), pH 8.0, were added to the mixture and vortexed briefly to mix. DNA was precipitated using 300mM NaOAc, pH 5.0, 100mM $MgCl_2$ and 75% ethanol, washed twice in ethanol:TE 3:1, and the resulting DNA pellet re-suspended in 50µl hybridisation buffer (100mM NaCl, 10mM Tris, pH 7.5,

5mM EDTA). DNA was subsequently transformed into chemically competent NEB Turbo cells (New England Biolabs) for plasmid propagation.

2.9.2.3 Completing Final Construct

The completed URA, exons 2-5, and DRA were ligated together to complete the *Hsd11b2* floxed construct. 25µg of completed construct was linearised using restriction enzyme SmaI, and purified by phenol/chloroform extraction as follows. Briefly, 1 volume of phenol (pH 7.9) was added, and mixed by constant gentle rotation for 20 minutes. This was then centrifuged for 5 minutes at 13 000 rpm and the top aqueous layer removed into a fresh tube. Next, half the total reaction volume of phenol was added, along with half chloroform:amlyalcohol 24:1, to the aqueous solution. This was mixed for 5 minutes, and then centrifuged as before for 2 minutes. Again the top layer was removed, and 1 volume of chloroform:amlyalcohol 24:1 was added. This was mixed for 5 minutes and centrifuged for 2 minutes, as before. The top layer was removed, and 1 volume of isopropanol added and mixed until homogeneous. This mix was then centrifuged for 2 minutes, and the supernatant from the resulting DNA pellet removed. The DNA pellet was washed in 180µl 70% ethanol. This was centrifuged for 2 minutes, supernatant removed, and the DNA pellet allowed to air dry. The final DNA pellet was then re-suspended in 20µl phosphate buffered saline (PBS; Sigma).

2.9.3 Introducing Completed Construct into Embryonic Stem Cells

Cell culture media (50ml foetal calf serum (FCS) (Sigma), 200mM glutamine (GIBCO, Invitrogen), 100mM sodium pyruvate (GIBCO), 5ml non-essential amino acids (GIBCO), 0.5ml 1000x β-mercaptoethanol (Sigma), 0.5ml LIF (GIBCO) and 450ml 1xBHK21 Glasgows media (GIBCO)) was removed from

three T75 flasks (IWAKI, Barloworld Scientific, Stone, Staffordshire, UK) of 80% confluent embryonic stem (ES) cells. The specific ES cells used had been previously derived from a 129 mouse line (agouti coat colour; E14TG2a cell line (129/OlaHsd)) (Hooper et al., 1987). Cells were then washed with 1 x PBS (Lonzo, Cambrex, Charles City, Iowa, USA), and 3ml of TVN (trypsin, chick serum, ETDA Na salt 1.85g/l, PBS) was added to each flask and incubated at 37°C for 5 minutes. 7ml of fresh media was then added to each flask, and the contents of all three flasks were pooled together and centrifuged at 1000xg for 3 minutes. The resulting cell pellet was re-suspended in 780µl PBS. 20µl of prepared linearised floxed *Hsd11b2* construct DNA (as described above) was mixed with the ES cell re-suspension, and the mixture transferred to a 2mm electroporation cuvette (Equibio Ltd, Ashford, UK). The mixture was then electroporated using an Easyject Plus instrument (Equibio) at 240 Volts, 450 µFaraday, and incubated at room temperature for 10 minutes in order introduce the targeting construct into the ES cell DNA. Next, 10ml fresh media was added and seeded between 10 10cm plates (IWAKI) with 19ml of fresh media (i.e. add 1ml of mixture to each), and incubated at 37°C overnight. All flasks and plates were previously coated with gelatine (GIBCO).

2.9.4 Neomycin Selection of Targeted Embryonic Stem Cells

Electroporated ES cells were grown in standard ES cell media, as described above, supplemented with 200µg/ml of the antibiotic G418 (Calbiochem, EMD Chemicals Inc., San Diego, USA) for neomycin selection of cells positive for targeting construct DNA incorporation. Cells were fed with fresh media plus G418 as required. Over a number of days, many of the

plated cells died off, but resistant ES cells survived to form clusters attached to the gelatine matrix of the plates.

After approximately 2 weeks, surviving clones were picked and transferred to individual wells in a 96-well plate (IWAKI). Briefly, cell culture media was changed one hour before picking commenced. This media was then removed and replaced with PBS. Clones were picked using a P10 pipette tip and moved along with 3ml PBS to a well of a 96 well plate containing 5µl TVN, and incubated at 37°C for 5 minutes. Then 150µl of media plus G418 was added and transferred to another well within a 96 well plate that had been pre-coated with gelatine. When the selected cells became confluent, they were moved to 24-well plates (IWAKI), and when confluent again, they were subsequently divided for DNA harvesting and freezing down stocks.

Briefly, fresh media was applied to cell cultures, removed 1 hour later, and the cells washed with PBS. 200µl of TVN was added to each well and incubated at 37°C for 5 minutes. Cells were re-suspended in 200µl of fresh media, and one-third was transferred to clean tube for DNA preparation. This aliquot was centrifuged at 13 000 rpm for 5 minutes, and the pellet stored at -20°C. The remaining two-thirds were transferred into a 15ml falcon tube (Greiner Bio One GmbH, Frickenhausen, Germany) for freezing down. The tube was centrifuged at 1000xg for 3 minutes, and the resulting pellet re-suspended in 85µl of freezing media (10% DMSO (Sigma), 10% FCS, 80% media), and finally transferred into a 1.5ml cryogenic freezing vial (Nalgene Cryoware, Rochester, NY, USA). Frozen down stocks were stored in liquid nitrogen storage.

2.9.5 PCR Screening for Homologous Recombination

ES cell DNA pellets previously selected for targeting construct incorporation (by neomycin selection) that had been stored at -20°C were thawed. Subsequently, 200µl of lysis buffer (100mM Tris.HCl, pH8.5, 5mM EDTA, 0.2% SDS, 200mM NaCl, 100µg/ml proteinase K (Roche)) was added, and incubated at 55°C overnight with constant, gentle rotation. Next, 1 volume of isopropanol was added and mixed well. This mix was then centrifuged at 13 000 rpm for 10 minutes. Supernatant was removed, and the resultant pellet was allowed to air-dry. Once dry, the pellet was re-suspended in 50µl 1xTE buffer, and stored short-term at 4°C (long-term storage at -20°C).

2.9.5.1 PCR Screening

Primers were designed to allow for the detection of targeted insertion of the *Hsd11b2* floxed construct into ES cells by homologous recombination. Primers were designed as follows: Forward A (*Hsd11b2* exon 1) 5'-CTGCTGGCTGCTCTCGACTG-3'; Reverse B (*Hsd11b2* exon 2) 5'–TCTTAGCTGTCTCCTTGCCA–3'; Reverse C (Neomycin cassette) 5'–TGTCAAGACCGACCTGTCCG–3'; Reverse D (5' Neomycin insert) 5'–GGCAGAGCCTATAACGAGTC–3' (primers synthesised by MWG Bio-tech, Ebersberg, Germany). PCR reactions were carried out using Finnzymes Phusion High-Fidelity DNA polymerase (NEB). PCR program was as follows: 98°C for 1 minute, cycle: 98°C 15 seconds, 67°C 30 seconds, 72°C 2 minutes (repeat cycle 33 times), 72°C 7 minutes. PCR reactions were carried out on a DNA Engine PCR machine (MJ Research DNA). PCR samples were analysed by agarose gel electrophoresis.

2.9.5.2 Fluorescent PCR Screening

Fluorescent detection PCR reactions with ES cell DNA were carried out using an ABI Prism 7000 Sequence Detection System machine. Primers were designed using Primer Express program (Applied Biosystems, http://www.appliedbiosystems.com/support/apptech/) as follows: Forward (*Hsd11b2* exon1) 5'-TGGCTGGATCGCGTTGT-3'; Reverse (*lox*P site) 5'-ATGTATGCTATACGAAGTTATTAGGT-3'. A positive control plasmid (containing *Hsd11b2* exon 1 and a *lox*P site) was constructed using the 5' external probe and pL451 plasmids described previously, in order to optimise reactions and act as a positive control for real reactions. Negative ES cell DNA was spiked with the equivalent molar concentration of 1 copy per genome of the positive control plasmid per genome volume of DNA. SYBR Green Taq Mastermix (ABI, Foster City, California, USA) was used, and PCR cycle was as follows: 95°C 10 minutes, cycle: 95°C 15 seconds, 60°C 1 minute (repeat cycle 40 times), 72°C 2 minutes.

2.9.6 Southern Hybridisation for Homologous Recombination

ES cell DNA used previously screened by fluorescent PCR (as described above) was purified further by phenol/chloroform method, as described earlier, with the final DNA pellet re-suspend in 40µl 1xTE buffer. Half of the final volume (20µl) was then used for subsequent reactions, with the remainder stored at -20°C. DNA was digested with either BamHI (3' external probe) or HindIII (5' external probe) restriction enzymes, separated by gel electrophoresis, and transferred to a Hybond nylon membrane (Amersham Bioscience, Little Chalfont, Bucks, UK). Once transfer was complete (generally overnight), the membrane was placed in 3MM chromatography paper (Whatman International Ltd, Maidstone, UK) and baked at 80 °C for 2

hours to permanently bond the DNA to the membrane. The membrane was then pre-hybridised to reduce background by incubating at 65°C for 3 hours in warmed hybridisation mix (0.5M $NaPO_4$, 7% SDS, 1mM EDTA, pH 7.4) plus 1 mM denatured salmon sperm DNA. The membrane was then hybridised overnight at 65°C with constant agitation, with a phosphate-32 (^{32}P)-dCTP labelled 3′ or 5′ external probe. 3′ and 5′ external probes were isolated from sub-clone plasmids using PstI/ScaI (350 bp fragment) and HpaI/XhoI (500 bp fragment), respectively. 10ng of probe DNA was labelled with $\alpha^{32}P$-dCTP (Amersham) for Southern hybridisation using Ready-To-Go DNA Labelling Beads (-dCTP; Amersham), according to manufacturers protocol. Labelled DNA was purified through a NAP-5 sephadex column (Amersham), and added to hybridisation buffer used previously during pre-hybridisation. After overnight incubation, hybridised membranes were rinsed briefly in 3xSSC buffer (20xSSC = 3M NaCl, 0.3M Na citrate), then twice for 15 minutes in 20mM Na2HPO4 pH 7.2, 1mM ETDA pH 8.0, 5% SDS, twice for 15 minutes in 20mM Na2HPO4 pH 7.2, 1mM ETDA pH 8.0, 1% SDS, and then rinsed again in 3xSSC. Next, membranes were washed in 0.1% SDS plus 0.5% SSC, and finally in 0.1% SDS plus 0.1% SSC. All washes were carried out at 65°C with constant rotation. The washed membrane was then wrapped in cling film, exposed to BioMax light film (Kodak, Sigma) in a light-proof cassette at - 80°C for an appropriate length of time, and the film was then developed on a Konica SRX-101 medical film processor (Konica Minolta, Tokyo, Japan).

2.9.7 Blastocyst Injection of Embryonic Stem Cells

ES cell clones that were confirmed positive for both 5′ and 3′ end homologous recombination by Southern hybridisation were introduced from

in vitro culture to a surrogate blastocyst by microinjection. The blastocyst injections and implantations were carried out by a University of Edinburgh in-house service (Genetic Intervention and Screening Technologies). Offspring were screened for ES cell uptake into genome by chimeric coat colouring. Chimeric offspring were then entered into a breeding program with C57BL6/J mice, and resultant offspring were screened for germline inclusion of the targeting construct by agouti coat colour.

2.9.7.1 Counting Chromosomes in Embryonic Stem Cells

The Karyotype of the ES cells to be blastocyst injected was checked before injection. 1 mg/ml Colcemid (Invitrogen) was added to the ES cell culture flasks and incubated at 37°C for one hour. Then the media was removed, and cells were washed with PBS, and incubated with trypsin for 3 minutes. The cells were then centrifuged at 1000 rpm for 5 minutes to harvest. Supernatant was removed and the cells were re-suspended in 1.5 ml fresh medium. 10 ml of 0.075 M KCl (pre-warmed to 37°C) was added slowly drop by drop to the tube containing the cells, mixing gently throughout. This was then incubated at 37°C for 15 minutes. Next, 2 - 3 drops of ice-cold fixative solution (3:1 mix of methanol:acetic acid), mixed, and centrifuged for 5 minutes at 1000 rpm. Supernatant was removed, and up to 10 ml of fresh ice-cold fixative solution added drop by drop, as before. Again the mix was centrifuged, supernatant removed and the addition of fixative solution repeated. This procedure was repeated twice more. After the final fixation, the cells were re-suspended in 0.5 ml fixative solution, dropped onto glass slides from an approximately 10 cm distance, and allowed to air-dry. Slides were finally viewed under a microscope (Nikon, Tokyo, Japan) and chromosome numbers of individual ES cells were counted. Ten chromosome counts were performed on individual cells from each clone that was put

forward for microinjection (see Table 2.1 for results of chromosome spreads, and Figure 6.7 for photograph of example chromosome spreads).

Clone Number	28	63	182
Chromosome Spread Number	Number of Chromosomes (Karyotype)		
1	40	39	40
2	40	40	41
3	41	40	40
4	40	40	40
5	38	40	38
6	38	38	40
7	40	40	40
8	40	41	40
9	42	40	41
10	40	40	40
% 40 chromosomes	60	70	70

Table 2.1 Chromosome Counting in ES Cell Spreads
Normal mouse chromosome number (Karyotype) is 40 chromosomes per cell.

2.10 LacZ Expression Detection

2.10.1 Kidney Perfusion Fixation

Mice heterozygous for both *Hoxb7* and ROSA26 allele were used for kidney fixation perfusions (ROSA26 null littermates were used as controls). Animals were anaesthetised I.P. with a mixture of ketamine hydrochloride (Vetalar, Pfizer Ltd., Kent, UK) and medetomidine hydrochloride (Domitor, Pfizer): 1.5 units of ketamine, 2 units of medetomidine and 8.25 units of water administered at 0.5ml/g body weight. Perfusion was carried out via

hepatic artery cannulation using Polyethylene tubing (PE90, Portex fine bore polyethylene tubing; Jencons) with 15mls cold PBS over a 5 minute period. This was followed by perfusion of 15mls of cold glutaraldehyde fixative solution (5mM EGTA, 100mM $MgCl_2$, 0.1M NaH_2PO_4 and 0.2% glutaraldehyde in PBS) over 5 minutes. The kidneys were removed and stored in glutaraldehyde fixative for 2 hours at 4°C. Kidneys were then sliced bivalve and moved to a 15% sucrose solution for 4 hours, followed by a 30% sucrose solution overnight, both at 4°C.

2.10.2 Microtome Sectioning

Preserved kidneys halves were mounted in OCT embedding matrix (Raymond A Lamb Lab Supplies, Eastbourne, East Sussex, UK) using Bright Cryospray 134 (Jencons) for rapid matrix setting. 10μM thick sections were then sliced using a microtome (Microtome blades were Carbon Steel C35 from Feather Safety Razor Co., Osaka, Japan) inside a cryostat (Bright Model OTF) onto Super Frost Plus microscope slides (BDH). Cryostat conditions were set to -15°C for specimen and -25°C for chamber. Section slides were stored at -20°C until further use.

2.10.3 X-Gal Staining

Previously mounted kidney sections were transferred directly from -20°C storage into β-galactosidase (LacZ) fixative solution (4% paraformaldehyde, 0.02% NP40, 0.01% sodium deoxycholate, 5mM EGTA and 2mM MgCl2) for 15 minutes at 4°C. Slides were then washed twice for 5 minutes each in LacZ wash buffer (2mM MgCl2, 0.02% NP40 and 0.01% sodium deoxycholate). Next, the slides were stained overnight at 37°C in darkness in LacZ staining

buffer (2mM MgCl2, 0.02% NP40, 0.01% sodium deoxycholate, 5mM potassium ferricyanide, 5mM potassium ferrocyanide and 1mg/ml X-gal). They were then rinsed twice in PBS for 5 minutes each, and transferred to eosin solution for 1- 2 minutes. Slides were then washed in distilled water and mounted directly with aqueous mounting medium (Shandon Immu-Mount, Thermo Scientific). They were finally sealed with clear nail varnish.

2.11 Statistical Analyses

All data (with the exception of Box and Whisker plots) are presented as means ± standard error (SE). After tests for Gaussian distribution, comparisons were made using either unpaired *t* test or analysis of variants ANOVA with Bonferroni *post hoc* test, as appropriate. Balance results are resented as Box and Whisker plots, where normal distribution is not assumed. Statistical comparisons were made using Prism 5 (GraphPad Software, San Diego, California, USA).

Chapter 3

Hsd11b2 Heterozygous Mice Have a Salt-Sensitive Phenotype

3.1 Introduction

The principal mineralocorticoid aldosterone is the classical ligand for the MR, but similarities in steroid structure permit the glucocorticoid cortisol (corticosterone in rodents) to share an equal affinity with aldosterone for the MR (Arriza et al., 1987). The co-localisation of MR with the enzyme 11β-HSD2 in tissues such as the kidney acts to maintain MR-aldosterone ligand specificity by converting the active cortisol to its inactive 11-keto metabolite, cortisone (dehydrocorticosterone in rodents). A down-regulation in the function and/or expression of 11β-HSD2 compromises this specificity by permitting cortisol to bind and inappropriately activate MR. This allows glucocorticoids to act as mineralocorticoids at the MR, and the negative feedback homeostasis of the RAAS is disrupted. This in turn results in an unregulated increased expression of MR target genes, which are important in maintaining electrolyte and BP balance. Consequences of this deregulation can include increased renal sodium reabsorbtion, leading to hypertension and potentially permanent renal and cardiac damage.

SAME is a clinical condition in which mutations in the HSD11B2 gene result in ablation of functional protein (also referred to as type I SAME in the literature) (White, 2001). This rare autosomal recessive disease presents in childhood with severe hypertension and hypokalemia, with low plasma renin and aldosterone levels, all of which can be attributed to MR over-activation. Although SAME is rare, the wider clinical significance of HSD11B2 functional mutations is highlighted by the following observations. In a Brazilian kindred, the heterozygous parent of a SAME patient was found to have late on-set mineralocorticoid hypertension, suggesting that genotypes in the HSD11B2 gene that lead to reduced (not ablated) enzyme function may have a phenotypic correlation (Li et al., 1997). Patients

homozygous for specific HSD11B2 mutations presenting with mild low-renin hypertension have been previously termed as type II SAME (Mantero et al., 1996; Wilson et al., 1998). An in-depth study into an extensive consanguineous Sardinian pedigree with SAME type II showed late on-set mineralocorticoid hypertension and impaired cortisol metabolism in affected individuals (Li et al., 1998). Interestingly in this study, the heterozygote state was linked to subtle changes in cortisol metabolism, and one such individual was hypertensive. Compound heterozygotes of SAME also exist, where each allele contains has a separate HSD11B2 mutation in the affected individual (Dave-Sharma et al., 1998; Kitanaka et al., 1997; Lavery et al., 2003). Furthermore, epidemiological human studies have shown that HSD11B2 polymorphic variation is present within the general population (Bocchi et al., 2004), and some research has highlighted a potential link between certain polymorphisms and essential and/or SS hypertension (Alikhani-Koupaei et al., 2007; Mariniello et al., 2005). Interestingly, the phenotypes of some essential hypertension patients indicate that a mineralocorticoid effect may be contributing towards the hypertension, such as positive correlations between BP and plasma sodium levels, and increased urinary cortisol metabolites (Ferrari et al., 2000). These observational studies into the effects of mutations affecting 11β-HSD2 enzyme activity emphasise the need to investigate the penetrance of HSD11B2 polymorphisms in hypertensive populations.

In depth analysis of impaired 11β-HSD2 enzyme activity in essential hypertension is difficult in human subjects. So far, over 30 different HSD11B2 mutations associated with type I and II SAME have been identified (Hammer and Stewart, 2006). However, it is difficult to correlate genotype with phenotype severity, as it is complex to predict what effects the genotype

has on enzyme function *in vivo*. *In vitro* studies on the enzyme activities of specific HSD11B2 mutations have been performed in transfected cell studies, but these have shown that the enzyme activity of the mutated 11β-HSD2 is greatly impaired, if not completely abolished, failing to predictably correlate genotype with phenotype (Lavery et al., 2003; Mune et al., 1995). Further studies of specific HSD11B2 mutations have suggested that mechanisms of action may include impaired 11β-HSD2 protein stability leading to a shortened enzymatic half-life (Atanasov et al., 2007; Nunez et al., 1999), as well as deficiencies in substrate binding capacity (Carvajal et al., 2003).

To assist physiological investigations into impaired 11β-HSD2 enzyme activity, an 11β-HSD2 full knockout mouse was generated by gene targeting (Kotelevtsev et al., 1999). Characterisation of the *Hsd11b2* null mouse model (*Hsd11b2*$^{-/-}$) confirms reproduction of all of the major phenotypes of SAME. Investigations using a synthetic glucocorticoid and monitoring of the sodium/potassium urinary excretion ratio suggested that the molecular mechanism underlying SAME phenotype is inappropriate MR activation by endogenous glucocorticoids (Kotelevtsev et al., 1999). Histological examination also revealed that renal damage is present in the distal nephron of *Hsd11b2*$^{-/-}$ mice. A recent study determined a mechanistic timeline of the development and maintenance of SAME in *Hsd11b2*$^{-/-}$ mice (Bailey et al., 2008), identifying impaired sodium excretion as a key process in the etiology of hypertension.

A definitive investigation into reduced 11β-HSD2 enzyme activity and a direct link to hypertension (SS hypertension in particular) is lacking. This study proposes that the *Hsd11b2* heterozygote null mouse (*Hsd11b2*$^{+/-}$) may represent an ideal rodent model of reduced 11β-HSD2 activity. Experimental investigations using this model could prove informative, especially in the

setting of excess dietary salt intake, and play a key role towards understanding the contributions that HSD11B2 polymorphisms are having towards hypertension within the general human population.

3.2 Results

3.2.1 *Hsd11b2* Heterozygous Mice Have Reduced Enzyme Activity and Display a Salt-Sensitive BP

11β-HSD2 enzyme activity was measured in kidney homogenates from *Hsd11b2* wild-type mice (*Hsd11b2*$^{+/+}$) and *Hsd11b2*$^{+/-}$ mice on a standard or a high sodium diet after three weeks (Figure 3.1). The *Hsd11b2*$^{+/-}$ mice had

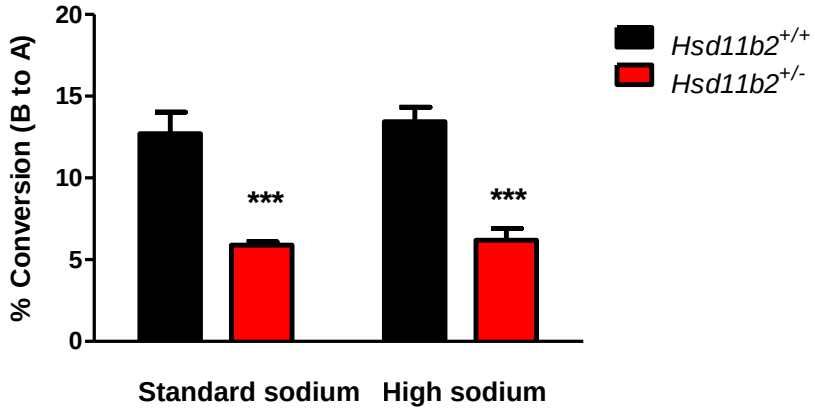

Figure 3.1. 11β-HSD2 enzyme activity in kidney homogenates from *Hsd11b2*$^{+/+}$ and *Hsd11b2*$^{+/-}$ mice on a standard and a high sodium diet (n = 6 for both groups on both diets). Measured as the % conversion of corticosterone (B) to dehydrocorticosterone (A). *Hsd11b2*$^{+/-}$ mice have a significantly lower conversion rate than *Hsd11b2*$^{+/+}$ mice on both diets; dietary sodium content does not affect either genotype. ******* P < 0.001. Data are means ± SEM.

approximately 50% 11β-HSD2 enzyme activity when compared to the *Hsd11b2*$^{+/+}$ mice on either sodium diet; dietary sodium content did not affect enzyme activity in either genotype. These results confirm that *Hsd11b2*$^{+/-}$ mice have a reduced 11β-HSD2 enzyme activity compared to *Hsd11b2*$^{+/+}$,

proving that having only one functional *Hsd11b2* allele decreases enzyme activity.

The effect of dietary sodium upon BP was investigated by using the tail cuff method to measure systolic BP (SBP) in *Hsd11b2*$^{+/-}$ and *Hsd11b2*$^{+/+}$ mice (Figure 3.2). On a standard sodium diet, SBP was similar for both genotypes. High

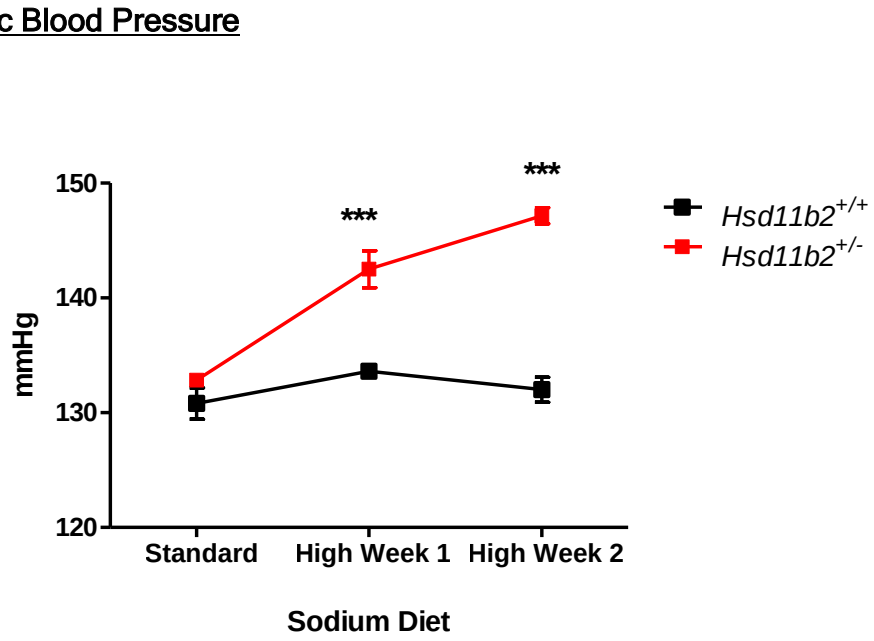

Figure 3.2. Systolic BP (SBP) measured using tail plethysmography in *Hsd11b2*$^{+/+}$ and *Hsd11b2*$^{+/-}$ mice on a standard sodium diet, and after 1 and 2 weeks on a high sodium diet (n = 5 and 6, respectively). SBP was comparable between *Hsd11b2*$^{+/-}$ and *Hsd11b2*$^{+/+}$ mice on a standard sodium diet. High sodium diet did not significantly alter SBP in *Hsd11b2*$^{+/+}$ mice. SBP was significantly increased in *Hsd11b2*$^{+/-}$ mice after 1 and 2 weeks on a high sodium diet. ******* P < 0.001. Data are means ± SEM.

sodium diet had no effect upon the SBP of *Hsd11b2*$^{+/+}$ mice, confirming that *Hsd11b2*$^{+/+}$ mice do not have a SS BP. *Hsd11b2*$^{+/-}$ mice displayed a significant increase in SBP after one week on the high sodium diet compared to a standard sodium diet, and also compared to *Hsd11b2*$^{+/+}$ mice after one week on a high salt diet. This increase remained stable after two weeks on the high

salt diet. These observations show that in conscious *Hsd11b2*$^{+/-}$ mice, SBP increases on a high salt diet compared to *Hsd11b2*$^{+/+}$ mice.

3.2.2 Metabolic Studies in Conscious Animals

To investigate the contribution of sodium and water balance towards the SS BP of *Hsd11b2*$^{+/-}$ mice, daily urine and electrolyte excretion was measured in *Hsd11b2*$^{+/-}$ and *Hsd11b2*$^{+/+}$ mice on different sodium diets from metabolic cage samples.

3.2.2.1 Sodium Balance

On a standard sodium diet, both genotypes had similar levels of dietary sodium intake and urinary sodium excretion; overall sodium balance was neutral (Figure 3.3). When placed on a high sodium diet, the dietary sodium intake aptly increased, with both groups of mice consuming similar levels throughout the study (Figure 3.3a). The *Hsd11b2*$^{+/+}$ mice responded to the increased sodium load with a rapid increase in their urinary sodium excretion after one day on the high sodium diet, and maintained a steady level of excretion for the duration of the study (Figure 3.3b). The *Hsd11b2*$^{+/-}$ mice also increased their urinary sodium excretion in response to the high sodium diet; however, for the first two days of the high sodium diet regime their excretion was significantly less than that of the *Hsd11b2*$^{+/+}$ mice (Figure 3.3b). This difference in natriuresis is reflected in overall sodium balance, as *Hsd11b2*$^{+/-}$ mice display a significantly positive sodium balance for the period of Day 1 - 3 compared with *Hsd11b2*$^{+/+}$ mice, which maintain a neutral sodium balance (Figure 3.3c). After the first few days, sodium excretion rates were comparable between the genotypes, and *Hsd11b2*$^{+/-}$ mice were restored to a neutral sodium balance. Daily faecal sodium excretion was also measured in

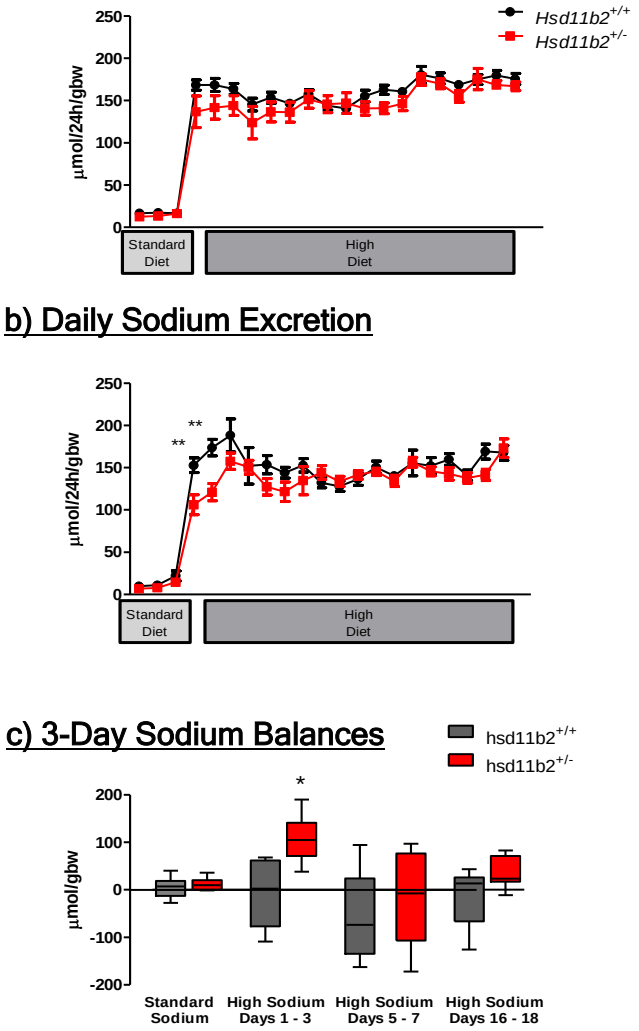

Figure 3.3. Metabolic cage sodium analysis in *Hsd11b2*$^{+/+}$ and *Hsd11b2*$^{+/-}$ mice on a standard and a high sodium diet (n = 7 and 10, respectively). **a)** Dietary sodium intake and **b)** urinary sodium excretion were measured during 24 hour periods. These data were then used to calculate **c)** sodium balance over three-day periods. Dietary sodium intake did not differ between *Hsd11b2*$^{+/+}$ and *Hsd11b2*$^{+/-}$ mice on either sodium diet; high sodium diet caused a significant increase in sodium intake ($P < 0.001$). Sodium excretion was equal between *Hsd11b2*$^{+/-}$ and *Hsd11b2*$^{+/+}$ mice on a standard sodium diet; high sodium diet caused a significant increase in excretion in both groups ($P < 0.001$), with *Hsd11b2*$^{+/-}$ mice excreting significantly less than *Hsd11b2*$^{+/+}$ mice for the first 2 days. This was reflected in sodium balance as *Hsd11b2*$^{+/-}$ mice had a significantly positive balance compared to *Hsd11b2*$^{+/+}$ mice for high sodium diet days 1 – 3 period. At all other time points sodium excretion and balance were equal between genotypes. ***** $P < 0.05$; ****** $P < 0.01$; ******* $P < 0.001$. Data are means ± SEM or medians and ranges (**c)**.

these mice and was found not to differ significantly between genotypes, and had no significant effect upon sodium balance results (data not shown).

3.2.2.2 Water Balance

Drinking water intake and urine flow rate (UFR) were not significantly different between *Hsd11b2*$^{+/+}$ and *Hsd11b2*$^{+/-}$ mice on a standard sodium diet (Figure 3.4a and b); water balance was also similar in both genotypes and was always significantly positive (Figure 3.4d). *Hsd11b2*$^{+/+}$ mice greatly increased both water intake and UFR after one day on a high sodium diet, and these increases were sustained for the duration of the high sodium diet study period (Figure 3.4a and b). *Hsd11b2*$^{+/-}$ mice also showed polydipsia and polyuria following transition to a high sodium diet, and although there was a trend during the first 48 hours for drinking water intake and UFR to be lower compared to *Hsd11b2*$^{+/+}$ mice, this was not statistically significant. Water balance was significantly increased for both groups on a high sodium diet compared to a standard sodium diet; the two genotypes did not differ in their water balance at any period (Figure 3.4d).

Faecal water content was significantly higher in *Hsd11b2*$^{+/+}$ mice compared to *Hsd11b2*$^{+/-}$ mice on a standard sodium diet (Figure 3.4d). However, once placed on a high sodium diet, both genotypes displayed significant reductions in their faecal water content. The faecal water content remained similar between the two groups for the remainder of the experiment. This suggests that faecal water content is tightly regulated by dietary sodium levels in both genotypes. Overall, faecal water loss is normally quite small, and the comparison of the UFR and the faecal water content during these experiments highlights this (compare Figure 3.4b and c). As a result, faecal water values were not included in the overall water balance calculations.

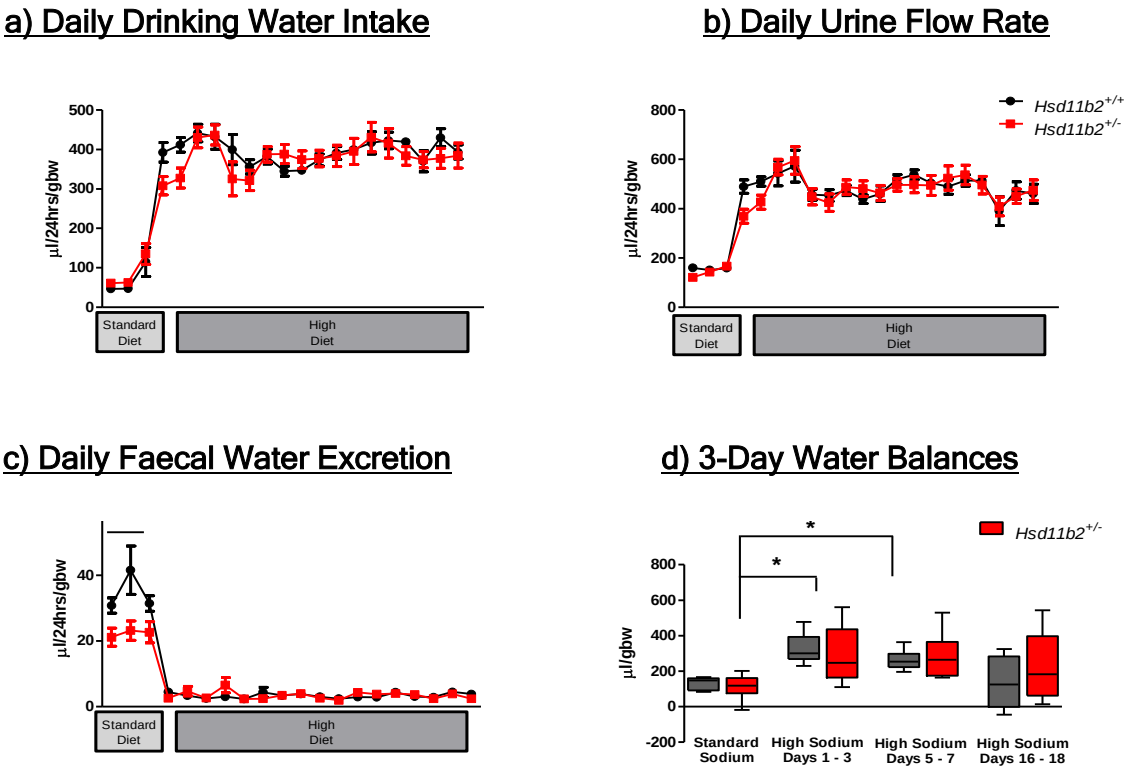

Figure 3.4. Metabolic cage water analysis in *Hsd11b2*$^{+/+}$ and *Hsd11b2*$^{+/-}$ mice on a standard and a high sodium diet (n = 7 and 10, respectively). **a)** Drinking water intake, **b)** urine flow rate (UFR) and **c)** faecal water content were measured during 24 hour periods. These data were then used to calculate **d)** water balance over three-day periods. Drinking water intake did not differ between *Hsd11b2*$^{+/+}$ and *Hsd11b2*$^{+/-}$ mice on either sodium diet; high sodium diet caused a significant increase in sodium intake ($P < 0.001$). UFR was also equal between *Hsd11b2*$^{+/-}$ and *Hsd11b2*$^{+/+}$ mice on a standard and a high sodium diet; high sodium diet caused a significant increase in the UFR of both groups ($P < 0.001$). *Hsd11b2*$^{+/+}$ mice have a greater faecal water content than *Hsd11b2*$^{+/-}$ mice on a standard sodium diet. High sodium diet significantly decreased the faecal water content for both genotypes ($P < 0.001$) to similar levels to one another. Sodium balance was equal between both genotypes at all periods measured; high sodium diet caused a significant increase in positive water balance for both *Hsd11b2*$^{+/+}$ and *Hsd11b2*$^{+/-}$ mice. * $P < 0.05$; ** $P < 0.01$. Data are means ± SEM or medians and ranges (**d)**.

3.2.2.3 Potassium Balance

The dietary intake of potassium was not different between the *Hsd11b2*$^{+/+}$ and *Hsd11b2*$^{+/-}$ mice at any point during both standard and high sodium diet feeding (Figure 3.5a). However, the change in sodium diet had a significant

a) Daily Potassium Intake

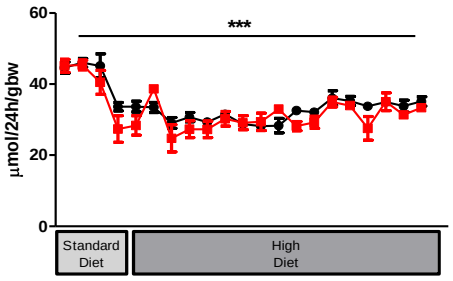

b) Daily Potassium Excretion

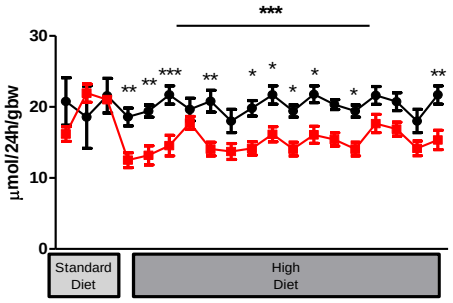

c) 3-Day Potassium Balances

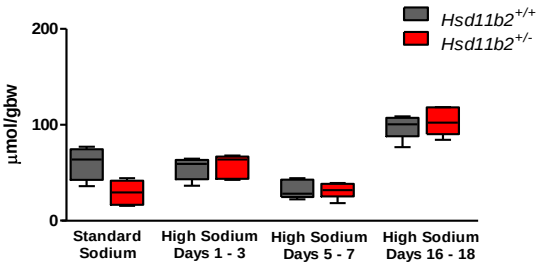

Figure 3.5. Metabolic cage potassium analysis in *Hsd11b2*$^{+/+}$ and *Hsd11b2*$^{+/-}$ mice on a standard and a high sodium diet (n = 7 and 10, respectively). **a)** Dietary potassium intake and **b)** urinary potassium excretion were measured during 24 hour periods. These data were then used to calculate **c)** potassium balance over three-day periods. Dietary potassium intake did not differ between *Hsd11b2*$^{+/+}$ and *Hsd11b2*$^{+/-}$ mice on either sodium diet; however moving to a high sodium diet caused a significant decrease in potassium intake (***). Potassium excretion was equal between *Hsd11b2*$^{+/-}$ and *Hsd11b2*$^{+/+}$ mice on a standard sodium diet; high sodium diet caused a significant decrease in excretion for *Hsd11b2*$^{+/-}$ mice only for the entire dietary period (***). Potassium balance was equal between both genotypes at all time points assessed. ***** P < 0.05; ****** P < 0.01; ******* P < 0.001. Data are means ± SEM or medians ranges (**c)**.

effect upon the dietary potassium intake of both groups. In terms of 24 hour urinary potassium excretion, there is no difference between the two genotypes on a standard sodium diet (Figure 3.5b). When the mice are moved onto the high sodium diet, the *Hsd11b2*$^{+/+}$ mice do not significantly alter their urinary potassium excretion compared to the standard sodium diet. The *Hsd11b2*$^{+/-}$ mice display a significant decrease in their urinary potassium excretion compared to their standard sodium diet excretion values, and also compared to *Hsd11b2*$^{+/+}$ mice for most of the high sodium diet period (Figure 3.5b). Three day potassium balance values did not reflect this difference in potassium excretion between the genotypes, as balance values were not significantly different from one another for any of the periods investigated (Figure 3.5c).

3.2.3 Steroid Concentrations in Plasma and Urine

Plasma concentrations of aldosterone and corticosterone were measured in terminal samples obtained from *Hsd11b2*$^{+/+}$ and *Hsd11b2*$^{+/-}$ mice on a standard sodium diet and after three weeks on a high sodium diet. The urinary excretion of aldosterone and corticosterone were measured during standard and high sodium diet feeding in 24 hour urine samples collected from metabolic cages.

3.2.3.1 Aldosterone

Plasma aldosterone concentration was significantly lower in *Hsd11b2*$^{+/-}$ mice than *Hsd11b2*$^{+/+}$ mice on a standard sodium diet (Figure 3.6a). After three weeks on a high sodium diet, plasma aldosterone levels were appropriately down regulated for both genotypes, but remained significantly lower in the *Hsd11b2*$^{+/-}$ group than the *Hsd11b2*$^{+/+}$ group (Figure 3.6a).

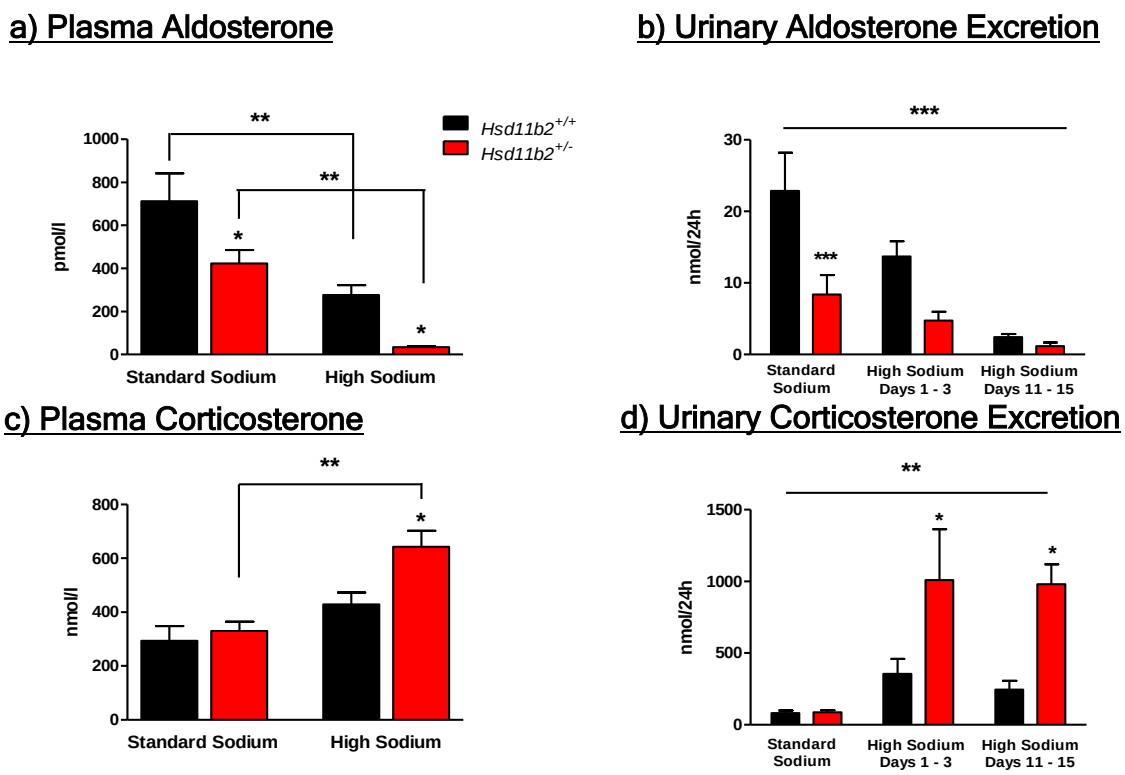

Figure 3.6. Plasma **a)** aldosterone and **c)** corticosterone were measured in *Hsd11b2*$^{+/+}$ and *Hsd11b2*$^{+/-}$ mice on a standard sodium diet or after three weeks on a high sodium diet (n = 9 for *Hsd11b2*$^{+/+}$ on standard diet for both steroids; n = 12 and 7 respectively for *Hsd112b*$^{+/-}$ on a standard diet; n = 9 and 7 respectively for *Hsd11b2*$^{+/+}$ on a high sodium diet; n = 8 and 7 respectively for *Hsd11b2*$^{+/-}$ on a high sodium diet). Urinary **b)** aldosterone and **d)** corticosterone were measured over three day periods from metabolic cage collected urines during both standard and high sodium diet feeding (n = 6 for both groups). Plasma aldosterone was significantly lower in *Hsd11b2*$^{+/+}$ mice than *Hsd11b2*$^{+/-}$ mice on both sodium diets; high sodium diet caused a significant decrease in plasma aldosterone in both genotypes. Urinary aldosterone excretion was also significantly lower for *Hsd11b2*$^{+/-}$ mice than *Hsd11b2*$^{+/+}$ mice; high sodium diet caused a significant decrease in aldosterone concentration in both genotypes at Days 1 – 3 ($P < 0.05$), and then decreases further at Days 11 – 15 ($P < 0.001$). Plasma corticosterone concentration was comparable between *Hsd11b2*$^{+/-}$ and *Hsd11b2*$^{+/+}$ mice on a standard sodium diet; high sodium diet had no effect upon *Hsd11b2*$^{+/+}$ concentration, but caused a significant increase in *Hsd11b2*$^{+/-}$ mice. Plasma corticosterone levels were also comparable between *Hsd11b2*$^{+/+}$ and *Hsd11b2*$^{+/-}$ mice on a standard sodium diet. Both groups had a significant increase on a high sodium diet, with the *Hsd11b2*$^{+/-}$ mice having a significantly greater increase at both Days 1 – 3 and 11 - 15. ***** $P < 0.05$; ****** $P < 0.01$; ******* $P < 0.001$. Data are means ± SEM.

24 hour urinary aldosterone excretion was measured over key periods from metabolic cage urine samples. Urine samples were measured in addition to the plasma samples as it was important to corroborate trends observed in samples collected under terminal conditions with conscious, unstressed levels. As with the plasma data, concentrations of urinary aldosterone excretion were higher in *Hsd11b2*$^{+/+}$ mice than *Hsd11b2*$^{+/-}$ mice on a standard sodium diet (Figure 3.6b). Urinary aldosterone excretion for both genotypes was reduced upon induction of the high sodium diet, and the *Hsd11b2*$^{+/-}$ mice displayed decreased concentrations compared to the *Hsd11b2*$^{+/+}$ mice.

3.2.3.2 Corticosterone

Plasma corticosterone was similar between *Hsd11b2*$^{+/-}$ and *Hsd11b2*$^{+/+}$ mice on a standard sodium diet (Figure 3.6c). After three weeks on a high sodium diet, the *Hsd11b2*$^{+/+}$ mice showed no significant difference in their plasma corticosterone levels compared to the standard sodium diet conditions, although there was a trend towards an increase. Plasma corticosterone levels were significantly greater in *Hsd11b2*$^{+/-}$ mice after three weeks on a high sodium diet compared with a standard sodium diet, and also when compared with the *Hsd11b2*$^{+/+}$ group on the high sodium diet (Figure 3.6c).

Urinary corticosterone concentration was measured over key periods, as with aldosterone. There was no significant difference in the urinary excretion of corticosterone between the two groups on a standard sodium diet (Figure 3.6d). Once moved to the high sodium diet, both groups increased their excretion of corticosterone at days 1 - 3, with the *Hsd11b2*$^{+/-}$ group showing a significantly greater increase compared with the *Hsd11b2*$^{+/+}$ group. These increases persisted at days 11 - 15 of the high sodium diet regime, with the statistical difference between the two groups maintained (Figure 3.6d).

3.2.4 Renal Clearance Study

Renal clearance surgery was performed upon *Hsd11b2*$^{+/+}$ and *Hsd11b2*$^{+/-}$ mice on either a standard sodium diet or after three weeks on a high sodium diet. This allowed for acute, *in vivo* measurements of renal hemodynamics and electrolyte status, as well as the response to bolus administration of the ENaC antagonist amiloride.

3.2.4.1 Mean Arterial BP

Mean arterial BP (MABP) was measured by carotid artery cannulation in *Hsd11b2*$^{+/+}$ and *Hsd11b2*$^{+/-}$ mice that had been maintained on either standard or high sodium diet for three weeks (Figure 3.7). On a standard sodium diet, MABP was comparable between the two genotypes. A high sodium diet had no effect upon MABP of *Hsd11b2*$^{+/+}$ mice. After three weeks on a high sodium

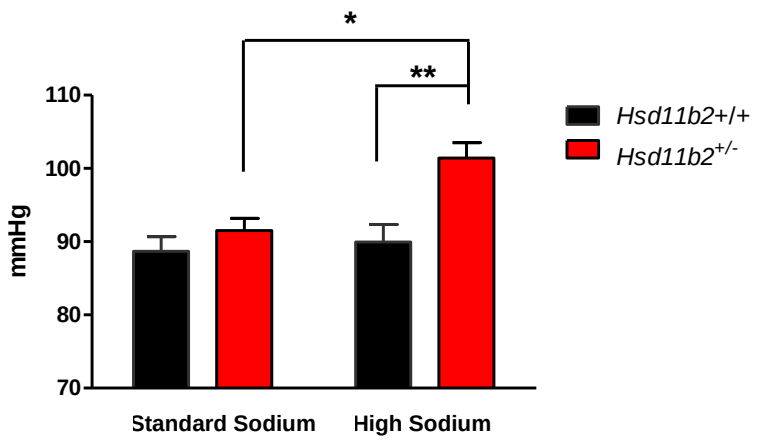

Figure 3.7. Mean arterial BP (MABP) measurements made during renal clearance surgery in *Hsd11b2*$^{+/+}$ and *Hsd11b2*$^{+/-}$ mice on a standard sodium diet (n = 8 for both groups), and after 3 weeks on a high sodium diet (n = 9 and 8, respectively). *Hsd11b2*$^{+/+}$ and *Hsd11b2*$^{+/-}$ mice have similar values for MABP on a standard sodium diet. High sodium diet does not affect MABP of *Hsd11b2*$^{+/+}$ mice. *Hsd11b2*$^{+/-}$ mice have a significantly increased MABP on a high sodium diet compared to a standard sodium diet, and also to *Hsd11b2*$^{+/+}$ mice on a high sodium diet. ***** P < 0.05; ****** P < 0.01. Data are means ± SEM.

diet, the *Hsd11b2*$^{+/-}$ mice had a greater MABP compared to either sodium-loaded *Hsd11b2*$^{+/+}$ mice, and *Hsd11b2*$^{+/-}$ mice on a standard sodium diet. These direct measurements of MABP corroborate the results obtained for SBP in conscious mice, confirming a SS BP phenotype in *Hsd11b2*$^{+/-}$ mice.

3.2.4.2 Renal Hemodynamics

The renal hemodynamics of *Hsd11b2*$^{+/+}$ and *Hsd11b2*$^{+/-}$ mice were measured after three weeks on either a standard or a high sodium diet. On a standard diet the *Hsd11b2*$^{+/-}$ mice had a significantly greater glomerular filtration rate (GFR) than *Hsd11b2*$^{+/+}$ mice (Figure 3.8a). This difference in GFR was also evident in mice fed the high sodium diet for three weeks. There was no effect of sodium diet upon GFR in the *Hsd11b2*$^{+/-}$ group, however post hoc analysis reveals that *Hsd11b2*$^{+/+}$ mice had a significantly lower GFR on the high compared to the standard sodium diet.

On a standard sodium diet there was no difference in renal blood flow (RBF) between *Hsd11b2*$^{+/+}$ and *Hsd11b2*$^{+/-}$ mice (Figure 3.8b). After three weeks on a high sodium diet, the *Hsd11b2*$^{+/-}$ group had a significantly lower RBF compared to the *Hsd11b2*$^{+/+}$ group.

Filtration fraction (FF) was comparable between the two genotypes on a standard sodium diet (Figure 3.8c). Movement to a high sodium diet caused a significant decrease in the FF of *Hsd11b2*$^{+/+}$ mice and a significant increase in the FF of *Hsd11b2*$^{+/-}$ mice, compared to their standard values; overall this resulted in a highly significant difference between the FF of the two genotypes on a high sodium diet.

On a standard sodium diet, the renal vascular resistance (RVR) was comparable between the two genotypes (Figure 3.8d). High sodium diet had no effect upon RVR in *Hsd11b2*$^{+/+}$ mice, but resulted in a significant increase in

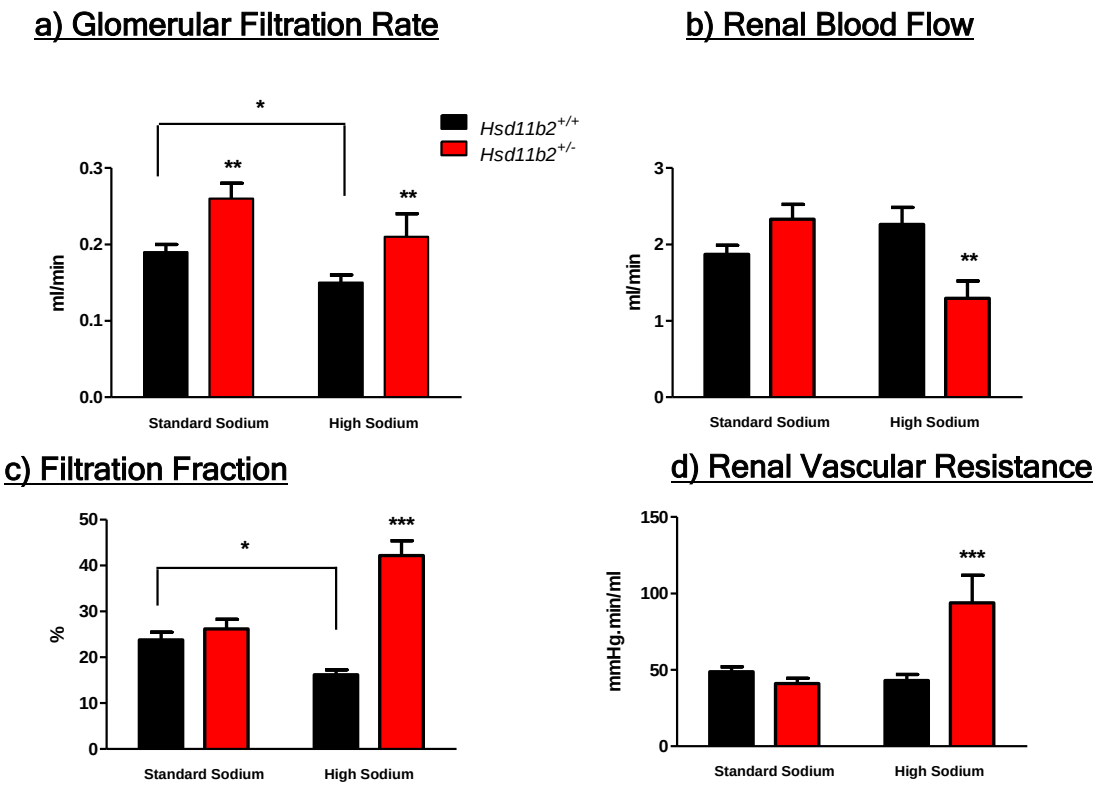

Figure 3.8. Renal hemodynamics were measured during renal clearance surgery in *Hsd11b2*$^{+/+}$ and *Hsd11b2*$^{+/-}$ mice on a standard sodium diet (n = 8 and 9 respectively) or after three weeks on a high sodium diet (n = 8 and 7, respectively). **a)** Glomerular filtration rate (GFR) was greater in *Hsd11b2*$^{+/-}$ mice on both sodium diets; high sodium diet caused a significant decrease in the GFR of *Hsd11b2*$^{+/+}$ mice and had no effect in *Hsd11b2*$^{+/-}$ mice. **b)** Renal blood flow (RBF) was comparable between both genotypes on a standard sodium diet; high sodium diet caused a significant decrease in *Hsd11b2*$^{+/-}$ RBF and had no effect upon *Hsd11b2*$^{+/+}$ RBF. **c)** Filtration fraction (FF) was equal between *Hsd11b2*$^{+/+}$ and *Hsd11b2*$^{+/-}$ mice on a standard sodium diet, and a high sodium diet caused a significant decrease in FF for *Hsd112b*$^{+/+}$ mice and a significant increase for *Hsd11b2*$^{+/-}$ mice, compared to standard sodium diet values. *Hsd11b2*$^{+/-}$ mice displayed a significantly greater FF than *Hsd11b2*$^{+/+}$ mice on a high sodium diet. **d)** Renal vascular resistance (RVR) was also equal between genotypes on a standard sodium diet. *Hsd11b2*$^{+/-}$ mice displayed a significant increase in RVR on a high sodium diet; high sodium diet had no effect upon *Hsd11b2*$^{+/+}$ mice. ***** P < 0.05; ****** P < 0.01; ******* P < 0.001. Data are means ± SEM.

Hsd11b2$^{+/-}$ mice compared to standard sodium diet values and *Hsd11b2*$^{+/+}$ mice on a high sodium diet.

3.2.4.3 Urine and Plasma Electrolytes

Urinary sodium and potassium excretion, as well as plasma concentrations, were measured in anaesthetised *Hsd11b2*$^{+/+}$ and *Hsd11b2*$^{+/-}$ mice after three weeks on either a standard or a high sodium diet.

On a standard sodium diet, *Hsd11b2*$^{+/-}$ mice excreted significantly less sodium in their urine than the *Hsd11b2*$^{+/+}$ mice (Figure 3.9a). The increase in dietary sodium intake caused an overall significant increase in sodium excretion in both genotypes, but sodium excretion was still significantly lower in *Hsd11b2*$^{+/-}$ mice compared to *Hsd11b2*$^{+/+}$ mice. The plasma sodium concentrations were similar between both genotypes on the standard and the high sodium diet, with the high sodium diet causing an overall significant increase in concentration across the two genotypes, but with no significant difference between the two groups (Figure 3.9b).

On a standard sodium diet, *Hsd11b2*$^{+/-}$ mice excreted significantly more potassium than *Hsd11b2*$^{+/+}$ mice (Figure 3.9c). After three weeks on a high sodium diet, both groups excreted less potassium than on the standard sodium diet, and there was no difference in terms of potassium excretion between the two genotypes; the overall effect of diet upon potassium excretion is highly significant (Figure 3.9c). The plasma potassium concentrations were similar between the two groups on the standard sodium diet (Figure 3.9d). Three weeks on a high sodium diet caused a significant decrease in the plasma potassium concentration of *Hsd11b2*$^{+/-}$ mice compared to *Hsd11b2*$^{+/+}$ mice, whose plasma potassium levels were not effected by changes in sodium diet (Figure 3.9d).

3.2.4.4 Response to Amiloride Administration

In order to assess ENaC-mediated sodium reabsorbtion, a bolus dose of the antagonist amiloride was administered by I.V. injection. These data are

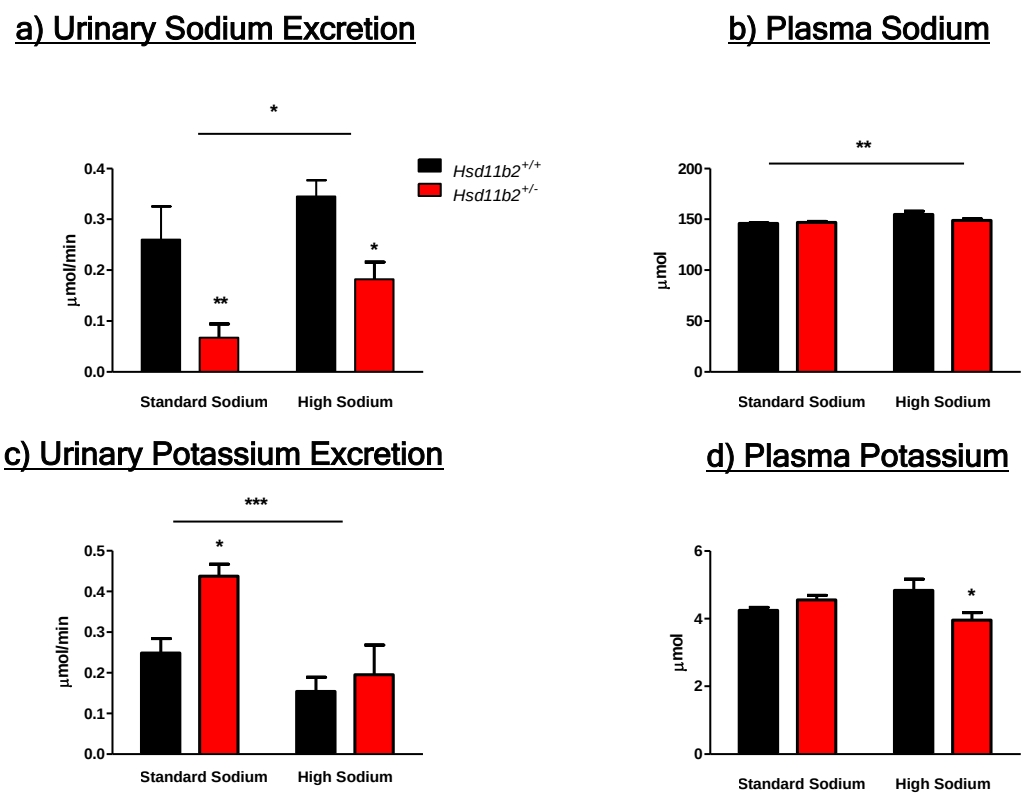

Figure 3.9. Urine and plasma electrolytes were measured during renal clearance surgery in *Hsd11b2*$^{+/+}$ and *Hsd11b2*$^{+/-}$ mice on a standard sodium diet (n = 8 and 9, respectively) or after three weeks on a high sodium diet (n = 8 and 7, respectively). **a)** Urinary sodium excretion was significantly greater in *Hsd11b2*$^{+/+}$ mice than *Hsd11b2*$^{+/+}$ on both sodium diets, with the high sodium diet causing an overall significant increase in sodium excretion for both genotypes. **b)** Plasma sodium levels were comparable between both genotypes on both diets; a high sodium diet caused a significant increase or both. **c)** *Hsd11b2*$^{+/-}$ mice had a greater urinary potassium excretion rate than *Hsd11b2*$^{+/+}$ mice on a standard sodium diet; urinary potassium excretion was decreased in both genotypes to similar levels on a high sodium diet. Plasma potassium was comparable between genotypes on a standard sodium diet, high sodium diet caused a significant decrease for *Hsd11b2*$^{+/-}$ mice and had no effect upon *Hsd11b2*$^{+/+}$ mice. ***** P < 0.05; ****** P < 0.01; ******* P < 0.001. Data are means ± SEM.

presented as the net change in a given variable, calculated from the same individual animal before and after amiloride administration.

On a normal sodium diet, amiloride administration caused a small decrease in the MABP of both groups (Figure 3.10a). On a high sodium diet it caused a significantly greater decrease in MABP; again the response was similar

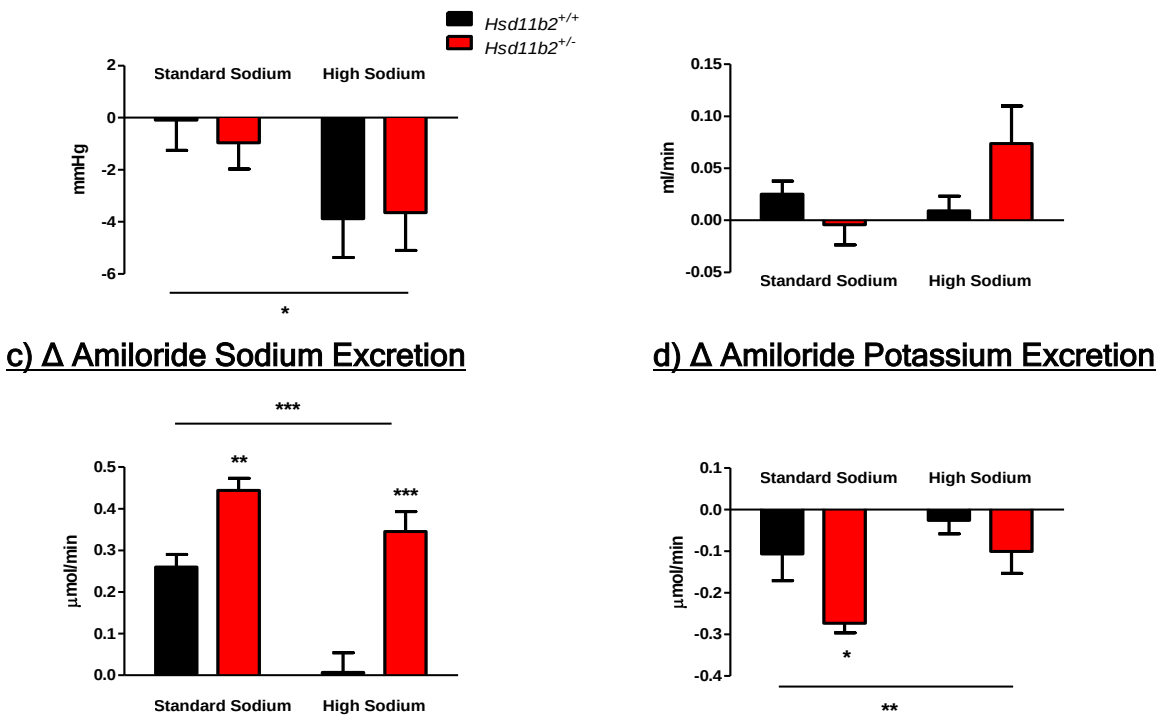

Figure 3.10. The effects of amiloride during renal clearance surgery in *Hsd11b2*$^{+/+}$ and *Hsd11b2*$^{+/-}$ mice on a standard sodium diet (n = 8 for both groups) or after three weeks on a high sodium diet (n = 9 and 7, respectively). Δ amiloride was calculated as the difference between measurements before and after amiloride administration. **a)** MABP was significantly decreased in both *Hsd11b2*$^{+/+}$ and *Hsd11b2*$^{+/+}$ mice on a high sodium diet compared to a standard sodium; there was no difference between genotypes on either diet. **b)** GFR was not significantly affected by amiloride administration on either diet for either genotype. **c)** Amiloride had a significantly greater effect upon urinary sodium excretion in *Hsd11b2*$^{+/-}$ compared to *Hsd11b2*$^{+/+}$ on both sodium diets. High sodium diet significantly reduced sodium excretion in *Hsd11b2*$^{+/+}$ mice compared to *Hsd11b2*$^{+/-}$ mice where it had little effect. **d)** Potassium excretion was reduced significantly mice in *Hsd11b2*$^{+/-}$ mice on a standard sodium diet than in *Hsd11b2*$^{+/+}$ mice. High sodium diet caused a significant decrease in amiloride-sensitive potassium excretion in both genotypes; the response was comparable between genotypes. ***** P < 0.05; ****** P < 0.01; ******* P < 0.001. Data are means ± SEM.

between the genotypes (Figure 3.10a). Acute administration of amiloride produced no significant effects upon the GFR of the *Hsd11b2*$^{+/+}$ or *Hsd11b2*$^{+/-}$ groups on either the standard or the high sodium diet (Figure 3.10b).

Amiloride administration increased urinary sodium excretion for both genotypes on a standard sodium diet. The net effect amiloride was significantly greater in the *Hsd11b2*$^{+/-}$ mice compared to the *Hsd11b2*$^{+/+}$ mice (Figure 3.10c). On a high sodium diet amiloride-sensitive sodium reabsorbtion was abolished in *Hsd11b2*$^{+/+}$ mice; this is consistent with an appropriate down regulation of ENaC-mediated sodium reabsorbtion (Figure 3.10c). The *Hsd11b2*$^{+/-}$ mice, however, do not appear to be appropriately regulating their ENaC-mediated sodium reabsorbtion in response to the high sodium diet; the natriuretic response to amiloride was significantly greater than that of the *Hsd11b2*$^{+/+}$ mice (Figure 3.10c).

The effects of amiloride administration on potassium excretion were also measured. On a standard sodium diet, amiloride reduced potassium excretion for both genotypes, having a significantly greater antikaliuretic effect in the *Hsd11b2*$^{+/-}$ compared to the *Hsd11b2*$^{+/+}$ mice (Figure 3.10d). Amiloride had significantly less of an effect upon potassium excretion on the high sodium diet compared to the standard sodium diet (Figure 3.10d). The overall effect was similar for both genotypes, although the *Hsd11b2*$^{+/-}$ group showed a trend towards a greater reduction in potassium excretion than the *Hsd11b2*$^{+/+}$ group (not statistically significant).

3.2.5 Molecular Mechanisms - Benzamil Study

To further assess the contributions of ENaC activity towards the SS phenotypes of *Hsd11b2*$^{+/-}$ mice, metabolic cage and renal clearance studies described earlier in this chapter were repeated in *Hsd11b2*$^{+/+}$ and *Hsd11b2*$^{+/-}$

mice on a standard and a high sodium diet with the addition of chronic administration of the ENaC antagonist benzamil.

3.2.5.1 Metabolic Cage Studies

On a standard sodium diet, both *Hsd11b2*$^{+/+}$ and *Hsd11b2*$^{+/-}$ mice had comparable levels of urinary sodium excretion (Figure 3.11a). The rate of sodium excretion increased significantly for both groups when they were administered benzamil on the standard sodium diet, with values remaining comparable between the two groups (Figure 3.11a).

Sodium balance data for key periods both before and after high sodium diet administration illustrated that there were no differences in the sodium balance between the two genotypes at any point (Figure 3.11b). This suggests that benzamil administration is rescuing the impaired sodium excretion observed in *Hsd11b2*$^{+/-}$ mice on a high sodium diet (compare Figure 3.11b with 3.3c). Water balance also does not vary between the *Hsd11b2*$^{+/+}$ and *Hsd11b2*$^{+/-}$ groups at any stage during the study (Figure 3.11c).

3.2.5.2 Renal Clearance Studies

After three weeks on a high sodium diet with chronic benzamil administration, the MABP was similar between the two genotypes (Figure 3.12a); this suggests that benzamil administration is rescuing the high sodium diet-induced increases in BP observed in *Hsd11b2*$^{+/-}$ mice on a high sodium diet (compare Figure 3.12a with Figure 3.2 and 3.7). GFR was significantly greater for *Hsd11b2*$^{+/-}$ mice compared to *Hsd11b2*$^{+/+}$ mice (Figure 3.12b). These values were lower than on a high sodium diet alone, although the overall significant difference between the genotypes remains (compare Figure 3.12b with Figure 3.8a). This implies that the changes in sodium balance and MABP observed in *Hsd11b2*$^{+/-}$ mice with benzamil treatment are

a) Urinary Sodium Excretion - Benzamil Effects

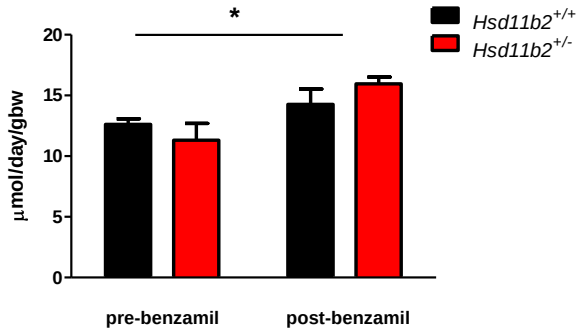

b) 3-Day Sodium Balances – Benzamil Effects

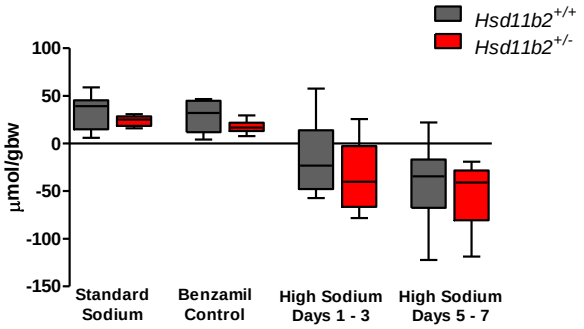

c) 3-Day Water Balances – Benzamil Effects

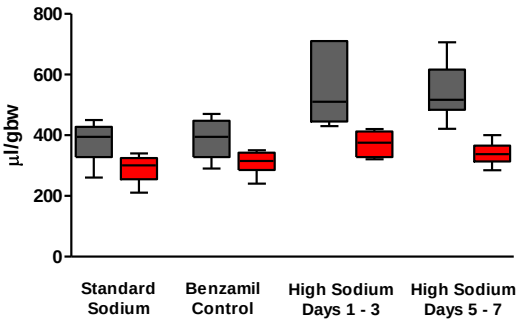

Figure 3.11. Benzamil treatment during a metabolic cage study (n = 6 for both groups). **a)** Urinary sodium excretion on a standard sodium diet before and after benzamil treatment; 3-day **b)** sodium and **c)** water balances before and after benzamil on a standard sodium diet, and with benzamil on a high sodium diet. Benzamil treatment on a standard sodium diet significantly increased urinary sodium excretion in both genotypes. There was no significant difference in terms of **b)** sodium balance or **c)** water balance between *Hsd11b2*$^{+/+}$ and *Hsd112b*$^{+/-}$ mice during any period. ***** P < 0.05. Data are means ± SEM (a) or medians and ranges.

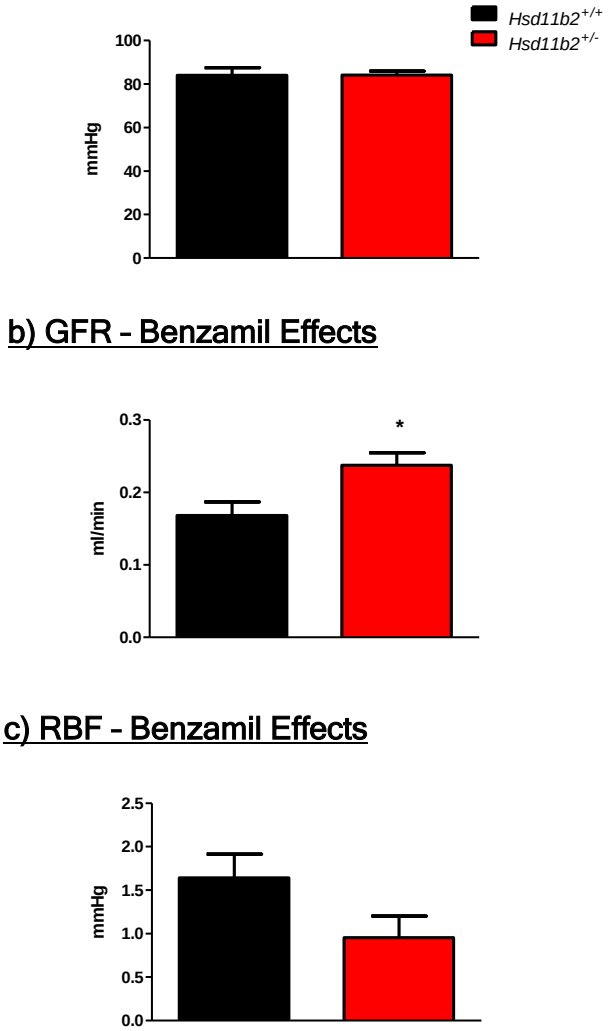

3.12. Benzamil treatment effects upon MABP and renal hemodynamics. MABP and renal hemodynamics were measured during renal clearance surgery in *Hsd11b2*$^{+/+}$ and *Hsd11b2*$^{+/-}$ mice after three weeks on a high sodium diet with benzamil treatment (n = 6 for both groups). **a)** MABP was equal between *Hsd11b2*$^{+/-}$ and *Hsd11b2*$^{+/+}$ mice. **b)** GFR was significantly greater in *Hsd11b2*$^{+/-}$ mice compared to *Hsd11b2*$^{+/+}$ mice. **c)** RBF was equal between *Hsd11b2*$^{+/+}$ and *Hsd11b2*$^{+/-}$ mice. ***** $P < 0.05$. Data are means ± SEM.

not mediated by changes in GFR.

There was a trend for the *Hsd11b2*$^{+/-}$ group to have a lower RBF than the *Hsd11b2*$^{+/+}$ group with benzamil treatment; however, this was not significant

(Figure 3.12c). The values for RBF for both groups were less than on a high sodium diet without benzamil treatment (compare Figure 3.12c with Figure 3.8b).

Benzamil treatment caused a increase in urinary sodium excretion in both genotypes compared to non-treatment on a high sodium diet (compare Figure 3.13a with Figure 3.9a). In addition, *Hsd11b2*$^{+/-}$ mice now excrete

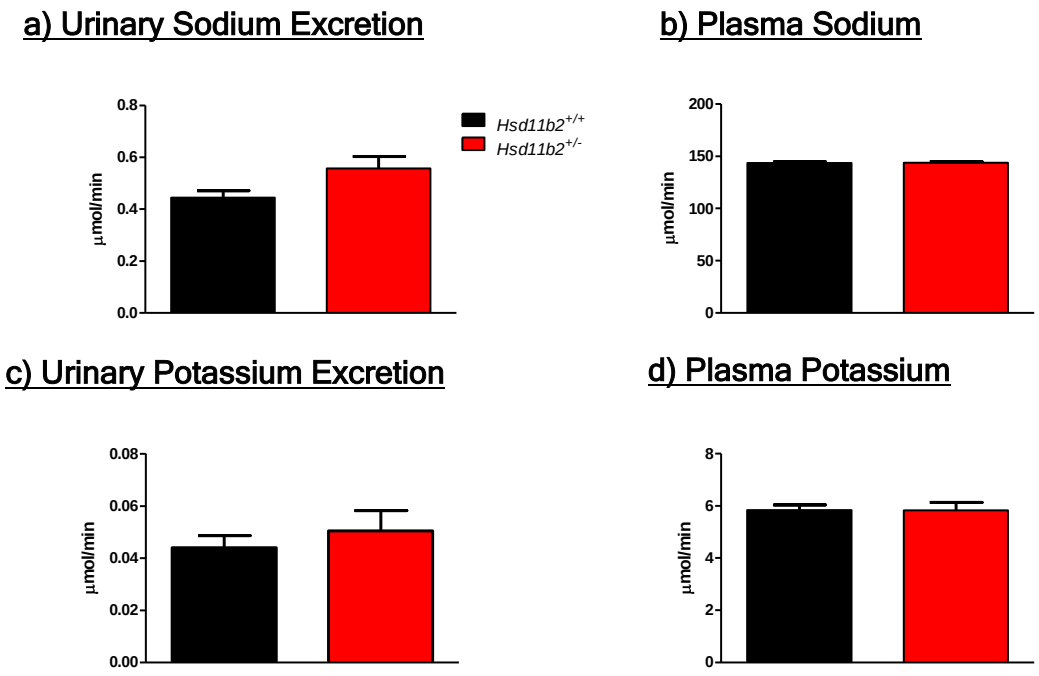

Figure 3.13. Urine and plasma electrolytes were measured during renal clearance surgery in *Hsd11b2*$^{+/+}$ and *Hsd11b2*$^{+/-}$ mice on a high sodium diet with benzamil treatment (n = 6 for both groups). There were no significant differences between *Hsd11b2*$^{+/+}$ and *Hsd11b2*$^{+/-}$ mice in terms of **a)** urinary sodium excretion, **b)** plasma sodium, **c)** urinary potassium excretion, or **d)** plasma potassium. Data are means ± SEM.

similar levels of urinary sodium compared with *Hsd11b2*$^{+/+}$ mice (Figure 3.13a). Potassium excretion was not altered by benzamil treatment in either group (Figure 3.13c compared to Figure 3.9b). Urinary potassium excretion was greatly down regulated on a high sodium diet with benzamil treatment compared to a high sodium diet alone (compare Figure 3.13c with Figure

3.9c); there was no significant difference between the two groups. The plasma potassium concentration of *Hsd11b2*$^{+/-}$ mice was greater after benzamil administration, resulting in the significant difference between the genotypes being abolished (compare Figure 3.13d with Figure 3.9d).

Values obtained after acute amiloride administration were not significantly different from the pre-amiloride values for any of the measured parameters in the renal clearance study for either genotype (data not shown). Thus, amiloride administration had no effect upon the physiology of these mice when they were receiving chronic benzamil administration; this can be attributed to the chronic mini pump dosing of benzamil being appropriate to completely inhibit ENaC activity.

3.2.6 Molecular Mechanisms - Spironolactone Study

To further assess the contributions of MR activation towards the SS phenotypes of *Hsd11b2*$^{+/-}$ mice, metabolic cage and renal clearance studies described earlier in this chapter were repeated in *Hsd11b2*$^{+/+}$ and *Hsd11b2*$^{+/-}$ mice on a standard and a high sodium diet with chronic administration of the MR antagonist spironolactone.

3.2.6.1 Metabolic Cage Studies

On a standard sodium diet, both *Hsd11b2*$^{+/+}$ and *Hsd11b2*$^{+/-}$ mice had equal levels of urinary sodium excretion (Figure 3.14a). Spironolactone administration on the standard sodium diet resulted in a decreased rate of urinary sodium excretion in *Hsd11b2*$^{+/+}$ mice compared with *Hsd11b2*$^{+/-}$ mice (Figure 3.14a).

Sodium balance data for key periods both before and after high sodium diet administration illustrated that there were no differences in the sodium

a) Urinary Sodium Excretion - Spironolactone Effects

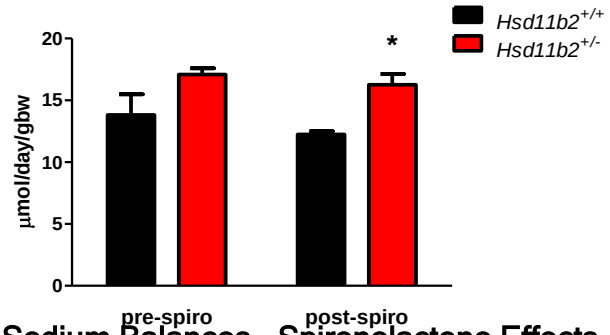

b) 3-Day Sodium Balances – Spironolactone Effects

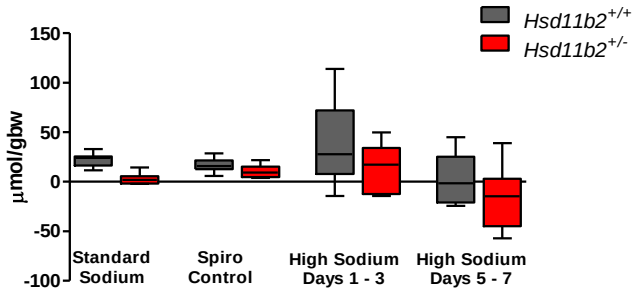

c) 3-Day Water Balances – Spironolactone Effects

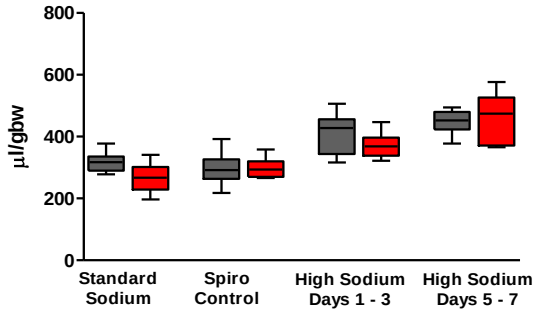

Figure 3.14. Spironolactone treatment during a metabolic cage study (n = 9 for both groups). **a)** Urinary sodium excretion on a standard sodium diet before and after spironolactone treatment; 3-day **b)** sodium and **c)** water balances before and after spironolactone on a standard sodium diet, and with spironolactone on a high sodium diet. Spironolactone treatment on a standard sodium diet caused a significant decrease in urinary sodium excretion in for *Hsd11b2*$^{+/+}$ mice compared to *Hsd11b2*$^{+/-}$ mice. There was no significant difference in terms of **b)** sodium balance or **c)** water balance between *Hsd11b2*$^{+/+}$ and *Hsd112b*$^{+/-}$ mice during any period. ***** $P < 0.05$. Data are means ± SEM for **a)**, and as the median, interquartile range and full range for **b)** and **c)**.

balance between the two genotypes at any point (Figure 3.14b). This suggests that spironolactone administration is rescuing the impaired sodium excretion observed in *Hsd11b2*$^{+/-}$ mice on a high sodium diet only (compare Figure 3.14b with 3.3c). Water balance also does not vary between the *Hsd11b2*$^{+/+}$ and *Hsd11b2*$^{+/-}$ groups at any stage during the study (Figure 3.14c).

3.2.6.2 Renal clearance studies

After three weeks on a high sodium diet with spironolactone administration, the MABP was significantly reduced for both *Hsd11b2*$^{+/-}$ and *Hsd11b2*$^{+/+}$ mice compared to a high sodium diet alone; the significant difference between the two genotypes remained (compare Figure 3.15a with Figure 3.7). This suggests that spironolactone treatment is causing a significant reduction in BP that is universal in spite of genotype and starting BP. There was no significant difference in the GFR values between the two groups with spironolactone treatment (Figure 3.15b). GFR was increased in *Hsd11b2*$^{+/+}$ mice on a high sodium diet with spironolactone treatment compared to a high sodium diet alone (compare Figure 3.15b and 3.8a); there was no change in *Hsd11b2*$^{+/-}$ GFR with spironolactone treatment. RBF was reduced in both genotypes with spironolactone treatment on a high sodium diet (compare Figure 3.15c with Figure 3.8b). Spironolactone abolished the significant effect of genotype upon RBF (Figure 3.15c).

Urinary sodium excretion was significantly increased with spironolactone administration on a high sodium diet compared to high sodium diet alone (compare Figure 3.16a with Figure 3.9a). A significant decrease in sodium excretion in the *Hsd11b2*$^{+/-}$ group compared with the *Hsd11b2*$^{+/+}$ group remained (Figure 3.16a). There was no difference between the two groups for plasma sodium concentration or urinary potassium excretion with spironolactone treatment, and these values did not differ significantly from

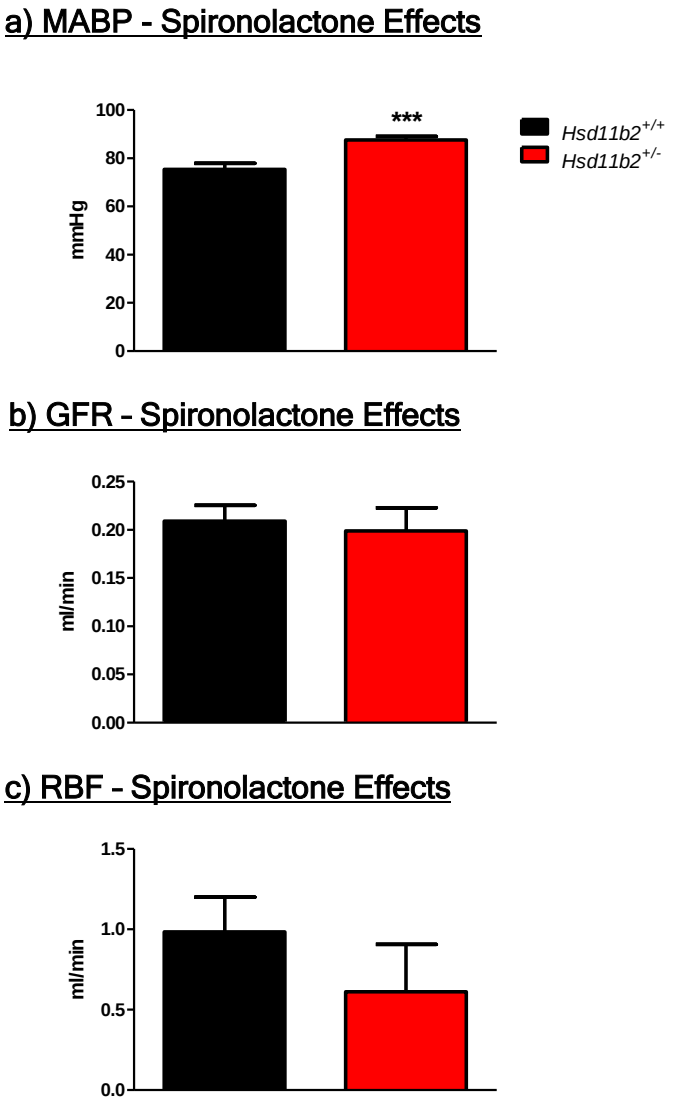

Figure 3.15. Spironolactone treatment effects upon MABP and renal hemodynamics. MABP and renal hemodynamics were measured during renal clearance surgery in *Hsd11b2*$^{+/+}$ and *Hsd11b2*$^{+/-}$ mice after three weeks on a high sodium diet with spironolactone treatment (n = 8 for both groups). **a)** MABP was significantly greater in *Hsd11b2*$^{+/-}$ mice compared to *Hsd11b2*$^{+/+}$ mice. **b)** GFR and **c)** RBF were equal between *Hsd11b2*$^{+/+}$ and *Hsd11b2*$^{+/-}$ mice. ******* $P < 0.001$. Data are means ± SEM.

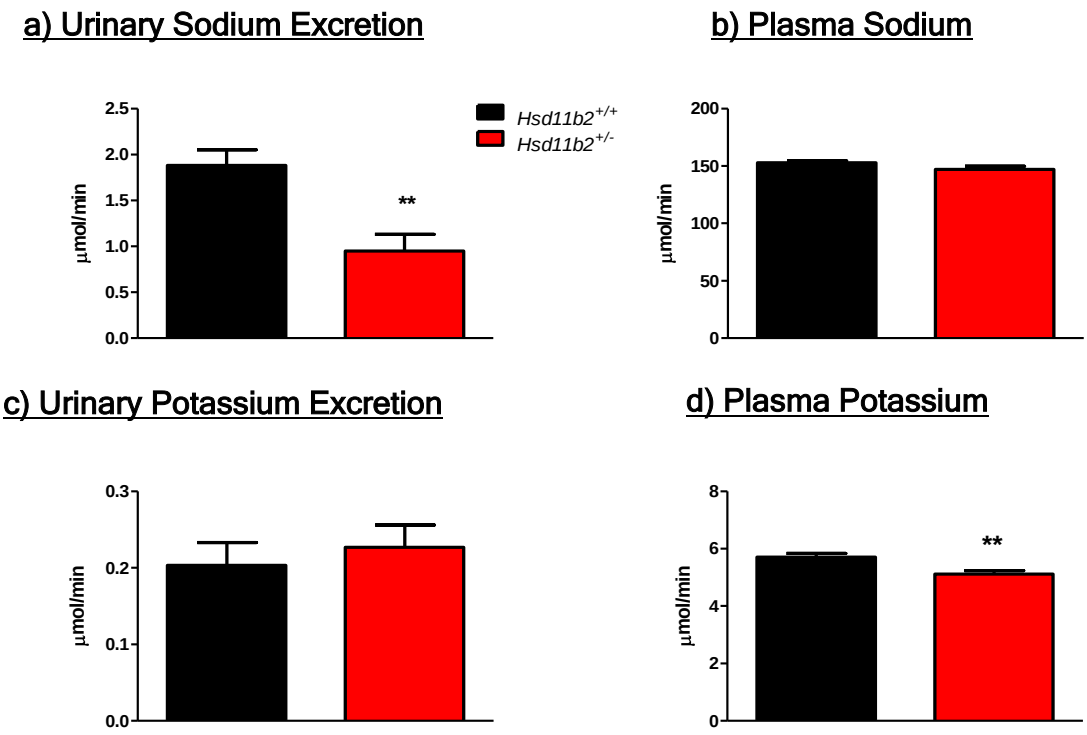

Figure 3.16. Urine and plasma electrolytes were measured during renal clearance surgery in *Hsd11b2*$^{+/+}$ and *Hsd11b2*$^{+/-}$ mice on a high sodium diet with spironolactone treatment (n = 8 for both groups). **a)** *Hsd11b2*$^{+/-}$ mice excreted significantly less sodium than *Hsd11b2*$^{+/+}$ mice. There were no significant differences between *Hsd11b2*$^{+/+}$ and *Hsd11b2*$^{+/+}$ mice in terms of **b)** plasma sodium, or **c)** urinary potassium excretion. **d)** *Hsd11b2*$^{+/-}$ mice had significantly lower plasma potassium levels compared to *Hsd11b2*$^{+/-}$ mice**.** ****** P < 0.01. Data are means ± SEM.

the high sodium diet only study (compare Figure 3.16b and c with Figure 3.9b and c, respectively). Plasma potassium levels were significantly lower for the *Hsd11b2*$^{+/-}$ mice than the *Hsd11b2*$^{+/+}$ mice, reflecting what is seen without spironolactone treatment on a high sodium diet (compare Figure 3.16d with Figure 3.9d).

3.3 Discussion

This chapter describes the discovery and initial characterisation of SS phenotypes of the *Hsd11b2*$^{+/-}$ mouse model. *Hsd11b2*$^{+/-}$ mice were first characterised in conjunction with the *Hsd11b2*$^{-/-}$ model when it was initially generated (Kotelevtsev et al., 1999). Using *Hsd11b2*$^{+/+}$ littermates as controls, investigations involving the three different genotypes found striking phenotypes associated with the *Hsd11b2*$^{-/-}$ animals that reflected the characteristics of SAME, the human genetic disorder associated with 11β-HSD2 ablation. Although the *Hsd11b2*$^{+/-}$ mice were found to have reduced 11β-HSD2 enzyme activity in placenta homogenates and reduced renal 11β-HSD2 mRNA expression, in terms of plasma electrolytes and BP they did not differ from the control *Hsd11b2*$^{+/+}$ group and displayed no obvious phenotypes (Kotelevtsev et al., 1999).

Interest in the possibility of reduced 11β-HSD2 enzyme activity having BP effects arises from epidemiological human studies that have shown HSD11B2 polymorphic variation is present within the general population (Bocchi et al., 2004). In addition, some research has highlighted a potential link between certain HSD11B2 polymorphisms and essential and/or SS hypertension (Alikhani-Koupaei et al., 2007; Mariniello et al., 2005). Furthermore other human studies into SAME type II (Mantero et al., 1996; Wilson et al., 1998) and heterozygosity in the families of SAME type I and II patients (Li et al., 1997; Li et al., 1998) have suggested that reduced 11β-HSD2 expression may be associated with hypertension. Together, these observations suggested that the *Hsd11b2*$^{+/-}$ mouse model could pose a more interesting model than the original characterising study would suggest, especially if challenged with a high salt dietary intake.

3.3.1 Hsd11b2 Heterozygous Mice Have a Salt-Sensitive Phenotype

3.3.1.1 Dietary Salt Intake and 11β-HSD2 Enzyme Activity

In the study that described the original characterisation of the *Hsd11b2*$^{+/+}$ model, 11β-HSD2 enzyme activity was measured in placental homogenates of *Hsd11b2*$^{+/+}$, *Hsd11b2*$^{+/-}$, and *Hsd11b2*$^{-/-}$ mice. *Hsd11b2*$^{+/-}$ mice were shown to have approximately 67% enzyme activity compared to *Hsd11b2*$^{+/+}$ mice (Kotelevtsev et al., 1999). In the current study renal 11β-HSD2 enzyme activity was measured using *Hsd11b2*$^{+/+}$ and *Hsd11b2*$^{+/-}$ kidney homogenates, and *Hsd11b2*$^{+/-}$ mice were found to have approximately 50% activity compared with the *Hsd11b2*$^{+/+}$ mice on both a standard and a high sodium diet (measured as the percentage conversion of corticosterone to deoxycorticosterone in the presence of NAD^+; Figure 3.1). A control using *Hsd11b2*$^{-/-}$ kidney homogenates in the same assay series showed conversion to be minimal (1.3 ± 0.14% conversion; data not shown); this is likely to reflect endogenous 11β-HSD1 dehydrogenase activity. This confirms that reduced functional allele number for *Hsd11b2* results in reduced renal enzyme activity in these transgenic mice. Also, the enzyme activity results indicate that dietary salt content has no effect upon *in vivo* 11β-HSD2 activity for either genotype.

Previous studies have had conflicting results as to whether or not there is an effect of dietary sodium content upon both 11β-HSD2 mRNA expression and enzyme activity (Franco-Saenz et al., 1999; Ingram et al., 1996; McKinnell et al., 2000). McKinnell *et al* reported that renal 11β-HSD2 enzyme activity was decreased in rats in a high sodium diet compared to a low sodium diet. However, studies into Hsd11b2 mRNA expression showed that in the medullary collecting ducts there was no change in expression between the

diets. Franco-Saenz *et al* compared renal Hsd11b2 mRNA expression between Dahl SS and SR rats on a low or a high sodium diet, and found that a high salt diet almost doubled Hsd11b2 mRNA expression in both rat strains compared to a low sodium diet. It must be highlighted that both of these studies were conducted by comparing low sodium diet values against those obtained on a high sodium diet. Clearly there will be a massive difference in sodium intake between the two diets in these studies; comparisons made during the current study are more reasonable as they are between normal and a high sodium diet conditions. In addition, the observation that one of these studies found a decrease in enzyme activity on a high sodium diet (and no change in mRNA levels) whereas the other found an increase in mRNA levels on a high sodium diet is inconsistent. Another study investigating the effects of dietary salt content upon 11β-HSD2 enzyme activity in human subjects (assessed as the urinary steroid metabolite ratio) found that their dietary sodium content had no effect upon 11β-HSD2 enzyme activity in non-hypertensive subjects (Ingram et al., 1996). Therefore, the current studies finding that a standard versus a high sodium diet has no effect upon 11β-HSD2 enzyme activity is relevant in terms of previously published studies.

3.3.1.2 Salt-Sensitive Blood Pressure

As the literature suggests that the hypertensive phenotype associated with 11β-HSD2 heterozygosity in humans was linked to high salt diet, the BP response of *Hsd11b2*$^{+/+}$ and *Hsd11b2*$^{+/-}$ mice exposed to a high sodium diet was investigated. In both conscious and anesthetised *Hsd11b2*$^{+/-}$ mice a high sodium diet was found to increase BP (SBP and MABP, respectively) compared to *Hsd11b2*$^{+/+}$ mice (approximately 10mmHg for measurements; Figure 3.2 and 3.7). *Hsd11b2*$^{+/+}$ mice did not display a SS-BP, an observation

in agreement with published works regarding the C57BL6 mouse strain (Ni et al., 2003; Ye et al., 2006).

The tail cuff SBP measurements for both genotypes on a standard sodium diet are greater than would normally be expected for a conscious mouse. This is most likely attributable to the stress of the mice being held in a restraint tube whilst the measurements are being made. This stress factor was reduced by training the mice to become used to handling and being held in the restraint tube (as described in Materials and Methods section; Chapter 2, section 2.3), but could not be completely removed. This was why it was important to validate these SBP findings with another BP measurement; MABP by carotid artery cannulation. The MABP values obtained were lower than the average MABP value for a mouse (approximately 110 mmHg at rest). This is due to the measurements being made under anaesthetic, which consequently leads to a reduction in MABP values. Although the values were lower than they would be in conscious animals, the differences observed between the genotypes remain characteristic of the SS BP phenotype, and consistent with the BP values obtained by tail cuff.

Overall, these results are direct evidence that reduced 11β-HSD2 activity is linked to SS BP in these mice. They validate indirect observations from human population studies suggesting a relationship between HSD11B2 polymorphisms affecting enzyme activity and SS and/or essential hypertension (Agarwal et al., 1994; Alikhani-Koupaei et al., 2007; Carvajal et al., 2005; Lovati et al., 1999; Mariniello et al., 2005).

3.3.1.3 Sodium Balance

Given the important role of sodium handling in SAME and other related corticosteroid disorders, it was reasonable to assume that sodium balance may be playing an important part in the SS phenotype of *Hsd11b2*$^{+/-}$ mice.

Measurements of urinary sodium excretion in conscious mice revealed that *Hsd11b2*$^{+/-}$ mice displayed a transient blunted natriuresis during the first few days of the diet regime, compared to the *Hsd11b2*$^{+/+}$ mice (Figure 3.3a). Differences in dietary sodium intake between the genotypes were not responsible for these observations as food intake was similar throughout (Figure 3.3b). These observations were reinforced by the 3-day sodium balance data (periods were divided into 3-day stages as the control data on the standard sodium diet was collected over 3 days), and suggest that *Hsd11b2*$^{+/-}$ mice are unable to excrete an increased dietary sodium load as efficiently as *Hsd11b2*$^{+/+}$ mice at the beginning of a high sodium diet regime.

Urinary sodium excretion results from the renal clearance experiments showed that after three weeks on a high sodium diet *Hsd11b2*$^{+/-}$ mice continue to excrete significantly less sodium than *Hsd11b2*$^{+/+}$ mice in an acute setting after three weeks on the high sodium diet (Figure 3.9a). This is in contrast to the 24 hour measurements, which show that the natriuresis of *Hsd11b2*$^{+/-}$ mice was equal to that of *Hsd11b2*$^{+/+}$ mice at this time point. Important differences between these two measurements are that one is obtained from unrestrained conscious animals over a 24 hour period, and the other under anaesthesia over a 40 minute period. Another difference is that during the renal clearance studies the ability of the kidney to handle sodium is being pushed beyond normal physiological circumstances due to the infusion of 0.9% saline. There is an implication that there may be a circadian regulation element to the discrepancy in sodium excretion. That is that *Hsd11b2*$^{+/-}$ mice may have an altered circadian rhythm in terms of sodium excretion and BP on a high sodium diet. Certainly in human subjects with SS hypertension, a "non-dipper" BP phenotype has been observed which is believed to enhance nocturnal pressure natriuresis so as to compensate for a diminished

natriuresis during the daytime (Kimura et al., 2010). In addition, balance studies from the 1970s using the DOCA-salt rat model highlighted a circadian rhythm of DOCA sodium positive balance escape (Mohring and Mohring, 1972; Mohring et al., 1970). It was observed in these studies that the sodium balance of the DOCA-salt rats returned to control values between 7pm – 7am after four days treatment, but that sodium retention persisted between 7am – 7pm. A circadian rhythm of sodium excretion may explain the discrepancies observed between these two collection types, and a division of the metabolic cage collections into 2 consecutive 12 hour periods per day would help to ascertain if there was a circadian element to the natriuresis phenotype of the *Hsd11b2*$^{+/-}$ mice.

The impaired sodium excretion of the *Hsd11b2*$^{+/-}$ mice during renal clearance studies was not accompanied by an increase in plasma sodium concentration compared to *Hsd11b2*$^{+/+}$ mice, as under conditions of both a standard and a high sodium diet, plasma sodium concentrations were similar between the two genotypes (Figure 3.9b). There was a significant increase in plasma sodium concentration on a high sodium diet compared to the standard sodium diet (Figure 3.9b), presumably a consequence of the increased dietary intake of sodium and corresponding with the increase in urinary sodium excretion that both genotypes display when moved to a high sodium diet. This observation ties in with the circadian non-dipper phenotype hypothesis, so that the BP of *Hsd11b2*$^{+/-}$ mice would be elevated in an effort to match the natriuresis of *Hsd11b2*$^{+/+}$ mice over a 24 hour period, thus maintaining stable plasma sodium levels at the expense of a high BP.

3.3.1.4 Water Balance

Water balance in terms of drinking water intake and UFR was analysed during the metabolic cage experiments. At all points of urine output, water

intake and overall water balance, there were no significant differences between the genotypes (Figure 3.4a, b and c). For both genotypes at all time points, the water balance was significantly different from zero, indicating that in relation to water intake and urinary output, the mice were always in a positive water balance. It must be taken into consideration that the measurement of any insensible water loss (such as from skin and lungs) and water loss from sweat (mice possess sweat glands in their feet) cannot be accounted for in these experiments. It is therefore unlikely that the mice were actually in such a positive water balance, especially as water loss from these other sources can be significant. However, what the water balance values do highlight is that there is no difference between the 2 genotypes even when the sodium balance is significantly positive for the *Hsd11b2*$^{+/-}$ mice during the initial high sodium diet period (Figure 3.3c and 3.4d). The traditional view is that sodium accumulation is accompanied by water retention which can lead to an increase in extracellular volume (ECV) and an increased BP. Generally, the kidneys are responsible for the regulation of ECV so as to maintain a stable BP by controlling total body sodium content. However evidence is accumulating to suggest that large amounts of sodium can be accumulated without water retention accompanying it (Titze, 2009). In particular, studies performed in rats have found that during high salt diet feeding the accumulation of sodium storage in the skin is increased, and suggest that the skin is an osmotically inactive sodium reservoir that accumulates sodium when dietary sodium is in excess (Titze et al., 2003). Of particular interest it has been found that sodium accumulation is excess in comparison to water accumulation in a model of mineralocorticoid excess (the deoxycorticosterone acetate (DOCA)-salt rat); 75 – 80% of sodium retention was found to be in abundance over water (Titze et al., 2005). This

was contributed towards by both osmotically inactive skin storage and an osmotically neutral sodium retention balance by potassium loss, thus allowing for maintenance of ECV homeostasis despite an increased total body sodium accumulation. Therefore, the absence of any significant difference between the water retention of the two genotypes does not necessarily mean that the *Hsd11b2*$^{+/-}$ mice are not in a positive sodium balance.

The one aspect where there was a difference in terms of water excretion between the two genotypes is with regards to faecal water content (Figure 3.4d). On a standard sodium diet, the *Hsd11b2*$^{+/-}$ mice had significantly less water content in their faeces compared to the *Hsd11b2*$^{+/+}$ mice. Once placed on a high sodium diet both genotypes significantly decreased their faecal water content to similar levels (Figure 3.4d). This suggests that faecal water content is tightly regulated by an increase in dietary sodium in both genotypes. 11β-HSD2 expression is well documented in epithelial cells of the colon, where it is assumed to play a protective role in MR activation, analogous to the kidney (Fuller and Verity, 1990; Moore et al., 2000). It is possible that under normal dietary conditions the *Hsd11b2*$^{+/-}$ model is displaying increased colonic water reabsorbtion (reflected by a reduced level of faecal water content) due to inappropriate activation of MR/GR target genes. Overall, faecal water loss is normally quite small, and the comparison of the volume urine produced and the faecal water content during these experiments highlights this (compare Figure 3.4a and d). For this reason (and because there is no difference in faecal water content once the animals are placed on a high sodium diet) faecal water measurements were excluded from total water balance calculations.

3.3.1.5 Potassium Balance

The differences observed for dietary potassium intake for both groups of mice when they are moved from a standard to a high sodium diet are most likely due to a difference in the dietary potassium content of the two sodium diets (Figure 3.5a). The potassium content of the standard sodium diet was 0.67%, and in the high sodium diet this was slightly less at 0.5%. However, this 0.16% difference in potassium content is enough to cause a significant difference in the dietary potassium intake between the two diets; this is not due to the mice eating less food over all on the high sodium diet as this was not significantly different (see Figure 4.9c). A decrease in potassium intake can trigger a decrease in aldosterone secretion (Williams, 2005), but as the lower potassium dietary content is being administered in conjunction with very high levels of dietary sodium intake, it is unlikely that these small changes in potassium intake would have any significant effect in comparison the large changes for sodium.

In the 24 hour metabolic cage urine samples there was no difference in the potassium excretion between the two genotypes on a standard sodium diet, and the *Hsd11b2*$^{+/-}$ mice excreted significantly less than the *Hsd11b2*$^{+/+}$ mice for the entire high sodium diet period (Figure 3.5b). This is in contrast to the renal clearance urinary potassium excretion values, where on a standard sodium diet the *Hsd11b2*$^{+/-}$ mice excreted significantly more urinary potassium than the *Hsd11b2*$^{+/+}$ mice, and on a high sodium diet there was no difference between the two groups; both had significantly down-regulated their potassium excretion compared to standard diet conditions (Figure 3.9c). These contrasting results may relate back to the comments made in relation to sodium excretion regarding the circadian rhythm of electrolyte excretion, and how this may be altered in the *Hsd11b2*$^{+/-}$ mice on a high sodium diet,

and so we will now refer to urinary potassium excretion as the 24 hour metabolic cage values.

Overall, the plasma potassium levels are also conflicting in terms of the urinary excretion profile; values are similar between genotypes on a standard sodium diet, and *Hsd11b2*$^{+/-}$ mice display a significantly lower plasma concentration compared to *Hsd11b2*$^{+/+}$ mice on a high sodium diet (Figure 3.9d). This suggests that even though the *Hsd11b2*$^{+/-}$ mice are excreting less urinary potassium on a high sodium diet, they also possess a lower plasma potassium concentration, compared to *Hsd11b2*$^{+/+}$ mice. The reduced plasma potassium levels are consistent with the phenotypes reported for SAME patients and the *Hsd11b2*$^{-/-}$ mouse model, where hypokalemia accompanies hypertension. However, if the potassium lost from the extracellular fluid (ECF) is not being excreted in the urine, then where is it moving to? It is known that excess aldosterone can cause potassium to move from the ECF into the intracellular fluid (ICF), particularly of muscle cells, which ultimately leads to a decrease in plasma potassium levels (McDonough et al., 2002). These ICF stores act as a buffer against unregulated increases in ECF potassium concentrations. This could be due to an MR-mediated increase in Na-K-ATPase expression and activity in skeletal muscle tissue. Although aldosterone is very low in *Hsd11b2*$^{+/-}$ mice on a high sodium diet, we have demonstrated that corticosterone levels are greatly increased, so perhaps this is stimulating increased Na-K-ATPase potassium uptake in muscle ICF via activation of both the MR and the GR (which also mediates Na-K-ATPase expression).

Faecal potassium excretion was not assessed during these studies, and so altered excretion and/or reabsorption by this route cannot be discounted as contributing towards these results. In particular, the omission of these

values may explain the positive potassium balance observed for both genotypes at all periods assessed (Figure 3.5c).

3.3.1.6 Renal Hemodynamics

The GFR represents the volume of fluid filtered by the kidneys from the plasma per unit of time. GFR can be measured using a substance that is feely filtered at the glomerular filtration barrier from plasma, but is neither reabsorbed nor secreted within the renal tubules. A classic example of such a substance is the naturally occurring plant polysaccharide inulin, whose clearance from plasma can be used as a direct measurement of GFR. Under the experimental conditions of renal clearance, it is possible to directly infuse inulin into the jugular vein at a known concentration rate, and to measure its clearance as a fraction of how much is measured in the plasma and the urine at a certain time point (see Materials and Methods chapter for further details). Variation in GFR is a crucial determinant of renal function, as it will effect fundamental changes in renal hemodynamics.

After three weeks on both the standard and the high sodium diet, *Hsd11b2*$^{+/-}$ mice had a greater GFR than *Hsd11b2*$^{+/+}$ mice (Figure 3.8a). There was also an overall effect of diet upon GFR in the *Hsd11b2*$^{+/+}$ mice who had a lower GFR on the high compared to the standard sodium diet. This did not happen with the *Hsd11b2*$^{+/-}$ group. Deciphering these results on their own is complicated as there are many variables that contribute towards the GFR, as with any capillary filtration barrier. The GFR is determined by the net filtration pressure as well as the permeability and the surface area of the capillaries. Increased GFR in the *Hsd11b2*$^{+/-}$ group is suggestive of increased (renal) arterial pressure and/or increased efferent arteriole resistance i.e. changes to hydrostatic pressure. Nonetheless, without knowing more about other factors of the renal hemodynamics it is impossible to say what exactly

is causing the changes observed here. GFR will also be increased if the kidneys themselves are physically are larger. However, analysis of kidneys weights from the two genotypes shows that they are the same size regardless of genotype or diet (data not shown).

In order to try and establish the causes of the altered GFR in Hsd11b2$^{+/-}$ mice, other renal hemodynamic parameters were investigated. The kidney receives the highest blood flow of any organ in the body. This high supply of blood is to supply enough plasma for high rates of GFR to be sustained, which in turn is required to allow the kidneys to constantly monitor and adapt to any changes in electrolyte and water balance. Thus, the mechanisms that regulate RBF are similar to those that govern GFR. RBF is determined by the renal arterial pressure and the contractility of the smooth muscle of the renal arterioles. As it is plasma that is filtered at the glomerular filtration barrier, not blood, RBF is calculated using effective renal plasma flow (RPF) and hematocrit values (see Material and Methods Chapter for further details). Effective RPF can be measured in renal clearance experiments by infusing the substance *p*-aminohippuric acid (PAH), and measuring its subsequent concentration in both plasma and urine. PAH is suitable for these measurements as it is freely filtered at the glomerulus, and almost all that is not filtered is secreted by the renal tubule within one systemic circulation of blood. This results in a very high extraction ratio (>90%), giving an accurate representation of the volume of plasma that the kidney is filtering per unit of time.

There was no difference in the RBF on a standard sodium diet between the *Hsd11b2*$^{+/+}$ and *Hsd11b2*$^{+/-}$ groups of mice (Figure 3.8b). However, after three weeks on a high sodium diet, the *Hsd11b2*$^{+/-}$ group had a significantly lower RBF compared to the *Hsd11b2*$^{+/+}$ group. Thus, RBF was affected by a high

sodium diet in the *Hsd11b2*$^{+/-}$ mice. The changes in the GFR and RBF of both genotypes on different sodium diets were reflected in the filtration fraction (FF) calculations; FF represents the fraction of renal plasma flow that is filtered through the glomerular capillaries and is calculated as a ratio of the GFR and the RPF. On a standard sodium diet, the FF was similar for the two groups, implying that the difference in GFR was not significantly affecting FF as a result of similar RBF being maintained (Figure 3.8c). On high sodium diet, the FF of the *Hsd11b2*$^{+/+}$ mice decreases, reflecting the decrease in GFR, whereas the *Hsd11b2*$^{+/-}$ mice have a highly significant increase in FF after three weeks on a high sodium diet, presumably a consequence of the significant decrease in RBF under these conditions.

Auto regulation feedback mechanisms are in place to keep the GFR and RBF relatively constant when the system is faced with changes in BP. This in turn is designed to keep the levels of water and solutes within balance by controlling their renal excretion. The increased GFR in the *Hsd11b2*$^{+/-}$ mice compared to the *Hsd11b2*$^{+/+}$ mice is present regardless of dietary sodium content. This suggests that this genotype has a compensatory increase in GFR which maintains a normal BP under conditions of standard sodium diet. However, when moved to a high sodium diet, the increase in GFR is still observed, but it is now accompanied by an increase in MABP and decrease in RPF. This could be indicative of changes within renal vascular resistance (RVR), in that either or both the efferent and afferent arterioles are different.

Indeed when RVR was calculated, values for both genotypes were equal on a standard sodium diet (when RBF and MABP are also equal), and high sodium diet had no effect upon *Hsd11b2*$^{+/+}$ mice (when RBF and MABP also remain the same). However, the *Hsd11b2*$^{+/-}$ mice displayed a significant increase in RVR on a high sodium diet, which corresponds with their

decreased RBF and increased MABP under such conditions (Figure 3.8d). This suggests that the renal vasculature is contracted in the *Hsd11b2*$^{+/-}$ mice on a high sodium diet, although it is not possible to deduce whether this is occurring in the efferent or the afferent arteriole from these experiments. 11β-HSD2 activity is present in arteriole smooth muscle cells (Hatakeyama et al., 2001) and also vascular endothelial cells (Gong et al., 2008), and the contractile response of the vasculature has been linked to glucocorticoid metabolism (Souness et al., 2002). In addition, on a mixed MF1 background, *Hsd11b2*$^{-/-}$ mice were found to have enhanced vascular constriction to norepinephrine, and their relaxation response was also impaired (Hadoke et al., 2001); it must however be pointed out that these observations may have been attributable to the mixed strain background of these mice, as on a congenic C57Bl6/J background these experiments are not reproducible (Bailey et al., 2008). This implies that 11β-HSD2 expression in tissues other than the kidney may be significantly contributing towards the SS BP phenotype of *Hsd11b2*$^{+/-}$ mice.

3.3.2 Steroids

The phenotype of the *Hsd11b2*$^{+/-}$ mice on a high sodium diet ultimately arises from a deficiency of 11β-HSD2 enzyme activity, and presumably this has effects upon the availability, occupancy, and activation of the MR to both aldosterone and corticosterone. Therefore, measuring the concentrations of these two hormones in both the urine and plasma of the animals on both sodium diets was undertaken in the hope of gaining further insights into the mechanisms underlying the observed phenotypes.

Under standard diet conditions, the plasma and urine aldosterone levels of *Hsd11b2*$^{+/-}$ mice were significantly lower than for *Hsd11b2*$^{+/+}$ mice (Figure 3.6a

and b). This suggests that during standard diet conditions, when no BP or sodium excretion phenotype is present, reduced 11β-HSD2 activity is resulting in a suppressed RAAS. Presumably, this is a consequence of enhanced MR activation under basal conditions due to reduced receptor protection by 11β-HSD2. A decrease in aldosterone typically reflects a down-regulated RAAS.

When the two groups of mice were moved onto a high sodium diet, they both down-regulated their urinary and plasma aldosterone concentrations, as is appropriate for the increase in dietary sodium intake (Figure 3.6a and b). The urinary aldosterone concentration decreased at Days 1 - 3 of the high sodium diet, and then was decreased even further at Days 11 - 15 for both genotypes (Figure 3.6b). The plasma aldosterone concentrations were measured after three weeks on either the standard or the high sodium diet, and were significantly less for both groups on the high sodium diet. In particular, the plasma concentrations of the *Hsd11b2*$^{+/-}$ group were very low on a high sodium diet. This implies that it is not aldosterone acting at the MR that is responsible for the phenotypes observed in the *Hsd11b2*$^{+/-}$ mice on a high sodium diet.

Plasma and urinary corticosterone levels were similar for both genotypes on a standard sodium diet (Figure 3.6c and d). In terms of urinary concentration, there was a significant increase for both genotypes at Days 1 - 3 of the high sodium diet, and similar levels at Day 11 - 15 also (Figure 3.6d). For the high sodium diet periods investigated, the *Hsd11b2*$^{+/-}$ mice had a significantly greater urinary corticosterone concentration than the *Hsd11b2*$^{+/+}$ mice. Plasma corticosterone concentration was also increased for the *Hsd11b2*$^{+/-}$ group after three weeks on a high sodium diet compared to a

standard sodium diet, but did not change for the *Hsd11b2*$^{+/+}$ group (Figure 3.6c).

When these steroid concentration data are analysed together, they suggest that it is increased corticosterone levels in the *Hsd11b2*$^{+/-}$ mice that are responsible for the observed phenotypes, and not aldosterone; although that is not to say that the reduced aldosterone levels are not having effects upon other physiological parameters in these mice, such as potassium balance, as discussed previously. The increased levels of corticosterone observed in the *Hsd11b2*$^{+/-}$ mice on a high sodium diet are likely to be either the result of increased corticosterone synthesis or decreased metabolism (presumably caused by a decrease in 11β-HSD2 activity). In addition, in is important to point out that the increase in corticosterone may also be over activating GRs as well as MRs. Therefore, the observed phenotypes could be a consequence of activation of either steroid receptor, or a combination of both. The properties of both aldosterone and corticosterone, and their respective regulatory systems, are investigated in more detail in Chapter 4.

3.3.3 Molecular Mechanisms

Although metabolic cage and renal clearance studies can assess and provide valuable insights into the function of many different renal processes, alone they are not sufficient to identify the contributions of specific nephron segments towards the observed phenotypes i.e. it is not possible to ascertain the nephron site(s) responsible for enhanced sodium reabsorption. In order to dissect this further, the potent ENaC blocker amiloride, and its derivative benzamil, were administered acutely and chronically, respectively. In addition, the MR antagonist spironolactone was also administered

chronically to the mice during a three week period of high sodium diet feeding.

3.3.3.1 Acute ENaC Blockade

ENaC is responsible for the reabsorption of sodium across the apical membrane of cells in the ASDN (see Figure 1.3). ENaC expression and activity have been shown to be regulated by MR activation (Snyder, 2005). As ENaC deregulation is known to be important in the pathogenesis of hypertension due to its involvement in sodium renal reabsorption, we decided to investigate the potential role of this sodium transporting channel in the *Hsd11b2*$^{+/-}$ SS phenotype. To do this, measurements made during the renal clearance studies (as described above) were repeated in the same animals after intravenous administration of the ENaC blocker amiloride.

Amiloride administration caused a significant decrease in MABP for both groups of mice on a high sodium diet compared to a standard sodium diet (Figure 3.10a). A change this rapid in MABP is unlikely to be due to amiloride effects upon renal sodium transport. The explanation may come in the form of ENaC expression in the central nervous system (CNS), and their suggested contribution towards the pathogenesis of SS hypertension (Abrams and Osborn, 2008). It is possible that the I.V. dose of amiloride is blocking these receptors in the CNS and that this is having an immediate impact upon the MABP. Why this response is exaggerated on a high sodium diet is unclear. The doses of amiloride administered in this study are unlikely to be affecting any other sodium transporters, as they have previously been rigorously tested for this (Dr. Matthew Bailey, unpublished results).

There was no significant change in GFR due to amiloride administration in either genotype on either sodium diet (Figure 3.10b), but there was for

sodium excretion (Figure 3.10.c); this demonstrates that these effects of amiloride upon sodium excretion are due to ENaC and not a change in GFR. The ENaC-mediated sodium reabsorption of the *Hsd11b2*$^{+/-}$ mice is significantly greater than that of the *Hsd11b2*$^{+/+}$ mice on a standard, suggesting that they have a greater expression and/or activity of ENaC under normal conditions. After three weeks on a high sodium diet, the difference between the two groups in terms of ENaC mediated sodium reabsorption becomes even more pronounced. The *Hsd11b2*$^{+/+}$ mice completely down-regulate their ENaC-mediated sodium reabsorption under the high sodium conditions, which is to be expected as the suppression of the RAAS due to high sodium intake reduces both ENaC expression and activity. The *Hsd11b2*$^{+/-}$ mice however do not down-regulate their ENaC-mediated sodium reabsorption, and it remains at level similar to that on a standard sodium diet; these levels are completely inappropriate for the level of dietary sodium intake and the plasma concentration of aldosterone. Therefore, this demonstrates that in the face of a high sodium diet and a greatly suppressed RAAS, the *Hsd11b2*$^{+/-}$ mice are still capable of maintaining significant levels of ENaC-mediated sodium reabsorption; that is ENaC are deregulated. This is highly suggestive of the increased levels of glucocorticoids observed in these mice playing a role in the regulation of ENaC, either via the MR or the GR, or more likely a combination of both.

Potassium excretion was significantly down-regulated in the *Hsd11b2*$^{+/-}$ compared to the *Hsd11b2*$^{+/+}$ mice on a standard sodium diet after amiloride administration (Figure 3.10d). The bigger difference in potassium excretion is most likely a due to the fact that they excrete more potassium under the renal clearance conditions on a standard sodium diet anyway (see above for discussion of potassium balance). The observation that both genotypes have

little change in their ENaC-mediated potassium excretion on a high sodium diet in response to amiloride is again reflective of the fact that both groups excrete significantly less potassium on a high sodium diet during these experiments.

3.3.3.2 Chronic ENaC Blockade

The results of acute ENaC blockade during renal clearance studies highlighted a potential role for the sodium channel in the pathogenesis of the SS phenotype in *Hsd11b2*$^{+/-}$ mice. In order to investigate this further, a chronic ENaC blockade study was designed whereby the ENaC blocker benzamil (a potent amiloride derivative) was administered continuously to both groups of mice during both a standard and a high sodium diet feeding regime during a metabolic cage study. A consistent administration of benzamil was achieved by surgical implantation of an osmotic mini-pump that would deliver the drug at a continuous rate for up to 4 weeks (see Materials and Methods Chapter for further details). After three weeks on a high sodium diet these mice were prepared for renal clearance.

The effects of benzamil administration caused a significant increase in urinary sodium excretion on a standard sodium diet during the metabolic cage control period (Figure 3.11a). This shows that the benzamil dose administered is sufficient to cause ENaC blockade, as reflected in an increased sodium excretion. Benzamil administration attenuated the positive sodium that had been previously observed in the *Hsd11b2*$^{+/-}$ mice for the first 3 day period on a high sodium diet, and there is no difference in water balance at any period between the two genotypes, as before (Figure 3.11b and c). Benzamil administration also attenuated the effects of a high sodium diet upon the MABP of *Hsd11b2*$^{+/-}$ mice, and both groups had similar values for MABP (Figure 3.12a). This suggests that increased sodium reabsorption

due to deregulated ENaC activity is important in the development of SS BP increase in *Hsd11b2*$^{+/-}$ mice. Benzamil administration does not however rescue the increased GFR of *Hsd11b2*$^{+/-}$ mice on a high sodium diet; this was not entirely surprising as the elevated GFR phenotype is observed in these mice on a standard sodium diet, and is therefore not due an increase in dietary sodium intake. The effects of a high sodium diet upon the RBF of *Hsd11b2*$^{+/-}$ mice are attenuated with benzamil treatment (Figure 3.12c) further emphasising the role of a high sodium diet in modifying the vascular reactivity of these mice.

In terms of urinary and plasma sodium and potassium measured during renal clearance studies, there was no difference for any of these measurements during the administration a high sodium diet with benzamil treatment (Figure 3.13), suggesting that the deregulation of these parameters in *Hsd11b2*$^{+/-}$ mice is due to ENaC function. The efficacy of the benzamil administration upon ENaC blockade was tested by administering an acute dose of amiloride during renal clearance studies, as before. There was no difference for any of the parameters measured for either genotype with amiloride administration, and so the dosing of benzamil was deemed to be sufficient for full ENaC blockade.

Both the acute and chronic blockade of ENaC with amiloride and benzamil, respectively, has highlighted the important role of deregulation of this sodium channel towards the phenotype of the *Hsd11b2*$^{+/-}$ mice. The deregulated activity of ENaC is undoubtedly due to the inappropriate over activation of the MR by corticosterone due to reduced 11β-HSD2 activity, and may also be contributed to by increased activation of the GR due to high levels of circulating corticosterone in these mice on a high sodium diet. Other contributing factors could be the deregulation of other proteins that

themselves act to regulate ENaC trafficking and activity, such as Nedd4-2 (Kamynina et al., 2001) and the WNKs (Huang and Kuo, 2007), both of which are also regulated by MR and GR transcription.

3.3.3.3 Chronic MR Blockade

The ENaC blockade studies demonstrate that regulation of this channel is deregulated in the *Hsd11b2*$^{+/-}$ mice and contributes towards their SS phenotype. In addition, both plasma and urinary steroid measurements suggest that an elevation in corticosteroid levels on a high sodium diet are also contributing towards their phenotype. As both ENaC density and activity can be regulated by MR activity, MR over activation due to reduced 11β-HSD2 activity and increased corticosteroid levels is a possible molecular mechanism for the SS phenotypes of *Hsd11b2*$^{+/-}$ mice. To investigate this further, a chronic MR blockade study was designed whereby the MR antagonist spironolactone was administered continuously to both *Hsd11b2*$^{+/+}$ and *Hsd11b2*$^{+/-}$ mice during standard and high sodium diet feeding regime during a metabolic cage study. A consistent administration of spironolactone was achieved by surgical implantation of an osmotic mini-pump, as with the benzamil study (see Materials and Methods Chapter for further details). After three weeks on a high sodium diet these mice were prepared for renal clearance.

The administration of spironolactone on a standard sodium diet during control metabolic cage collections caused a significant natriuresis in the *Hsd11b2*$^{+/-}$ mice compared to the *Hsd11b2*$^{+/+}$ mice (Figure 3.14a). This suggests that MR activation is contributing towards sodium reabsorption in the *Hsd11b2*$^{+/-}$ mice on a standard diet. Spironolactone administration has previously been shown have mild natriuretic effects (Sica, 2005). Spironolactone administration alleviated the significantly positive sodium

balance of *Hsd11b2*$^{+/-}$ mice on a high sodium diet, and there were no differences between the two genotypes for water balance (Figure 3.14b and c).

Although spironolactone reduced the MABP of *Hsd11b2*$^{+/-}$ after three weeks on a high sodium diet compared to a high sodium diet alone by approximately 14 mmHg (87.5±1.54 versus 101.4±2.11, respectively), it also reduced the MABP of *Hsd11b2*$^{+/+}$ mice by a similar amount (75.4±2.43 versus 89.95±2.4, respectively). Therefore, the effects of spironolactone are having a BP lowering effects of a similar magnitude regardless of genotype, and so the BP reducing effects seen here are not indicative of a "rescued" *Hsd11b2*$^{+/-}$ SS phenotype as a result of MR blockade. This is unusual as the BP lowering effects of spironolactone are well reported within hypertensive population studies (Nishizaka et al., 2003) but would not be expected to take place in normotensive subjects, such as the *Hsd11b2*$^{+/+}$ mice (Pratt et al., 2001). Another interesting observation is that although at first it appears that spironolactone administration had attenuated the increased GFR and decreased RBF of *Hsd11b2*$^{+/-}$ mice compared to *Hsd11b2*$^{+/+}$ mice on a high sodium diet (Figure 3.15b and c) it actually appears as though the spironolactone dosing has altered these parameters in the *Hsd11b2*$^{+/+}$ mice to give similar values to those of the *Hsd11b2*$^{+/-}$ mice.

In terms of urinary excretion and plasma concentrations of sodium and potassium, spironolactone would be expected to increase sodium excretion and decrease potassium excretion so that plasma potassium concentration increases. A common side-effect of spironolactone treatment in hypertensive patients is the onset of hyperkalemia due to decreased potassium excretion (a consequence of reduced ENaC and Na-K-ATPase activity under MR blockade) (Jansen et al., 2009). Although urinary excretion is increased

approximately 10-fold with spironolactone administration on a high sodium diet compared to without under renal clearance conditions (Figure 3.16c), the significant difference between the two genotypes remains, and plasma sodium levels are as without spironolactone treatment. Most strikingly, potassium excretion and plasma potassium levels are largely unaltered with spironolactone treatment (Figure 3.16c and d).

The unexpected results observed with spironolactone treatment prompted further investigation of the dosing regime by analysing terminal plasma samples from the mice for the presence of the spironolactone active metabolite, canrenone, by MS analysis (see Materials and Methods chapter). Canrenone is measured rather than spironolactone itself as the plasma concentration half life of spironolactone is 1.4 days compared to 16.5 days for canrenone (Sica, 2005). Canrenone was undetectable in the terminal plasma samples of all spironolactone-treated mice (data not shown). This suggests that the dosing regime adapted for use from the published study by MacDonald *et al* was not suitable for these experiments and that full MR blockade was not being achieved (MacDonald et al., 2000). This means that it is possible the vehicle solution of DMSO and propylene glycol used to solubilise spironolactone for the mini-pump dosing (spironolactone is notoriously difficult to solubilise in aqueous fluids (Sica, 2005)) may be having physiological effects. Although administration of this vehicle by mini-pump was reported not to cause any significant physiological changes in the original study (MacDonald et al., 2000), as vehicle control experiments were not performed here, there is a distinct possibility that the vehicle may be causing some of the effects observed here. A study that used a sheep model to investigate the cardiovascular effects of water-miscible solvents that are routinely used as drug carriers placed DMSO as causing a moderate

effect, and propylene glycol as having a marked effect (Laurent et al., 2007). In addition, DMSO is known to have significant effects upon membrane permeability (Jacob and de la Torre, 2009; Notman et al., 2006) which had been shown to promote the osmotic absorption of fluid in microvessels *in vitro* (Glass et al., 2006). Therefore, the effects of the spironolactone vehicle could well be having phenotypic effects that, in addition to the dosing of spironolactone being too low, are also responsible for the phenotypes observed in this study.

Although there was not enough time within the scale of these studies to repeat the chronic MR blockade with spironolactone in a different dosing regime, these experiments have since been successfully carried out. The spironolactone dosing was improved by dissolving the drug into silicon pellet and implanting this subcutaneously into the mice; canrenone measurements showed there was significant levels in their plasma. For further details, see the submitted manuscrpublished scientific paper in Appendix 2 of this thesis.

3.3.4 Summary

In summary, studies described within this chapter have proved that reduced enzyme activity of 11β-HSD2 in *Hsd11b2*$^{+/-}$ mice is responsible for a SS phenotype. Salt sensitivity in this model is associated with an increased BP, impaired sodium excretion and a failure to regulate ENaC-mediated sodium reabsorption appropriately for salt and steroid status. These phenotypes are observed in combination with changes to renal hemodynamics, and aldosterone and corticosteroid concentrations. Investigations into the molecular mechanisms underlying these phenotypes have shown ENaC blockade to alleviate symptoms. Unfortunately, a study investigating MR blockade gave indefinite data. Therefore, the molecular mechanisms behind

this SS phenotype need to be investigated in more detail; further studies of this thesis will investigate the effects of *Hsd11b2* heterozygosity on BP and steroid profiles (chapter 4), also and its effects upon steroid receptor regulation by a high sodium diet in terms of oxidative stress (chapter 5).

Chapter 4

Mineralocorticoid and Glucocorticoid Regulation

4.1 Introduction

The regulation of aldosterone and corticosterone, the two main MR ligands, may be altered in *Hsd11b2*$^{+/-}$ mice on a high sodium diet. The rationale behind this theory comes from observations made in the previous chapter, Chapter 3. Firstly, impaired ligand specificity of MR for aldosterone and improved corticosterone access, as demonstrated by a reduced 11β-HSD2 enzyme activity in *Hsd11b2*$^{+/-}$ mice, could alter the dynamics of these two corticosteroids in relation to MR regulation; this in turn could have feedback effects upon their production and/or regulation. Secondly, high sodium intake was shown to have a significant effect upon the concentrations of both aldosterone and corticosterone and this was exacerbated in *Hsd11b2*$^{+/-}$ mice compared to *Hsd11b2*$^{+/+}$ mice; this suggests that the regulation of mineralocorticoids and glucocorticoids may be distorted in *Hsd11b2*$^{+/-}$ mice.

4.1.1 Mineralocorticoid Regulation

4.1.1.1 Aldosterone and the RAAS

Aldosterone homeostasis is regulated by the RAAS homeostatic feedback loop (see Introduction Chapter and Figure 1.6). In the instance of ablated 11β-HSD2 enzyme activity, SAME patients have been shown to have a down-regulated RAAS, as endogenous renin activity and aldosterone concentration are typically low (Quinkler and Stewart, 2003). In addition, *Hsd11b2*$^{-/-}$ mice also have a suppressed RAAS, with plasma concentrations of renin and aldosterone, as well as kidney renin mRNA, significantly reduced compared to *Hsd11b2*$^{+/+}$ littermates (Bailey et al., 2008; Kotelevtsev et al., 1999). These observations suggest the RAAS is successfully regulated in

response to the severe hypertension observed in SAME patients and the *Hsd11b2*$^{-/-}$ transgenic mouse model.

Reduced aldosterone levels in *Hsd11b2*$^{+/-}$ mice on a standard sodium diet suggest a down regulated RAAS when no BP phenotype is present; an indication that lower concentrations of aldosterone may be required in order to maintain a normal phenotype under normal dietary conditions. Aldosterone levels are decreased further on a high sodium diet, implying that the RAAS is being appropriately regulated in response to increased sodium intake, albeit to a greater extent than in *Hsd11b2*$^{+/+}$ mice. These results suggest that *Hsd11b2*$^{+/-}$ mice have a constitutively suppressed RAAS that is exacerbated by a high sodium diet. This has implications for RAAS components other than aldosterone, such as the aldosterone pre-cursor AngII. In order to investigate RAAS regulation further, RAAS parameters were measured using stress-free terminal blood collections from *Hsd11b2*$^{+/+}$ and *Hsd11b2*$^{+/-}$ mice on standard and high sodium diets.

4.1.1.2 AT Receptors and the RAAS

AngII acts upon the adrenal gland to stimulate the production of aldosterone, so a reduction in aldosterone concentration implies that AngII is also down-regulated in *Hsd11b2*$^{+/-}$ mice. In addition, AngII has BP regulation effects other than promoting aldosterone synthesis. AngII mediates its effects via the AngII Type I and Type II receptors (AT_1 and AT_2) with the majority of physiological AngII effects are mediated by the AT_1 receptor. These include vasoconstriction, modulation of the central sympathetic nervous system, and changes in renal sodium handling (de Gasparo et al., 2000). Together, AngII effects mediated by AT_1 receptors serve to increase BP. The actions of AngII at AT_2 receptors are less well understood, however recent studies suggest they may exert counter-regulatory effects to oppose

AT_1-mediated vasoconstriction (for recent review see (Carey and Padia, 2008)). A constitutively suppressed RAAS could have feedback effects upon AT receptors, such as adaptive changes in the expression and/or binding properties of AT_1 receptors in the *Hsd11b2*$^{+/-}$ mice, and these changes could be exaggerated further under high dietary sodium. To investigate this, the vasoconstrictive response of *Hsd11b2*$^{+/+}$ and *Hsd11b2*$^{+/-}$ mice to acute AngI and AngII administration were assessed.

4.1.2 Glucocorticoid Regulation

The HPA axis is responsible for the homeostatic regulation of glucocorticoid synthesis and release (see Introduction Chapter and Figure 1.7). Plasma corticosterone concentrations are comparable between *Hsd11b2*$^{+/+}$ and *Hsd11b2*$^{-/-}$ mice on a standard sodium diet (Bailey et al., 2008), and SAME patients do not exhibit elevations in plasma cortisol concentration, despite evidence of impaired metabolism (Ulick et al., 1979; White et al., 1997). These findings support the concept that the phenotype of SAME patients and *Hsd11b2*$^{-/-}$ mice arise from improved glucocorticoid access to MR as a result of lack of 11β-HSD2 enzyme activity, and not an elevation in glucocorticoid concentration. In addition, the normal levels of plasma cortisol in SAME patients is indicative of an intact HPA axis negative feedback mechanism acting to maintain steady concentrations of circulating cortisol despite impaired metabolism (Palermo et al., 1996).

In light of these important findings, the observation made in Chapter 3 that an increased sodium intake significantly increases corticosterone concentrations in *Hsd11b2*$^{+/-}$ mice is intriguing; corticosterone concentrations were also increased in *Hsd11b2*$^{+/+}$ mice, but to a lesser extent. The increase in corticosterone concentration during exposure to a high sodium diet

corresponds with the timescale of when the phenotype of the *Hsd11b2*$^{+/-}$ mice presents, and suggests that sodium intake is fundamental to the increased levels observed. Increased corticosterone levels could be the result of either increased corticosterone production or decreased metabolism (i.e. a longer half-life), or a combination of both. Further investigations into the cause(s) of increased corticosterone concentrations are important, as they may be central as to why the *Hsd11b2*$^{+/-}$ phenotype presents only on a high sodium diet. Experiments were performed to assess how the HPA axis of these mice responded to stress, as an observed weight-loss phenotype implied the high sodium diet was initiating a stress-related phenotype; the *Hsd11b2*$^{+/-}$ mice may not be able to adapt to environmental stresses such as a change in diet as efficiently as the *Hsd11b2*$^{+/+}$ mice. These experiments also allowed for analysis of the acute post-stress metabolism of corticosterone, an important factor in a setting of reduced 11β-HSD2 enzyme activity.

4.2 Results: Aldosterone Regulation

4.2.1 RAAS Plasma Analysis

Measurements were made of key RAAS components in the plasma of *Hsd11b2*$^{+/-}$ and *Hsd11b2*$^{+/+}$ mice on both standard and high sodium diets. Plasma angiotensinogen (AGT) concentration was similar in both *Hsd11b2*$^{+/+}$ and *Hsd11b2*$^{+/-}$ mice, and was not affected by dietary sodium content (Figure 4.1).

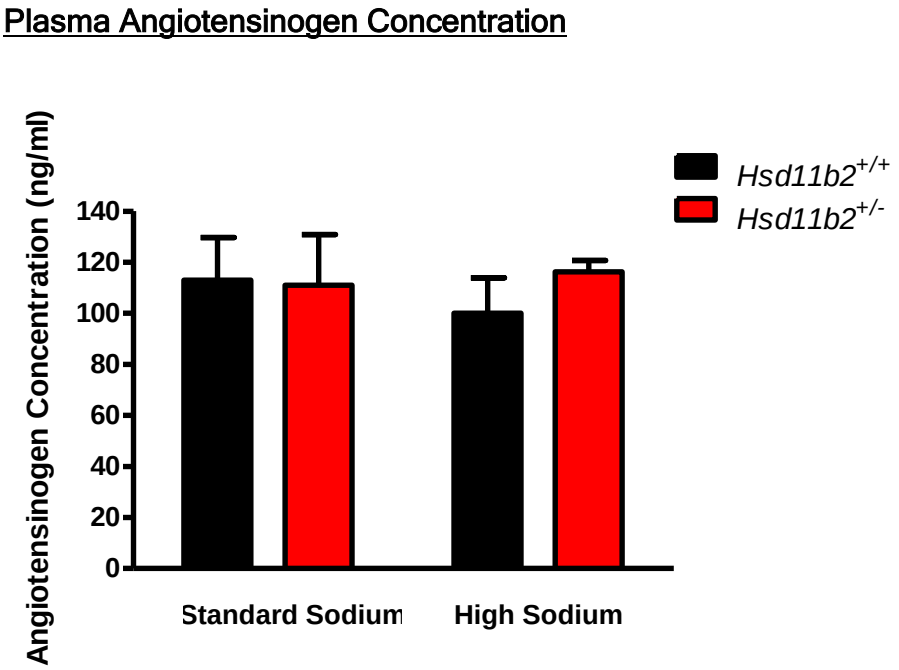

Figure 4.1. Plasma angiotensinogen concentration of *Hsd11b2*$^{+/+}$ and *Hsd11b2*$^{+/-}$ mice on a standard (n = 6 and 5, respectively) and high (n = 6 for both groups) sodium diet. There was no difference between the two groups and no effect of sodium diet upon plasma angiotensinogen concentration. Data are means ± SEM.

Circulating renin was measured as both plasma concentration and plasma renin activity (PRA). On a standard sodium, diet the plasma renin

concentration was comparable between *Hsd11b2*$^{+/+}$ and *Hsd11b2*$^{+/-}$ mice (Figure 4.2a).

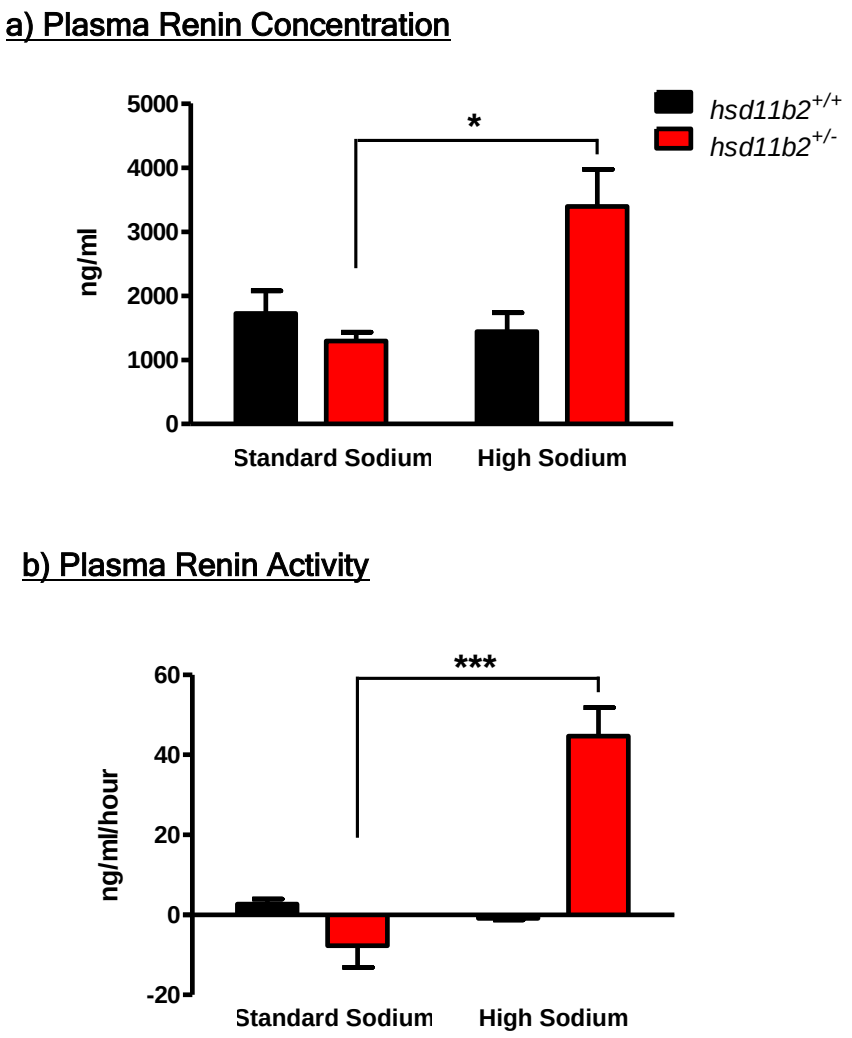

Figure 4.2. **a)** Plasma renin concentration and **b)** plasma renin activity of *Hsd11b2*$^{+/+}$ and *Hsd11b2*$^{+/-}$ mice on a standard (n = 6 for both groups) and high (n = 5 and 7, respectively) sodium diet. Plasma renin concentration and activity are significantly greater in *Hsd11b2*$^{+/-}$ mice on a high sodium diet compared to a standard sodium diet. Diet has no effect upon *Hsd11b2*$^{+/+}$ mice for either measurement. All data are means ± SEM. ***** P < 0.05; ******* P < 0.001.

After three weeks on a high sodium, *Hsd11b2*$^{+/-}$ mice displayed a significant increase in plasma renin concentration compared to both sodium-loaded *Hsd11b2*$^{+/+}$ mice and *Hsd11b2*$^{+/-}$ mice on a standard sodium diet. PRA was

similar between both groups on a standard sodium diet (Figure 4.2b). The high sodium diet had no effect upon the renin activity of *Hsd11b2*$^{+/+}$ mice, but caused a significantly greater level of PRA in *Hsd11b2*$^{+/-}$ mice.

4.2.2 Angiotensin I and II Dose Responses

4.2.2.1 Maximal BP Response

Increasing doses of AngI and II were administered to anaesthetised *Hsd11b2*$^{+/+}$ and *Hsd11b2*$^{+/-}$ mice with MABP measured throughout. The maximal BP response (MBPR) was calculated by subtracting the baseline MABP value before, and maximal MABP recorded after, the drug administration (see Figure 4.3 for details).

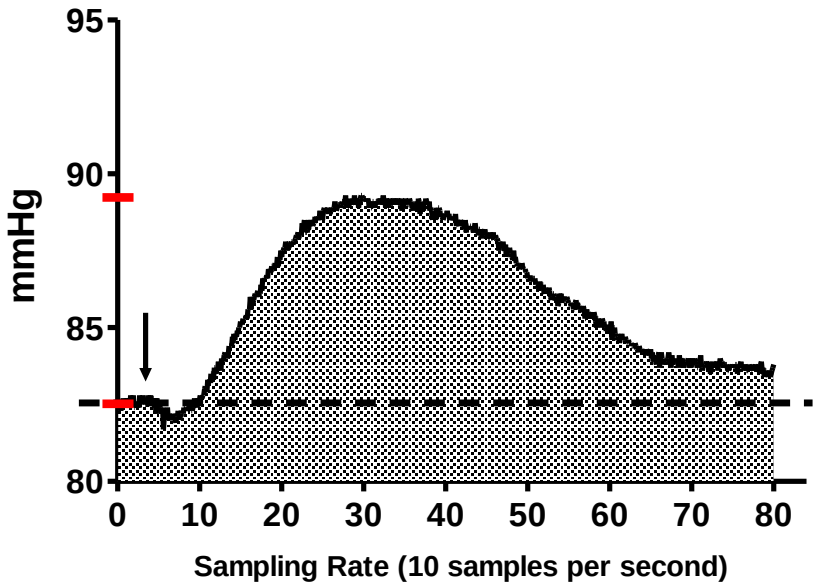

Figure 4.3. An example of a typical MABP dose response curve generated in response to AngI or AngII administration. Red lines on Y axis demonstrate the difference between baseline BP and maximal BP response to administration; presented as the maximal BP response. The horizontal dotted line represents the bottom range of the area under the curve measurements, as determined by baseline BP. The specific BP response shown here was generated from an *Hsd11b2*$^{+/+}$ mouse administered 1.125ng of AngI on a standard sodium diet. The black arrow demonstrates the moment of AngI IV administration.

On a standard sodium diet genotype had a significant effect upon the MBPR of the two groups across a range of AngI doses, with *Hsd11b2*$^{+/-}$ mice displaying an increased sensitivity compared to *Hsd11b2*$^{+/+}$ mice, irrespective of dose concentration (Figure 4.4). This pattern persists following 3 weeks

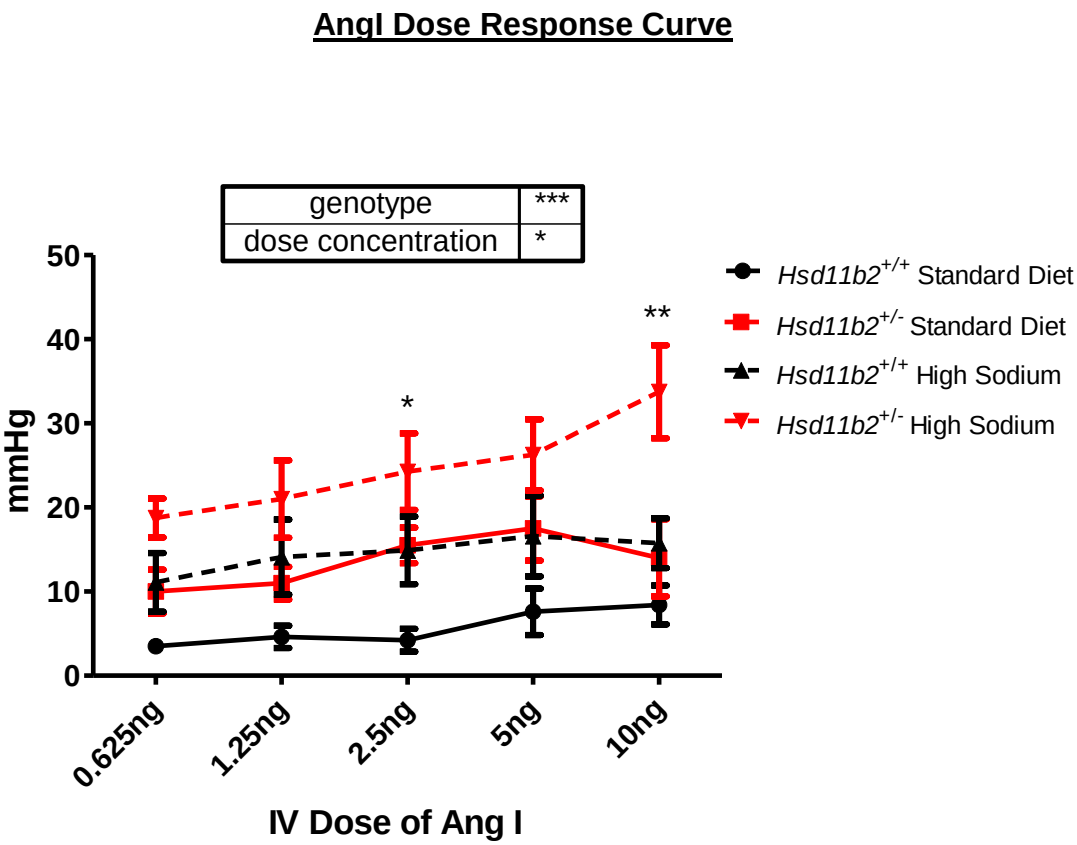

Figure 4.4. The BP effects of acute AngI IV administration at different doses. Maximal BP response of *Hsd11b2*$^{+/+}$ and *Hsd11b2*$^{+/-}$ mice on a standard sodium diet (n = 5 and 6, respectively) and on a high sodium diet (n = 5 for both groups), *Hsd11b2*$^{+/-}$ mice have greater BP response compared to *Hsd11b2*$^{+/+}$ mice on both sodium diets, with a high sodium diet significantly increasing values for both groups. The response under both dietary conditions is highly significantly different in terms of genotype (***) and significantly different in terms of AngI dose concentration. All data are means ± SEM. * $P < 0.05$; ** $P < 0.01$; *** $P < 0.001$.

on a high sodium diet, with AngI administration causing larger MBPR in *Hsd11b2*$^{+/-}$ mice compared to *Hsd11b2*$^{+/+}$ mice (Figure 4.4). When MBPR

values are compared within genotypes on different sodium diets, it becames apparent that the high sodium diet is increasing MBPR for both genotypes compared to standard sodium diet values (Figure 4.4).

The MBPR for AngII on a standard sodium diet shows a similar relationship for both genotypes to that of AngI, with *Hsd11b2*$^{+/-}$ displaying a greater MBPR compared to *Hsd11b2*$^{+/+}$ mice at all doses (Figure 4.5). After three

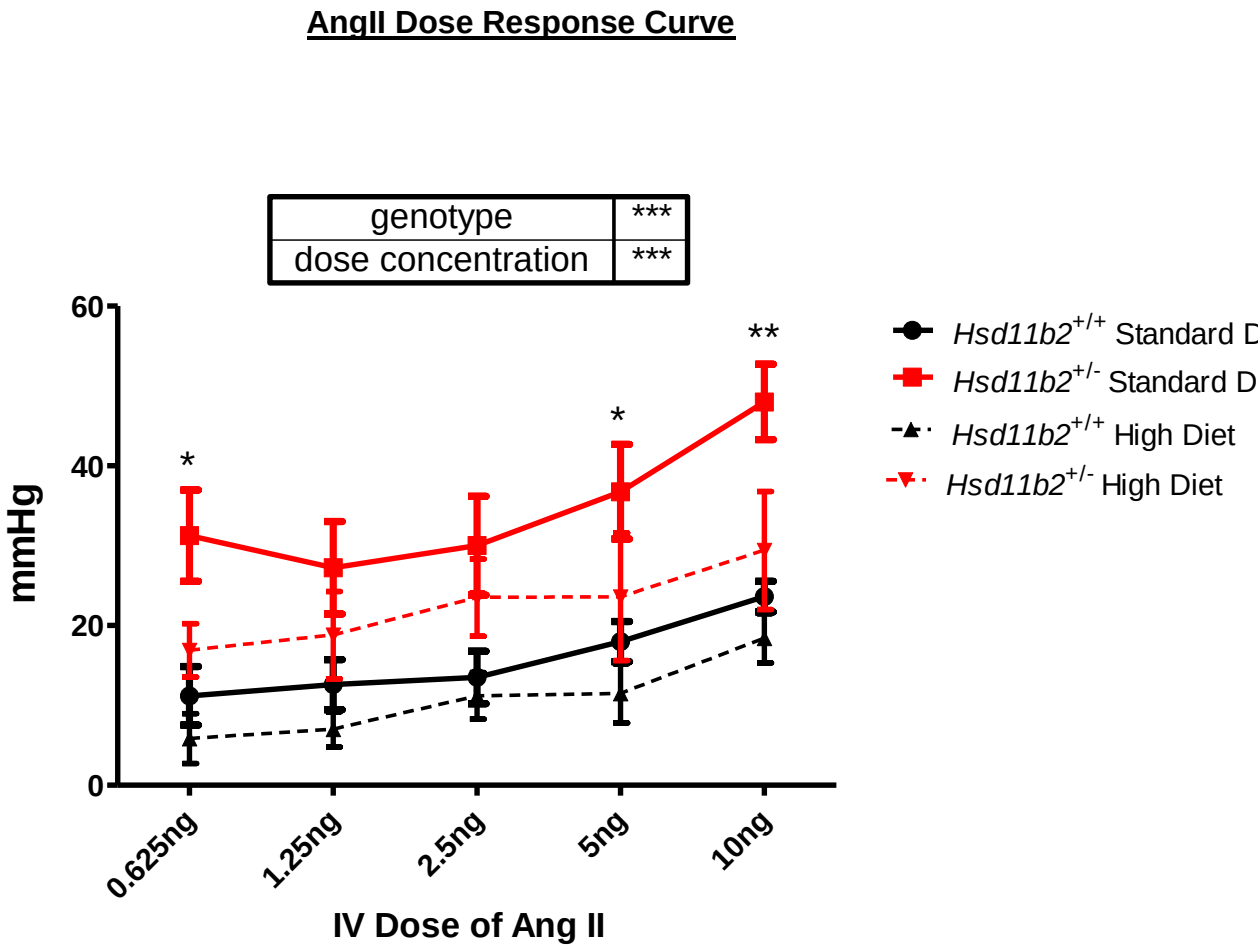

Figure 4.5. The BP effects of acute AngII IV administration at different doses. Maximal BP response of *Hsd11b2*$^{+/+}$ and *Hsd11b2*$^{+/-}$ mice on a standard sodium diet (n = 6 and 5, respectively) **and** on a high sodium diet (n = 5 for both groups), *Hsd11b2*$^{+/-}$ mice have greater BP response compared to *Hsd11b2*$^{+/+}$ mice on both sodium diets, with a high sodium diet significantly increasing values for both groups. The response under both dietary conditions is highly significantly different in terms of genotype AngII dose concentration (***). All data are means ± SEM. ***** P < 0.05; ****** P < 0.01; ******* P < 0.001.

weeks on a high sodium diet, the *Hsd11b2*$^{+/-}$ mice continue to display increased MBPR compared to the *Hsd11b2*$^{+/+}$ mice (Figure 4.5). Comparison of the MBPR within genotypes on different sodium diets shows that high sodium diet had a significant effect upon increasing the MBPR for both *Hsd11b2*$^{+/+}$ and *Hsd11b2*$^{+/-}$ mice (Figure 4.5). The responses to AngII were larger than those to AngI at all points for both genotypes on both sodium diets. It is important to point out that for these dose response experiments the vehicle used to administer AngI and II (0.9% saline) had no effects upon BP recorded (results not shown). The injection volume for each dose is 50µl, making a total of 250µl fluid injected in each group of experiments.

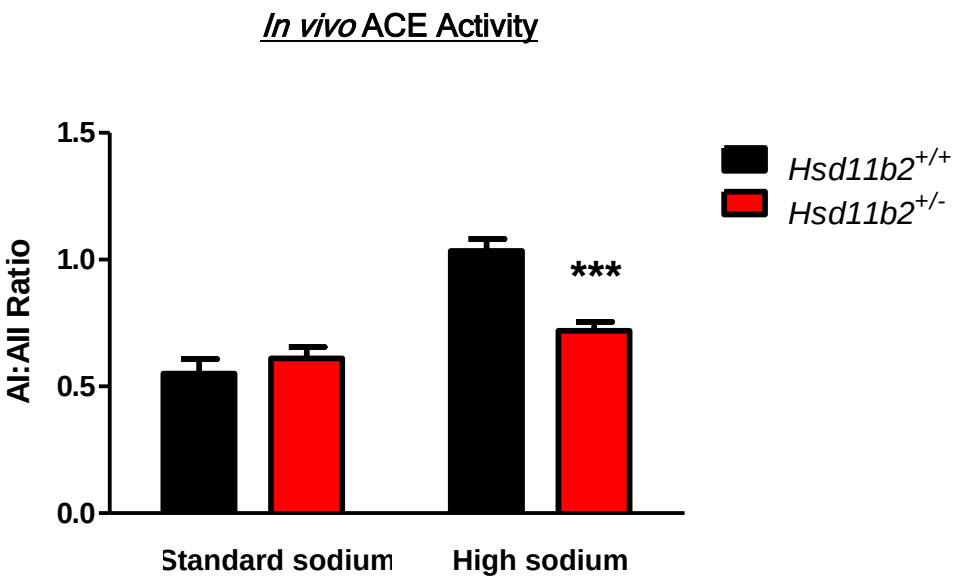

Figure 4.6. *In vivo* plasma ACE activity of *Hsd11b2*$^{+/+}$ and *Hsd11b2*$^{+/-}$ mice, measured as the ratio between the AngI and AngII maximal BP responses on a standard (n = 5 for both groups) and high (n = 5 for both groups) sodium diet. *Hsd11b2*$^{+/-}$ mice have significantly greater ACE activity on a high sodium diet compared to the *Hsd11b2*$^{+/+}$ mice. Data are means ± SEM. ******* P < 0.001.

Calculating the difference between the AngI and AngII MBPR in individual mice as a ratio allowed for an *in vivo* estimation of Angiotensin Converting Enzyme (ACE) activity. On a standard sodium diet both groups have similar levels of ACE activity (Figure 4.6). On a high sodium diet, the *Hsd11b2*$^{+/+}$ mice have down regulated their ACE activity in response to the high sodium diet. *Hsd11b2*$^{+/-}$ mice have a significantly greater ACE activity than *Hsd11b2*$^{+/+}$ mice on a high sodium diet, and have not adjusted their ACE activity appropriately for the dietary sodium content, displaying similar values to those measured on a standard sodium diet.

It is important to point out that enzymes other than ACE can also catalyse the conversion of AngI to AngII, such as chymostatin-sensitive angiotensin-generating enzyme (chymase) (Urata et al., 1993). The catalytic activity of chymase for the conversion of AngI to AngII has been shown to be 20-fold greater than that of ACE (Dell'Italia et al., 1995). A study investigating the contribution of ACE versus chymase was carried out using an ACE knockout mouse model (Wei et al., 2002). These studies showed that while chymase may provide an important mechanism in maintaining steady-state AngII levels in AngII-target tissues, ACE activity is essential to AngII formation in vascular space. Therefore, this interpretation of ACE activity may not be entirely accurate as other enzymes can also catalyse the same reaction.

4.2.2.2 Area under the Curve Analysis

The extent of the response to the AngI and II doses described above were also analysed by measuring the area under the BP curves produced in response to these administrations (does response curves (DRC); see Figure 4.3 for example). This analysis allowed for the investigation of potential effects of genotype and/or sodium diet upon the magnitude of the BP

response. The magnitude and duration of a BP response to AngI and II can provide insight(s) into the receptor ligand relationship.

On a standard sodium diet *Hsd11b2*$^{+/-}$ mice have a significantly greater BP response than *Hsd11b2*$^{+/+}$ mice to AngI in terms of area under the curve (AUC) analysis (Figure 4.7a). This difference was significant in terms of both

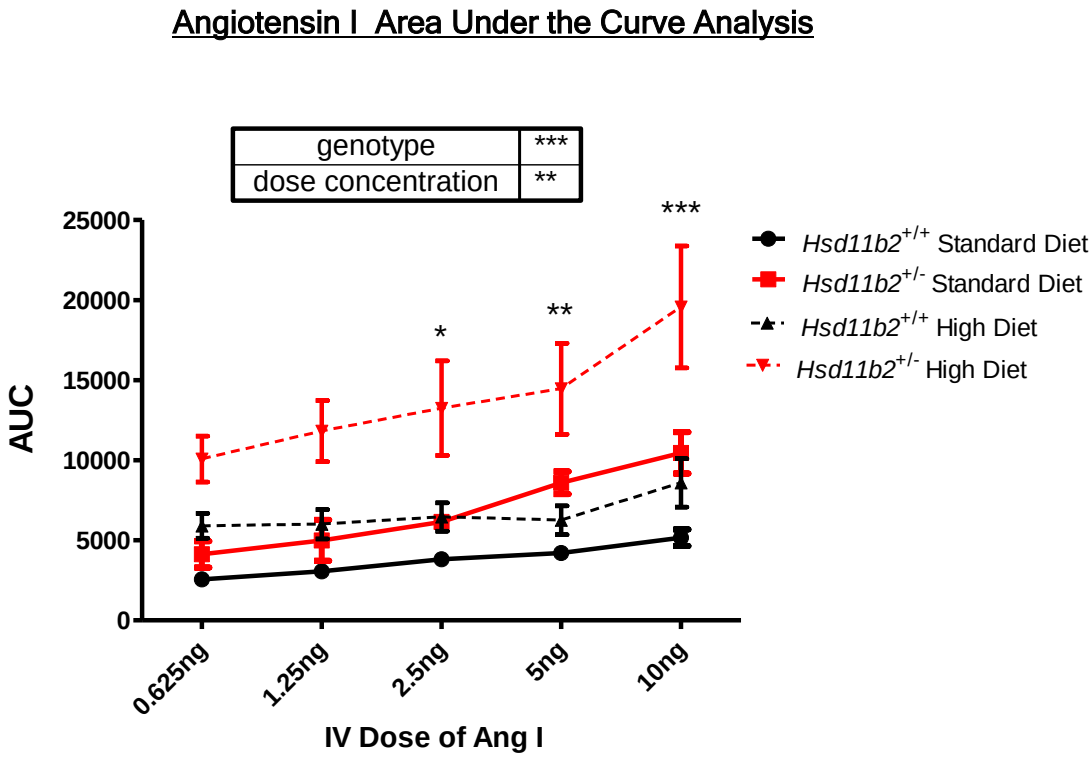

Figure 4.7. Area under the curve (AUC) values for BP responses to acute AngI IV administration at different doses. The values for *Hsd11b2*$^{+/+}$ and *Hsd11b2*$^{+/-}$ mice on a standard sodium diet (n = 4 for both groups) **and** a high sodium diet (n = 4 for both groups),. *Hsd11b2*$^{+/-}$ mice have greater AUC values compared to *Hsd11b2*$^{+/+}$ mice on both sodium diets, with a high sodium diet significantly increasing values for both groups. All data are means ± SEM. ***** P < 0.05; ******* P < 0.01; ******* P < 0.001.

genotype and dose concentration, especially at the higher end of the dose range. A similar pattern was also observed after three weeks on a high sodium diet, although AUC values for both *Hsd11b2*$^{+/+}$ and *Hsd11b2*$^{+/-}$ mice were greater than on a standard sodium diet (Figure 4.7b). When the effects

of dietary sodium content were compared across individual genotypes, the effects of a high sodium diet upon AUC was significant in both groups compared to a standard sodium diet; values were always greater in *Hsd11b2*$^{+/-}$ mice than *Hsd11b2*$^{+/+}$ mice (Figure 4.7c and d).

AngII administration on a standard sodium diet had a significantly greater effect upon the AUC values in *Hsd11b2*$^{+/-}$ mice compared to *Hsd11b2*$^{+/+}$ mice (Figure 4.8a). This was especially prominent at higher AngII concentrations.

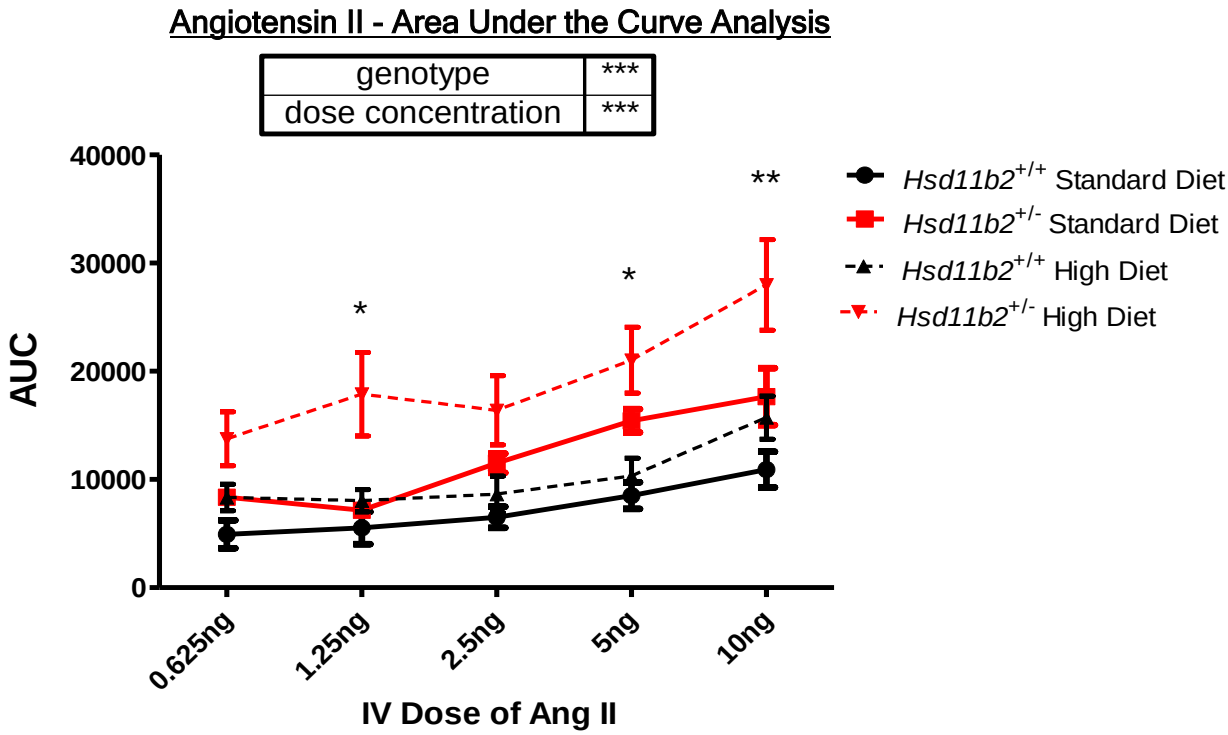

Figure 4.8. Area under the curve (AUC) values for BP responses to acute AngII IV administration at different doses. The values for *Hsd11b2*$^{+/+}$ and *Hsd11b2*$^{+/-}$ mice on a standard sodium diet (n = 4 for both groups) **and** a high sodium diet (n = 4 for both groups). *Hsd11b2*$^{+/-}$ mice have greater AUC values compared to *Hsd11b2*$^{+/+}$ mice on both sodium diets, with a high sodium diet significantly increasing values for both groups. All data are means ± SEM. ***** P < 0.05; ****** P < 0.01; ******* P < 0.001

.

A similar pattern was observed after three weeks on a high sodium diet, again with dose concentration having an effect (Figure 4.8b). AUC values

were greater at all dose concentrations for both genotypes on a high sodium diet compared to a standard sodium diet (Figure 4.8c and d), with *Hsd11b2*$^{+/-}$ mice always having greater values than *Hsd11b2*$^{+/+}$ mice.

4.3 Results: Corticosterone Regulation

4.3.1 Body Weights and Food Intake

The body weights and food intake of *Hsd11b2*$^{+/+}$ and *Hsd11b2*$^{+/-}$ mice were recorded daily during the metabolic cage experiments described in Chapter 3. Upon further investigation, these data suggested that there may be a stress-related phenotype occurring in the *Hsd11b2*$^{+/-}$ mice on a high sodium diet.

In relation to individual body weight, *Hsd11b2*$^{+/-}$ mice lost significantly more weight than *Hsd11b2*$^{+/+}$ mice during the high sodium diet feeding period (Figure 4.9a). The body weight difference between the two genotypes is shown in terms of the total body weight difference over this period in Figure 4.9b. Daily food intake was also recorded over this period; there was no significant difference for food intake between *Hsd11b2*$^{+/+}$ and *Hsd11b2*$^{+/-}$ mice for the entire period of high sodium diet feeding (Figure 4.9c).

At the end of the high sodium diet regime the mice were culled and certain tissues were dissected for further analysis. This included the epididymal fat pads, the weights of which were calculated in relation to total body weight. The epididymal fat pads were analysed to try and ascertain the source of the weight-loss observed in the *Hsd11b2*$^{+/-}$ mice. The fat pads of the *Hsd11b2*$^{+/-}$ mice weighed significantly less than those of the *Hsd11b2*$^{+/+}$ mice (Figure 4.9d). This demonstrates that the total body weight losses observed in the *Hsd11b2*$^{+/-}$ mice over the high sodium diet period are reflected in epididymal

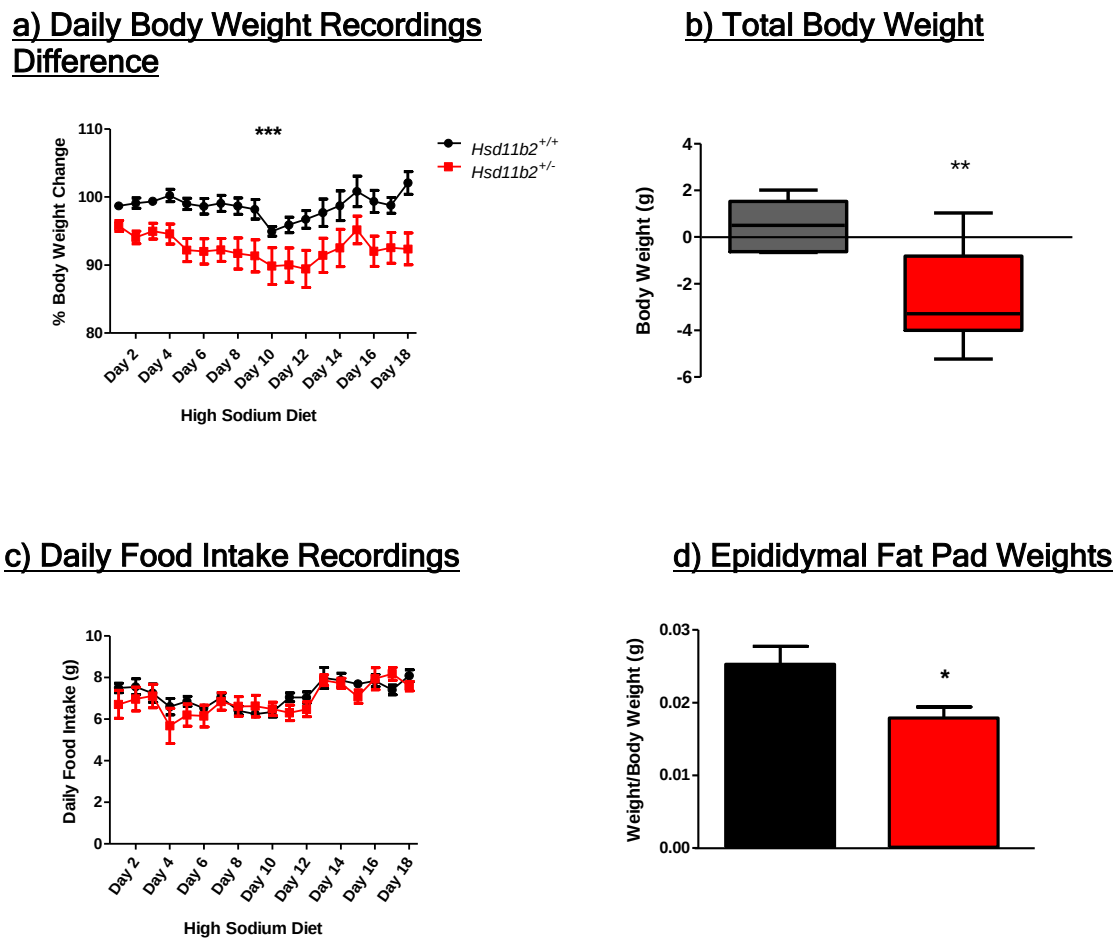

Figure 4.9. Body weights and food intake of *Hsd11b2*$^{+/+}$ and *Hsd11b2*$^{+/-}$ mice (n = 7 and 8, respectively). **a)** The daily body weights were recorded for mice in metabolic cages during high sodium diet feeding and presented as % body weight loss from baseline measurements; **b)** presents data in **a)** as the total difference in body weight over the high sodium diet feeding period; **c)** daily food intake recordings made over the same period; **d)** post-mortem weights of dissected epididymal fat pads. *Hsd11b2*$^{+/-}$ mice lost significantly more weight on a high sodium diet compared to *Hsd11b2*$^{+/+}$ mice. This was not due to a decrease in food intake, and was reflected in their epididymal fat pad weight. All data are means ± SEM. ***** P < 0.05; ****** P < 0.01 ******* P < 0.001.

fat pad deposits. Kidney and adrenal weights were also analysed, and no differences were observed between genotypes or different sodium diets.

4.3.2 HPA Axis Testing – Corticosterone Response

The ability to respond to stress was assessed in *Hsd11b2*$^{+/+}$ and *Hsd11b2*$^{+/-}$ mice on both a standard and a high sodium diet by measuring corticosterone levels before and after exposure to an intense, short-term stressor (see Chapter 2, Figure 2.3 for experimental design).

The two genotypes had similar baseline corticosterone plasma concentrations on the standard sodium diet; these values remained stable for both groups of mice after three weeks on the high sodium diet (Figure 4.10a). After exposure to stress, plasma corticosterone concentration increased greatly, with values for both genotypes on both diets comparable (Figure 4.10b). The animals were then allowed 90 minutes to recover from the stress. After this recovery period, a final plasma corticosterone concentration measurement was obtained. On a standard sodium diet there was no difference between the recovery corticosterone concentrations of *Hsd11b2*$^{+/+}$ and *Hsd11b2*$^{+/-}$ mice (Figure 4.10c); values were greatly reduced compared to stress plasma corticosterone concentrations. After three weeks on a high sodium diet, the recovery corticosterone concentration for *Hsd11b2*$^{+/-}$ mice was significantly greater than on a standard sodium diet, and than that of *Hsd11b2*$^{+/+}$ mice on a high sodium diet.

As the increased concentration of plasma corticosterone after recovery on a high sodium diet in high sodium diet fed *Hsd11b2*$^{+/+}$ mice suggests an impaired corticosterone metabolism, these values were analysed further in order to calculate the % decay (calculated as a % of the stress measurement corticosterone concentration remaining in the recovery measurement concentration). As predicted by the recovery plasma corticosterone concentrations, on a standard sodium diet the % decay of plasma corticosterone in *Hsd11b2*$^{+/+}$ and *Hsd11b2*$^{+/-}$ were similar to one another

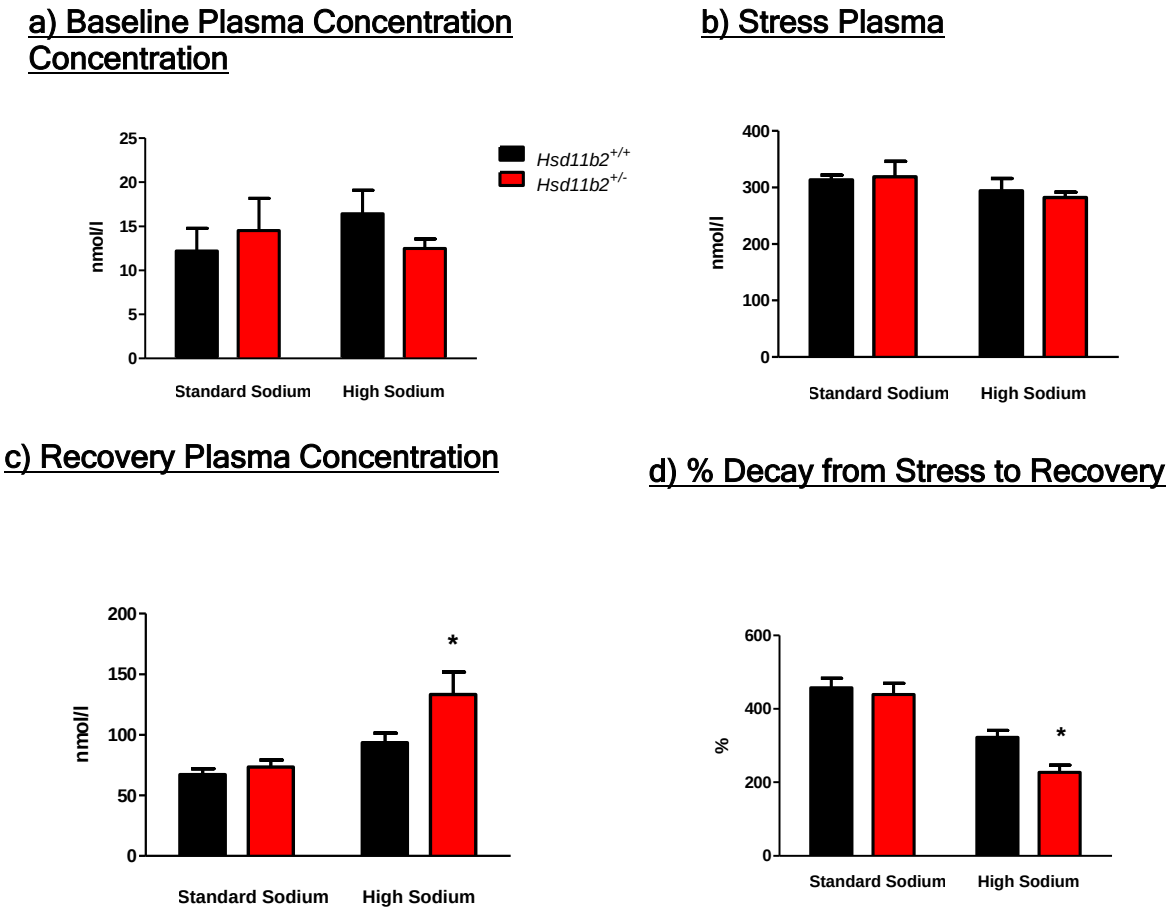

Figure 4.10. **a)** Baseline **b)** stress and **c)** recovery plasma corticosterone concentrations of *Hsd11b2*$^{+/+}$ and *Hsd11b2*$^{+/-}$ mice on a standard, and after three weeks on a high, sodium diet (n = 9 for both groups). There was no difference in terms of baseline and stress plasma corticosterone concentrations. *Hsd11b2*$^{+/-}$ mice had a significantly greater recovery plasma corticosterone concentration compared to *Hsd11b2*$^{+/+}$ mice on a high sodium diet. **d)** These values were then calculated as the % decay of plasma corticosterone concentration compared to stress values; *Hsd11b2*$^{+/-}$ have a significantly lower rate of decay than *Hsd11b2*$^{+/+}$ mice on a high sodium diet. All data are means ± SEM. ***** P < 0.05.

(Figure 4.10d). After three weeks on a high sodium diet, the % decay for the *Hsd11b2*$^{+/-}$ group was significantly decreased compared to *Hsd11b2*$^{+/+}$ mice, and also to *Hsd11b2*$^{+/-}$ mice on a standard sodium diet.

4.4 Discussion

This chapter describes investigations into the regulation of aldosterone and corticosterone in *Hsd11b2*$^{+/-}$ mice in relation to their SS phenotype. Regulation of the homeostatic feedback loops controlling production of these hormones (the RAAS and HPA axis, respectively) is important as they are equal in their affinity for the MR. MR activation is key in the phenotype of this mouse model as reduced 11β-HSD2 activity changes the way in which these ligands can interact with the receptor.

4.4.1 Aldosterone Regulation

4.4.1.1 RAAS Analysis

The reduction in concentration of both urinary and plasma aldosterone observed in *Hsd11b2*$^{+/-}$ mice when they are moved from a standard to a high sodium diet implies that they have a functional RAAS that is responding appropriately to an increased dietary sodium load. However, the significantly lower aldosterone concentrations of *Hsd11b2*$^{+/-}$ mice compared to *Hsd11b2*$^{+/+}$ mice on both diets implies that there is a tonic suppression of the RAAS in these mice even when no BP or sodium retention phenotype is present. This suggests that on a standard sodium diet reduced aldosterone concentrations are required to maintain normal BP and natriuresis in the face of impaired 11β-HSD2 enzyme activity. This is presumably to prevent over-activation of the MR by aldosterone as the reduced 11β-HSD2 activity is permitting improved glucocorticoid access to the MR. In light of these results, investigations were carried out to assess RAAS regulation in *Hsd11b2*$^{+/-}$ mice in more depth. Plasma concentrations and enzyme activities

of certain RAAS parameters under both standard and high sodium diet conditions were measured.

AGT is an inactive peptide that is the precursor of AngI. Genetic linkage studies involving AGT have found a strong correlation between sequence variations in the AGT gene and essential hypertension within the human population (Jeunemaitre et al., 1992). In addition, transgenic mouse studies in which the AGT gene was expressed in increasing copy number from 1 to 4 showed correlation between AGT gene copy number and BP; BP rose approximately 8mmHg for each increase in gene copy number (Kim et al., 1995). Given its effects upon BP homeostasis, it was therefore important to investigate if AGT was playing a role in this model of increased BP. Plasma concentrations of AGT were comparable between *Hsd11b2*$^{+/-}$ and *Hsd11b2*$^{+/+}$ mice on both sodium diets; dietary sodium content had no effect upon concentration. Therefore, AGT deregulation is unlikely to be involved in the BP increase of *Hsd11b2*$^{+/-}$ mice on a high sodium diet.

Renin is the enzyme responsible for the cleavage of AGT into AngI, and is produced in specialised cells of the juxtaglomerular apparatus known as granular cells. Renin can be released in response to a number of different physiological stimuli such as a fall in systolic BP, reduced concentration of sodium in the distal nephron (as detected by the macula densa), or sympathetic nervous system activity via β_1 adrenergic receptors (Schweda et al., 2007). Two methods were used to measure renin in this study in order to obtain both plasma concentration and enzyme activity (PRA). This is important as renin plasma concentration is not always a reflection of PRA and vice versa. PRA assesses the rate-limiting enzymatic step in the production of AngI (and therefore also AngII) and also takes into account substrate (AGT) availability. As AGT availability has already been

discounted as contributing towards increased BP in this model by direct measurements, differences in PRA can therefore be assessed in light of renins enzymatic activity alone. Plasma renin concentration was increased in *Hsd11b2*$^{+/-}$ mice on a high sodium diet. This is in contrast to the suppressed RAAS that was predicted from the low plasma and urinary aldosterone concentrations previously reported in Chapter 3. This suggests that the *Hsd11b2*$^{+/-}$ mice are releasing inappropriate levels of renin in response to a high sodium diet. Results from the PRA assay also show that *Hsd11b2*$^{+/-}$ mice have inappropriately elevated PRA under increased sodium diet conditions, demonstrating that the increase in plasma renin concentration is not an adaptive mechanism to combat low PRA.

In light of the observed increase in PRA, the decreased plasma potassium concentration observed in *Hsd11b2*$^{+/-}$ mice on a high sodium diet in Chapter 3 may be significant (Figure 3.9d). Studies from the 1970s in both humans and rats found a relationship between reduced plasma potassium concentrations and increased PRA (Brunner et al., 1970; Sealey et al., 1970). These studies demonstrated that PRA was increased in states of potassium depletion associated with a low plasma aldosterone concentration. They hypothesised that increased PRA may play a role in the renal conservation of potassium under conditions of low aldosterone, and that potassium may modify renin secretion directly by acting on the juxtaglomerular cells of the kidney, or by inducing changes in renal tubular secretion. This hypothesis may go some way towards explaining the reduction in urinary potassium excretion observed in *Hsd11b2*$^{+/-}$ mice on a high sodium diet compared to on a standard sodium diet and *Hsd11b2*$^{+/+}$ mice on both diets (Figure 3.9c). That is, reduced plasma potassium concentrations in the *Hsd11b2*$^{+/-}$ mice on a high sodium diet may be stimulating an increase in the release and/or activity of renin so

as to conserve potassium. Another potential explanation comes from a recent study which found increased levels of urinary catecholamine excretion in *Hsd11b2*$^{-/-}$ mice (Bailey et al., 2008). This implies that the sympathetic nervous system may be promoting excess renin release via activation of β_1 adrenergic receptors. Urinary catecholamine measurements in *Hsd11b2*$^{+/-}$ mice could identify if the high sodium diet causes changes in sympathetic nervous system activity.

The studies described here are limited to plasma concentrations of RAAS parameters. While this is extremely useful for analysing renin and angiotensin effects at a circulating systemic level, the contributions of intra-tissue Renin-Angiotensin System (RAS) have not been assessed in these studies. In particular, many studies have implicated the intra-renal RAS as an important factor in hypertension; especially as there can be marked differences between renin and angiotensin levels in the kidney and the plasma, and even within different compartments of the kidney; for review see (Kobori et al., 2007). Additional analysis of tissue RAS parameters could provide further insights into the development of elevated BP and impaired natriuresis on a high sodium diet in *Hsd11b2*$^{+/-}$ mice.

4.4.1.2 Angiotensin Dose Responses

A tonic suppression of the RAAS in *Hsd11b2*$^{+/-}$ mice may have feedback effects upon the function of AT receptors, such as AT_1. Altered levels of circulating RAAS components could cause adaptive changes in the expression and/or binding properties of AT receptors in *Hsd11b2*$^{+/-}$ mice; these changes could be exaggerated further under high dietary sodium as the RAAS is further suppressed. To investigate this theory, the BP response to I.V. doses of both AngI and AngII were measured in *Hsd11b2*$^{+/+}$ and *Hsd11b2*$^{+/-}$ mice on both a standard and a high sodium diet. In addition to providing

information about the AT receptors by using both AngI and AngII, and measuring the difference between the responses to each, these studies provided further information about ACE activity.

AngI and II were administered in increasing doses, with any BP changes observed being allowed to return back to baseline measurements before the next injection dose. The time frame of this experiment is not long enough to observe any genomic effects that the I.V. injections may cause. Therefore, all observations can largely be interpreted as the vasoconstrictive effects of AngII on the vasculature, although as it was not possible to measure heart rate (HR) during these experiments due to technical restraints, the contribution of HR changes in response to AngI and AngII administrations cannot be discounted.

The BP response to AngI was significantly greater in the *Hsd11b2*$^{+/-}$ group compared to the *Hsd11b2*$^{+/+}$ group on both sodium diets; however the response was greater for both genotypes on a high sodium diet (Figure 4.4). A similar pattern was observed with AngII administration, although the responses were always greater than with AngI (Figure 4.5). This shows that although high dietary sodium is causing changes in the AT receptor response to AngI and AngII in both genotypes, the affect is always greater in the *Hsd11b2*$^{+/-}$ group. The extent of the BP response to the AngI and II doses were further analysed by calculating and analysing AUC values. On a standard and a high sodium diet, for both AngI and AngII, *Hsd11b2*$^{+/-}$ mice had a significantly greater AUC BP response compared to *Hsd11b2*$^{+/+}$ mice. This shows that both genotype and sodium diet effect the BP response as measured in this way. The magnitude and duration of the BP response to AngI and II suggests that the receptor ligand relationship is altered in *Hsd11b2*$^{+/-}$ mice, and this is further exacerbated by a high sodium diet.

Investigations by Ruan *et al* have revealed how AT_1 receptors adapt in rats exposed to high or low sodium diets (Ruan et al., 1997). These investigations showed that on high sodium diet there was a parallel increase in AT_1 receptor mRNA and receptor density in afferent arterioles, implying a casual link between dietary sodium and AT_1 receptor expression. Overall, receptor expression increased two-fold on high sodium diet compared with low sodium diet. Further investigations for the current studies could investigate whether a change in receptor density accounts for the different responses to AngI and II observed on different sodium diets, and also if there is a difference between genotypes on the same diet. In addition, GR activation has been proposed to up regulate AT_1 mRNA and receptor expression (Guo et al., 1995; Sato et al., 1994), and this presents a potential correlation between the observed increases in corticosterone concentration and the exaggerated responses to AngII on a high sodium diet in *Hsd11b2*$^{+/-}$ mice. Thus, the increased concentrations of glucocorticoids in these mice may promote increases in AT_1 receptor expression, thus explaining at least in part the potency of AngII bolus injections. Furthermore, some studies have found a link between increased glucocorticoid levels and increased AT_1 receptor ligand binding (Shelat et al., 1999a; Shelat et al., 1999b), although it should also be pointed out that others find no link between the two (Ruan et al., 1997; Sato et al., 1994). In addition, changes in the expression of AT_2 receptors may also be contributing to the increased vascular contractility observed in *Hsd11b2*$^{+/-}$ mice. Increased AngII levels (Bonnet et al., 2001) and a sodium restricted diet (Siragy et al., 2000) have both been shown to increase AT_2 receptor expression, so it is entirely possible that the suppressed RAAS and increased sodium intake could be having the opposite effect in the *Hsd11b2*$^{+/-}$ mice. Whether the increased dietary sodium intake is modifying

receptor number and/or ligand binding efficiency in AT_1 and AT_2 receptors remains to be established. Quantitative PCR and studies using AT receptor antagonists, such as Losartan, would help to address this. It is also worth noting that there may be additional differences between the genotypes in terms of small resistance vessels that may also be having an effect upon the observed differences in their response to AngI and II. Resistance vessels are the primary site of vascular resistance, the hallmark of arterial hypertension. AngII is involved in the contractile response to flow in resistance arteries, and both AngII and dietary salt can be responsible for structural changes within the vascular (Simon, 2004). A study by Csiky *et al* demonstrated that in normotensive rats, 7 - 10 day treatment with a high salt diet potentiated the vasoconstrictor responses to AngII, independently of BP changes (Csiky and Simon, 1997). The authors go on to suggest a possible mechanism for this change: extracellular sodium is a determinant of the transmembrane sodium gradient, which in turn determines the magnitude of vasoconstrictor responses to agonists whose mode of action includes stimulating sodium influx, such as AngII. Therefore, the increases we see in vasoconstriction in response to AngI and II in both sets of mice may be due to these effects of a high sodium diet, the results of which could be magnified in *Hsd11b2*$^{+/-}$ mice compared to *Hsd11b2*$^{+/+}$ mice due to differences in resistance vessel remodelling.

In addition, the difference in the responses to AngI and AngII between the genotypes implies that there may be a difference in ACE activity and/or concentration. ACE activity was investigated further by calculating the ratio of the AngI to AngII BP response. This showed that the *Hsd11b2*$^{+/-}$ mice do not appropriately adapt their ACE activity in response to a high sodium diet

as the *Hsd11b2*$^{+/+}$ mice do. This implies a further failure of the RAAS to adapt appropriately to a high sodium diet in *Hsd11b2*$^{+/-}$ mice.

4.4.1.3 11β-HSD2 and AT Receptors

In addition to AngII and sodium levels potentially affecting AT receptor expression, it has been ascertained from preeclampsia studies that a decrease in 11β-HSD2 activity may also contribute towards an altered expression of AT receptors (Lanz et al., 2003). In normal pregnancies, there is a resistance to translate high AngII plasma levels (caused by a natural RAAS activation during pregnancy) into increased BP. However, this resistance is lost in preeclampsic pregnancies, where sensitivity to AngII increases (Gant et al., 1973) and a higher expression of AT_1 receptors is observed (Thapa et al., 2004). Preeclampsia has been associated with reduced levels of 11β-HSD2 activity, linking increased sensitivity to AngII with reduced 11β-HSD2 activity (Causevic and Mohaupt, 2007). These effects are thought to be mediated via increased glucocorticoid levels (in the face of reduced metabolism by 11β-HSD2) up-regulating AT_1 receptor expression. Whereas in preeclampsia it has been suggested that high levels of AngII may be negatively regulating 11β-HSD2 expression via actions mediated by the AT receptors (Lanz et al., 2003), these observations can be translated to studies in the *Hsd11b2*$^{+/-}$ mice as they have a genetically modified reduction in 11β-HSD2 activity.

4.4.2 Corticosterone Regulation

4.4.2.1 Body Weights and Food Intake

The body weights of individual mice were recorded daily during the metabolic cage studies described in Chapter 3. Before any experimental

measurements were made, the mice were given 5 days to acclimatise to being housed in the metabolic cages. At the beginning of the acclimatisation period body weight decreased for both groups of mice. This was not unexpected as mice typically lose weight upon introduction to a metabolic cage due to the stress of a new environment; the 5 day acclimatisation period was deliberately introduced to try and minimise the interference of this natural stress upon experimental measurements (Gomez-Sanchez and Gomez-Sanchez, 1991; Hoppe et al., 2009). After 5 days the body weights of the mice in both groups stabilised and experimental measurements began. Body weights remained relatively stable during the 3 day period of control collections on a standard sodium diet. However, once placed on a high sodium diet, the % body weight change in *Hsd11b2*$^{+/-}$ mice declined significantly compared to the *Hsd11b2*$^{+/+}$ mice. The weight loss observed in the *Hsd11b2*$^{+/-}$ group upon high sodium diet induction, combined with the observation that both groups eat similar amounts of food, implies that the change in sodium diet is inducing a weight-loss phenotype in *Hsd11b2*$^{+/-}$ mice. This weight loss might reflect an altered fat metabolism as post-mortem analysis of epididymal fat pads revealed that they weighed significantly less in *Hsd11b2*$^{+/-}$ mice than *Hsd11b2*$^{+/+}$ mice after three weeks on a high sodium diet (Figure 4.9d). Studies of mouse 11β-HSD2 expression sites have found no evidence of 11β-HSD2 expression in fat tissue (Moore et al., 2000) so this decrease is probably attributable to the overall weight loss phenotype. In addition, differences in water retention are unlikely to account for the weight differences as both genotypes were always equal for water balance (Chapter 3, Figure 3.4d).

Published studies concerning salt and glucose tolerance may help to explain the weight loss and smaller fat pads in *Hsd11b2*$^{+/-}$ mice on a high sodium diet.

There is literature linking SS and glucose tolerance (Giner et al., 2001). Some studies suggest that the serum- and glucocorticoid-inducible kinase (SGK1) may be involved in pathogenesis of glucose intolerance as salt intake-induced low aldosterone levels would decrease SGK1 transcription, thus decreasing SGK1-dependent uptake of glucose into tissues such as fat and liver (Boini et al., 2006; Ullrich et al., 2005). However, as the *Hsd11b2*$^{+/-}$ mice will likely maintain SGK1 expression due to high circulating glucocorticoid levels, *Hsd11b2*$^{+/-}$ mice are unlikely to develop insulin-resistance via this route. Therefore, an inappropriate over-expression of SGK1 under conditions of high sodium diet could be involved in the weight-loss phenotype observed; the opposite effect of a suppressed RAAS may occur in *Hsd11b2*$^{+/-}$ mice on a high sodium diet due to MR over activation by excess glucocorticoids. Investigating SGK1 expression and the glucose tolerance of these mice may help to assess these contributions towards this salt-induced phenotype. In addition, the corticosterone concentrations observed in Chapter 3 may indicate an inability of *Hsd11b2*$^{+/-}$ mice to regulate their HPA axis appropriately on a high sodium diet. This is of particular note as stressful situations are known to provoke weight loss.

4.4.2.2 HPA Axis Testing

A series of experiments were designed to test the HPA axis in *Hsd11b2*$^{+/-}$ mice and their ability to react to stressful situations on both a standard and a high sodium diet. These experiments showed that a high sodium diet had no effect upon the production of corticosterone under conditions of acute stress. However, what they did highlight was a deficiency in the metabolism of plasma corticosterone after exposure to stress in *Hsd11b2*$^{+/-}$ mice on a high sodium diet.

A previous study in which the anxiety state and HPA axis stress reaction was investigated in *Hsd11b2*$^{+/+}$, *Hsd11b2*$^{+/-}$ and *Hsd11b2*$^{-/-}$ littermates showed that *Hsd11b2*$^{-/-}$ mice display an increased anxiety phenotype compared to *Hsd11b2*$^{+/+}$ mice (Holmes et al., 2006). The *Hsd11b2*$^{+/-}$ mice displayed no anxiety phenotype, and neither the *Hsd11b2*$^{+/-}$ nor the *Hsd11b2*$^{-/-}$ mice had any changes in HPA axis reactivity testing for corticosteroid or ACTH levels compared with *Hsd11b2*$^{+/+}$ littermates. However, it is important to point out that these experiments were carried out on a standard sodium diet and so it was deemed important to investigate this on a high sodium diet. Whilst suggesting there is a stress phenotype associated with 11β-HSD2 ablation, but not reduced activity, it should be pointed out that these studies also found a significant difference between the birth weights of the three genotypes. That is, there was a direct correlation between 11β-HSD2 activity and birth weight, with *Hsd11b2*$^{+/+}$ mice being heaviest, *Hsd11b2*$^{-/-}$ mice the lightest, and *Hsd11b2*$^{+/-}$ mice falling in the middle. This suggests that *Hsd11b2*$^{+/-}$ mice may have a body weight phenotype, as reflected by epididymal fat pad weight analysis. Also, the stress tests used here were measurements of acute stress, not chronic exposure as is taking place with exposure to a high sodium diet. Therefore, the possibility of a chronic stress phenotype relating to body weight changes may well still be relevant.

4.4.2.3 Glucocorticoid Metabolism

The emergence of reduced glucocorticoid metabolism under conditions of impaired 11β-HSD2 function is highlighted by studies in SAME patients measuring urinary levels of cortisol and cortisone metabolites (5α- and 5β-tetrahydrocortisol (THF) and tetrahydrocortisone (THE), respectively) (Monder et al., 1986). An increased THF/THE ratio is routinely used as a biochemical marker of SAME as the higher ratio is associated with reduced

11β-HSD2 activity. This can be interpreted as more cortisol is being metabolised via this pathway due to deficiencies in the 11β-HSD2 metabolism to corticosterone route, therefore the ratio of cortisol metabolite to corticosterone metabolite is greater.

A reduction in corticosteroid metabolism in *Hsd11b2*$^{+/-}$ mice (therefore leading to the increased concentrations observed in both plasma and urine) could reflect reduced 11β-HSD2 enzyme activity. However, since this activity is not further modified by high sodium intake (Figure 3.1), it is not clear why differences in corticosterone levels are only evident on a high sodium diet. Therefore, if the ability of 11β-HSD2 to metabolise corticosterone has not changed in this setting, then some other reaction to the increased sodium intake must be causing corticosterone levels to increase. Of particular interest is the observation that corticosterone concentrations increase in *Hsd11b2*$^{+/+}$ mice as well as *Hsd11b2*$^{+/-}$ mice on a high sodium diet, although not to the same extent (Figure 3.6). This suggests that the high sodium diet per se may enhance corticosterone levels, an effect amplified by low 11β-HSD2 activity.

Whatever the cause(s) of the corticosteroid increase it appears that in *Hsd11b2*$^{+/-}$ mice, under normal dietary conditions, the reduction in corticosteroid metabolism is not sufficient to cause a measurable phenotype in terms of BP. Under these conditions, the reduction in 11β-HSD2 activity is presumably compensated for by other forms of metabolism, such as the 5α- and β-reductases. However, when the levels of corticosterone are increased on a high sodium diet, the compensatory pathway of metabolism can no longer sustain the level of metabolism required to maintain a normal phenotype, and the *Hsd11b2*$^{+/-}$ mice present with an elevated BP and impaired natriuresis. To address the mechanism of this effect further, it will

be important to establish the effect of increased sodium intake upon other factors involved in both glucocorticoid production and metabolism, such as ACTH levels and 5α- and β-reductase metabolites, respectively. It will also be important to investigate other potential consequences of increased sodium intake that could cause these phenotypes to occur.

4.4.3 Summary

In summary, the studies described here show that the regulation of both aldosterone and corticosterone appears to be deregulated in *Hsd11b2*$^{+/-}$ mice on a both standard and a high sodium diet. On a standard sodium diet, this does not result in a phenotype (as far as is measured within the experiments presented here); the deregulation of both steroids is exacerbated by a high sodium diet, and it is only then that the natriuresis and BP phenotypes of the *Hsd11b2*$^{+/-}$ mice present. This suggests that high levels of dietary sodium are inducing changes in these mice that render them unable to cope physiologically, as they could before on a standard sodium diet, in the face of reduced 11β-HSD2 enzyme activity. Mineralocorticoids and glucocorticoids, via their many physiological effects, undoubtedly play an important role in the mechanism(s) of the SS phenotype of *Hsd11b2*$^{+/-}$ mice, although exactly why an increased sodium intake alters some of these effects is yet to be established.

Chapter 5

Salt-Sensitivity and Oxidative Stress

5.1 Introduction

There is strong evidence from a number of studies that SS BP may be linked to renal oxidative stress (Manning et al., 2005; Taylor et al., 2006; Tian et al., 2005). Oxidative stress-induced changes in intracellular reductive-oxygen reaction balance may determine the ligand specificity of transcription factor regulation (Liu et al., 2005; Zhang et al., 2002). A link between sodium intake, oxidative stress and MR ligand specificity begins to emerge that may further explain why reduced 11β-HSD2 activity causes a SS BP increase.

5.1.1 Oxidative Stress

Reactive oxygen species (ROS) are highly reactive, short-lived derivatives of oxygen metabolism that are produced in all biological systems and play an important role physiologically. Examples of endogenously produced ROS include superoxide radical ($O_2^{\cdot-}$), hydrogen peroxide (H_2O_2), and nitric oxide (NO), which all play important roles in vascular biology (Roberts and Sindhu, 2009). ROS are normally inactivated and rendered harmless by a series of endogenous antioxidant enzymes (such as superoxide dismutase (SOD), catalase (CAT) and glutathione peroxidase (GPX)) and also by dietary antioxidant compounds (such as Vitamin C and E). Oxidative stress occurs when the net amount of ROS produced exceeds the buffering capacity of the antioxidants available; this can be the result of increased ROS production, decreased availability of antioxidants, or a combination of the two. Under conditions of oxidative stress, elevated ROS levels can act to enhance lipid peroxidation, cause DNA damage and induce protein modifications, thus leading to cellular dysfunction.

5.1.2 Oxidative Stress and Hypertension

Oxidative stress has been well documented in models of AngII-dependent hypertension (Kawada et al., 2002; Wilcox, 2002). However, there is also substantial evidence of oxidative stress in the development hypertension where the RAAS is suppressed (Beswick et al., 2001; Nicod et al., 2000). A link between oxidative stress and high BP causing renal inflammation and damage has also been demonstrated in models of SS hypertension, such as the Dahl SS rat (Meng et al., 2002; Tian et al., 2008). These studies may be relevant in the *Hsd11b2*$^{+/-}$ model of SS hypertension where the RAAS has been shown to be suppressed on a high sodium diet (Chapter 4).

Although ROS are short-lived, they leave a detectable trace of modified oxidative products which act as surrogate markers for oxidative stress. Two such markers, the F_2-isoprostanes and NADPH oxidase subunits, are up regulated in different models of experimental hypertension (Paravicini and Touyz, 2008). The F_2-isoprostanes are a family of eicosanoids produced by the oxidation of arachidonic acid by ROS that are frequently used as marker of oxidative stress *in vivo* (Davi et al., 1999; Pratico et al., 2001; Roberts and Morrow, 2000). NADPH oxidase is a major producer of ROS in both the kidney and the vasculature. NADPH oxidase consists of a number of subunits, both cytosolic and membrane-bound, which form the functional enzyme complex. These include p47phox, p67phox (both cytosolic), gp91phox, Nox1, Nox4 and p22phox (all membrane-bound). Different subunits have different expression patterns throughout the kidney (for review of kidney NAPDH oxidases see (Gill and Wilcox, 2006)). NADPH oxidase can be regulated by vasoconstrictive hormones, such as AngII, as well as by growth factors and mechanical stimuli such as shear stress and

stretch (Lassegue and Clempus, 2003). In addition, pharmacological approaches suggest that the effect of RAAS activation in AngII-dependent hypertensive models may in part be attributable to MR in *Nox2*$^{-/-}$ mice (Johar et al., 2006) and Ren-2 transgenic rats (Lastra et al., 2008).

5.1.3 Increased Salt Loading and Oxidative Stress

A study where a high sodium diet was fed to normal rats who did not develop SS hypertension highlighted a potential direct link between high sodium intake and renal oxidative stress (Kitiyakara et al., 2003). Measurements of urinary markers of oxidative stress (8-isoprostane (8-iso-PGF2α) and malonyldialdehyde) and real-time PCR assessment of NADPH oxidase subunits showed that salt loading *per se* was inducing oxidative stress in the kidneys of normal rats. Another more recent study reinforces these observations as again high sodium loading in rats resulted in increase urinary excretion of 8-iso-PGF2α and increases in both NADPH oxidase subunit expression and enzyme activity (Johns et al., 2010).

5.1.4 Treatment of Hypertension with Antioxidants

Further evidence of the potential importance of oxidative stress and high BP comes from studies where hypertension has been successfully treated with antioxidants (for review see (Manning et al., 2005). In spontaneously hypertensive rats (SHR) a two week administration of the SOD mimetic antioxidant 4-hydroxy-2, 2, 6, 6-tetramethyl piperidinoxyl (TEMPOL) reduced both BP and renal excretion of F_2-isoprostanes (Schnackenberg and Wilcox, 1999). TEMPOL treatment of DOCA-salt hypertensive rats, along with another antioxidant pyrrolidinedithiocarbamate (PDTC), attenuated

both the high BP and renal inflammation observed in this hypertensive model (Beswick et al., 2001). In addition to the successes of SOD-mimetic antioxidants, the administration of Vitamin C and E to Dahl SS rats on a high sodium diet significantly reduced renal O_2^{-} release, blood pressure, and renal damage (Tian et al., 2005).

5.1.5 Summary

The contribution of oxidative stress towards the SS phenotype of *Hsd11b2*$^{+/-}$ mice was investigated in conscious and anaesthetised mice. Urinary levels of the oxidative stress marker 8-iso-PGF2α were measured in mice on a standard and then a high sodium diet using the metabolic cage approach as described previously. Parallel studies were performed in which mice received the antioxidant drug TEMPOL in combination with a high sodium diet. Renal clearance experiments were also performed to investigate BP and renal function. This is of particular relevance as changes in local oxidative stress balance have been shown to be involved in the regulation of receptor-ligand activation of the GR (Okamoto et al., 1999; Tanaka et al., 1999), a dynamic that is altered in *Hsd11b2*$^{+/-}$ mice due to improved glucocorticoid access to the MR.

5.2 Results

5.2.1 Metabolic Cage Studies

The daily urinary excretion of the oxidative stress marker 8-iso-PGF2α was measured in conscious *Hsd11b2*$^{+/+}$ and *Hsd11b2*$^{+/-}$ mice first on a standard, and then on a high, sodium diet. 8-iso-PGF2α levels were similar between the two genotypes on a standard sodium diet (Figure 5.1).

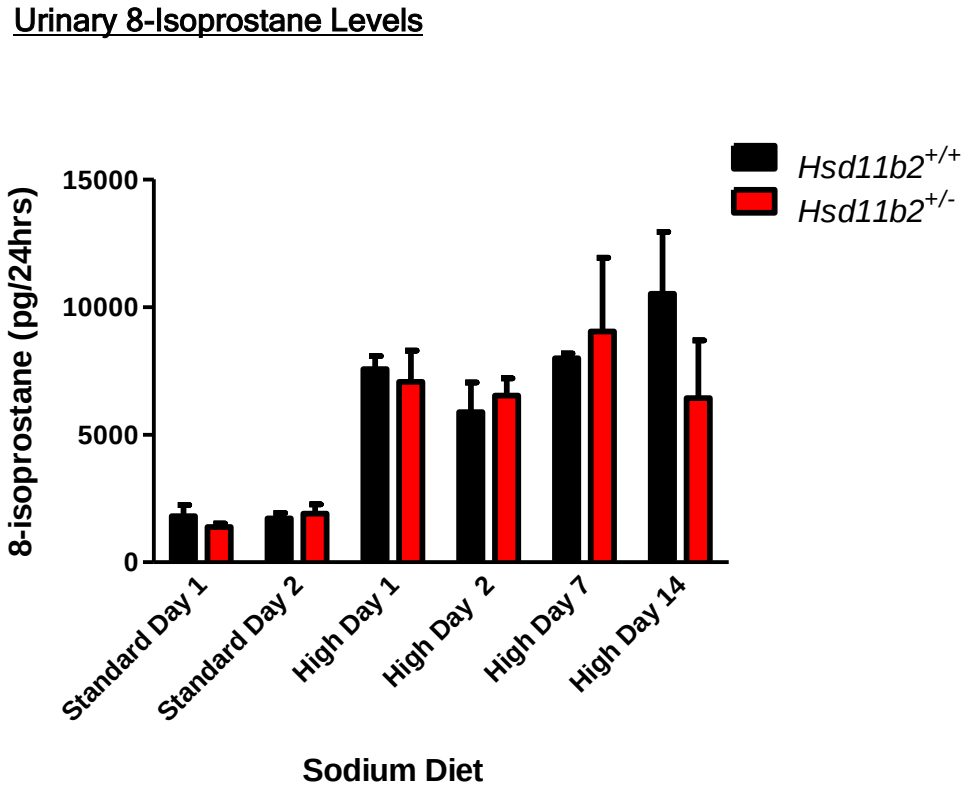

Figure 5.1. 24 hour urinary 8-isoprostane concentration of *Hsd11b2*$^{+/+}$ and *Hsd11b2*$^{+/-}$ mice on a standard and a high sodium diet (n = 4 for both groups). There was no difference between the two groups on either sodium diet. High sodium diet causes a significant increase in 8-isoprostane levels on Day 1; $P < 0.001$. Data are means ± SEM.

Transition to a high sodium diet caused a substantial increase in urinary 8-iso-PGF2α excretion in both genotypes and there was no significant

difference between the two genotypes during the time points investigated. These results suggested that a high salt diet was causing oxidative stress in both genotypes, and the effect of the antioxidant drug TEMPOL was therefore measured.

TEMPOL did not affect sodium excretion on a standard sodium diet in either *Hsd11b2*$^{+/+}$ or *Hsd11b2*$^{+/-}$ mice (Figure 5.2a). The natriuretic response to high sodium feeding was unaffected by TEMPOL in *Hsd11b2*$^{+/+}$ mice. *Hsd11b2*$^{+/-}$ mice showed an improved sodium excretion and no longer exhibited a period of positive sodium balance (Figure 5.2b and c compared with Figure 3.3b and c, Chapter 3).

TEMPOL treatment did not change the 24 hour urine flow rate water on a standard sodium diet in either genotype, with both *Hsd11b2*$^{+/+}$ and *Hsd11b2*$^{+/-}$ mice excreting similar volumes (Figure 5.3a). The urine flow rate on a high sodium diet is similar for the two groups during TEMPOL treatment (Figure 5.3b), and in agreement with this, water balance is not significantly altered by the change in dietary sodium content during TEMPOL treatment (Figure 5.3c).

5.2.2 Renal Clearance Studies

After three weeks on a high sodium diet with TEMPOL administration, mice were prepared for renal clearance surgery. MABP measurements showed that TEMPOL treatment attenuated the BP increases observed in *Hsd11b2*$^{+/-}$ mice on a high sodium diet; both genotypes had similar values (Figure 5.4a compared to Figure 3.7). In terms of renal hemodynamics, TEMPOL treatment also appeared to attenuate the increased GFR previously observed in *Hsd11b2*$^{+/-}$ mice compared to *Hsd11b2*$^{+/+}$ mice on both a standard and a high

a) TEMPOL Treatment Sodium Excretion Control

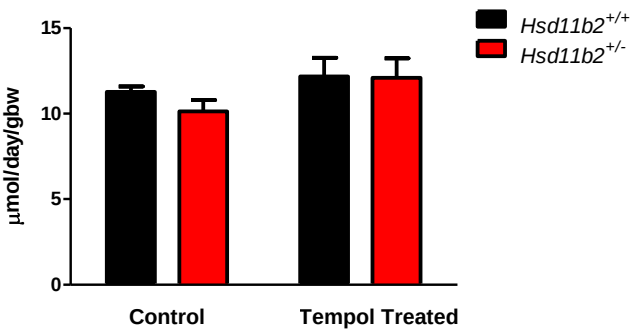

b) Daily Sodium Excretion during TEMPOL Treatment

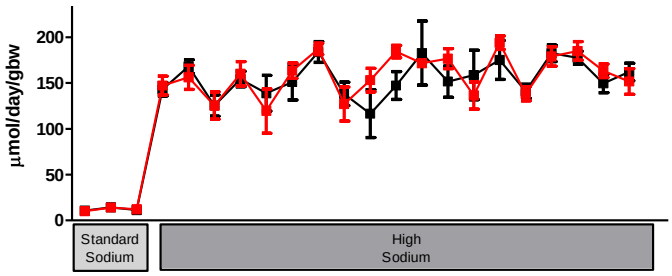

c) Sodium Balance during TEMPOL Treatment

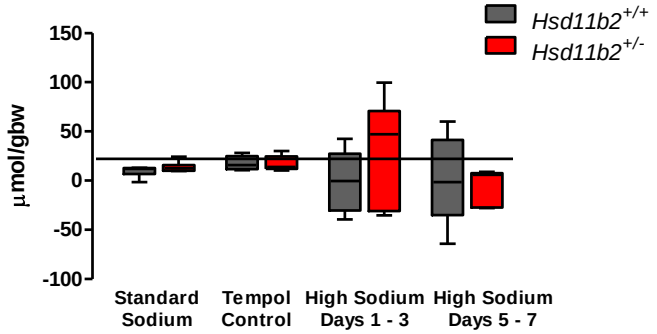

Figure 5.2. TEMPOL treatment metabolic cage study (n = 8 for both groups). Urinary sodium excretion **a)** on a standard sodium diet before and after TEMPOL treatment, and **b)** recorded daily on a standard and high sodium diet with TEMPOL treatment. TEMPOL treatment on a standard sodium diet had no effect upon urinary sodium excretion. High sodium diet caused a significant increase in urinary sodium excretion ($P < 0.001$); there was no difference between *Hsd11b2*$^{+/+}$ and *Hsd11b2*$^{+/-}$ mice. **c)** Sodium balance was calculated using sodium intake and urinary sodium excretion over 3 day periods. There was no significant difference between genotypes during any period. Data are means ± SEM for **a)** and **b)**, and as the median, interquartile range and full range for **c)**.

a) TEMPOL Treatment Urine Flow Rate Control

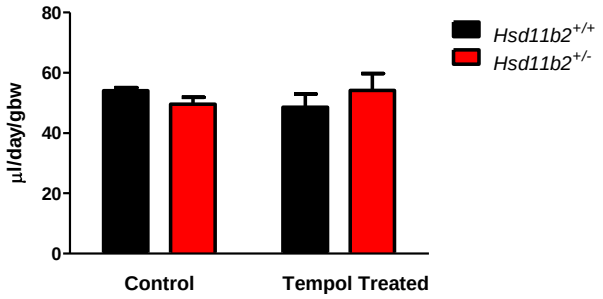

b) Daily Urine Flow Rate during TEMPOL Treatment

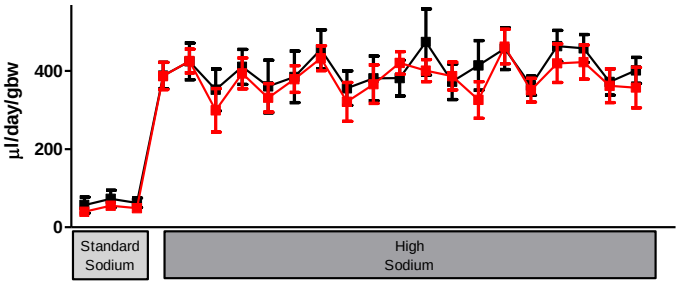

c) Water Balance during TEMPOL Treatment

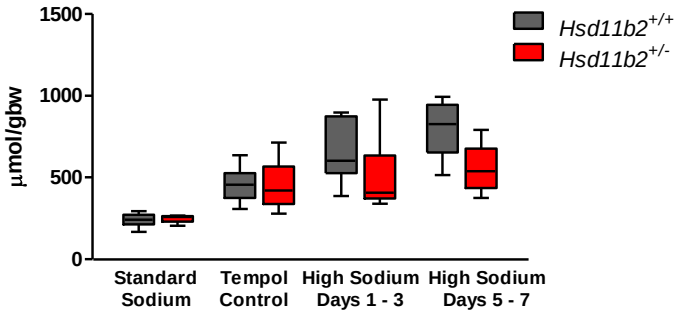

Figure 5.3. TEMPOL treatment metabolic cage study (n = 8 for both groups). Urine flow rate (UFR) **a)** on a standard sodium diet before and after TEMPOL treatment, and **b)** recorded daily on a standard and high sodium diet with TEMPOL treatment. TEMPOL treatment on a standard sodium diet had no effect upon UFR. High sodium diet caused a significant increase in UFR ($P < 0.001$); there was no difference between *Hsd11b2*$^{+/+}$ and *Hsd11b2*$^{+/-}$ mice. **c)** Water balance was calculated using drinking water intake and urinary UFR over 3 day periods. There was no significant difference between genotypes during any period. Data are means ± SEM for **a)** and **b)**, and as the median, interquartile range and full range for **c)**.

. a) MABP

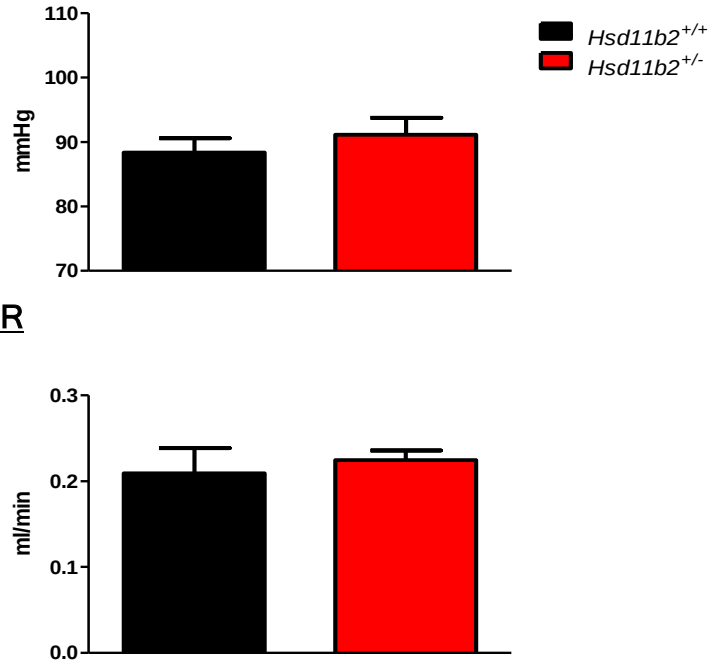

Figure 5.4. Measurements made during renal clearance surgery after 3 weeks on a high sodium diet with TEMPOL treatment of **a)** mean arterial BP (MABP) and **b)** glomerular filtration rate (GFR) (n = 8 for both groups). *Hsd11b2*$^{+/+}$ and *Hsd11b2*$^{+/-}$ mice have similar values for MABP and GFR. Data are means ± SEM.

sodium diet (Figure 5.4b compared to Figure 3.8a, Chapter 3). Measurements of the urine excretion and plasma concentration of sodium and potassium were also obtained. These were not different for any of the values between the genotypes on a high sodium diet with TEMPOL treatment (Figure 5.5a - d).

After baseline measurements for MABP, GFR, and plasma electrolytes had been made, measurements were repeated in the same mice after an I.V. dose of the ENaC blocker amiloride. Differences in MABP and GFR measurements after amiloride administration were not significantly different between the two genotypes (Figure 5.6a and b). Differences in the urinary excretion of sodium and potassium were also measured; there was no difference in terms

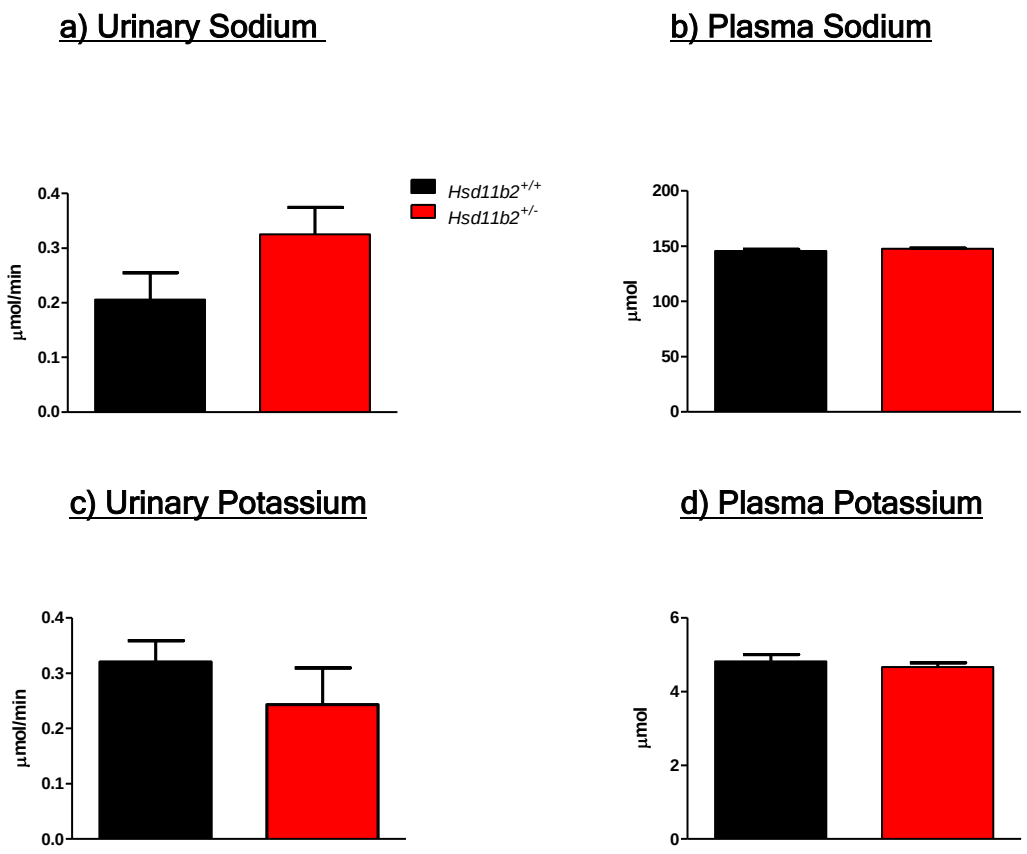

Figure 5.5. Urine and plasma electrolytes (n = 8 for both groups). Measurements made during renal surgery after 3 weeks on a high sodium diet with TEMPOL treatment of **a)** urinary sodium, **b)** plasma sodium, **c)** urinary potassium, and **d)** plasma potassium concentrations. There is no significant difference in the plasma and urinary concentrations of both sodium and potassium between *Hsd11b2*$^{+/+}$ and *Hsd11b2*$^{+/-}$ mice. Data are means ± SEM.

of potassium excretion, but *Hsd11b2*$^{+/+}$ mice exhibited a significantly greater increase in urinary sodium excretion after amiloride administration than *Hsd11b2*$^{+/-}$ mice (Figure 5.6c and d).

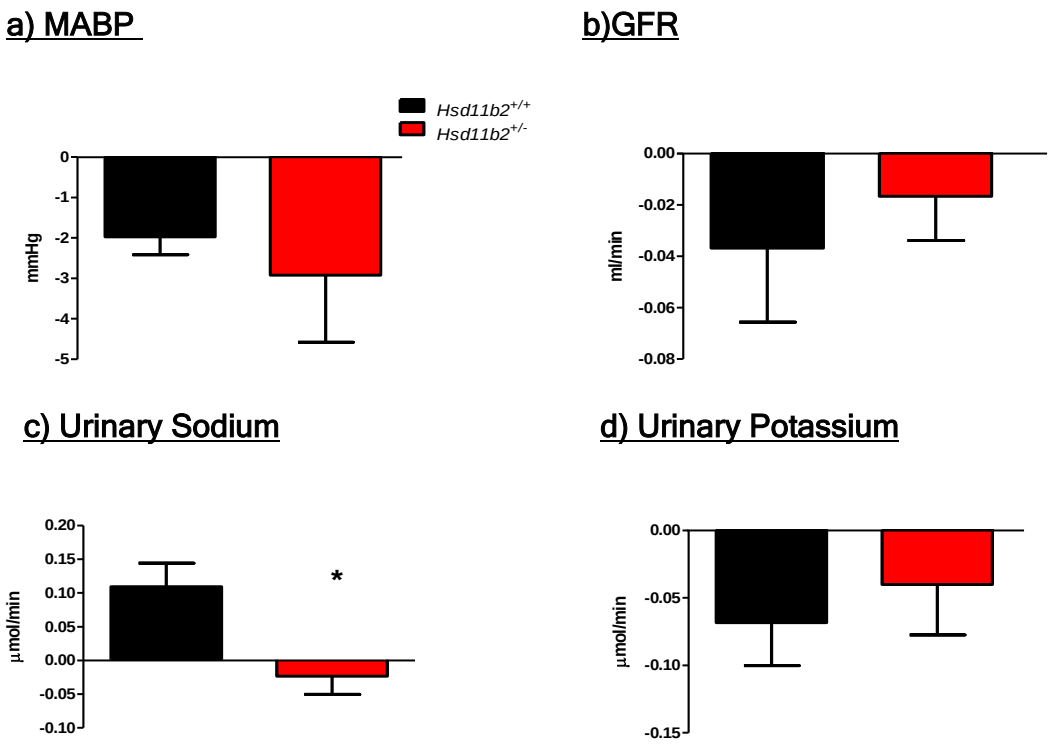

Figure 5.6. The effects of amiloride administration during renal surgery after 3 weeks on a high sodium diet with TEMPOL treatment upon **a)** MABP, **b)** GFR, **c)** urinary sodium excretion, and **d)** urinary potassium excretion (n = 8 for both groups). There is no significant difference in the effect of amiloride upon MABP, GFR, or urinary potassium excretion between the two groups. Amiloride causes significantly more sodium excretion in *Hsd11b2*$^{+/+}$ mice compared to *Hsd11b2*$^{+/-}$ mice, where it has little effect. ***** $P < 0.05$. Data are means ± SEM.

5.2.3 TEMPOL Effects upon 8-Iso-PGF2α Urinary Excretion

To establish if the observed improvements in the SS phenotype of *Hsd11b2*$^{+/-}$ mice during TEMPOL treatment was a consequence of reduced renal oxidative stress, 8-iso-PGF2α levels were measured in 24 hour urine collections.

On a standard sodium diet, TEMPOL administration caused no difference in 8-iso-PGF2α excretion between *Hsd11b2*$^{+/+}$ and *Hsd11b2*$^{+/-}$ mice (Figure 5.7a). On Day 1 of the high sodium diet, there was no significant change in 8-iso-

a) Urinary 8-Isoprostane Levels during TEMPOL Treatment

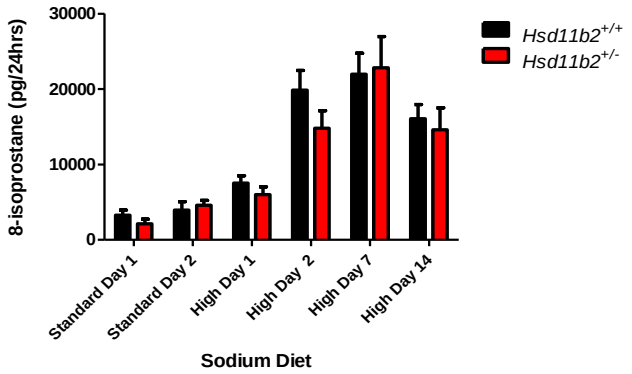

b) Urinary 8-Isoprostane Levels during TEMPOL Treatment - *Hsd11b2*$^{+/+}$

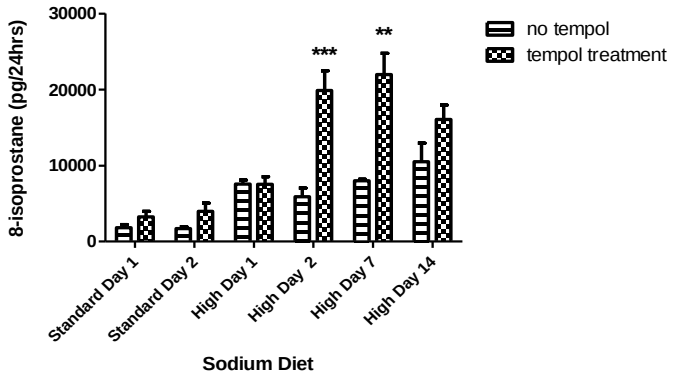

c) Urinary 8-Isoprostane Levels during TEMPOL Treatment - *Hsd11b2*$^{+/-}$

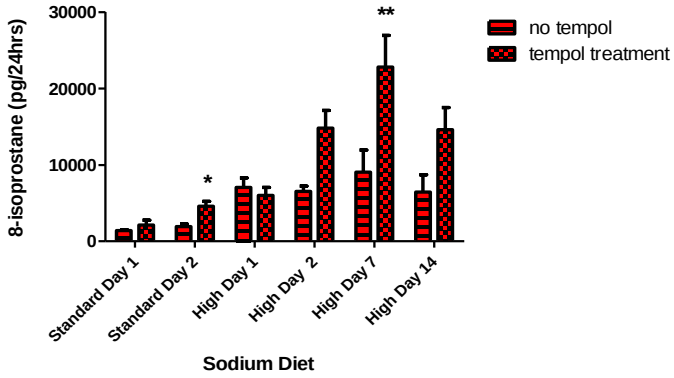

Figure 5.7. 24 hour urinary 8-isoprostane concentration of **a)** *Hsd11b2*$^{+/+}$ and *Hsd11b2*$^{+/-}$ mice on a standard and a high sodium diet with TEMPOL treatment, and **b)** *Hsd11b2*$^{+/+}$ and **c)** *Hsd11b2*$^{+/-}$ mice only on both diets (n = 4 for both genotypes). There was no difference between the two groups on either sodium diet. High sodium diet causes a significant increase in 8-isoprostane levels on Day 2 ($P < 0.001$), with Day 1 not differing significantly from the standard sodium results. TEMPOL treatment had an overall significant effect upon 8-isoprostane excretion in *Hsd11b2*$^{+/+}$ mice on different sodium diets ($P < 0.001$), with post-hoc significance at Day 2 and 7 on a high sodium diet. TEMPOL also had an overall

significant effect upon 8-isoprostane excretion in *Hsd11b2*$^{+/-}$ mice between the two sodium diets ($P < 0.001$), with post-hoc significance at Day 2 on a standard sodium diet and Day 7 on a high sodium diet. ***** $P < 0.05$; ****** $P < 0.01$; ******* $P < 0.001$. Data are means ± SEM.

PGF2α levels compared to on a standard sodium diet for either group. On Day2 of the high sodium diet, there was a significant increase in 8-iso-PGF2α excretion that continued on Day 7 and Day 14.

The 8-iso-PGF2α levels on the standard and high sodium diets were then compared within the individual genotypes. There was no significant effect of TEMPOL treatment on the 8-iso-PGF2α excretion on a standard sodium diet or on Day 1 of the high sodium diet for either *Hsd11b2*$^{+/+}$ and *Hsd11b2*$^{+/-}$ mice (Figure 5.7b and c, respectively). However, both groups showed an unexpected trend for increased levels of 8-iso-PGF2α after Day 2 on the high sodium diet.

5.3 Discussion

This chapter describes a salt-induced increase in urinary excretion of the oxidative stress marker 8-iso-PGFα in both *Hsd11b2*$^{+/+}$ and *Hsd11b2*$^{+/-}$ mice. TEMPOL administration in conjunction with a high sodium diet prevented the development of both impaired natriuresis and increased BP in *Hsd11b2*$^{+/-}$ mice, but did not alter the excretion of 8-iso-PGFα.

5.3.1 A High Sodium Diet Increases Oxidative Stress

The salt-induced increase in the urinary excretion of 8-iso-PGF2α was similar in both groups, and was not exacerbated by reduced enzyme activity of 11β-HSD2. Therefore, it is the high sodium diet *per se* that is causing the perceived increases in oxidative stress and not a secondary effect of the hypertension observed in *Hsd11b2*$^{+/-}$ mice on a high sodium diet. This is in agreement with previous studies where a high sodium diet has been shown to cause oxidative stress independently of increased BP (Johns et al., 2010; Kitiyakara et al., 2003). The identification of increases in additional markers of oxidative stress, such as using real-time PCR to quantify NADPH Oxidase subunits in the kidney, would further support this finding that a high salt diet induces oxidative stress in these mice.

5.3.2 Antioxidant Administration Rescues *Hsd11b2*$^{+/-}$ Salt-Sensitive Phenotype

Administration of TEMPOL was used in an attempt to provide anti-oxidant therapy. TEMPOL is a small molecule cell-permeable SOD mimetic that catalyses the dismutation of O_2^{-} into metabolic oxygen & H_2O_2, and acts as an

important antioxidant defence in cells (for review see (Wilcox and Pearlman, 2008)). Many of the phenotypes associated with salt-loading in *Hsd11b2*$^{+/-}$ mice were attenuated by TEMPOL administration. Surprisingly, TEMPOL actually increased ENaC-mediated sodium reabsorption in the *Hsd11b2*$^{+/+}$ mice on a high sodium diet with TEMPOL administration (Figure 5.6c). This suggests that TEMPOL administration was somehow causing ENaC not to be down regulated in *Hsd11b2*$^{+/+}$ mice on a high sodium diet. Analysis of plasma aldosterone and glucocorticoid levels in these mice during TEMPOL treatment may provide further insights as to why this may be.

Overall, these studies showed that administration of TEMPOL at the same time as the high sodium diet was therapeutically successful. However, this effect cannot be attributed to the restoration of a favourable REDOX state as TEMPOL did not reduce 8-iso-PGFα excretion in either group, and this was even increased at some time points. In many studies of oxidative stress-related hypertension, TEMPOL administration is sufficient to reduce both BP and 8-iso-PGF2α levels (Brands et al., 2004; Knight et al.; Schnackenberg and Wilcox, 1999; Welch et al., 2005). However, some studies also describe the ability of TEMPOL to reduce BP without effecting 8-iso-PGF2α levels. Williams *et al* reported that TEMPOL administration in Sprague-Dawley rats had no effect upon plasma 8-iso-PGF2α levels after three days on a high sodium diet compared to no-TEMPOL controls, despite lowering arterial BP; after seven days, 8-iso-PGF2α levels were actually increased compared to controls (Williams et al., 2004). A different study using TEMPOL to treat ACTH-induced hypertension followed a similar pattern. TEMPOL treatment at day 8 of ACTH treatment reversed hypertension and pre-treatment for four days before ACTH administration partially prevented it, but 8-iso-

PGF2α levels remained elevated under both circumstances (Zhang et al., 2003).

There are several possible explanations for these findings. SOD mimetics, such as TEMPOL, may cause accumulation of H_2O_2 in the kidney (Makino et al., 2003). This potentially happens due to the method of SOD action. SODs work to reduce ROS by catalysing $O_2^{\cdot-}$ to metabolic oxygen and H_2O_2. H_2O_2 is a much less reactive ROS than $O_2^{\cdot-}$, and unlike $O_2^{\cdot-}$ it can diffuse across cell membranes avoiding excessive accumulation in regions of production (Antunes and Cadenas, 2000). This means that a high concentration of TEMPOL may be leading to reduced levels of highly reactive $O_2^{\cdot-}$ at the expense of increased levels of less-reactive H_2O_2. The increased levels of H_2O_2 may then result in the high levels of 8-iso-PGF2α excretion observed during TEMPOL treatment in both *Hsd1b2*$^{+/+}$ and *Hsd11b2*$^{+/-}$ mice. The dosing of TEMPOL chosen for this study (2 mmol/l administered on drinking water – see Materials and Methods Chapter) has been previously used in many published studies of TEMPOL administration in rats; perhaps it is too high a dose for studies in mice and caused increased production of H_2O_2 which lead to increased levels of 8-iso-PGF2α.

In addition, some studies suggest that TEMPOL administration may decrease central sympathetic nerve responses, which could also explain the rescue of increased BP and impaired natriuresis without reducing 8-iso-PGF2α levels (Lu et al., 2004; Shokoji et al., 2003); sympathetic nerve function in these studies could be assessed by measuring the levels of catecholamines in 24 hour urine collections. However, other studies in which TEMPOL rescues increases in blood pressure in spontaneously hypertensive rats show catecholamine levels not to be affected by TEMPOL administration (Welch et al., 2005). It will be important to measure the concentration of

catecholamines in the urine of *Hsd11b2*$^{+/+}$ and *Hsd11b2*$^{+/-}$ mice before and during TEMPOL treatment to confirm the action of TEMPOL rescue in these experiments. TEMPOL treatment has also been shown in numerous animal studies to restore the agonist-induced endothelium-dependent vasodilation, and this may well be contributing to the anti-hypertensive effects seen in these experiments (Simonsen et al., 2009). In addition, the modulation of potassium channels has also been suggested as a mechanism for the antihypertensive actions of TEMPOL. TEMPOL-induced vasodilation was enhanced in perfused mesenteric arteries from DOCA salt hypertensive rats, and these effects could be reduced by application of a vascular large-conductance calcium-activated potassium (BK_{Ca}) channel blocker (Xu et al., 2005). In addition, TEMPOL may also enhance vasodilation through modulation of ATP-sensitive potassium channels (Chen et al., 2007). This may be particularly relevant to the *Hsd11b2*$^{+/-}$ model as potassium homeostasis has been shown to be altered (see Chapter 3).

These studies could also be repeated using a different antioxidant drug to see if the rescue effects of TEMPOL can be replicated.

5.3.4 11β-HSD2, REDOX Balance and MR Regulation

The suggestion that oxidative stress caused by a high sodium diet may be contributing to the SS phenotypes of *Hsd11b2*$^{+/-}$ mice is particularly interesting in terms of 11β-HSD2 activity and MR ligand-activation regulation, and may be a reason why the SS phenotypes only occur on a high sodium diet. Studies using cloned 11β-HSD2 protein have shown that *in vitro* conversion of cortisol to corticosterone displays a linear dose response (Ferrari et al., 1996). Glucocorticoids therefore technically have "improved" access to MR in the *Hsd11b2*$^{+/-}$ mice at all times, but this appears to have no

physiological consequences under normal sodium diet conditions. Further investigations studying the binding of tracer ^{3}H-aldosterone in kidney, colon, heart and hippocampal extracts, suggest that MR are always highly occupied by glucocorticoids, but not always activated (Funder and Myles, 1996). This poses the question why does glucocorticoid activation of MR, and the consequential detrimental effects, only occur when the system is exposed to increased levels of sodium? A possible explanation begins with studies showing a link between increased salt intake and renal oxidative stress (Gill and Wilcox, 2006). If a high sodium diet changes the oxidative stress state of the kidney, then the local REDOX (reduction-oxidation reaction) balance would be altered. It has been suggested that changes in the REDOX balance of MR and 11β-HSD2 target tissues may alter the ability of glucocorticoids to activate the MR (Funder, 2005). That is, under a normal REDOX state, glucocorticoids can occupy MR, but do not necessarily activate them. However, when something acts to change the intracellular REDOX state, such as high sodium diet, this permits glucocorticoids to activate the MR.

REDOX state is also affected by the balance between reduced and oxidised molecular pairs, including NAD(P)H/NAD(P). This is a balance that will be affected locally by a reduced activity of 11β-HSD2, as the conversion of cortisol to cortisone by 11β-HSD2 requires the reduction of NAD to NADH. It has been estimated that under resting conditions the intracellular levels of NAD are approximately 700-fold greater than NADH, and that generation of NADH by 11β-HSD2 can produce major changes to this ratio (Funder, 2004). In a physiological situation where the conversion of cortisol to cortisone is reduced, such as the *Hsd11b2*$^{+/-}$ mice, the local REDOX balance will be altered compared to normal. And if excessive ROS is being produced under conditions of a high sodium diet, these two factors together may contribute

towards MR transcriptional activation becoming altered due to a REDOX imbalance, thus permitting glucocorticoids to cause unregulated increases in MR activity. The REDOX-sensitive activation of other transcription factors has previously been demonstrated, such as the carboxyl-terminal binding protein (CtBP) (Fjeld et al., 2003; Liu et al., 2005; Zhang et al., 2002). In addition, *in vitro* studies showing REDOX-dependent regulation of GR nuclear import increase the possibility that MR activation may be regulated by REDOX state as well (Okamoto et al., 1999; Tanaka et al., 1999).

5.3.5 Summary

In summary, these studies show that a high sodium diet is inducing oxidative stress in both *Hsd11b2*$^{+/+}$ and *Hsd11b2*$^{+/-}$ mice, and that treatment with the antioxidant TEMPOL alleviates the SS phenotypes of *Hsd11b2*$^{+/-}$ mice. This suggests a direct link between salt intake, the REDOX balance of 11β-HSD2 expressing cells, and the ability of glucocorticoids to activate MR, as the SS phenotype of *Hsd11b2*$^{+/-}$ mice. This is particularly relevant as previous studies have suggested that MR is always occupied by glucocorticoids, but not always activated. REDOX balance may work in synergy with 11β-HSD2 to prevent MR activation by glucocorticoids under normal circumstances, but when REDOX balance is altered, it acts as a molecular switch in the control of MR ligand activation.

Chapter 6 Part 1

Generating a Floxed 11β-HSD2 Mouse

6p1.1 Introduction

The expression of 11β-HSD2 in sites other than the kidney could have important contributions to the phenotypes observed in the *Hsd11b2*$^{+/-}$ SS model described in earlier chapters, and also in SAME patients and the *Hsd11b2*$^{+/+}$ mouse model. In order to dissect the contributions made towards the phenotype by reduced or removed 11β-HSD2 activity at these different sites of expression, a targeting construct was developed to allow for conditional spatial deletion of the *Hsd11b2* gene by homologous recombination. This was achieved by employing Cre/*lox*P recombinase technology (for reviews see (Branda and Dymecki, 2004; Ryding et al., 2001)), which requires the flanking of the region of genomic DNA that encodes for the functional protein of interest by 2 *lox*P sites. The gene of interest is then said to be "floxed". When the 2 *lox*P sites are in the same orientation, Cre (a site-specific bacterial recombinase) can recombine the DNA strands on either side of the floxed region, thus deleting the floxed gene (Ghosh and Van Duyne, 2002). Expression of Cre recombinase can be regulated spatially or temporally, by placing it under the transcriptional control of either a tissue-specific or an inducible promoter. Thus, when the mouse with a floxed gene of interest is crossed with a transgenic mouse expressing Cre recombinase in a tissue or cell-type specific manner, the resulting offspring will have conditional deletion of the gene of interest. Expression of the gene will be normal in all other expression sites other than that targeted by Cre recombinase expression. This chapter describes the molecular techniques used for building a transgenic mouse model with a floxed *Hsd11b2* gene.

6p1.2 Results

6p1.2.1 Targeting Construct Design

6p1.2.1.1 Clone pS141

The plasmid clone pS141 (previously derived in the research group from bacterial artificial chromosome (BAC) RP23-410B24) was used to generate the original *Hsd11b2*$^{-/-}$ mouse model (Kotelevtsev et al., 1999). The pS141 clone is 15 kilo bases (Kb) in length, and spans the entire *Hsd11b2* gene, as well as additional upstream and downstream areas. This clone was already available within the research group (a kind gift from Dr. Yuri Kotelevstev), and had been previously transformed into a commercially available pBluescript vector (Stratagene), and was used to develop the new *Hsd11b2* floxed construct. The pS141 clone was transformed into competent *E. coli* cells; positive uptake of the pS141 was confirmed by ampicillin-resistance, which is conferred by the pBluescript vector. Positive colonies were grown in liquid broth (LB) culture, and DNA from these was purified (as described in Materials and Methods Chapter).

Approximately 20 Kb of the RP23-410B24 BAC sequence (which spans the 15Kb genomic clone pS141) was analysed by a web tool (http://tools.neb.com/NEB_cutter2) to generate a map of restriction enzyme sites. This was subsequently used to design a step-by-step construct building strategy (Figure 6.1). To begin with, the purified pS141 plasmid DNA was digested with the restriction enzyme XbaI to separate out the founding sub-clones to be used for building the final floxed *Hsd11b2* gene targeting construct.

a) *Hsd11b2* Floxed Targeting Construct Design

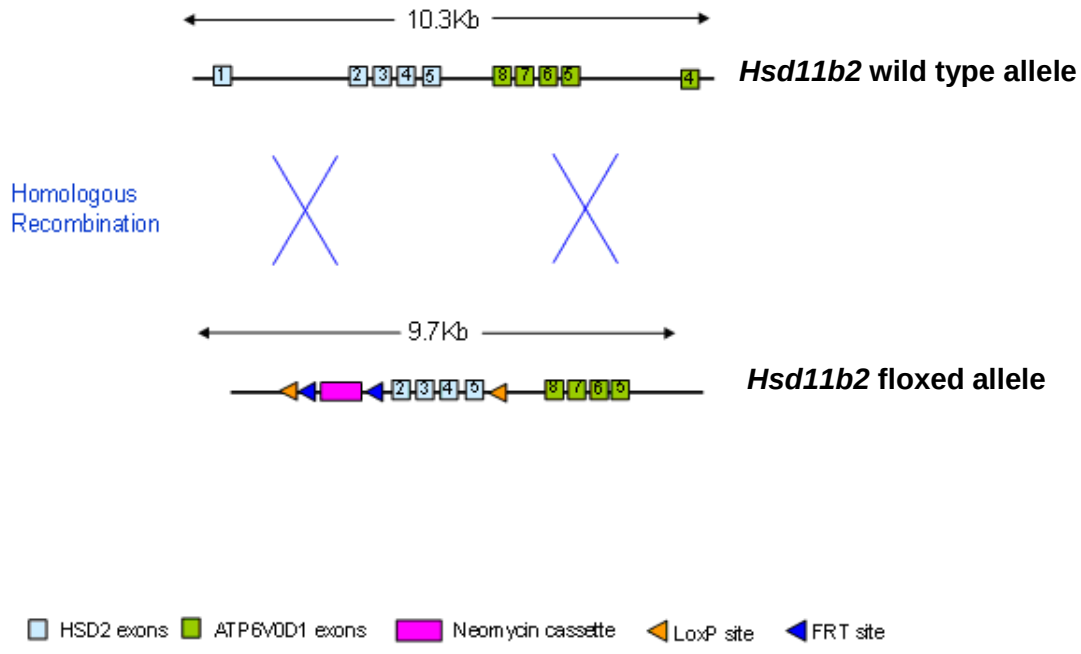

b) Schematic Flow Diagram of *hsd11b2* Floxed Targeting Construct

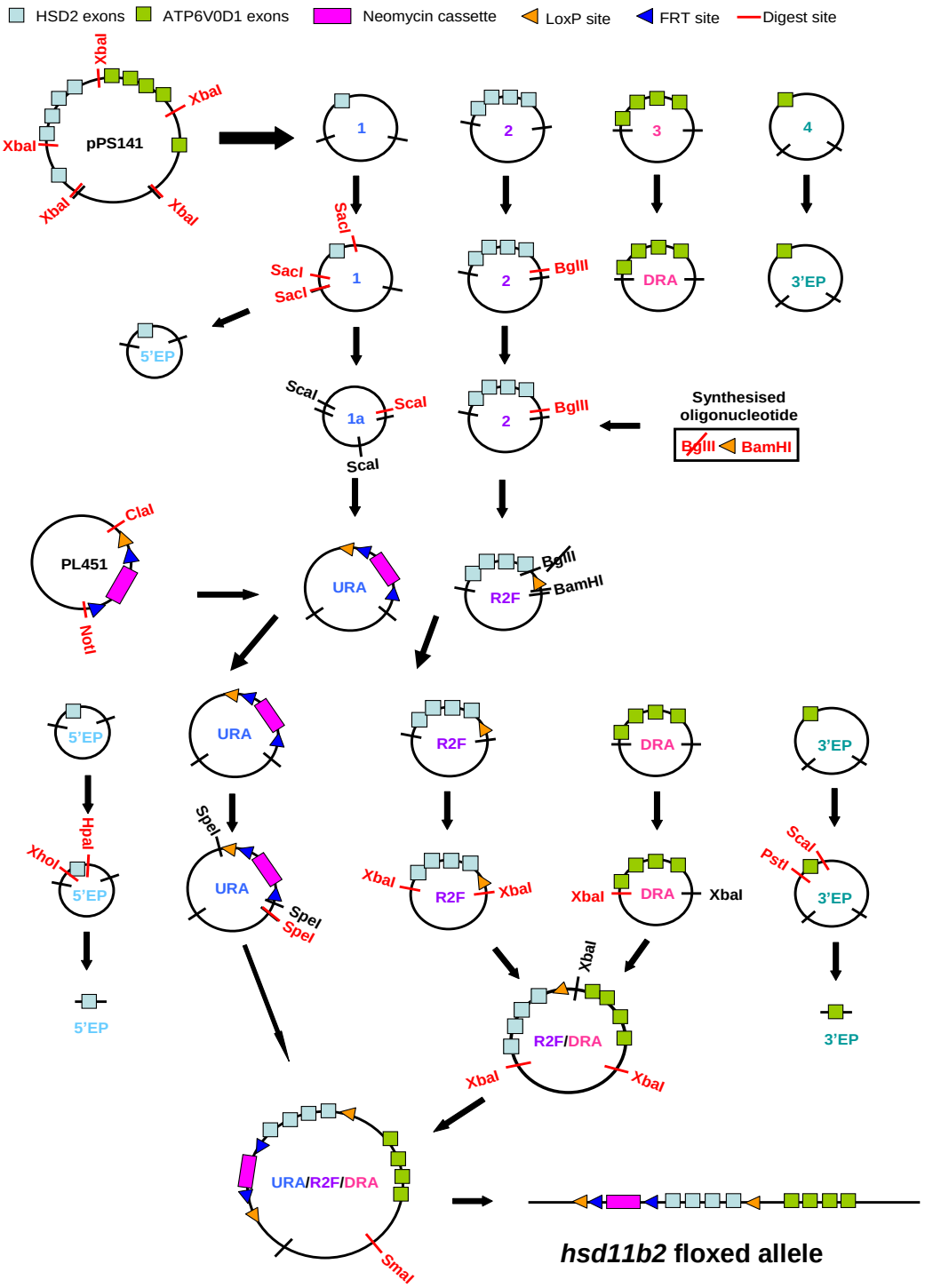

Figure 6.1. *Hsd11b2* Floxed Targeting Construct. **a)** *Hsd11b2* floxed construct design. **b)** *Hsd11b2* floxed construct step-by-step assembly plan.

6p1.2.1.2 Upstream Recombination Arm

The pS141 sub-clone that was to become the upstream recombination arm (URA) initially contained *Hsd11b2* exon 1 with both upstream and downstream intron sequence (labelled as "1" in Figure 6.1). Exon 1 was separated from this sub-clone by a SacI restriction enzyme digest, and put aside for future use as a 5 prime end (5') external probe (EP) for detecting homologous recombination of the completed construct. The sub-clone (labelled "1a" in Figure 6.1) now contained sequence from intron 1. A fragment containing the upstream *lox*P site and a neomycin resistance cassette was isolated from plasmid pL451 (Chapter 2; Figure 2.4) (Liu et al., 2003) by a ClaI/NotI double restriction enzyme digest. The neomycin resistance cassette was flanked by two FRT sites. The FRT/Flip recombinase system is analogous to the *lox*P/Cre recombinase system, and therefore permits the selectable removal of the neomycin cassette from the targeting construct if required. The isolated fragment containing these factors was inserted into the URA sub-clone at an open ScaI restriction site by a blunt-ended ligation. The URA sub-clone has three ScaI restriction sites, so insertion at the correct site had to be achieved by a partial digest to attain a linearised plasmid (Figure 6.2b). Insertion at the correct ScaI restriction site was subsequently identified by diagnostic restriction digest analysis.

6p1.2.1.3 Floxed Region and Downstream Recombination Arm

Exons 2 – 5 of the *Hsd11b2* gene had been chosen as the region to be removed under a Cre-*lox*P recombination event as deletion of this region in the original knock-out mouse had been show to be appropriate for full protein ablation (Kotelevtsev et al., 1999). The pS141 sub-clone containing exons 2 – 5 (labelled as "2" in Figure 6.1) required the insertion of a downstream *lox*P site to become the region to flox (R2F). This was achieved

URA ScaI Restriction Enzyme Partial Digest

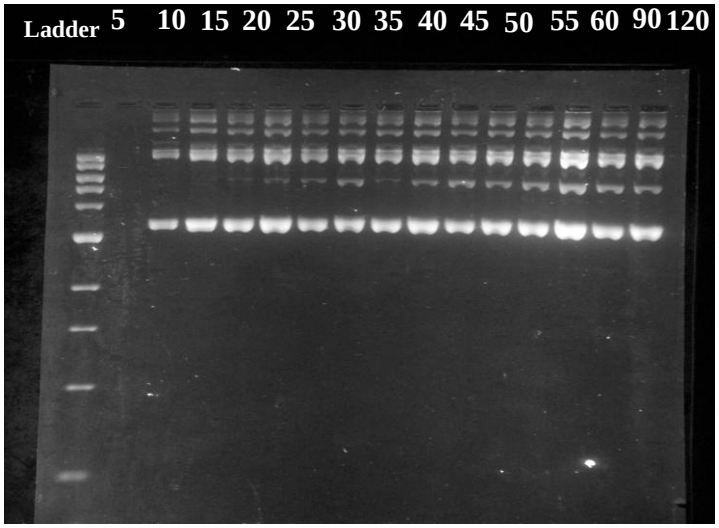

Figure 6.2. *Hsd11b2* Floxed Construct Assembly. Agarose gel electrophoresis separation of URA sub-clone ScaI restriction enzyme partial digest for subsequent insertion of *lox*P-FRT-Neomycin cassette by ligation. 5.5 Kb represents linearised DNA fragment, which was consequently excised from gel and DNA purified. Restriction digest times in minutes are illustrated along the top of figure.

using the Linker Tailing Method (Lathe et al., 1984), as detailed in the Materials and Methods chapter. Briefly, forward and reverse transcribing oligonucleotides were designed to encode for a 34 bp *lox*P site, and a novel 3 prime (3') BamHI restriction site. The ends of the oligonucleotides were designed to be compatible with an open BglII restriction site, and also to introduce a deliberate bp change to the original BglII restriction site to render it un-cleavable i.e. to destroy it. The R2F sub-clone was opened at a BglII restriction site and the *lox*P-BamHI oligonucleotides were synthesised and inserted. Correctly orientated clones were firstly identified by diagnostic restriction digest analysis, and *lox*P site orientation identified by bp sequencing. The finished R2F insert was removed from its vector backbone by an XbaI restriction digest, and ligated into the downstream recombination

arm sub-clone (DRA; labelled as "3" in Figure 6.1) opened at its extreme 5' XbaI restriction site.

The DRA sub-clone contained exons 5 – 8 of the neighbouring ATP6V0D1 gene (Pietrement et al., 2006) and required no further modifications. The ATP6V0D1 gene runs in the opposite orientation to *Hsd11b2*, and the terminal exons of the gene are separated by only a short intron sequence (less than 1Kb). As this sequence has the potential to contain important regulatory elements for the transcription of either or both genes, the decision was made to include this segment and ATP6V0D1 exons 5 - 8 in the DRA. The decision was also made to keep modifications within this region to a minimum during targeting construct building.

The ligation of the R2F insert into the DRA was achieved by partial digestion, as described before with the URA, as the DRA has two XbaI restriction sites. The R2F/DRA insert was then excised from its vector backbone by another XbaI partial restriction digest, and ligated into the URA opened at an extreme 3' SpeI restriction site. This plasmid was then linearised by a SmaI restriction digest to give the final *Hsd11b2* floxed targeting construct.

6p1.2.1.4 5' and 3' External Probes

5' and 3' EPs are required in order to verify homologous recombination of the targeting construct into the mouse genome. This was performed by Southern hybridisation, which will be discussed in more detail later. The EPs must recognise an area out with the targeting construct so that they can distinguish between genomic DNA with and without the insertion of the targeting construct. Probes were designed to give a different sized product for hybridisation depending upon whether the allele was wild type or gene targeted for *Hsd11b2*. The probes were made mostly from exon sequence as

this is more sequence specific than intron sequence, and thus less likely to result in non-specific hybridisation and a false or ambiguous result.

Briefly, the 5′ EP contained *Hsd11b2* exon 1 and was isolated from the same pS141 sub-clone as the URA (discussed in section 6p1.2.2; Figure 6.1). This was "trimmed" further to contain less non-specific intron sequence by isolating exon 1 with an XhoI/HpaI double restriction enzyme digest. The 3′ EP was isolated directly from a pS141 sub-clone (labelled "4" in Figure 6.1) and contained exon 4 of the ATP6V0D1 gene. The 3′ EP was also "trimmed" by a restriction enzyme digest (PstI/ScaI) to contain less intron sequence (to make it more sequence specific).

6p1.2.2 Introducing the *Hsd11b2* Targeting Construct into ES Cells

6p1.2.2.1 Electroporation

In order for a targeting construct to become incorporated into the mouse genomic DNA by homologous recombination, it must first be introduced into cultured embryonic stem (ES) cells. To achieve this, the completed *Hsd11b2* floxed construct was introduced into mouse ES cells (had been originally derived from a blastocyst inner cell mass (ICM)) in order to achieve stable inheritance of the transgenic allele (Evans and Kaufman, 1981). These ES cells had been previously derived from a 129 mouse line (chinchilla coat colour; E14TG2a cell line (129/OlaHsd)) (Hooper et al., 1987), and introduction of the targeting construct was performed by electroporation. The mouse ES cells were grown to 80% confluence in standard ES cell culture media (as detailed in the Materials and Methods chapter). ES cells were then washed and pelleted (as described in the Materials and Methods chapter) ready for electroporation. Meanwhile, approximately 20μg of linearised

Hsd11b2 floxed targeting construct DNA was prepared (as described in the Materials and Methods chapter). This was then mixed with the pelleted ES cells, and the mix was electroporated at 240 Volts.

6p1.2.2.2 Neomycin Selection of Positive ES Clones

To establish which ES cells had integrated the construct into their genome, the neomycin antibiotic resistance cassette that had been incorporated into the final targeting construct was utilised. G418 is an antibiotic used to select cells that contain the gene for neomycin resistance, and this was added to the culture media used to nurture the electroporated ES cells. Cells that do not contain the neomycin gene (and therefore have not incorporated the targeting construct) will die in the presence of G418, and those that do contain it will thrive. The cell cultures were incubated with G418 for up to two weeks, after which colonies derived from individual ES cell clones were selected and propagated in separate culture wells (see Materials and Methods chapter). ES cells selected this way will contain the targeting construct, but this screening method can not differentiate between homologous recombination into the genome and a random insertion event.

6p1.2.3 Screening for Homologous Recombination

6p1.2.3.1 PCR Screening Results

The recombination arms of the targeting construct should favour insertion by homologous recombination, but the construct may also be randomly inserted into the genome. Traditionally, a Southern hybridisation screen involving 3' and 5' EPs is developed to screen for homologous recombination. However, this is a lengthy and time-consuming process that requires high amounts of ES cell DNA and the use of radioactive isotopes. A PCR screen was therefore

developed as a primary screen to identify ES cell clones that were likely to contain a homologous recombination event. These ES cell clones were then taken forward for validation screening by Southern hybridisation.

Primers were designed to amplify over regions of the *Hsd11b2* gene that would reveal whether any targeting construct insertion was homologous or not (Figure 6.3). A ubiquitous forward primer was designed to be paired with 3 different reverse primers (primer sequences are detailed in Materials and Methods chapter). Primer pair A - B was designed check the integrity of the homologous recombination crossover point, and to give a size difference in product to indicate presence or absence of the targeting construct. Primer pair A - C was intended to confirm the presence and the position of the

PCR ES Cell Screening Strategy

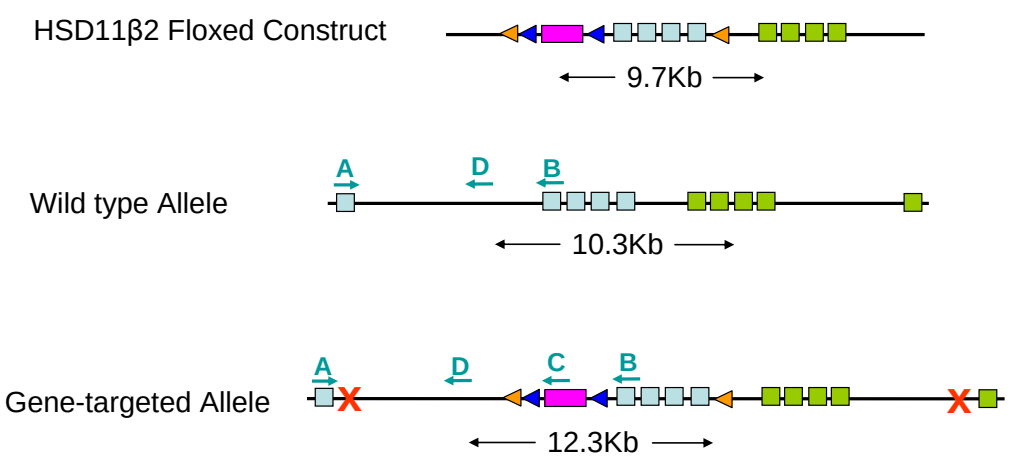

Primers	Wild Type	Gene Targeted
A - B	3.2 Kb	5.1 Kb
A - C	-	3.7 Kb
A - D	1.4 Kb	1.4 Kb

Forward Primer A (HSD2 exon 1) – 5' - ctg ctg gct gct ctc gac tg - 3'
Reverse Primer B (HSD2 exon 2) – 5' – tct tag ctg tct cct tgc ca – 3'
Reverse Primer C (Neo cassette) – 5' – tgt caa gac cga cct gtc cg – 3'
Reverse Primer D (5' Neo insert) – 5' – ggc aga gcc tat aac gag tc – 3'

Figure 6.3. Primer design and expected PCR product sizes for both wild type and gene-targeted alleles. Primer position on DNA represented by blue letters A - D. Cross-over points of DNA homologous recombination of hsd11b2 floxed constrict represented by red X.

Neomycin resistance cassette, thus verifying the presence and position of the targeting construct. Finally, primer pair A - D was also designed to ensure the integrity of the homologous recombination crossover point (a contingency in case the A - B PCR product was too large to synthesis efficiently). PCR reaction conditions were optimised using un-transfected ES cell DNA as a template, and DNA extracted from neomycin-selected ES cells (as detailed in the Materials and Methods chapter) was screened initially using the A - B primer pair. This proved to be a problematic PCR reaction to optimise, presumably because the expected PCR products were relatively large (wild type allele 3.2Kb and gene-targeted allele 5.2Kb). Consequently, A - D and A - C primer pairs were attempted, but they too proved to be problematical, and a reliable and robust PCR assay proved difficult to establish.

6p1.2.3.2 Fluorescent PCR Screening Results

Due to the difficulties mentioned with the traditional PCR methods, a quantitative fluorescent-based approach for PCR screening was also developed. This was similar to a real-time PCR approach, using the same instrument and reagents, but different in that an absolute detection of a specific a nucleic acid sequence was being looked for, not a relative quantification of that detection. Primers were calculated using an online program for designing real-time assay primers (as described in detail in the Materials and Methods chapter), which are generally designed to amplify over an area up to a few hundred bp in length. The optimal design for this new PCR assay was to amplify between *Hsd11b2* exon 1 and the upstream *lox*P site, an area which covers approximately 2.8Kb. This would result in a positive assay signal if the *loxP* site was in the correct region and no signal if it was not. As described in the Materials and Methods chapter, a positive

control plasmid (containing *Hsd11b2* exon 1 and a *lox*P site) was constructed using the 5′ EP and pL451 plasmid to act as a positive control in screening reactions. This plasmid was designed to amplify a product that would be smaller in size than the real product, so that any suspicion of DNA sample contamination could be accounted for. A primer matrix reaction was carried out using positive control DNA to analyse what concentrations would give the best results (Figure 6.4a). This was performed using a SYBR Green probe, as this is activated for fluorescent detection by any double stranded DNA, thus removing the need for a DNA sequence-specific probe. Once this had been calculated, the sensitivity of the assay was tested by using the positive control DNA at different concentrations per genome. The outcome of the real-time PCR was validated by agarose gel electrophoresis to visualise the DNA product. The DNA of the neomycin selection positive ES clones was then screened by this assay. ES cell clones with a cross threshold value of over 30 (approximately 25% of total samples) were expanded and carried forward for further screening analysis by Southern hybridisation (Figure 6.4 b).

6p1.2.3.3 Southern Hybridisation Screening Results

A Southern hybridisation screen was designed to verify homologous recombination of the targeting construct using EPs to the 5′ and 3′ ends (Figure 6.5; 6p1.2.4). ES cell genomic DNA taken forward from primary fluorescent PCR screening was purified further using a phenol/chloroform protocol (see Materials and Methods chapter). The DNA was then digested using the BamHI restriction enzyme for 3′ EP and HindIII restriction enzyme for 5′ EP. 3′ EP screening of the DNA was performed in the first instance, as the results of this screen had proved easier to interpret during optimisation than the 5′ EP.

a) SYBR Green PCR Primer Matrix CTs

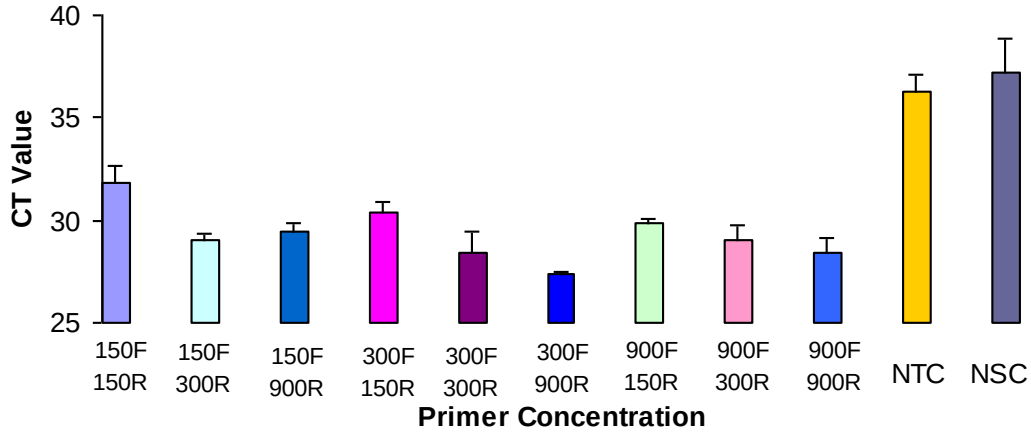

b) CT Values for PCR ES Cell Screening

Well	Sample Name	Detector	Task	CT	Well	Sample Name	Detector	Task	CT
A1	271	Test1	Unknown	Undetermined	A1	271	Test1	Unknown	Undetermined
A2	272	Test1	Unknown	Undetermined	A2	272	Test1	Unknown	Undetermined
A3	273	Test1	Unknown	Undetermined	A3	273	Test1	Unknown	Undetermined
A4	274	Test1	Unknown	Undetermined	A4	274	Test1	Unknown	Undetermined
A5	275	Test1	Unknown	Undetermined	A5	275	Test1	Unknown	Undetermined
A6	276	Test1	Unknown	Undetermined	A6	276	Test1	Unknown	Undetermined
A7	277	Test1	Unknown	Undetermined	A7	277	Test1	Unknown	Undetermined
A8	278	Test1	Unknown	Undetermined	A8	278	Test1	Unknown	Undetermined
A9	279	Test1	Unknown	Undetermined	A9	279	Test1	Unknown	Undetermined
A10	280	Test1	Unknown	Undetermined	A10	280	Test1	Unknown	Undetermined
A11	281	Test1	Unknown	37.18	A11	281	Test1	Unknown	37.18
A12	282	Test1	Unknown	34.68	A12	282	Test1	Unknown	34.68
B1	283	Test1	Unknown	Undetermined	B1	283	Test1	Unknown	Undetermined
B2	284	Test1	Unknown	Undetermined	B2	284	Test1	Unknown	Undetermined
B3	285	Test1	Unknown	Undetermined	B3	285	Test1	Unknown	Undetermined
B4	286	Test1	Unknown	Undetermined	B4	286	Test1	Unknown	Undetermined
B5	287	Test1	Unknown	Undetermined	B5	287	Test1	Unknown	Undetermined
B6	288	Test1	Unknown	Undetermined	B6	288	Test1	Unknown	Undetermined
B7	289	Test1	Unknown	Undetermined	B7	289	Test1	Unknown	Undetermined
B8	290	Test1	Unknown	Undetermined	B8	290	Test1	Unknown	Undetermined
B9	291	Test1	Unknown	Undetermined	B9	291	Test1	Unknown	Undetermined
B10	292	Test1	Unknown	Undetermined	B10	292	Test1	Unknown	Undetermined
B11	293	Test1	Unknown	Undetermined	B11	293	Test1	Unknown	Undetermined
B12	294	Test1	Unknown	Undetermined	B12	294	Test1	Unknown	Undetermined
C1	295	Test1	Unknown	Undetermined	C1	295	Test1	Unknown	Undetermined
C2	296	Test1	Unknown	37.19	C2	296	Test1	Unknown	37.19
C3	297	Test1	Unknown	Undetermined	C3	297	Test1	Unknown	Undetermined
C4	298	Test1	Unknown	Undetermined	C4	298	Test1	Unknown	Undetermined
C5	299	Test1	Unknown	Undetermined	C5	299	Test1	Unknown	Undetermined
C6	300	Test1	Unknown	Undetermined	C6	300	Test1	Unknown	Undetermined
C7	301	Test1	Unknown	Undetermined	C7	301	Test1	Unknown	Undetermined
C8	302	Test1	Unknown	Undetermined	C8	302	Test1	Unknown	Undetermined
C9	303	Test1	Unknown	Undetermined	C9	303	Test1	Unknown	Undetermined
C10	304	Test1	Unknown	Undetermined	C10	304	Test1	Unknown	Undetermined
C11	305	Test1	Unknown	35.47	C11	305	Test1	Unknown	35.47
C12	306	Test1	Unknown	33.77	C12	306	Test1	Unknown	33.77
D1	307	Test1	Unknown	Undetermined	D1	307	Test1	Unknown	Undetermined
D2	308	Test1	Unknown	Undetermined	D2	308	Test1	Unknown	Undetermined
D3	309	Test1	Unknown	Undetermined	D3	309	Test1	Unknown	Undetermined
D4	310	Test1	Unknown	Undetermined	D4	310	Test1	Unknown	Undetermined
D5	311	Test1	Unknown	36.43	D5	311	Test1	Unknown	36.43
D6	312	Test1	Unknown	Undetermined	D6	312	Test1	Unknown	Undetermined
D7	313	Test1	Unknown	36.81	D7	313	Test1	Unknown	36.81
D8	314	Test1	Unknown	36.03	D8	314	Test1	Unknown	36.03
D9	315	Test1	Unknown	Undetermined	D9	315	Test1	Unknown	Undetermined
D10	316	Test1	Unknown	Undetermined	D10	316	Test1	Unknown	Undetermined
D11	317	Test1	Unknown	36.76	D11	317	Test1	Unknown	36.76
D12	318	Test1	Unknown	36.89	D12	318	Test1	Unknown	36.89
E1	319	Test1	Unknown	Undetermined	E1	319	Test1	Unknown	Undetermined
E2	320	Test1	Unknown	Undetermined	E2	320	Test1	Unknown	Undetermined
E3	321	Test1	Unknown	Undetermined	E3	321	Test1	Unknown	Undetermined
E4	322	Test1	Unknown	36.97	E4	322	Test1	Unknown	36.97
E5	323	Test1	Unknown	36.63	E5	323	Test1	Unknown	36.63
E6	324	Test1	Unknown	Undetermined	E6	324	Test1	Unknown	Undetermined
E7	325	Test1	Unknown	Undetermined	E7	325	Test1	Unknown	Undetermined
E8	326	Test1	Unknown	Undetermined	E8	326	Test1	Unknown	Undetermined
E9	327	Test1	Unknown	Undetermined	E9	327	Test1	Unknown	Undetermined
E10	328	Test1	Unknown	Undetermined	E10	328	Test1	Unknown	Undetermined
E11	329	Test1	Unknown	Undetermined	E11	329	Test1	Unknown	Undetermined
E12	330	Test1	Unknown	Undetermined	E12	330	Test1	Unknown	Undetermined
F1	331	Test1	Unknown	Undetermined	F1	331	Test1	Unknown	Undetermined
F2	332	Test1	Unknown	Undetermined	F2	332	Test1	Unknown	Undetermined
F3	333	Test1	Unknown	37.06	F3	333	Test1	Unknown	37.06
F4	334	Test1	Unknown	Undetermined	F4	334	Test1	Unknown	Undetermined
F5	335	Test1	Unknown	Undetermined	F5	335	Test1	Unknown	Undetermined
F6	336	Test1	Unknown	Undetermined	F6	336	Test1	Unknown	Undetermined
F7	337	Test1	Unknown	Undetermined	F7	337	Test1	Unknown	Undetermined
F8	338	Test1	Unknown	37.26	F8	338	Test1	Unknown	37.26
F9	339	Test1	Unknown	Undetermined	F9	339	Test1	Unknown	Undetermined
F10	340	Test1	Unknown	Undetermined	F10	340	Test1	Unknown	Undetermined
F11	341	Test1	Unknown	Undetermined	F11	341	Test1	Unknown	Undetermined
F12	342	Test1	Unknown	Undetermined	F12	342	Test1	Unknown	Undetermined
G1	343	Test1	Unknown	Undetermined	G1	343	Test1	Unknown	Undetermined
G2	344	Test1	Unknown	Undetermined	G2	344	Test1	Unknown	Undetermined
G3	345	Test1	Unknown	Undetermined	G3	345	Test1	Unknown	Undetermined
G4	346	Test1	Unknown	Undetermined	G4	346	Test1	Unknown	Undetermined
G5	347	Test1	Unknown	Undetermined	G5	347	Test1	Unknown	Undetermined
G6	348	Test1	Unknown	37.23	G6	348	Test1	Unknown	37.23
G7	349	Test1	Unknown	Undetermined	G7	349	Test1	Unknown	Undetermined
H1	ES + spike	Test1	Unknown	32.41	H1	ES + spike	Test1	Unknown	32.41
H2	ES	Test1	Unknown	Undetermined	H2	ES	Test1	Unknown	Undetermined
H3	BI6	Test1	Unknown	Undetermined	H3	BI6	Test1	Unknown	Undetermined
H4		Test1	NTC	Undetermined	H4		Test1	NTC	Undetermined

Figure 6.4. Real-time PCR screening strategy for ES cells. **a)** Bar chart showing the CTs for different combinations of Forward (F) and Reverse (R) primer concentrations in a SYBR Green fluorescent detection PCR reaction. All primer concentrations are in nM. NTC = no template control; NSC = non spike control. **b)** Example of results obtained from SYBR Green PCR screening of ES cells targeted for hsd11b2 floxed construct positive for neomycin selection, using primer concentration of 300nM forward and 900nM reverse. Positive CT results are highlighted in pink.

a) 3' External Probe Schematic

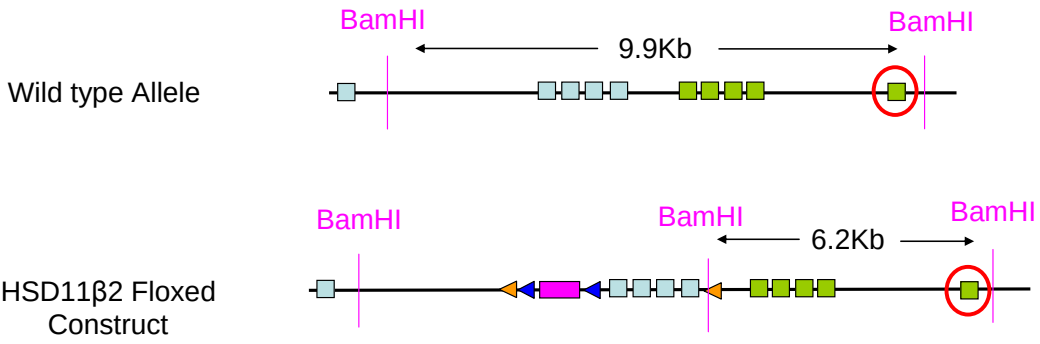

b) 5' External Probe Schematic

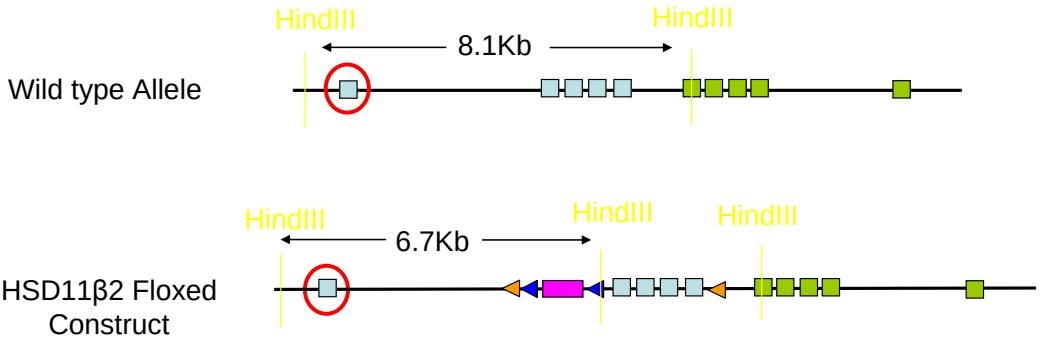

Figure 6.5. 3' and 5' external probe design. **a)** Schematic representation of the 3' external probe (circled in red) and the different sizes that Southern hybridisation with the probe would generate according to wild type or gene-targeting allele after a BamHI restriction enzyme digest. **b)** Schematic representation of the 5' external probe and the different sizes that Southern of hybridisation with the probe would generate according to wild type or gene-targeting allele after a HindIII restriction enzyme digest.

Digests were separated by agarose gel electrophoresis, transferred to a nitrocellulose membrane, and subsequently analysed for radioactively-labelled probe hybridisation. Clones that gave a positive result for the 3′ EP (Figure 6.6a) were consequently probed for the 5′ EP (Figure 6.6b), as verification of homologous recombination is required at both ends of the targeting construct.

6p1.2.4 Blastocyst Injection and Chimeric Mouse Breeding

6p1.2.4.1 Blastocyst Injection of ES Cells

Three separate ES cell clones (named 28, 63 and 128) that were confirmed positive for both 5′ and 3′ end homologous recombination by Southern hybridisation were introduced from *in vitro* culture to a surrogate blastocyst by microinjection. Karyotype was checked before injection (Figure 6.7; see Materials and Methods chapter for details). Manipulated blastocysts were then transplanted into psuedopregnant female mice for implantation and gestation. The blastocyst injections and implantations were carried out by a University of Edinburgh in-house service (Genetic Intervention and Screening Technologies). Refer to Table 6.1 for blastocyst injection statistics.

6p1.2.4.2 Chimeras and Floxed Allele Germline Transmission

During embryonic development of the injected blastocysts, the targeted floxed allele will become incorporated into the embryonic germline, where the pluripotency of the ES cells will allow them to become integrated into the embryo at all consequent tissue lineages (Ledermann, 2000). As the resulting offspring are essentially derived from the cells of two different embryos (the targeted ES cells and the microinjected blastocyst), they are referred to as chimeras. The production of a chimera is an essential stage in the generation of a transgenic mouse, and it can be used to advantage for screening of successful targeting allele genome integration. If the ES cell line and the donor embryo are derived from mouse lineages that express different coat colours, then a chimeric offspring can be easily identified by its "patchy" coat appearance. This is an indication that the genotypes from both the targeted ES cells and the donor blastocyst were incorporated into the germline of the resulting offspring.

a) 3' External Probe Southern Hybridisation Blot

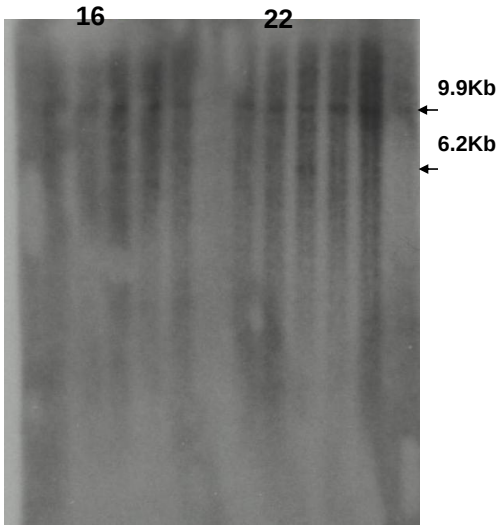

b) 5' External Probe Southern Hybridisation Blot

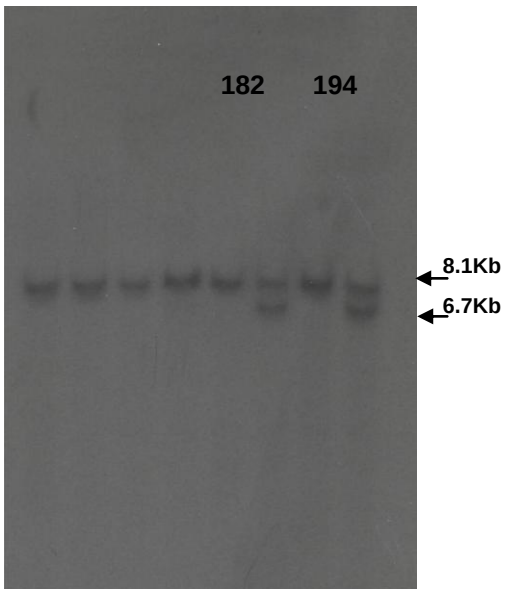

Figure 6.6. Southern hybridisation blots of 3' and 5' external probes. **a)** Southern membrane of BamHI restriction enzyme digested ES cell DNA transferred from an agarose gel to a nitrocellulose membrane, probed with radioactively-labelled 3' external probe. Samples 16 and 22 represent ES clones positive for insertion of the hsd11b2 floxed targeting construct by homologous recombination at the 3' end. **b)** Southern membrane of HindIII restriction enzyme digested ES cell DNA transferred from an agarose gel to a nitrocellulose membrane, probed with radioactively-labelled 5' external probe. Samples 182 and 194 represent ES clones positive for insertion of the hsd11b2 floxed targeting construct by homologous recombination at the 5' end.

ES Cell Chromosome Spreads

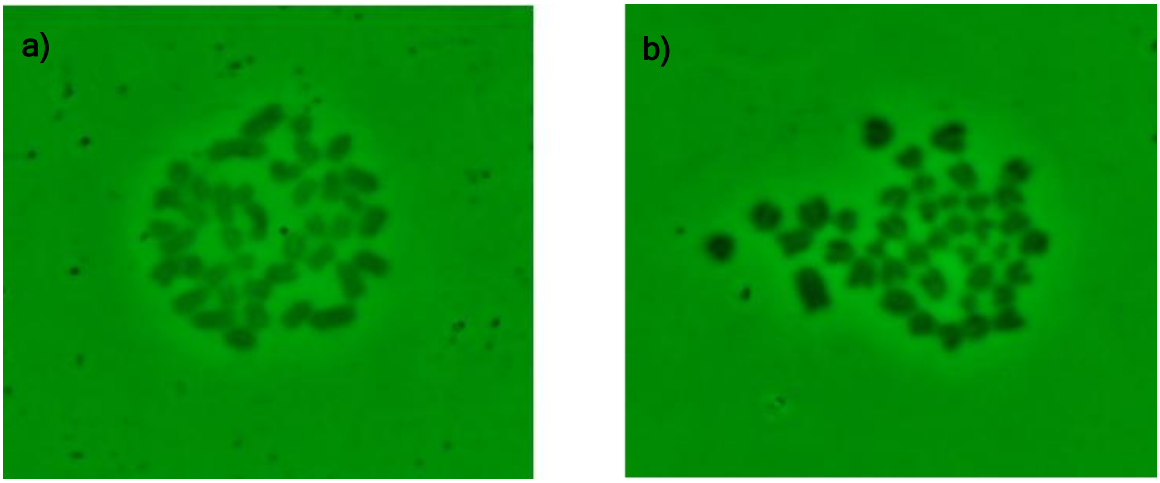

Figure 6.7. ES cell karyotyping. Photos of ES cell spreads for checking karyotypes of cells. Both ES cell clone 28 **a)** and 63 **b)** have a normal mouse karyotype of 40.

For the *Hsd11b2* floxed construct targeting, the ES cells used have been previously derived from a 129 mouse line (agouti coat colour) and they were injected into C57BL/6 blastocysts (black coat colour). Any resultant offspring will be screened for floxed allele integration by chimeric coat colour (a mixture of black and agouti; see Figure 6.8 for photos). In total, from five separate rounds of injections seven individual chimeras were obtained (refer to Table 6.1 for statistics).

Chimera Photographs

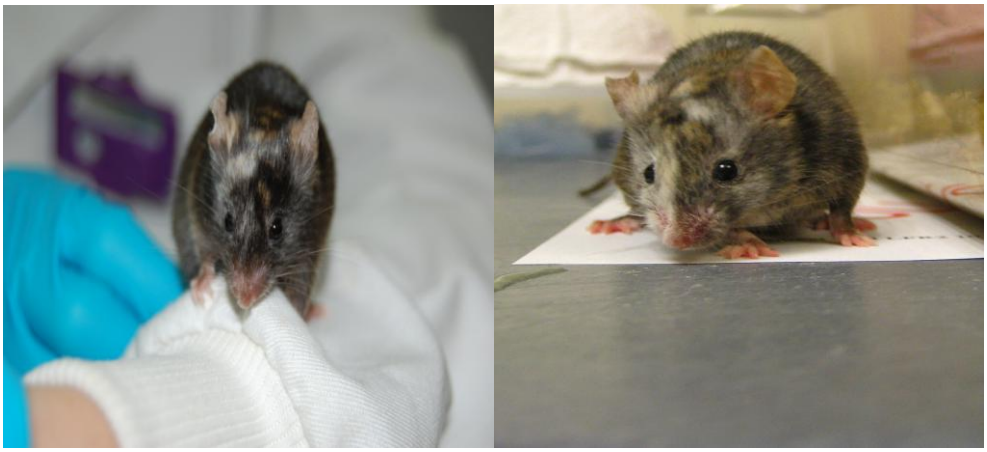

Figure 6.8. Photographs of chimera 1 and 4 representing "patchy" coat colouring characteristic of chimeric mice.

Injection Statistics

Injection set	Clone Number	Blastocyst Injections	Pregnant Surrogates	Live Offspring Births	Chimeric Offspring
1	182	124	4	4	3
2	182	61	3	9	0
3	28	53	4	6	1
4	63	130	8	27	0
5	28 & 63	98	4	11	3

Table 6.1. Blastocyst injection statistics

Once chimeric offspring were weaned, a breeding program commenced, pairing them with C57BL/6 wild-type mice. The results of these breeding programs is the last step in producing a new transgenic mouse line, as for the new line to continue and be used experimentally, the targeted allele must be incorporated into the germline of the chimeric offspring. That is, although all chimeric offspring will contain a mixture of cells derived from both the targeted ES cells and the donor blastocyst, if none of the targeted cells are being passed onto the next generation via the germline, then the targeted allele will not be transmitted. Black coat-colour (blastocyst donor coat colour) progeny do not contain the introduced targeted allele, whereas successful germline transmission is detected by agouti coat-colour (ES cell line coat-colour). The seven chimeras produced a combined total of 169 weaned pups, all of which were black in coat colour (see Table 6.2 for statistics).

Breeding Statistics

Chimera no.	Injection set	DOB	Sex	Pups weaned	Black Pups	Agouti Pups
1	1	12/02/2008	Male	0	n/a	n/a
2	1	12/02/2008	Female	18	18	0
3	1	12/02/2008	Male	66	66	0
4	3	01/12/2008	Male	0	n/a	n/a
15	5	31/03/2009	Female	0	n/a	n/a
16	5	31/03/2009	Female	23	23	0
29	5	31/03/2009	Male	62	62	0

Table 6.2. Chimera Breeding Program Statistics

As can be seen in Table 6.2, chimera 1, 4 and 15 did not produce any offspring. Chimera 4 was in a breeding program for a number of months, but failed to produce any offspring (despite rotation of numerous female partners) so was presumed to be sterile. Chimera 15 was found unexpectedly dead at 8 weeks old; no obvious cause of death could be identified from a basic autopsy. Chimera 1 was found to have an infected abscess near his penis at 5 months of age and was consequently culled; this abscess being the presumed cause of his failure to produce any offspring. Approximately three months after the abscess was discovered in chimera 1, chimera 3 developed a similar lesion. This time a full necropsy was performed by in-house rodent pathologist Dr David Brownstein, which identified the abscess as an infected preputial gland abscess with skin fistula (see Appendix 1). A literature search for possible causes of the perputial gland abscess identified a *Staphylococcus aureus* bacterial infection as a possible cause (Hong and Ediger, 1978). Tests for *Staphylococcus aureus* could have been carried out on tissue harvested from the autopsied male, but as this is a common infection found in a high percentage of the general

population (Wertheim et al., 2005; Yu et al., 2002), a positive result would be ambiguous.

Unfortunately, all resulting progeny from the successfully breeding chimeras were black, signifying that the chimeras had not transmitted the transgenic allele to their progeny.

6p1.3 Discussion

6p1.3.1 Summary of Gene Targeting Construct

The *Hsd11b2* floxed gene targeting construct was designed and built to allow for conditional deletion of 11β-HSD2 in a site-specific manner using the Cre/*lox*P recombination technology. The construct was specifically designed to include exons 2 - 5 of the *Hsd11b2* gene. These were flanked by two *lox*P sites facing in the same direction to allow for removal of this region of DNA from the genome upon exposure to Cre recombinase. There was also a neomycin cassette flanked by two FRT sites (again facing in the same direction) positioned between the 5' *lox*P site and *Hsd11b2* exon 2. This was to permit independent removal of the neomycin cassette in ES cells, if required. Exons 5 - 8 of the neighbouring ATP6V0D1 gene are included within the DRA of the targeting construct for two main reasons. Firstly, their inclusion allows for the recombination arm to be longer, as longer recombination arms have been shown to be beneficial in promoting a higher frequency of homologous recombination (Inbar et al., 2000). Secondly, because these two genes terminate within a few Kbs of one another, this region is likely to be important for their transcriptional regulation, and so it is favourable to minimise sequence disruption within this region.

Once the completed targeting construct had been verified by DNA sequencing, it was introduced into an ES cell line. The ES cells were initially screened for integration of the introduced targeting construct by exploiting the antibiotic resistance of cells positive for integration (due to the neomycin cassette of the targeting construct). However, while this screening method can reliably detect construct integration into the ES cell genome, it cannot

distinguish between a random insertion event and genuine homologous recombination. In order to try and make the secondary screening for homologous recombination more efficient than the traditional approach by Southern hybridisation of EPs, a PCR-based screening strategy was developed. This approach was first attempted using a traditional PCR strategy; however the long length of PCR products required to produce reliable evidence of a homologous recombination event proved difficult to optimise. Consequently, a fluorescence-based PCR approach was instead adopted. This proved more successful, and allowed the number of ES cell clones put forward for further screening by Southern hybridisation to be reduced by approximately two-thirds. Southern hybridisation screening was first carried out using the 3′ EP. Clones that were positive for this probe were then put forward for Southern hybridisation screening with the 5′ EP. Consequently, three separate ES cell clones were chosen to go forward for blastocyst injection.

6p1.3.2 Chimera Breeding Program and Germline Transmission

The results of the blastocyst injections were poorer than would normally be expected (Table 6.1); with the number of pregnant surrogates low, and live offspring production also lower than normal. Despite this, seven chimeras were successfully produced, and were all entered into breeding programs with C57Bl6 mice. Unfortunately, the floxed *Hsd11b2* allele never progressed to germline status. As a result of the poor blastocyst injection statistics and the resultant failure of the targeted allele to become germline, diagnostic tests were carried out upon the ES cell line to try and determine why this had happened. These tests revealed that all three of the injected ES cell clones had a mycoplasma infection (mycoplasma testing performed by Mrs. Audrey

Peter, Senior Technician, Molecular Physiology Lab). Mycoplasma-infected ES cells have been shown to affect germline transmission from chimeras (Markoullis et al., 2009). Infection can also lead to a reduction in the number of pups born, a lower frequency of chimeric pups, and a higher frequency of embryo death and implanted blastocyst re-absorption (Bradley, 1987). This is a likely explanation for the low numbers observed. This then has a knock-on effect regarding chimera numbers, as lower pregnancies means less chance of producing a germline chimera. In addition, a mycoplasma infection can also cause genitourinary infections in humans, and so could be the cause of the infections that were observed affecting the genitalia of two male chimeras (Appendix 1).

These unfortunate events mean the process of producing a floxed *Hsd11b2* transgenic line from start to finish could not be realised in the time frame of these studies. However, there is the potential that the completed construct can be re-transfected into clean ES cells and the process carried forward to successful germline transmission of the floxed *Hsd11b2* allele.

6p1.3.3 Future Direction: the Importance of Phenotypic Characterisation Before Site-Specific Deletion of a Floxed Allele

Once the *Hsd11b2* floxed line has been successfully established, it will be important to establish its phenotype before selectively removing *Hsd11b2* in the CD, especially on different sodium diets. This will ensure that phenotypes observed in the CD-specific 11β-HSD2 knockout model (i.e. *Hsd11b2* floxed/*HoxB7* Cre line (to be discussed in more detail in Chapter 6 Part 2) cross offspring) are due to the spatial removal of the gene of interest, and not an effect of floxing the gene; i.e. the gene of interest must function as normal until excised by interbreeding with a recombinase-expressing mouse

line. The insertion of extra regions of DNA (such as the neomycin selection cassette) in the introns or near the promoter of the gene of interest when generating a targeting construct can have stochastic effects upon the normal function of that gene (Kwan, 2002). It can also have effects upon the transcriptional regulation of neighbouring genes (Olson et al., 1996). These effects can be overcome by flanking the neomycin cassette for selectable removal, as was done with FRT in the floxed construct described here. Occasionally this phenomenon can render the transgenic allele hypomorphic; that is expression of the gene of interest may be reduced rather than ablated. This perceived shortcoming of gene targeting experiments has conversely been exploited by some researchers in order to produce models of gene mutations with varying degrees of phenotypic severity (Meyers et al., 1998; Nagy et al., 1998).

Chapter 6 Part 2

Characterising a Cre Line

6p2.1 Introduction

As discussed in Part 1 of Chapter 2, a Cre/*lox*P transgenic approach is being undertaken in order establish spatial conditional deletion of 11β-HSD2 in a mouse model. The kidney is an attractive candidate for first employing this technique, as it is a major expression site of 11β-HSD2, and SAME is classically held to be a renal disease. This theory is supported by the observation that kidney transplantation in a SAME patient rescued the phenotype, and consequent clinical analysis revealed the new kidney was expressing functional 11β-HSD2 (Palermo et al., 2000). Therefore, investigating the specific contribution of renal 11β-HSD2 towards the phenotypes reported in SAME patients, and the *Hsd11b2*$^{-/-}$ mouse model, will be important in understanding the pathology 11β-HSD2 ablation. Also, the role of the kidney in the development of SS BP in the *Hsd11b2*$^{+/-}$ model (see Chapter 3) further strengthens the case for exploring the specific roles that renal 11β-HSD2 expression plays towards the pathology of impaired protein expression.

The particular expression site of 11β-HSD2 within the mouse kidney is in the distal nephron (Condon et al., 1997). More specifically, the connecting tubule (CNT) and the principal cells of the collecting duct (CD) of mice show strong expression for 11β-HSD2 (Cole, 1995) (Campean et al., 2001). One particular study also finds occasional 11β-HSD2 expression (at both RNA and protein levels) in the distal convoluted tubule (DCT) (Campean et al., 2001); although it must be pointed out that expression is seen in transitional segmental portions and in the minority of sections. There are a small number of kidney Cre lines that would be appropriate for CD-specific deletion of 11β-HSD2 (for review see (Rubera et al., 2009)). One of these is the AQP2 Cre line, which has Cre recombinase expression under the control of the AQP2 gene

promoter with specific expression in the CD and the late CNT (Ronzaud et al., 2007). Both the human and mouse AQP2 promoter have been previously used in Cre recombinase mouse lines to target floxed genes in the CD principal cells. However, both of these models have been shown to have leaky expression patterns of transgene activity, with Cre recombinase expression demonstrated in non-renal tissues (Nelson et al., 1998) (Zharkikh et al., 2002) (Ge et al., 2005). As 11β-HSD2 is expressed in other tissues, using this particular Cre could remove 11β-HSD2 in sites other than the kidney, thus compromising any observations made using the floxed *Hsd11b2* model.
An attractive alternative to the AQP2 Cre line is the *HoxB7* Cre line. This Cre line does not cover the entire 11β-HSD2 expression sites in the ASDN (CD only, not CNT or DCT). However, studies have suggested that the role of the proximal and the distal ASDN in water and sodium balance are different in that the proximal segments regulate balance short-term, where as the distal ASDN (i.e. CD) regulates the long-term balance (Rubera et al., 2003). This makes the *HoxB7* Cre a worthwhile model to investigate the role of 11β-HSD2 expression in the long-term regulation of sodium and water balance homeostasis.

6p2.1.1 Hox Genes

The family of Homeobox genes (*Hox*) encode transcription factors that are key regulators of embryonic axis formation, and tight regulation of these genes is essential for embryonic morphogenesis (Deschamps et al., 1999). In addition, the *Hox* family also specify additional differentiation events in both embryonic and adult tissues (Yaron et al., 2001). 39 different *Hox* genes have been identified over 4 different chromosomal compartments, and the genes

are sub-classed depending upon their chromosomal compartment positioning (*Hox*1 - 4).

The particular *Hox* gene of interest here, *HoxB7*, was previously known as *Hox2.3*. The initial expression characterisation of *HoxB7* was performed by Northern hybridisation analysis in mouse embryonic tissues (Deschamps et al., 1987). These experiments showed expression according to a temporally and spatially restricted pattern in the embryonic central and peripheral nervous system, and in derivatives of the axial, lateral plate and intermediate mesoderm (Deschamps et al., 1987). To investigate the effects of different regions within the *HoxB7* promoter and enhancer upon differential gene expression *in vivo*, Deschamps and colleagues generated several chimeric transcription units composed of *HoxB7* upstream sequences encompassing its promoters and enhancers and the bacterial *LacZ* reporter gene to generate transgenic mouse lines (Kress et al., 1990). One of the chimeric transgene constructs showed particularly strong expression in the epithelium within the urogenital system derived from the mesonephric duct, a site of high *HoxB7* expression. Expression of the construct (as identified by LacZ expression) was not observed in any other region of normal *HoxB7* expression. This observation was later exploited by another group to develop Cre mouse line using the original vector described above containing a 1.3 kb *HoxB7* enhancer/promoter that targets expression in the urogenital system only (Yu et al., 2002).

6p2.1.2 HoxB7 Cre Line: Previously Published Observations

The *HoxB7* Cre reporter line expresses Cre recombinase under the control of the above described *HoxB7* promoter/enhancer, specifically within the mesonephric duct and its derivatives (Yu et al., 2002). The original paper

describing this model demonstrates detailed analysis of the spatial and temporal expression of the Cre recombinase using a *ROSA* 26 reporter mouse line. Cre activity was detected in the mesonephric duct as early as embryonic day 9.5 (E9.5). It was subsequently detected throughout the ureteric bud from its initiation at E10.25, and was clearly able to initiate recombination-mediated expression of the *ROSA* reporter gene in all ureteric bud epithelial cells by E12.5.

Another study using the *HoxB7* Cre line, this time to selectively remove α-ENaC subunits from the CD, also investigated the expression of the recombinase at a tissue level (Rubera et al., 2003). Again using the *ROSA* 26 *LacZ* reporter line, they showed that Cre recombinase could be detected in the entire CD, and that tissue samples from lung, colon, skin, liver, heart and brain were all negative for expression. This study also investigated the efficiency of recombination by the Cre recombinase in CD cells. They demonstrated the efficiency to be high by using immunohistochemistry to detect the α-ENaC subunit; less than 1.5% α-ENaC positive cells were detected in the CDs of transgenic mice (Rubera et al., 2003).

The *HoxB7* Cre model was purchased as two breeding pairs from the Jackson Laboratories website (http://jaxmice.jax.org/info/index.html). The line is maintained on a hemizygous background (*HoxB7*$^{+/-}$) as homozygocity is embryonic lethal. For further detailed Cre expression characterisation for embryonic, post-natal and adult tissues, see Cre expression resource option on the Jackson Laboratories website (http://cre.jax.org/HoxB7/HoxB7-Cre.html).

6p2.2 Results

6p2.2.1 Detecting Cre Recombinase Expression

6p2.2.1.1 *ROSA 26* LacZ Reporter Line

Although the *HoxB7* Cre line has previously been used to drive deletion in the CD, the specific location of Cre recombinase in the kidney was investigated by cross-breeding *HoxB7*$^{+/-}$ mice with the *ROSA* 26 LacZ Cre reporter strain (Friedrich and Soriano, 1991). This transgenic reporter model expresses an introduced construct in all cell types that contains a LacZ expression gene. The ubiquitous expression of the LacZ gene is prevented by a floxed stop codon. In the presence of Cre recombinase, the stop codon is excised and expression of the LacZ gene will be observed in tissues where Cre is present. LacZ gene expression is detected as β-galactosidase activity, and this is done by means of X-Gal staining.

The kidneys of mice identified by PCR-based screening as heterozygous for both the *HoxB7* and the *ROSA* 26 allele were perfusion-fixed with glutaraldehyde (*HoxB7* Cre mice were used as negative controls), and stained for LacZ expression with X-Gal solution, as detailed in the Materials and Methods chapter. The results showed positive staining of CDs, and this staining was not observed in control kidney sections (Figure 6.9). As can be seen, the X-Gal staining is exclusive to a sub-population of cells within the CDs; as this population makes up the majority of the CD cells, these are most likely to be the principal cells, with the unstained remainder presumed to be the minority intercalated cell population. This study is consistent with the previous reports in the literature that *HoxB7* Cre recombinase expression in the kidney is exclusive to the principal cells of the CD.

Renal *HoxB7* Cre Recombinase Expression

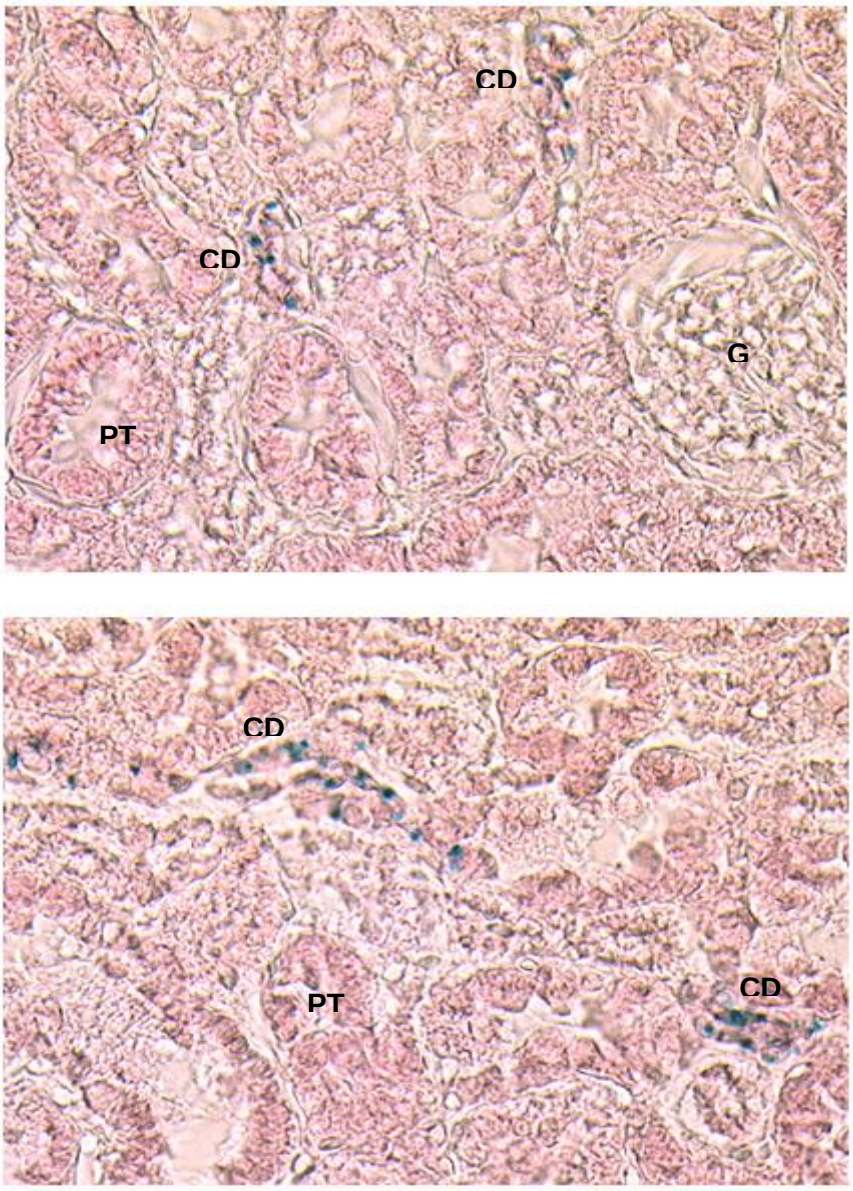

Figure 6.9. Kidney sections from a Hoxb7/ROSA26 heterozygote mouse stained with X-Gal to detect LacZ expression. **CD** = collecting duct; **G** = glomerulosa; **PT** = proximal tubule. Blue staining represents LacZ expression.

6p2.2.2 Characterising *HoxB7* Cre Mice - Effects of a High Sodium Diet

A detailed physiological assessment of the *HoxB7* Cre line is lacking in the literature and will be important for characterisation of future CD-specific

11β-HSD2 deletion. It is important to define the phenotype in terms of 11β-HSD2 deletion separately from contributions to the phenotype due to the *HoxB7* transgene. It is particularly important in this instance to establish any phenotypes associated with the *HoxB7* Cre line in relation changes in sodium diet content, as the *Hsd11b2*$^{+/-}$ mice have been shown to have a SS phenotype (Chapter 3). It is therefore essential to determine that these SS phenotypes are not present in the Cre line. The value of investigating hypomorphic alleles is previously discussed in Chapter 6 Part 1.

Experiments for renal and blood pressure phenotyping was performed in anesthetised mice as before (Chapter 3). Cohorts for the experiments consisted of *H*oxB7$^{+/-}$ mice and wild-type littermates (*HoxB7*$^{+/+}$) maintained on either a normal sodium diet, or a high sodium diet for three weeks prior to phenotyping experiments. As shown in Figure 6.10a, MABP was not different between the two genotypes, and was not influenced by dietary sodium content in either genotype.

This strongly suggests that *HoxB7*$^{+/-}$ transgenic mice do not have a salt-sensitive blood pressure phenotype. Acute amiloride administration also did not significantly alter MABP in either genotype on both sodium diets (results not shown).

Figure 6.10b shows that GFR values do not differ significantly between genotypes. It can also be observed that sodium diet had no effect upon GFR in either genotype. Urinary sodium excretion (E_{Na}) was also measured in these groups of mice. On a standard sodium diet, both genotypes have similar levels E_{Na} (Figure 6.10c). After three weeks on a high sodium diet, the E_{Na} is significantly increased to similar levels for both genotypes. E_{Na} was also measured after acute amiloride administration, and the difference between pre- and post-amiloride administration calculated (Δ amiloride).

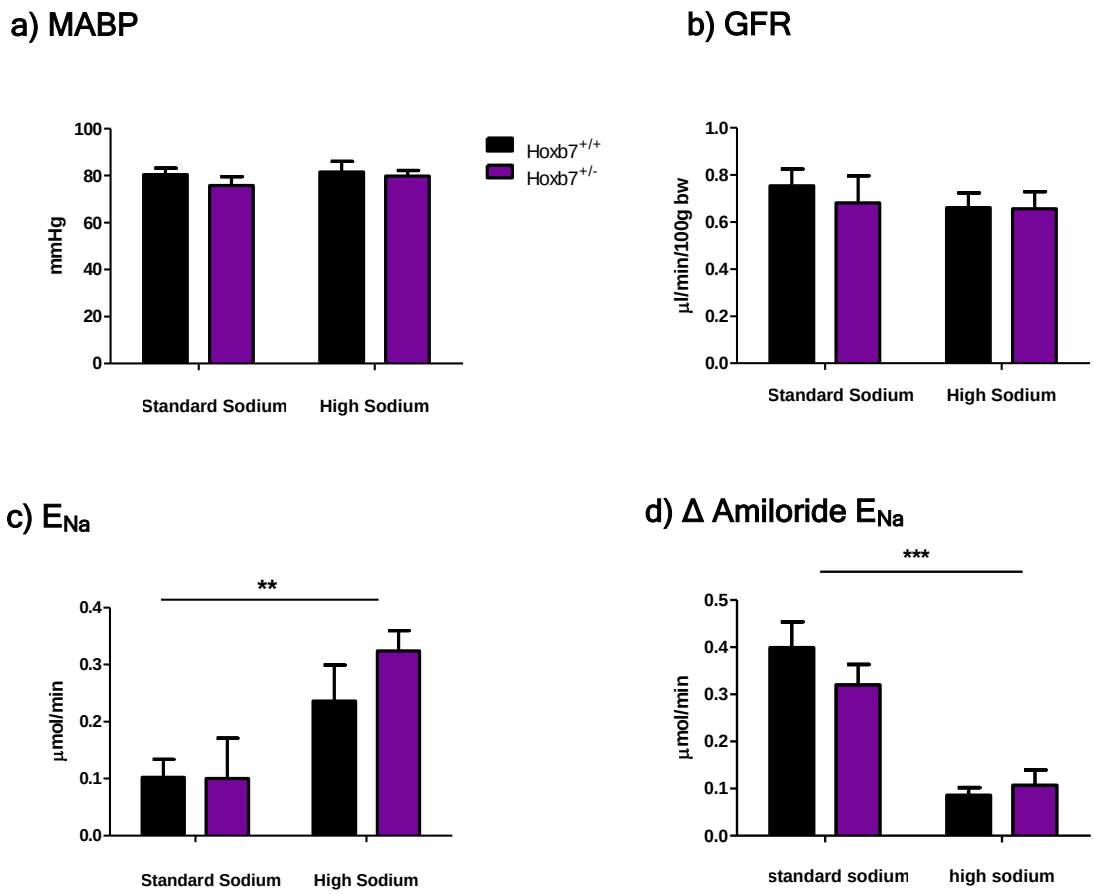

Figure 6.10. MABP, GFR, E_{Na}, and E_{Na} after amiloride administration in anaesthetised Hoxb7$^{+/+}$ and Hoxb7$^{+/-}$ mice after three weeks on either a standard (n = 7 for both groups) or high (n = 6 and 5, respectively) sodium diet. **a)** Overall statistical analysis of MABP after three weeks on either a standard or high sodium diet shows that there is no significant effect upon MABP of either diet or genotype. **b)** GFR values are expressed as mls of FITC-labelled inulin filtered across the glomerular filter barrier from plasma per minute, as measured from both urine and plasma. Overall statistical analysis reveals that there is no significant effect of genotype or sodium diet upon GFR. **c)** Statistical analysis shows there is a significant effect of diet upon urinary sodium excretion (E_{Na}) (** = $P < 0.01$), but that there is no significant effect of genotype upon the values on either dietary regime. **d)** Overall analysis shows there is a highly significant effect of dietary sodium upon Δ E_{Na} after amiloride administration (*** = $P < 0.001$), but there is no significant effect of genotype either before or after. Data are mean ± SEM. Statistical analysis by 2 way ANOVA.

These results show that on a standard sodium diet, both *HoxB7*$^{+/+}$ and *HoxB7*$^{+/-}$ mice greatly increase their E_{Na}, consistent with acute ENaC blockade (Figure 6.10d). After three weeks on a high sodium diet, the Δ amiloride

ENa values are significantly lower than for those on the standard sodium diet for both genotypes, but this difference is equal between the two genotypes (Figure 6.10d). This suggests that the *HoxB7*$^{+/-}$ mice are regulating their ENaC expression and sodium excretion appropriately for the level of sodium in their diet; deregulation in this system is a predominant finding reported in the characterisation of the *Hsd11b2*$^{+/-}$ mice on a high sodium diet. This is an important observation as it verifies that any changes to natriuresis, with particular reference to the role of ENaC in the process, which may occur when an *Hsd11b2* conditional knockout model is produced, are not due to any underlying phenotype effects of the *HoxB7* Cre genotype.

6p2.3 Discussion

HoxB7 Cre will allow for conditional deletion of 11β-HSD2 when cross-bred with a floxed *Hsd11b2* line. In particular, the *Hoxb7* Cre line will remove 11β-HSD2 expression in the CD of the ASDN, which includes the cortical CD (CCD) and the outer and inner medullary CD (OMCD and IMCD, respectively) (Rubera et al., 2003). Published observations and the LacZ reporter experiments described here demonstrate that Cre recombinase activity in this line is indeed confined to this region of the kidney (Rubera et al., 2003; Yu et al., 2002) and that the recombinase activity of the Cre is strong (Rubera et al., 2003).

Just as it will be important to establish any baseline phenotypes in the *Hsd11b2* floxed line, the same is true for the *HoxB7* Cre line. Any underlying phenotypes of the model that are not identified before cross-breeding with the *Hsd11b2* floxed line could compromise the phenotypic investigations of the new conditional model. The phenotyping experiments performed here suggest that the Cre transgene is not affecting the BP or renal sodium handling in the *HoxB7* Cre line. These investigations were pursued further by also assessing the mice under conditions of physiological stress; namely a high sodium diet regime. The model did not differ in phenotype from the wild-type controls, again suggesting that the transgene is not having an influence upon phenotype.

Overall, the investigations described in this chapter recommend the *HoxB7* Cre line as an appropriate choice for generating a kidney CD-specific *Hsd11b2* knockout mouse model. This model will be important for investigating the renal contributions towards the phenotypes of the already established *Hsd11b2*$^{+/+}$ and *Hsd11b2*$^{+/-}$ models of hypertension.

Chapter 7

Discussion

This thesis describes the initial characterisation of the SS phenotype of *Hsd11b2*$^{+/-}$ mice. The inspiration for these studies came from research into human populations which suggested that polymorphisms in the HSD11B2 gene may be associated with essential and/or SS hypertension. Ferrari *et al* identified the heterozygous parent of a SAME patient as having hypertension, as well as a homozygous SAME patient with a mild mutation that caused only a hypertensive phenotype rather than full blown SAME (Ferrari et al., 2000). This led the authors to suggest that the degree of 11β-HSD2 activity *in vivo* may influence the severity of the hypertensive phenotype. They then went on to prove that a HSD11B2 polymorphism (CA repeat allele) was associated with SS hypertension. Studies of cell lines transfected with HSD11B2 allele variants have highlighted the effects of different polymorphisms upon differences in enzyme activity (Alikhani-Koupaei et al., 2007; Lavery et al., 2003). Conversely, a study by Melander *et al* found no correlation between HSD11B2 polymorphisms and essential hypertension using patients THF/THE ratio as a guide to *in vivo* 11β-HSD2 activity (Melander et al., 2003). However, another study by Poch *et al* demonstrated reduced 11β-HSD2 activity associated with essential hypertension in biopsied salivary glands of hypertensive patients for whom the THF/THE ratio was not significantly different compared to normotensive controls (Poch et al., 2001); they concluded that the THF/THE ratio is not an ideal marker of *in vivo* enzyme activity.

We have advanced upon these human population association and *in vitro* cell line studies to provide the first direct *in vivo* evidence that reduced 11β-HSD2 enzyme activity causes a SS BP phenotype. This is an important finding as it supports the theory that HSD11B2 polymorphisms within the general population contribute towards essential and/or SS hypertension.

Therefore, the *Hsd11b2*$^{+/-}$ mouse is an excellent *in vivo* model to use for dissecting molecular mechanisms that underlie SS BP.

The altered sodium handling and renal hemodynamics of *Hsd11b2*$^{+/-}$ mice on a high sodium diet is highly suggestive of a renal aspect to the BP phenotype. The major role that the kidney plays in BP homeostasis is well documented. The case study of a kidney transplant fully rescuing the phenotype of a SAME patient also highlights the important role of the kidney in the development of these phenotypes (Palermo et al., 2000) Therefore, our investigations into the molecular mechanisms underlying the salt sensitivity of the *Hsd11b2*$^{+/-}$ mice focused upon the kidney in particular. Pharmacological interventions showed that the important renal sodium channel ENaC was playing a role in the development of SS phenotypes, as ENaC blockade prevented the phenotype from developing on a high sodium diet. Further studies into the involvement of ENaC in the *Hsd11b2*$^{+/-}$ SS phenotype could be carried out to enhance our understanding of this phenotype. These studies could include quantifying the expression of ENaC subunits by performing quantitive PCR upon dissected collecting ducts from *Hsd11b2*$^{+/-}$ and *Hsd11b2*$^{+/+}$ mice both before and after and high sodium diet, and seeing what effects diet and genotype have upon ENaC expression. Electrophysiology experiments could also be carried out upon split-open distal tubules from these mice to assess the functional activity of ENaC, and also immunostaining in order to determine the spatial location of ENaC at a cellular level. The expression of ENaC regulators, such as SGK1 and Nedd 4, may also prove insightful.

AngI and II dose response experiments highlighted the contributions that 11β-HSD2 expression in the vasculature may also be making towards these phenotypes. These experiments could be further developed by performing

quantitative PCR assays to assess AT receptor expression levels, and also myography of resistance vessels as the RVR and Ang I and II dose-response curves are suggestive of alterations in the vasculature of *Hsd11b2*$^{+/-}$ mice, particularly in the setting of a high sodium diet. These studies could also be repeated using AT receptor antagonists, such as Losartan, to pharmacologically characterise the BP responses to Ang I and II.

The ability of the *Hsd11b2*$^{+/-}$ mice to significantly reduce their aldosterone levels on a high sodium diet suggested that they are capable of regulating their RAAS in response to dietary salt load. An unexpected finding was the significant increases in corticosterone in these mice on a high sodium diet. These increased levels are most likely responsible for the phenotype of the *Hsd11b2*$^{+/-}$ mice, whether via MR, GR or, more likely, a combination of both. Studies performed in this thesis with the MR antagonist spironolactone proved inconclusive, and an investigation with a GR antagonist would be of great interest. Since the completion of my PhD studies, these experiments have been successfully carried by others in the research group (see Appendix 2 of this thesis for published scientific paper in the journal Hypertension that includes these further experiments). In addition, the elevated glucocorticoid levels suggested that a stress-related phenotype due to the high sodium diet may have developed. HPA axis testing showed that the *Hsd11b2*$^{+/-}$ mice were not synthesising or releasing greater amounts of corticosterone in response to an acute stress on a high sodium diet. However, this testing did highlight the impaired ability of the *Hsd11b2*$^{+/-}$ mice to metabolise corticosterone in comparison to the *Hsd11b2*$^{+/+}$ mice, but only under high sodium diet conditions. This would suggest that the high sodium diet was affecting 11β-HSD2 activity, but our enzyme activity assay showed this not to be the case. The high sodium diet may therefore be influencing other mediators of

corticosterone metabolism or regulation, such as the 5α- and β-reductases. It would be interesting to measure the THF/THE ration in these mice to see if a high sodium diet affects this pathway of glucocorticoid metabolism. We also thought it important to investigate other effects that a high sodium diet may be causing as the *Hsd11b2*$^{+/-}$ phenotype may arise as a failure of the mice to respond appropriately to the physiological stresses that associate with sodium loading.

As previously mentioned, an interesting observation in these studies is that the *Hsd11b2*$^{+/-}$ mice only present with a phenotype different from the *Hsd1b2*$^{+/+}$ mice when they are confronted with increased dietary sodium. Studies using cloned 11β-HSD2 protein have shown that *in vitro* conversion of cortisol to corticosterone displays a linear dose response (Ferrari et al., 1996). Glucocorticoids therefore technically have "improved" access to MR in the heterozygote model, but this appears to have no physiological consequences under normal salt conditions. Further investigations studying the binding of tracer ^{3}H-aldosterone in kidney, colon, heart and hippocampal extracts, suggest MR are always highly occupied by glucocorticoids, but not necessarily activated (Funder and Myles, 1996). This poses the question why does glucocorticoid activation of MR, and the consequential detrimental effects, only occur when the *Hsd11b2*$^{+/-}$ mice are exposed to levels of increased sodium?

A possible explanation begins with the observation in some studies showing a link between increased salt intake and renal oxidative stress (Gill and Wilcox, 2006). It has been suggested that a change in the REDOX state of MR and 11β-HSD2 target tissues may change the ability of glucocorticoids to activate the MR (Funder, 2005). That is, under a normal REDOX state, glucocorticoids can occupy the MR, but do not activate the MR. However,

when something acts to change the intracellular REDOX state, such as high sodium diet, this permits the glucocorticoids to activate the MR. The link between increased sodium and an altered REDOX state seems to arise from an increase in oxidative stress. Markers of oxidative stress, such as the isoprostanes and NADPH Oxidase subunits, have been found as up regulated in different models of experimental hypertension (Paravicini and Touyz, 2008). Our studies showed that high sodium diet induced a urinary marker of oxidative stress in both genotypes, and that co-administration of an antioxidant drug with a high sodium diet alleviated the SS phenotype of *Hsd11b2*$^{+/-}$ mice. However, the antioxidant drug did not attenuate the urinary oxidative stress marker, and so further experiments are required to fully analyse the contribution of oxidative stress to the phenotype of this model, such as quantitative PCR measurements of NADPH Oxidase subunits, as well as repeating the experiments with a antioxidant drug that works via a different mechanism(s) to assess the validity of the TEMPOL treatment.

The link between *Hsd11b2* heterozygosity, dietary sodium intake and our observed phenotype is likely to be a complicated one involving glucocorticoid regulation, MR target genes, and the control of ligand-receptor regulation. The most important factor is that despite the differences we see in phenotype between *Hsd11b2*$^{+/-}$ and *Hsd11b2*$^{+/+}$ mice, these only present on a high sodium diet, and are therefore the result of a relationship between this and a decrease in 11β-HSD2 enzyme activity, and not either on its own. Therefore, the important question that these studies have raised is why do *Hsd11b2*$^{+/-}$ mice only present with a phenotype under increased dietary sodium? The answer to this is likely to prove insightful in clinical treatments for hypertension not only for individuals with HSD11B2 polymorphisms, but for SS hypertension in general.

References

Abrams, J.M., Osborn, J.W., 2008. A role for benzamil-sensitive proteins of the central nervous system in the pathogenesis of salt-dependent hypertension. Clin Exp Pharmacol Physiol 35, 687-694.

Agarwal, A.K., Monder, C., Eckstein, B., White, P.C., 1989. Cloning and expression of rat cDNA encoding corticosteroid 11 beta-dehydrogenase. J Biol Chem 264, 18939-18943.

Agarwal, A.K., Mune, T., Monder, C., White, P.C., 1994. NAD(+)-dependent isoform of 11 beta-hydroxysteroid dehydrogenase. Cloning and characterization of cDNA from sheep kidney. J Biol Chem 269, 25959-25962.

Agarwal, A.K., Rogerson, F.M., Mune, T., White, P.C., 1995. Analysis of the human gene encoding the kidney isozyme of 11 beta-hydroxysteroid dehydrogenase. J Steroid Biochem Mol Biol 55, 473-479.

Agarwal, R., 2002. Rapid microplate method for PAH estimation. Am J Physiol Renal Physiol 283, F236-241.

Aizawa, Y., Kamimura, N., Watanabe, H., Aizawa, Y., Makiyama, Y., Usuda, Y., Watanabe, T., Kurashina, Y., 2006. Cardiovascular risk factors are really linked in the metabolic syndrome: this phenomenon suggests clustering rather than coincidence. Int J Cardiol 109, 213-218.

Al-Dujaili, E.A., Mullins, L.J., Bailey, M.A., Andrew, R., Kenyon, C.J., 2009a. Physiological and pathophysiological applications of sensitive ELISA methods for urinary deoxycorticosterone and corticosterone in rodents. Steroids 74, 938-944.

Al-Dujaili, E.A., Mullins, L.J., Bailey, M.A., Kenyon, C.J., 2009b. Development of a highly sensitive ELISA for aldosterone in mouse urine: validation in physiological and pathophysiological states of aldosterone excess and depletion. Steroids 74, 456-462.

Alikhani-Koupaei, R., Fouladkou, F., Fustier, P., Cenni, B., Sharma, A.M., Deter, H.C., Frey, B.M., Frey, F.J., 2007. Identification of polymorphisms in the human 11beta-hydroxysteroid dehydrogenase type 2 gene promoter: functional characterization and relevance for salt sensitivity. FASEB J 21, 3618-3628.

Antunes, F., Cadenas, E., 2000. Estimation of H2O2 gradients across biomembranes. FEBS Lett 475, 121-126.

Arnaldi, G., Mancini, T., Polenta, B., Boscaro, M., 2004. Cardiovascular risk in Cushing's syndrome. Pituitary 7, 253-256.

Arriza, J.L., Weinberger, C., Cerelli, G., Glaser, T.M., Handelin, B.L., Housman, D.E., Evans, R.M., 1987. Cloning of human mineralocorticoid receptor complementary DNA: structural and functional kinship with the glucocorticoid receptor. Science 237, 268-275.

Atanasov, A.G., Ignatova, I.D., Nashev, L.G., Dick, B., Ferrari, P., Frey, F.J., Odermatt, A., 2007. Impaired protein stability of 11beta-hydroxysteroid dehydrogenase type 2: a novel mechanism of apparent mineralocorticoid excess. J Am Soc Nephrol 18, 1262-1270.

Bailey, M.A., Mullins, J.J., Kenyon, C.J., 2009. Mineralocorticoid and glucocorticoid receptors stimulate epithelial sodium channel activity in a mouse model of Cushing syndrome. Hypertension 54, 890-896.

Bailey, M.A., Paterson, J.M., Hadoke, P.W., Wrobel, N., Bellamy, C.O., Brownstein, D.G., Seckl, J.R., Mullins, J.J., 2008. A switch in the mechanism of hypertension in the syndrome of apparent mineralocorticoid excess. J Am Soc Nephrol 19, 47-58.

Baker, M.E., Chandsawangbhuwana, C., Ollikainen, N., 2007. Structural analysis of the evolution of steroid specificity in the mineralocorticoid and glucocorticoid receptors. BMC Evol Biol 7, 24.

Bandulik, S., Penton, D., Barhanin, J., Warth, R., 2010. TASK1 and TASK3 potassium channels: determinants of aldosterone secretion and adrenocortical zonation. Horm Metab Res 42, 450-457.

Beggah, A.T., Escoubet, B., Puttini, S., Cailmail, S., Delage, V., Ouvrard-Pascaud, A., Bocchi, B., Peuchmaur, M., Delcayre, C., Farman, N., Jaisser, F., 2002. Reversible cardiac fibrosis and heart failure induced by conditional expression of an antisense mRNA of the mineralocorticoid receptor in cardiomyocytes. Proc Natl Acad Sci U S A 99, 7160-7165.

Berger, S., Bleich, M., Schmid, W., Cole, T.J., Peters, J., Watanabe, H., Kriz, W., Warth, R., Greger, R., Schutz, G., 1998. Mineralocorticoid receptor knockout mice: pathophysiology of Na+ metabolism. Proc Natl Acad Sci U S A 95, 9424-9429.

Beswick, R.A., Zhang, H., Marable, D., Catravas, J.D., Hill, W.D., Webb, R.C., 2001. Long-term antioxidant administration attenuates mineralocorticoid hypertension and renal inflammatory response. Hypertension 37, 781-786.

Bocchi, B., Kenouch, S., Lamarre-Cliche, M., Muffat-Joly, M., Capron, M.H., Fiet, J., Morineau, G., Azizi, M., Bonvalet, J.P., Farman, N., 2004. Impaired 11-beta hydroxysteroid dehydrogenase type 2 activity in sweat gland ducts in human essential hypertension. Hypertension 43, 803-808.

Boini, K.M., Hennige, A.M., Huang, D.Y., Friedrich, B., Palmada, M., Boehmer, C., Grahammer, F., Artunc, F., Ullrich, S., Avram, D., Osswald, H., Wulff, P., Kuhl, D., Vallon, V., Haring, H.U., Lang, F., 2006. Serum- and glucocorticoid-inducible kinase 1 mediates salt sensitivity of glucose tolerance. Diabetes 55, 2059-2066.

Bongartz, L.G., Cramer, M.J., Doevendans, P.A., Joles, J.A., Braam, B., 2005. The severe cardiorenal syndrome: 'Guyton revisited'. Eur Heart J 26, 11-17.

Bonnet, F., Cooper, M.E., Carey, R.M., Casley, D., Cao, Z., 2001. Vascular expression of angiotensin type 2 receptor in the adult rat: influence of angiotensin II infusion. J Hypertens 19, 1075-1081.

Booth, R.E., Johnson, J.P., Stockand, J.D., 2002. Aldosterone. Adv Physiol Educ 26, 8-20.

Bradley, A., 1987. Production and analysis of chimaeric mice. In: Robertson E.J. (ed) Teratocarcinomas and embryonic stem cells. IRL Press, 113-151.

Branda, C.S., Dymecki, S.M., 2004. Talking about a revolution: The impact of site-specific recombinases on genetic analyses in mice. Dev Cell 6, 7-28.

Brands, M.W., Bell, T.D., Gibson, B., 2004. Nitric oxide may prevent hypertension early in diabetes by counteracting renal actions of superoxide. Hypertension 43, 57-63.

Brilla, C.G., Weber, K.T., 1992. Mineralocorticoid excess, dietary sodium, and myocardial fibrosis. J Lab Clin Med 120, 893-901.

Brown, R.W., Diaz, R., Robson, A.C., Kotelevtsev, Y.V., Mullins, J.J., Kaufman, M.H., Seckl, J.R., 1996. The ontogeny of 11 beta-hydroxysteroid dehydrogenase type 2 and mineralocorticoid receptor gene expression reveal intricate control of glucocorticoid action in development. Endocrinology 137, 794-797.

Brunner, H.R., Baer, L., Sealey, J.E., Ledingham, J.G., Laragh, J.H., 1970. The influence of potassium administration and of potassium deprivation on plasma renin in normal and hypertensive subjects. J Clin Invest 49, 2128-2138.

Cai, T.Q., Wong, B., Mundt, S.S., Thieringer, R., Wright, S.D., Hermanowski-Vosatka, A., 2001. Induction of 11beta-hydroxysteroid dehydrogenase type 1 but not -2 in human aortic smooth muscle cells by inflammatory stimuli. J Steroid Biochem Mol Biol 77, 117-122.

Campean, V., Kricke, J., Ellison, D., Luft, F.C., Bachmann, S., 2001. Localization of thiazide-sensitive Na(+)-Cl(-) cotransport and associated gene products in mouse DCT. Am J Physiol Renal Physiol 281, F1028-1035.

Campese, V.M., Park, J., 2006. The kidney and hypertension: over 70 years of research. J Nephrol 19, 691-698.

Carey, R.M., Padia, S.H., 2008. Angiotensin AT2 receptors: control of renal sodium excretion and blood pressure. Trends Endocrinol Metab 19, 84-87.

Carvajal, C.A., Gonzalez, A.A., Romero, D.G., Gonzalez, A., Mosso, L.M., Lagos, E.T., Hevia Mdel, P., Rosati, M.P., Perez-Acle, T.O., Gomez-Sanchez, C.E., Montero, J.A., Fardella, C.E., 2003. Two homozygous mutations in the 11 beta-hydroxysteroid dehydrogenase type 2 gene in a case of apparent mineralocorticoid excess. J Clin Endocrinol Metab 88, 2501-2507.

Carvajal, C.A., Romero, D.G., Mosso, L.M., Gonzalez, A.A., Campino, C., Montero, J., Fardella, C.E., 2005. Biochemical and genetic characterization of 11 beta-hydroxysteroid dehydrogenase type 2 in low-renin essential hypertensives. J Hypertens 23, 71-77.

Causevic, M., Mohaupt, M., 2007. 11beta-Hydroxysteroid dehydrogenase type 2 in pregnancy and preeclampsia. Mol Aspects Med 28, 220-226.

Chen, X., Patel, K., Connors, S.G., Mendonca, M., Welch, W.J., Wilcox, C.S., 2007. Acute antihypertensive action of Tempol in the spontaneously hypertensive rat. Am J Physiol Heart Circ Physiol 293, H3246-3253.

Chew, G.T., Gan, S.K., Watts, G.F., 2006. Revisiting the metabolic syndrome. Med J Aust 185, 445-449.

Christy, C., Hadoke, P.W., Paterson, J.M., Mullins, J.J., Seckl, J.R., Walker, B.R., 2003. 11beta-hydroxysteroid dehydrogenase type 2 in mouse aorta:

localization and influence on response to glucocorticoids. Hypertension 42, 580-587.

Churchill, P.C., Churchill, M.C., Bidani, A.K., 1992. Kidney cross transplants in Dahl salt-sensitive and salt-resistant rats. Am J Physiol 262, H1809-1817.

Cole, T.J., 1995. Cloning of the mouse 11 beta-hydroxysteroid dehydrogenase type 2 gene: tissue specific expression and localization in distal convoluted tubules and collecting ducts of the kidney. Endocrinology 136, 4693-4696.

Cole, T.J., Blendy, J.A., Monaghan, A.P., Krieglstein, K., Schmid, W., Aguzzi, A., Fantuzzi, G., Hummler, E., Unsicker, K., Schutz, G., 1995. Targeted disruption of the glucocorticoid receptor gene blocks adrenergic chromaffin cell development and severely retards lung maturation. Genes Dev 9, 1608-1621.

Condon, J., Ricketts, M.L., Whorwood, C.B., Stewart, P.M., 1997. Ontogeny and sexual dimorphic expression of mouse type 2 11beta-hydroxysteroid dehydrogenase. Mol Cell Endocrinol 127, 121-128.

Conn, J.W., Knopf, R.F., Nesbit, R.M., 1964. Clinical Characteristics of Primary Aldosteronism from an Analysis of 145 Cases. Am J Surg 107, 159-172.

Couture, R., Regoli, D., 1980. Vascular reactivity to angiotensin and noradrenaline in rats maintained on a sodium free diet or made hypertensive with desoxycorticosterone acetate and salt (DOCA/salt). Clin Exp Hypertens 2, 25-43.

Cowley, A.W., Jr., 1997. Genetic and nongenetic determinants of salt sensitivity and blood pressure. Am J Clin Nutr 65, 587S-593S.

Cowley, A.W., McCaa, R.E., 1976. Acute and chronic dose-response relationships for angiotensin, aldosterone, and arterial pressure at varying levels of sodium intake. Circ Res 39, 788-797.

Csiky, B., Simon, G., 1997. Synergistic vascular effects of dietary sodium supplementation and angiotensin II administration. Am J Physiol 273, H1275-1282.

Dahl, L.K., Heine, M., 1975. Primary role of renal homografts in setting chronic blood pressure levels in rats. Circ Res 36, 692-696.

Dahl, L.K., Heine, M., Tassinari, L., 1962. Role of genetic factors in susceptibility to experimental hypertension due to chronic excess salt ingestion. Nature 194, 480-482.

Dave-Sharma, S., Wilson, R.C., Harbison, M.D., Newfield, R., Azar, M.R., Krozowski, Z.S., Funder, J.W., Shackleton, C.H., Bradlow, H.L., Wei, J.Q., Hertecant, J., Moran, A., Neiberger, R.E., Balfe, J.W., Fattah, A., Daneman, D., Akkurt, H.I., De Santis, C., New, M.I., 1998. Examination of genotype and phenotype relationships in 14 patients with apparent mineralocorticoid excess. J Clin Endocrinol Metab 83, 2244-2254.

Davi, G., Ciabattoni, G., Consoli, A., Mezzetti, A., Falco, A., Santarone, S., Pennese, E., Vitacolonna, E., Bucciarelli, T., Costantini, F., Capani, F., Patrono, C., 1999. In vivo formation of 8-iso-prostaglandin f2alpha and platelet activation in diabetes mellitus: effects of improved metabolic control and vitamin E supplementation. Circulation 99, 224-229.

de Gasparo, M., Catt, K.J., Inagami, T., Wright, J.W., Unger, T., 2000. International union of pharmacology. XXIII. The angiotensin II receptors. Pharmacol Rev 52, 415-472.

Dell'Italia, L.J., Meng, Q.C., Balcells, E., Straeter-Knowlen, I.M., Hankes, G.H., Dillon, R., Cartee, R.E., Orr, R., Bishop, S.P., Oparil, S., et al., 1995. Increased ACE and chymase-like activity in cardiac tissue of dogs with chronic mitral regurgitation. Am J Physiol 269, H2065-2073.

Deng, A.Y., 1998. In search of hypertension genes in Dahl salt-sensitive rats. J Hypertens 16, 1707-1717.

Deschamps, J., de Laaf, R., Verrijzer, P., de Gouw, M., Destree, O., Meijlink, F., 1987. The mouse Hox2.3 homeobox-containing gene: regulation in differentiating pluripotent stem cells and expression pattern in embryos. Differentiation 35, 21-30.

Deschamps, J., van den Akker, E., Forlani, S., De Graaff, W., Oosterveen, T., Roelen, B., Roelfsema, J., 1999. Initiation, establishment and maintenance of Hox gene expression patterns in the mouse. Int J Dev Biol 43, 635-650.

Duprez, D.A., 2007. Aldosterone and the vasculature: mechanisms mediating resistant hypertension. J Clin Hypertens (Greenwich) 9, 13-18.

Elliott, P., Stamler, J., 2002. Evidence on salt and blood pressure is consistent and persuasive. Int J Epidemiol 31, 316-319; discussion 331-312.

Endemann, D.H., Touyz, R.M., Iglarz, M., Savoia, C., Schiffrin, E.L., 2004. Eplerenone prevents salt-induced vascular remodeling and cardiac fibrosis in stroke-prone spontaneously hypertensive rats. Hypertension 43, 1252-1257.

Etxabe, J., Vazquez, J.A., 1994. Morbidity and mortality in Cushing's disease: an epidemiological approach. Clin Endocrinol (Oxf) 40, 479-484.

Evans, M.J., Kaufman, M.H., 1981. Establishment in culture of pluripotential cells from mouse embryos. Nature 292, 154-156.

Ferrari, A.U., Franzelli, C., Daffonchio, A., Perlini, S., Dirienzo, M., 1996. Sympathovagal interplay in the control of overall blood pressure variability in unanesthetized rats. Am J Physiol 270, H2143-2148.

Ferrari, P., Lovati, E., Frey, F.J., 2000. The role of the 11beta-hydroxysteroid dehydrogenase type 2 in human hypertension. J Hypertens 18, 241-248.

Fjeld, C.C., Birdsong, W.T., Goodman, R.H., 2003. Differential binding of NAD+ and NADH allows the transcriptional corepressor carboxyl-terminal binding protein to serve as a metabolic sensor. Proc Natl Acad Sci U S A 100, 9202-9207.

Forte, J.G., Miguel, J.M., Miguel, M.J., de Padua, F., Rose, G., 1989. Salt and blood pressure: a community trial. J Hum Hypertens 3, 179-184.

Franco-Saenz, R., Shen, P., Lee, S.J., Cicila, G.T., Henrich, W.L., 1999. Regulation of the genes for 11beta-hydroxysteroid dehydrogenase type 1 and type 2 in the kidney of the Dahl rat. J Hypertens 17, 1089-1093.

Franco, V., Oparil, S., 2006. Salt sensitivity, a determinant of blood pressure, cardiovascular disease and survival. J Am Coll Nutr 25, 247S-255S.

Friedrich, G., Soriano, P., 1991. Promoter traps in embryonic stem cells: a genetic screen to identify and mutate developmental genes in mice. Genes Dev 5, 1513-1523.

Fuller, P.J., Verity, K., 1990. Mineralocorticoid receptor gene expression in the gastrointestinal tract: distribution and ontogeny. J Steroid Biochem 36, 263-267.

Funder, J., Myles, K., 1996. Exclusion of corticosterone from epithelial mineralocorticoid receptors is insufficient for selectivity of aldosterone action: in vivo binding studies. Endocrinology 137, 5264-5268.

Funder, J.W., 2004. Is aldosterone bad for the heart? Trends Endocrinol Metab 15, 139-142.

Funder, J.W., 2005. RALES, EPHESUS and redox. J Steroid Biochem Mol Biol 93, 121-125.

Funder, J.W., Carey, R.M., Fardella, C., Gomez-Sanchez, C.E., Mantero, F., Stowasser, M., Young, W.F., Jr., Montori, V.M., 2008. Case detection, diagnosis, and treatment of patients with primary aldosteronism: an endocrine society clinical practice guideline. J Clin Endocrinol Metab 93, 3266-3281.

Funder, J.W., Pearce, P.T., Smith, R., Smith, A.I., 1988. Mineralocorticoid action: target tissue specificity is enzyme, not receptor, mediated. Science 242, 583-585.

Gant, N.F., Daley, G.L., Chand, S., Whalley, P.J., MacDonald, P.C., 1973. A study of angiotensin II pressor response throughout primigravid pregnancy. J Clin Invest 52, 2682-2689.

Ge, Y., Stricklett, P.K., Hughes, A.K., Yanagisawa, M., Kohan, D.E., 2005. Collecting duct-specific knockout of the endothelin A receptor alters renal vasopressin responsiveness, but not sodium excretion or blood pressure. Am J Physiol Renal Physiol 289, F692-698.

Geller, D.S., Farhi, A., Pinkerton, N., Fradley, M., Moritz, M., Spitzer, A., Meinke, G., Tsai, F.T., Sigler, P.B., Lifton, R.P., 2000. Activating mineralocorticoid receptor mutation in hypertension exacerbated by pregnancy. Science 289, 119-123.

Ghosh, K., Van Duyne, G.D., 2002. Cre-loxP biochemistry. Methods 28, 374-383.

Giles, T.D., 2006. Circadian rhythm of blood pressure and the relation to cardiovascular events. J Hypertens Suppl 24, S11-16.

Gill, P.S., Wilcox, C.S., 2006. NADPH oxidases in the kidney. Antioxid Redox Signal 8, 1597-1607.

Giner, V., Coca, A., de la Sierra, A., 2001. Increased insulin resistance in salt sensitive essential hypertension. J Hum Hypertens 15, 481-485.

Girod, J.P., Brotman, D.J., 2004. Does altered glucocorticoid homeostasis increase cardiovascular risk? Cardiovasc Res 64, 217-226.

Glass, C.A., Perrin, R.M., Pocock, T.M., Bates, D.O., 2006. Transient osmotic absorption of fluid in microvessels exposed to low concentrations of dimethyl sulfoxide. Microcirculation 13, 29-40.

Glover, O'Shaughnessy, 2010. SPAK and WNK kinases? a new target for blood pressure treatment? Curr Opin Nephrol Hypertens.

Gomez-Sanchez, E.P., 1986. Intracerebroventricular infusion of aldosterone induces hypertension in rats. Endocrinology 118, 819-823.

Gomez-Sanchez, E.P., 1997. Central hypertensive effects of aldosterone. Front Neuroendocrinol 18, 440-462.

Gomez-Sanchez, E.P., Ganjam, V., Chen, Y.J., Liu, Y., Clark, S.A., Gomez-Sanchez, C.E., 2001. The 11beta hydroxysteroid dehydrogenase 2 exists as an inactive dimer. Steroids 66, 845-848.

Gomez-Sanchez, E.P., Gomez-Sanchez, C.E., 1991. 19-Nordeoxycorticosterone, aldosterone, and corticosterone excretion in sequential urine samples from male and female rats. Steroids 56, 451-454.

Gomez-Sanchez, E.P., Gomez-Sanchez, C.E., 1992. Central hypertensinogenic effects of glycyrrhizic acid and carbenoxolone. Am J Physiol 263, E1125-1130.

Gong, R., Morris, D.J., Brem, A.S., 2008. Variable expression of 11beta Hydroxysteroid dehydrogenase (11beta-HSD) isoforms in vascular endothelial cells. Steroids 73, 1187-1196.

Good, D.W., 2007. Nongenomic actions of aldosterone on the renal tubule. Hypertension 49, 728-739.

Group, I.C.R., 1988. Intersalt: an international study of electrolyte excretion and blood pressure. Results for 24 hour urinary sodium and potassium excretion. BMJ 297, 319-328.

Grundy, S.M., 2007. Metabolic syndrome: a multiplex cardiovascular risk factor. J Clin Endocrinol Metab 92, 399-404.

Guo, D.F., Uno, S., Ishihata, A., Nakamura, N., Inagami, T., 1995. Identification of a cis-acting glucocorticoid responsive element in the rat angiotensin II type 1A promoter. Circ Res 77, 249-257.

Guyton, A.C., 1990. The surprising kidney-fluid mechanism for pressure control--its infinite gain! Hypertension 16, 725-730.

Guyton, A.C., Coleman, T.G., Granger, H.J., 1972. Circulation: overall regulation. Annu Rev Physiol 34, 13-46.

Hadoke, P.W., Christy, C., Kotelevtsev, Y.V., Williams, B.C., Kenyon, C.J., Seckl, J.R., Mullins, J.J., Walker, B.R., 2001. Endothelial cell dysfunction in mice after transgenic knockout of type 2, but not type 1, 11beta-hydroxysteroid dehydrogenase. Circulation 104, 2832-2837.

Hammer, F., Stewart, P.M., 2006. Cortisol metabolism in hypertension. Best Pract Res Clin Endocrinol Metab 20, 337-353.

Harvey, B.J., Alzamora, R., Stubbs, A.K., Irnaten, M., McEneaney, V., Thomas, W., 2008. Rapid responses to aldosterone in the kidney and colon. J Steroid Biochem Mol Biol 108, 310-317.

Haseroth, K., Gerdes, D., Berger, S., Feuring, M., Gunther, A., Herbst, C., Christ, M., Wehling, M., 1999. Rapid nongenomic effects of aldosterone in mineralocorticoid-receptor-knockout mice. Biochem Biophys Res Commun 266, 257-261.

Hatakeyama, H., Inaba, S., Miyamori, I., 1999. 11beta-hydroxysteroid dehydrogenase in cultured human vascular cells. Possible role in the development of hypertension. Hypertension 33, 1179-1184.

Hatakeyama, H., Inaba, S., Miyamori, I., 2001. 11beta-hydroxysteroid dehydrogenase activity in human aortic smooth muscle cells. Hypertens Res 24, 33-37.

Hatakeyama, H., Inaba, S., Takeda, R., Miyamori, I., 2000. 11beta-hydroxysteroid dehydrogenase in human vascular cells. Kidney Int 57, 1352-1357.

Holmes, M.C., Abrahamsen, C.T., French, K.L., Paterson, J.M., Mullins, J.J., Seckl, J.R., 2006. The mother or the fetus? 11beta-hydroxysteroid dehydrogenase type 2 null mice provide evidence for direct fetal programming of behavior by endogenous glucocorticoids. J Neurosci 26, 3840-3844.

Holmes, M.C., Seckl, J.R., 2006. The role of 11beta-hydroxysteroid dehydrogenases in the brain. Mol Cell Endocrinol 248, 9-14.

Hong, C.C., Ediger, R.D., 1978. Perputial gland abscess in mice. Lab Anim Sci 28, 153-156.

Hooper, M., Hardy, K., Handyside, A., Hunter, S., Monk, M., 1987. HPRT-deficient (Lesch-Nyhan) mouse embryos derived from germline colonization by cultured cells. Nature 326, 292-295.

Hoppe, C.C., Moritz, K.M., Fitzgerald, S.M., Bertram, J.F., Evans, R.G., 2009. Transient hypertension and sustained tachycardia in mice housed individually in metabolism cages. Physiol Res 58, 69-75.

Huang, C.L., Kuo, E., 2007. Mechanisms of disease: WNK-ing at the mechanism of salt-sensitive hypertension. Nat Clin Pract Nephrol 3, 623-630.

Inbar, O., Liefshitz, B., Bitan, G., Kupiec, M., 2000. The relationship between homology length and crossing over during the repair of a broken chromosome. J Biol Chem 275, 30833-30838.

Ingram, M.C., Wallace, A.M., Collier, A., Fraser, R., Connell, J.M., 1996. Sodium status, corticosteroid metabolism and blood pressure in normal human subjects and in a patient with abnormal salt appetite. Clin Exp Pharmacol Physiol 23, 375-378.

Jacob, S.W., de la Torre, J.C., 2009. Pharmacology of dimethyl sulfoxide in cardiac and CNS damage. Pharmacol Rep 61, 225-235.

Jansen, P.M., Danser, A.H., Imholz, B.P., van den Meiracker, A.H., 2009. Aldosterone-receptor antagonism in hypertension. J Hypertens 27, 680-691.

Jeunemaitre, X., Soubrier, F., Kotelevtsev, Y.V., Lifton, R.P., Williams, C.S., Charru, A., Hunt, S.C., Hopkins, P.N., Williams, R.R., Lalouel, J.M., et al., 1992. Molecular basis of human hypertension: role of angiotensinogen. Cell 71, 169-180.

Johar, S., Cave, A.C., Narayanapanicker, A., Grieve, D.J., Shah, A.M., 2006. Aldosterone mediates angiotensin II-induced interstitial cardiac fibrosis via a Nox2-containing NADPH oxidase. FASEB J 20, 1546-1548.

Johns, E.J., O'Shaughnessy, B., O'Neill, S., Lane, B., Healy, V., 2010. Impact of Elevated Dietary Sodium Intake on Nad(P)H Oxidase and Sod in the Cortex and Medulla of the Rat Kidney. Am J Physiol Regul Integr Comp Physiol.

Kahle, K.T., Ring, A.M., Lifton, R.P., 2008. Molecular physiology of the WNK kinases. Annu Rev Physiol 70, 329-355.

Kahle, K.T., Wilson, F.H., Lalioti, M., Toka, H., Qin, H., Lifton, R.P., 2004. WNK kinases: molecular regulators of integrated epithelial ion transport. Curr Opin Nephrol Hypertens 13, 557-562.

Kamynina, E., Debonneville, C., Bens, M., Vandewalle, A., Staub, O., 2001. A novel mouse Nedd4 protein suppresses the activity of the epithelial Na+ channel. FASEB J 15, 204-214.

Kannel, W.B., 2000. Elevated systolic blood pressure as a cardiovascular risk factor. Am J Cardiol 85, 251-255.

Kantachuvesiri, S., Fleming, S., Peters, J., Peters, B., Brooker, G., Lammie, A.G., McGrath, I., Kotelevtsev, Y., Mullins, J.J., 2001. Controlled hypertension, a transgenic toggle switch reveals differential mechanisms underlying vascular disease. J Biol Chem 276, 36727-36733.

Kathiresan, S., Larson, M.G., Benjamin, E.J., Corey, D., Murabito, J.M., Fox, C.S., Wilson, P.W., Rifai, N., Meigs, J.B., Ricken, G., Lifton, R.P., Levy, D., Vasan, R.S., 2005. Clinical and genetic correlates of serum aldosterone in the community: the Framingham Heart Study. Am J Hypertens 18, 657-665.

Kato, N., 1999. Genetic analysis in Dahl salt-sensitive rats. Clin Exp Pharmacol Physiol 26, 539-540.

Kawada, N., Imai, E., Karber, A., Welch, W.J., Wilcox, C.S., 2002. A mouse model of angiotensin II slow pressor response: role of oxidative stress. J Am Soc Nephrol 13, 2860-2868.

Khaw, K.T., Bingham, S., Welch, A., Luben, R., O'Brien, E., Wareham, N., Day, N., 2004. Blood pressure and urinary sodium in men and women: the Norfolk Cohort of the European Prospective Investigation into Cancer (EPIC-Norfolk). Am J Clin Nutr 80, 1397-1403.

Kim, H.S., Krege, J.H., Kluckman, K.D., Hagaman, J.R., Hodgin, J.B., Best, C.F., Jennette, J.C., Coffman, T.M., Maeda, N., Smithies, O., 1995. Genetic control of blood pressure and the angiotensinogen locus. Proc Natl Acad Sci U S A 92, 2735-2739.

Kimura, G., Dohi, Y., Fukuda, M., 2010. Salt sensitivity and circadian rhythm of blood pressure: the keys to connect CKD with cardiovascular events. Hypertens Res 33, 515-520.

Kitanaka, S., Katsumata, N., Tanae, A., Hibi, I., Takeyama, K., Fuse, H., Kato, S., Tanaka, T., 1997. A new compound heterozygous mutation in the 11 beta-

hydroxysteroid dehydrogenase type 2 gene in a case of apparent mineralocorticoid excess. J Clin Endocrinol Metab 82, 4054-4058.

Kitiyakara, C., Chabrashvili, T., Chen, Y., Blau, J., Karber, A., Aslam, S., Welch, W.J., Wilcox, C.S., 2003. Salt intake, oxidative stress, and renal expression of NADPH oxidase and superoxide dismutase. J Am Soc Nephrol 14, 2775-2782.

Knight, S.F., Yuan, J., Roy, S., Imig, J.D., Simvastatin and tempol protect against endothelial dysfunction and renal injury in a model of obesity and hypertension. Am J Physiol Renal Physiol 298, F86-94.

Kobori, H., Nangaku, M., Navar, L.G., Nishiyama, A., 2007. The intrarenal renin-angiotensin system: from physiology to the pathobiology of hypertension and kidney disease. Pharmacol Rev 59, 251-287.

Koper, J.W., Stolk, R.P., de Lange, P., Huizenga, N.A., Molijn, G.J., Pols, H.A., Grobbee, D.E., Karl, M., de Jong, F.H., Brinkmann, A.O., Lamberts, S.W., 1997. Lack of association between five polymorphisms in the human glucocorticoid receptor gene and glucocorticoid resistance. Hum Genet 99, 663-668.

Kotelevtsev, Y., Brown, R.W., Fleming, S., Kenyon, C., Edwards, C.R., Seckl, J.R., Mullins, J.J., 1999. Hypertension in mice lacking 11beta-hydroxysteroid dehydrogenase type 2. J Clin Invest 103, 683-689.

Kramer, R.E., Gallant, S., Brownie, A.C., 1980. Actions of angiotensin II on aldosterone biosynthesis in the rat adrenal cortex. Effects on cytochrome P-450 enzymes of the early and late pathway. J Biol Chem 255, 3442-3447.

Kress, C., Vogels, R., De Graaff, W., Bonnerot, C., Meijlink, F., Nicolas, J.F., Deschamps, J., 1990. Hox-2.3 upstream sequences mediate lacZ expression in intermediate mesoderm derivatives of transgenic mice. Development 109, 775-786.

Kunes, J., Zicha, J., 2009. The interaction of genetic and environmental factors in the etiology of hypertension. Physiol Res 58 Suppl 2, S33-41.

Kwan, K.M., 2002. Conditional alleles in mice: practical considerations for tissue-specific knockouts. Genesis 32, 49-62.

Lalioti, M.D., Zhang, J., Volkman, H.M., Kahle, K.T., Hoffmann, K.E., Toka, H.R., Nelson-Williams, C., Ellison, D.H., Flavell, R., Booth, C.J., Lu, Y., Geller, D.S., Lifton, R.P., 2006. Wnk4 controls blood pressure and potassium

homeostasis via regulation of mass and activity of the distal convoluted tubule. Nat Genet 38, 1124-1132.

Landmesser, U., Hornig, B., Drexler, H., 2004. Endothelial function: a critical determinant in atherosclerosis? Circulation 109, II27-33.

Lanz, B., Kadereit, B., Ernst, S., Shojaati, K., Causevic, M., Frey, B.M., Frey, F.J., Mohaupt, M.G., 2003. Angiotensin II regulates 11beta-hydroxysteroid dehydrogenase type 2 via AT2 receptors. Kidney Int 64, 970-977.

Lassegue, B., Clempus, R.E., 2003. Vascular NAD(P)H oxidases: specific features, expression, and regulation. Am J Physiol Regul Integr Comp Physiol 285, R277-297.

Lastra, G., Whaley-Connell, A., Manrique, C., Habibi, J., Gutweiler, A.A., Appesh, L., Hayden, M.R., Wei, Y., Ferrario, C., Sowers, J.R., 2008. Low-dose spironolactone reduces reactive oxygen species generation and improves insulin-stimulated glucose transport in skeletal muscle in the TG(mRen2)27 rat. Am J Physiol Endocrinol Metab 295, E110-116.

Lathe, R., Kieny, M.P., Skory, S., Lecocq, J.P., 1984. Linker tailing: unphosphorylated linker oligonucleotides for joining DNA termini. DNA 3, 173-182.

Laurent, A., Mottu, F., Chapot, R., Zhang, J.Q., Jordan, O., Rufenacht, D.A., Doelker, E., Merland, J.J., 2007. Cardiovascular effects of selected water-miscible solvents for pharmaceutical injections and embolization materials: a comparative hemodynamic study using a sheep model. PDA J Pharm Sci Technol 61, 64-74.

Lavery, G.G., Ronconi, V., Draper, N., Rabbitt, E.H., Lyons, V., Chapman, K.E., Walker, E.A., McTernan, C.L., Giacchetti, G., Mantero, F., Seckl, J.R., Edwards, C.R., Connell, J.M., Hewison, M., Stewart, P.M., 2003. Late-onset apparent mineralocorticoid excess caused by novel compound heterozygous mutations in the HSD11B2 gene. Hypertension 42, 123-129.

Lazartigues, E., Feng, Y., Lavoie, J.L., 2007. The two fACEs of the tissue renin-angiotensin systems: implication in cardiovascular diseases. Curr Pharm Des 13, 1231-1245.

Le Menuet, D., Isnard, R., Bichara, M., Viengchareun, S., Muffat-Joly, M., Walker, F., Zennaro, M.C., Lombes, M., 2001. Alteration of cardiac and renal

functions in transgenic mice overexpressing human mineralocorticoid receptor. J Biol Chem 276, 38911-38920.

Ledermann, B., 2000. Embryonic stem cells and gene targeting. Exp Physiol 85, 603-613.

Levy, D.G., Rocha, R., Funder, J.W., 2004. Distinguishing the antihypertensive and electrolyte effects of eplerenone. J Clin Endocrinol Metab 89, 2736-2740.

Li, A., Li, K.X., Marui, S., Krozowski, Z.S., Batista, M.C., Whorwood, C.B., Arnhold, I.J., Shackleton, C.H., Mendonca, B.B., Stewart, P.M., 1997. Apparent mineralocorticoid excess in a Brazilian kindred: hypertension in the heterozygote state. J Hypertens 15, 1397-1402.

Li, A., Tedde, R., Krozowski, Z.S., Pala, A., Li, K.X., Shackleton, C.H., Mantero, F., Palermo, M., Stewart, P.M., 1998. Molecular basis for hypertension in the "type II variant" of apparent mineralocorticoid excess. Am J Hum Genet 63, 370-379.

Lifton, R.P., Dluhy, R.G., Powers, M., Rich, G.M., Cook, S., Ulick, S., Lalouel, J.M., 1992. A chimaeric 11 beta-hydroxylase/aldosterone synthase gene causes glucocorticoid-remediable aldosteronism and human hypertension. Nature 355, 262-265.

Lifton, R.P., Gharavi, A.G., Geller, D.S., 2001. Molecular mechanisms of human hypertension. Cell 104, 545-556.

Lin, R.C., Wang, X.L., Morris, B.J., 2003. Association of coronary artery disease with glucocorticoid receptor N363S variant. Hypertension 41, 404-407.

Liu, H., Colavitti, R., Rovira, II, Finkel, T., 2005. Redox-dependent transcriptional regulation. Circ Res 97, 967-974.

Liu, P., Jenkins, N.A., Copeland, N.G., 2003. A highly efficient recombineering-based method for generating conditional knockout mutations. Genome Res 13, 476-484.

Liu, X., Bellamy, C.O., Bailey, M.A., Mullins, L.J., Dunbar, D.R., Kenyon, C.J., Brooker, G., Kantachuvesiri, S., Maratou, K., Ashek, A., Clark, A.F., Fleming, S., Mullins, J.J., 2009. Angiotensin-converting enzyme is a modifier of hypertensive end organ damage. J Biol Chem 284, 15564-15572.

Lorenz, J.N., 2002. A practical guide to evaluating cardiovascular, renal, and pulmonary function in mice. Am J Physiol Regul Integr Comp Physiol 282, R1565-1582.

Losel, R., Schultz, A., Wehling, M., 2004. A quick glance at rapid aldosterone action. Mol Cell Endocrinol 217, 137-141.

Lotshaw, D.P., 2001. Role of membrane depolarization and T-type Ca2+ channels in angiotensin II and K+ stimulated aldosterone secretion. Mol Cell Endocrinol 175, 157-171.

Lovati, E., Ferrari, P., Dick, B., Jostarndt, K., Frey, B.M., Frey, F.J., Schorr, U., Sharma, A.M., 1999. Molecular basis of human salt sensitivity: the role of the 11beta-hydroxysteroid dehydrogenase type 2. J Clin Endocrinol Metab 84, 3745-3749.

Lu, N., Helwig, B.G., Fels, R.J., Parimi, S., Kenney, M.J., 2004. Central Tempol alters basal sympathetic nerve discharge and attenuates sympathetic excitation to central ANG II. Am J Physiol Heart Circ Physiol 287, H2626-2633.

Lu, N.Z., Wardell, S.E., Burnstein, K.L., Defranco, D., Fuller, P.J., Giguere, V., Hochberg, R.B., McKay, L., Renoir, J.M., Weigel, N.L., Wilson, E.M., McDonnell, D.P., Cidlowski, J.A., 2006. International Union of Pharmacology. LXV. The pharmacology and classification of the nuclear receptor superfamily: glucocorticoid, mineralocorticoid, progesterone, and androgen receptors. Pharmacol Rev 58, 782-797.

MacDonald, P., MacKenzie, S., Ramage, L.E., Seckl, J.R., Brown, R.W., 2000. Corticosteroid regulation of amiloride-sensitive sodium-channel subunit mRNA expression in mouse kidney. J Endocrinol 165, 25-37.

Magiakou, M.A., Smyrnaki, P., Chrousos, G.P., 2006. Hypertension in Cushing's syndrome. Best Pract Res Clin Endocrinol Metab 20, 467-482.

Makino, A., Skelton, M.M., Zou, A.P., Cowley, A.W., Jr., 2003. Increased renal medullary H2O2 leads to hypertension. Hypertension 42, 25-30.

Manning, R.D., Jr., Tian, N., Meng, S., 2005. Oxidative stress and antioxidant treatment in hypertension and the associated renal damage. Am J Nephrol 25, 311-317.

Mantero, F., Palermo, M., Petrelli, M.D., Tedde, R., Stewart, P.M., Shackleton, C.H., 1996. Apparent mineralocorticoid excess: type I and type II. Steroids 61, 193-196.

Mariniello, B., Ronconi, V., Sardu, C., Paglericcio, A., Galletti, F., Strazzullo, P., Palermo, M., Boscaro, M., Stewart, P.M., Mantero, F., Giacchetti, G., 2005. Analysis of the 11beta-hydroxysteroid dehydrogenase type 2 gene (HSD11B2) in human essential hypertension. Am J Hypertens 18, 1091-1098.

Markos, F., Healy, V., Harvey, B.J., 2005. Aldosterone rapidly activates Na+/H+ exchange in M-1 cortical collecting duct cells via a PKC-MAPK pathway. Nephron Physiol 99, p1-9.

Markoullis, K., Bulian, D., Holzlwimmer, G., Quintanilla-Martinez, L., Heiliger, K.J., Zitzelsberger, H., Scherb, H., Mysliwietz, J., Uphoff, C.C., Drexler, H.G., Adler, T., Busch, D.H., Schmidt, J., Mahabir, E., 2009. Mycoplasma contamination of murine embryonic stem cells affects cell parameters, germline transmission and chimeric progeny. Transgenic Res 18, 71-87.

Martinez-Arguelles, D.B., Papadopoulos, V., Epigenetic regulation of the expression of genes involved in steroid hormone biosynthesis and action. Steroids 75, 467-476.

Maser, E., Volker, B., Friebertshauser, J., 2002. 11 Beta-hydroxysteroid dehydrogenase type 1 from human liver: dimerization and enzyme cooperativity support its postulated role as glucocorticoid reductase. Biochemistry 41, 2459-2465.

Masuzaki, H., Paterson, J., Shinyama, H., Morton, N.M., Mullins, J.J., Seckl, J.R., Flier, J.S., 2001. A transgenic model of visceral obesity and the metabolic syndrome. Science 294, 2166-2170.

Masuzaki, H., Yamamoto, H., Kenyon, C.J., Elmquist, J.K., Morton, N.M., Paterson, J.M., Shinyama, H., Sharp, M.G., Fleming, S., Mullins, J.J., Seckl, J.R., Flier, J.S., 2003. Transgenic amplification of glucocorticoid action in adipose tissue causes high blood pressure in mice. J Clin Invest 112, 83-90.

McBride, M.W., Graham, D., Delles, C., Dominiczak, A.F., 2006. Functional genomics in hypertension. Curr Opin Nephrol Hypertens 15, 145-151.

McDonough, A.A., Thompson, C.B., Youn, J.H., 2002. Skeletal muscle regulates extracellular potassium. Am J Physiol Renal Physiol 282, F967-974.

McKinnell, J., Roscoe, D., Holmes, M.C., Lloyd-MacGilp, S.A., Kenyon, C.J., 2000. Regulation of 11beta-hydroxysteroid dehydrogenase enzymes by dietary sodium in the rat. Endocr Res 26, 81-95.

Melander, O., Frandsen, E., Groop, L., Hulthen, U.L., 2003. No evidence of a relation between 11beta-hydroxysteroid dehydrogenase type 2 activity and salt sensitivity. Am J Hypertens 16, 729-733.

Meneton, P., Ichikawa, I., Inagami, T., Schnermann, J., 2000. Renal physiology of the mouse. Am J Physiol Renal Physiol 278, F339-351.

Meneton, P., Jeunemaitre, X., de Wardener, H.E., MacGregor, G.A., 2005. Links between dietary salt intake, renal salt handling, blood pressure, and cardiovascular diseases. Physiol Rev 85, 679-715.

Meng, S., Roberts, L.J., 2nd, Cason, G.W., Curry, T.S., Manning, R.D., Jr., 2002. Superoxide dismutase and oxidative stress in Dahl salt-sensitive and -resistant rats. Am J Physiol Regul Integr Comp Physiol 283, R732-738.

Meyers, E.N., Lewandoski, M., Martin, G.R., 1998. An Fgf8 mutant allelic series generated by Cre- and Flp-mediated recombination. Nat Genet 18, 136-141.

Michailidou, Z., Carter, R.N., Marshall, E., Sutherland, H.G., Brownstein, D.G., Owen, E., Cockett, K., Kelly, V., Ramage, L., Al-Dujaili, E.A., Ross, M., Maraki, I., Newton, K., Holmes, M.C., Seckl, J.R., Morton, N.M., Kenyon, C.J., Chapman, K.E., 2008. Glucocorticoid receptor haploinsufficiency causes hypertension and attenuates hypothalamic-pituitary-adrenal axis and blood pressure adaptions to high-fat diet. FASEB J 22, 3896-3907.

Milford, D.V., 1999. Investigation of hypertension and the recognition of monogenic hypertension. Arch Dis Child 81, 452-455.

Missaghian, E., Kempna, P., Dick, B., Hirsch, A., Alikhani-Koupaei, R., Jegou, B., Mullis, P.E., Frey, B.M., Fluck, C.E., 2009. Role of DNA methylation in the tissue-specific expression of the CYP17A1 gene for steroidogenesis in rodents. J Endocrinol 202, 99-109.

Mohring, J., Mohring, B., 1972. Reevaluation of DOCA escape phenomenon. Am J Physiol 223, 1237-1245.

Mohring, J., Mohring, B., Just, S., 1970. Description of the DOCA escape phenomenon in the rat. Naunyn Schmiedebergs Arch Pharmakol 266, 406-407.

Monder, C., Shackleton, C.H., Bradlow, H.L., New, M.I., Stoner, E., Iohan, F., Lakshmi, V., 1986. The syndrome of apparent mineralocorticoid excess: its association with 11 beta-dehydrogenase and 5 beta-reductase deficiency and some consequences for corticosteroid metabolism. J Clin Endocrinol Metab 63, 550-557.

Moore, X.L., Hoong, I., Cole, T.J., 2000. Expression of the 11beta-hydroxysteroid dehydrogenase 2 gene in the mouse. Kidney Int 57, 1307-1312.

Morton, N.M., Holmes, M.C., Fievet, C., Staels, B., Tailleux, A., Mullins, J.J., Seckl, J.R., 2001. Improved lipid and lipoprotein profile, hepatic insulin sensitivity, and glucose tolerance in 11beta-hydroxysteroid dehydrogenase type 1 null mice. J Biol Chem 276, 41293-41300.

Morton, N.M., Paterson, J.M., Masuzaki, H., Holmes, M.C., Staels, B., Fievet, C., Walker, B.R., Flier, J.S., Mullins, J.J., Seckl, J.R., 2004. Novel adipose tissue-mediated resistance to diet-induced visceral obesity in 11 beta-hydroxysteroid dehydrogenase type 1-deficient mice. Diabetes 53, 931-938.

Mullins, L.J., Bailey, M.A., Mullins, J.J., 2006. Hypertension, kidney, and transgenics: a fresh perspective. Physiol Rev 86, 709-746.

Mune, T., Rogerson, F.M., Nikkila, H., Agarwal, A.K., White, P.C., 1995. Human hypertension caused by mutations in the kidney isozyme of 11 beta-hydroxysteroid dehydrogenase. Nat Genet 10, 394-399.

Nagata, K., Obata, K., Xu, J., Ichihara, S., Noda, A., Kimata, H., Kato, T., Izawa, H., Murohara, T., Yokota, M., 2006. Mineralocorticoid receptor antagonism attenuates cardiac hypertrophy and failure in low-aldosterone hypertensive rats. Hypertension 47, 656-664.

Nagy, A., Moens, C., Ivanyi, E., Pawling, J., Gertsenstein, M., Hadjantonakis, A.K., Pirity, M., Rossant, J., 1998. Dissecting the role of N-myc in development using a single targeting vector to generate a series of alleles. Curr Biol 8, 661-664.

Naray-Fejes-Toth, A., Fejes-Toth, G., 1996. Subcellular localization of the type 2 11beta-hydroxysteroid dehydrogenase. A green fluorescent protein study. J Biol Chem 271, 15436-15442.

Nelson, R.D., Stricklett, P., Gustafson, C., Stevens, A., Ausiello, D., Brown, D., Kohan, D.E., 1998. Expression of an AQP2 Cre recombinase transgene in

kidney and male reproductive system of transgenic mice. Am J Physiol 275, C216-226.

New, M.I., Wilson, R.C., 1999. Steroid disorders in children: congenital adrenal hyperplasia and apparent mineralocorticoid excess. Proc Natl Acad Sci U S A 96, 12790-12797.

Ni, X.P., Pearce, D., Butler, A.A., Cone, R.D., Humphreys, M.H., 2003. Genetic disruption of gamma-melanocyte-stimulating hormone signaling leads to salt-sensitive hypertension in the mouse. J Clin Invest 111, 1251-1258.

Nicod, L., Rodriguez, S., Letang, J.M., Viollon-Abadie, C., Jacqueson, A., Berthelot, A., Richert, L., 2000. Antioxidant status, lipid peroxidation, mixed function oxidase and UDP-glucuronyl transferase activities in livers from control and DOCA-salt hypertensive male Sprague Dawley rats. Mol Cell Biochem 203, 33-39.

Nishi, M., Kawata, M., 2007. Dynamics of glucocorticoid receptor and mineralocorticoid receptor: implications from live cell imaging studies. Neuroendocrinology 85, 186-192.

Nishizaka, M.K., Zaman, M.A., Calhoun, D.A., 2003. Efficacy of low-dose spironolactone in subjects with resistant hypertension. Am J Hypertens 16, 925-930.

Noda, Y., Sasaki, S., 2006. Regulation of aquaporin-2 trafficking and its binding protein complex. Biochim Biophys Acta 1758, 1117-1125.

Nogueira, E.F., Gerry, D., Mantero, F., Mariniello, B., Rainey, W.E., 2010. The role of TASK1 in aldosterone production and its expression in normal adrenal and aldosterone-producing adenomas. Clin Endocrinol (Oxf) 73, 22-29.

Notman, R., Noro, M., O'Malley, B., Anwar, J., 2006. Molecular basis for dimethylsulfoxide (DMSO) action on lipid membranes. J Am Chem Soc 128, 13982-13983.

Nunez, B.S., Rogerson, F.M., Mune, T., Igarashi, Y., Nakagawa, Y., Phillipov, G., Moudgil, A., Travis, L.B., Palermo, M., Shackleton, C., White, P.C., 1999. Mutants of 11beta-hydroxysteroid dehydrogenase (11-HSD2) with partial activity: improved correlations between genotype and biochemical phenotype in apparent mineralocorticoid excess. Hypertension 34, 638-642.

O'Reilly, M., Marshall, E., Macgillivray, T., Mittal, M., Xue, W., Kenyon, C.J., Brown, R.W., 2006. Dietary electrolyte-driven responses in the renal WNK kinase pathway in vivo. J Am Soc Nephrol 17, 2402-2413.

Oberleithner, H., 2005. Aldosterone makes human endothelium stiff and vulnerable. Kidney Int 67, 1680-1682.

Odermatt, A., Arnold, P., Stauffer, A., Frey, B.M., Frey, F.J., 1999. The N-terminal anchor sequences of 11beta-hydroxysteroid dehydrogenases determine their orientation in the endoplasmic reticulum membrane. J Biol Chem 274, 28762-28770.

Okamoto, K., Tanaka, H., Ogawa, H., Makino, Y., Eguchi, H., Hayashi, S., Yoshikawa, N., Poellinger, L., Umesono, K., Makino, I., 1999. Redox-dependent regulation of nuclear import of the glucocorticoid receptor. J Biol Chem 274, 10363-10371.

Olson, E.N., Arnold, H.H., Rigby, P.W., Wold, B.J., 1996. Know your neighbors: three phenotypes in null mutants of the myogenic bHLH gene MRF4. Cell 85, 1-4.

Page, L.B., Vandevert, D.E., Nader, K., Lubin, N.K., Page, J.R., 1981. Blood pressure of Qash'qai pastoral nomads in Iran in relation to culture, diet, and body form. Am J Clin Nutr 34, 527-538.

Palermo, M., Delitala, G., Sorba, G., Cossu, M., Satta, R., Tedde, R., Pala, A., Shackleton, C.H., 2000. Does kidney transplantation normalise cortisol metabolism in apparent mineralocorticoid excess syndrome? J Endocrinol Invest 23, 457-462.

Palermo, M., Shackleton, C.H., Mantero, F., Stewart, P.M., 1996. Urinary free cortisone and the assessment of 11 beta-hydroxysteroid dehydrogenase activity in man. Clin Endocrinol (Oxf) 45, 605-611.

Paravicini, T.M., Touyz, R.M., 2008. NADPH oxidases, reactive oxygen species, and hypertension: clinical implications and therapeutic possibilities. Diabetes Care 31 Suppl 2, S170-180.

Paterson, J.M., Holmes, M.C., Kenyon, C.J., Carter, R., Mullins, J.J., Seckl, J.R., 2007. Liver-selective transgene rescue of hypothalamic-pituitary-adrenal axis dysfunction in 11beta-hydroxysteroid dehydrogenase type 1-deficient mice. Endocrinology 148, 961-966.

Paterson, J.M., Seckl, J.R., Mullins, J.J., 2005. Genetic manipulation of 11beta-hydroxysteroid dehydrogenases in mice. Am J Physiol Regul Integr Comp Physiol 289, R642-652.

Pietrement, C., Sun-Wada, G.H., Silva, N.D., McKee, M., Marshansky, V., Brown, D., Futai, M., Breton, S., 2006. Distinct expression patterns of different subunit isoforms of the V-ATPase in the rat epididymis. Biol Reprod 74, 185-194.

Pitt, B., Remme, W., Zannad, F., Neaton, J., Martinez, F., Roniker, B., Bittman, R., Hurley, S., Kleiman, J., Gatlin, M., 2003. Eplerenone, a selective aldosterone blocker, in patients with left ventricular dysfunction after myocardial infarction. N Engl J Med 348, 1309-1321.

Pitt, B., Zannad, F., Remme, W.J., Cody, R., Castaigne, A., Perez, A., Palensky, J., Wittes, J., 1999. The effect of spironolactone on morbidity and mortality in patients with severe heart failure. Randomized Aldactone Evaluation Study Investigators. N Engl J Med 341, 709-717.

Poch, E., Gonzalez, D., Giner, V., Bragulat, E., Coca, A., de La Sierra, A., 2001. Molecular basis of salt sensitivity in human hypertension. Evaluation of renin-angiotensin-aldosterone system gene polymorphisms. Hypertension 38, 1204-1209.

Pradervand, S., Wang, Q., Burnier, M., Beermann, F., Horisberger, J.D., Hummler, E., Rossier, B.C., 1999. A mouse model for Liddle's syndrome. J Am Soc Nephrol 10, 2527-2533.

Pratico, D., Lawson, J.A., Rokach, J., FitzGerald, G.A., 2001. The isoprostanes in biology and medicine. Trends Endocrinol Metab 12, 243-247.

Pratt, J.H., Eckert, G.J., Newman, S., Ambrosius, W.T., 2001. Blood pressure responses to small doses of amiloride and spironolactone in normotensive subjects. Hypertension 38, 1124-1129.

Qin, W., Rudolph, A.E., Bond, B.R., Rocha, R., Blomme, E.A., Goellner, J.J., Funder, J.W., McMahon, E.G., 2003. Transgenic model of aldosterone-driven cardiac hypertrophy and heart failure. Circ Res 93, 69-76.

Quinkler, M., Stewart, P.M., 2003. Hypertension and the cortisol-cortisone shuttle. J Clin Endocrinol Metab 88, 2384-2392.

Quinn, S.J., Williams, G.H., 1988. Regulation of aldosterone secretion. Annu Rev Physiol 50, 409-426.

Roberts, C.K., Sindhu, K.K., 2009. Oxidative stress and metabolic syndrome. Life Sci 84, 705-712.

Roberts, L.J., Morrow, J.D., 2000. Measurement of F(2)-isoprostanes as an index of oxidative stress in vivo. Free Radic Biol Med 28, 505-513.

Robson, A.C., Leckie, C.M., Seckl, J.R., Holmes, M.C., 1998. 11 Beta-hydroxysteroid dehydrogenase type 2 in the postnatal and adult rat brain. Brain Res Mol Brain Res 61, 1-10.

Rocha, R., Funder, J.W., 2002. The pathophysiology of aldosterone in the cardiovascular system. Ann N Y Acad Sci 970, 89-100.

Roland, B.L., Li, K.X., Funder, J.W., 1995. Hybridization histochemical localization of 11 beta-hydroxysteroid dehydrogenase type 2 in rat brain. Endocrinology 136, 4697-4700.

Ronzaud, C., Loffing, J., Bleich, M., Gretz, N., Grone, H.J., Schutz, G., Berger, S., 2007. Impairment of sodium balance in mice deficient in renal principal cell mineralocorticoid receptor. J Am Soc Nephrol 18, 1679-1687.

Rossier, B.C., Canessa, C.M., Schild, L., Horisberger, J.D., 1994. Epithelial sodium channels. Curr Opin Nephrol Hypertens 3, 487-496.

Rosskopf, D., Schurks, M., Rimmbach, C., Schafers, R., 2007. Genetics of arterial hypertension and hypotension. Naunyn Schmiedebergs Arch Pharmacol 374, 429-469.

Ruan, X., Wagner, C., Chatziantoniou, C., Kurtz, A., Arendshorst, W.J., 1997. Regulation of angiotensin II receptor AT1 subtypes in renal afferent arterioles during chronic changes in sodium diet. J Clin Invest 99, 1072-1081.

Rubera, I., Hummler, E., Beermann, F., 2009. Transgenic mice and their impact on kidney research. Pflugers Arch 458, 211-222.

Rubera, I., Loffing, J., Palmer, L.G., Frindt, G., Fowler-Jaeger, N., Sauter, D., Carroll, T., McMahon, A., Hummler, E., Rossier, B.C., 2003. Collecting duct-specific gene inactivation of alphaENaC in the mouse kidney does not impair sodium and potassium balance. J Clin Invest 112, 554-565.

Ryding, A.D., Sharp, M.G., Mullins, J.J., 2001. Conditional transgenic technologies. J Endocrinol 171, 1-14.

Sacks, F.M., Svetkey, L.P., Vollmer, W.M., Appel, L.J., Bray, G.A., Harsha, D., Obarzanek, E., Conlin, P.R., Miller, E.R., 3rd, Simons-Morton, D.G., Karanja, N., Lin, P.H., 2001. Effects on blood pressure of reduced dietary sodium and the Dietary Approaches to Stop Hypertension (DASH) diet. DASH-Sodium Collaborative Research Group. N Engl J Med 344, 3-10.

Sato, A., Saruta, T., 2004. Aldosterone-induced organ damage: plasma aldosterone level and inappropriate salt status. Hypertens Res 27, 303-310.

Sato, A., Suzuki, H., Murakami, M., Nakazato, Y., Iwaita, Y., Saruta, T., 1994. Glucocorticoid increases angiotensin II type 1 receptor and its gene expression. Hypertension 23, 25-30.

Schelling, J.R., DeLuca, D.J., Konieczkowski, M., Marzec, R., Sedor, J.R., Dubyak, G.R., Linas, S.L., 1994. Glucocorticoid uncoupling of antiogensin II-dependent phospholipase C activation in rat vascular smooth muscle cells. Kidney Int 46, 675-682.

Schnackenberg, C.G., Wilcox, C.S., 1999. Two-week administration of tempol attenuates both hypertension and renal excretion of 8-Iso prostaglandin f2alpha. Hypertension 33, 424-428.

Schweda, F., Friis, U., Wagner, C., Skott, O., Kurtz, A., 2007. Renin release. Physiology (Bethesda) 22, 310-319.

Sealey, J.E., Clark, I., Bull, M.B., Laragh, J.H., 1970. Potassium balance and the control of renin secretion. J Clin Invest 49, 2119-2127.

Seckl, J.R., Holmes, M.C., 2007. Mechanisms of disease: glucocorticoids, their placental metabolism and fetal 'programming' of adult pathophysiology. Nat Clin Pract Endocrinol Metab 3, 479-488.

Seckl, J.R., Walker, B.R., 2004. 11beta-hydroxysteroid dehydrogenase type 1 as a modulator of glucocorticoid action: from metabolism to memory. Trends Endocrinol Metab 15, 418-424.

Sepehrdad, R., Chander, P.N., Singh, G., Stier, C.T., Jr., 2004. Sodium transport antagonism reduces thrombotic microangiopathy in stroke-prone spontaneously hypertensive rats. Am J Physiol Renal Physiol 286, F1185-1192.

Shelat, S.G., Flanagan-Cato, L.M., Fluharty, S.J., 1999a. Glucocorticoid and mineralocorticoid regulation of angiotensin II type 1 receptor binding and inositol triphosphate formation in WB cells. J Endocrinol 162, 381-391.

Shelat, S.G., King, J.L., Flanagan-Cato, L.M., Fluharty, S.J., 1999b. Mineralocorticoids and glucocorticoids cooperatively increase salt intake and angiotensin II receptor binding in rat brain. Neuroendocrinology 69, 339-351.

Shokoji, T., Nishiyama, A., Fujisawa, Y., Hitomi, H., Kiyomoto, H., Takahashi, N., Kimura, S., Kohno, M., Abe, Y., 2003. Renal sympathetic nerve responses to tempol in spontaneously hypertensive rats. Hypertension 41, 266-273.

Sica, D.A., 2005. Pharmacokinetics and pharmacodynamics of mineralocorticoid blocking agents and their effects on potassium homeostasis. Heart Fail Rev 10, 23-29.

Simon, G., 2004. Pathogenesis of structural vascular changes in hypertension. J Hypertens 22, 3-10.

Simonsen, U., Christensen, F.H., Buus, N.H., 2009. The effect of tempol on endothelium-dependent vasodilatation and blood pressure. Pharmacol Ther 122, 109-124.

Siragy, H.M., de Gasparo, M., Carey, R.M., 2000. Angiotensin type 2 receptor mediates valsartan-induced hypotension in conscious rats. Hypertension 35, 1074-1077.

Snyder, P.M., 2005. Minireview: regulation of epithelial Na+ channel trafficking. Endocrinology 146, 5079-5085.

Souness, G.W., Brem, A.S., Morris, D.J., 2002. 11 beta-Hydroxysteroid dehydrogenase antisense affects vascular contractile response and glucocorticoid metabolism. Steroids 67, 195-201.

Spat, A., 2004. Glomerulosa cell--a unique sensor of extracellular K+ concentration. Mol Cell Endocrinol 217, 23-26.

Staub, O., Abriel, H., Plant, P., Ishikawa, T., Kanelis, V., Saleki, R., Horisberger, J.D., Schild, L., Rotin, D., 2000. Regulation of the epithelial Na+ channel by Nedd4 and ubiquitination. Kidney Int 57, 809-815.

Stewart, P.M., Corrie, J.E., Shackleton, C.H., Edwards, C.R., 1988. Syndrome of apparent mineralocorticoid excess. A defect in the cortisol-cortisone shuttle. J Clin Invest 82, 340-349.

Stewart, P.M., Wallace, A.M., Valentino, R., Burt, D., Shackleton, C.H., Edwards, C.R., 1987. Mineralocorticoid activity of liquorice: 11-beta-hydroxysteroid dehydrogenase deficiency comes of age. Lancet 2, 821-824.

Stojiljkovic, L., Behnia, R., 2007. Role of renin angiotensin system inhibitors in cardiovascular and renal protection: a lesson from clinical trials. Curr Pharm Des 13, 1335-1345.

Swedberg, K., Eneroth, P., Kjekshus, J., Wilhelmsen, L., 1990. Hormones regulating cardiovascular function in patients with severe congestive heart failure and their relation to mortality. CONSENSUS Trial Study Group. Circulation 82, 1730-1736.

Swift, P.A., Markandu, N.D., Sagnella, G.A., He, F.J., MacGregor, G.A., 2005. Modest salt reduction reduces blood pressure and urine protein excretion in black hypertensives: a randomized control trial. Hypertension 46, 308-312.

Tanaka, H., Makino, Y., Okamoto, K., Iida, T., Yan, K., Yoshikawa, N., 1999. Redox regulation of the glucocorticoid receptor. Antioxid Redox Signal 1, 403-423.

Taylor, N.E., Glocka, P., Liang, M., Cowley, A.W., Jr., 2006. NADPH oxidase in the renal medulla causes oxidative stress and contributes to salt-sensitive hypertension in Dahl S rats. Hypertension 47, 692-698.

Thapa, L., He, C.M., Chen, H.P., 2004. Study on the expression of angiotensin II (ANG II) receptor subtype 1 (AT1R) in the placenta of pregnancy-induced hypertension. Placenta 25, 637-641.

Thiesson, H.C., Jensen, B.L., Bistrup, C., Ottosen, P.D., McNeilly, A.D., Andrew, R., Seckl, J., Skott, O., 2007. Renal sodium retention in cirrhotic rats depends on glucocorticoid-mediated activation of mineralocorticoid receptor due to decreased renal 11beta-HSD-2 activity. Am J Physiol Regul Integr Comp Physiol 292, R625-636.

Thompson, A., Han, V.K., Yang, K., 2002. Spatial and temporal patterns of expression of 11beta-hydroxysteroid dehydrogenase types 1 and 2 messenger RNA and glucocorticoid receptor protein in the murine placenta and uterus during late pregnancy. Biol Reprod 67, 1708-1718.

Thompson, A., Han, V.K., Yang, K., 2004. Differential expression of 11beta-hydroxysteroid dehydrogenase types 1 and 2 mRNA and glucocorticoid

receptor protein during mouse embryonic development. J Steroid Biochem Mol Biol 88, 367-375.

Tian, H.G., Guo, Z.Y., Hu, G., Yu, S.J., Sun, W., Pietinen, P., Nissinen, A., 1995. Changes in sodium intake and blood pressure in a community-based intervention project in China. J Hum Hypertens 9, 959-968.

Tian, N., Moore, R.S., Phillips, W.E., Lin, L., Braddy, S., Pryor, J.S., Stockstill, R.L., Hughson, M.D., Manning, R.D., Jr., 2008. NADPH oxidase contributes to renal damage and dysfunction in Dahl salt-sensitive hypertension. Am J Physiol Regul Integr Comp Physiol 295, R1858-1865.

Tian, N., Thrasher, K.D., Gundy, P.D., Hughson, M.D., Manning, R.D., Jr., 2005. Antioxidant treatment prevents renal damage and dysfunction and reduces arterial pressure in salt-sensitive hypertension. Hypertension 45, 934-939.

Titze, J., 2009. Water-free sodium accumulation. Semin Dial 22, 253-255.

Titze, J., Bauer, K., Schafflhuber, M., Dietsch, P., Lang, R., Schwind, K.H., Luft, F.C., Eckardt, K.U., Hilgers, K.F., 2005. Internal sodium balance in DOCA-salt rats: a body composition study. Am J Physiol Renal Physiol 289, F793-802.

Titze, J., Lang, R., Ilies, C., Schwind, K.H., Kirsch, K.A., Dietsch, P., Luft, F.C., Hilgers, K.F., 2003. Osmotically inactive skin Na+ storage in rats. Am J Physiol Renal Physiol 285, F1108-1117.

Ulick, S., Levine, L.S., Gunczler, P., Zanconato, G., Ramirez, L.C., Rauh, W., Rosler, A., Bradlow, H.L., New, M.I., 1979. A syndrome of apparent mineralocorticoid excess associated with defects in the peripheral metabolism of cortisol. J Clin Endocrinol Metab 49, 757-764.

Ullian, M.E., 1999. The role of corticosteriods in the regulation of vascular tone. Cardiovasc Res 41, 55-64.

Ullrich, S., Berchtold, S., Ranta, F., Seebohm, G., Henke, G., Lupescu, A., Mack, A.F., Chao, C.M., Su, J., Nitschke, R., Alexander, D., Friedrich, B., Wulff, P., Kuhl, D., Lang, F., 2005. Serum- and glucocorticoid-inducible kinase 1 (SGK1) mediates glucocorticoid-induced inhibition of insulin secretion. Diabetes 54, 1090-1099.

Uno, S., Guo, D.F., Nakajima, M., Ohi, H., Imada, T., Hiramatsu, R., Nakakubo, H., Nakamura, N., Inagami, T., 1994. Glucocorticoid induction of

rat angiotensin II type 1A receptor gene promoter. Biochem Biophys Res Commun 204, 210-215.

Urata, H., Boehm, K.D., Philip, A., Kinoshita, A., Gabrovsek, J., Bumpus, F.M., Husain, A., 1993. Cellular localization and regional distribution of an angiotensin II-forming chymase in the heart. J Clin Invest 91, 1269-1281.

van Rossum, E.F., Feelders, R.A., van den Beld, A.W., Uitterlinden, A.G., Janssen, J.A., Ester, W., Brinkmann, A.O., Grobbee, D.E., de Jong, F.H., Pols, H.A., Koper, J.W., Lamberts, S.W., 2004. Association of the ER22/23EK polymorphism in the glucocorticoid receptor gene with survival and C-reactive protein levels in elderly men. Am J Med 117, 158-162.

van Rossum, E.F., Lamberts, S.W., 2004. Polymorphisms in the glucocorticoid receptor gene and their associations with metabolic parameters and body composition. Recent Prog Horm Res 59, 333-357.

Van Tassell, B.W., Munger, M.A., 2007. Aliskiren for renin inhibition: a new class of antihypertensives. Ann Pharmacother 41, 456-464.

Walker, B.R., 2006. Cortisol--cause and cure for metabolic syndrome? Diabet Med 23, 1281-1288.

Walker, B.R., Connacher, A.A., Webb, D.J., Edwards, C.R., 1992. Glucocorticoids and blood pressure: a role for the cortisol/cortisone shuttle in the control of vascular tone in man. Clin Sci (Lond) 83, 171-178.

Warnock, D.G., 2001. Liddle syndrome: genetics and mechanisms of Na+ channel defects. Am J Med Sci 322, 302-307.

Webster, S.P., Ward, P., Binnie, M., Craigie, E., McConnell, K.M., Sooy, K., Vinter, A., Seckl, J.R., Walker, B.R., 2007. Discovery and biological evaluation of adamantyl amide 11beta-HSD1 inhibitors. Bioorg Med Chem Lett 17, 2838-2843.

Wei, C.C., Tian, B., Perry, G., Meng, Q.C., Chen, Y.F., Oparil, S., Dell'Italia, L.J., 2002. Differential ANG II generation in plasma and tissue of mice with decreased expression of the ACE gene. Am J Physiol Heart Circ Physiol 282, H2254-2258.

Weinberger, M.H., Miller, J.Z., Luft, F.C., Grim, C.E., Fineberg, N.S., 1986. Definitions and characteristics of sodium sensitivity and blood pressure resistance. Hypertension 8, II127-134.

Welch, W.J., Mendonca, M., Blau, J., Karber, A., Dennehy, K., Patel, K., Lao, Y.S., Jose, P.A., Wilcox, C.S., 2005. Antihypertensive response to prolonged tempol in the spontaneously hypertensive rat. Kidney Int 68, 179-187.

Wertheim, H.F., Melles, D.C., Vos, M.C., van Leeuwen, W., van Belkum, A., Verbrugh, H.A., Nouwen, J.L., 2005. The role of nasal carriage in Staphylococcus aureus infections. Lancet Infect Dis 5, 751-762.

White, P.C., 2001. 11beta-hydroxysteroid dehydrogenase and its role in the syndrome of apparent mineralocorticoid excess. Am J Med Sci 322, 308-315.

White, P.C., Mune, T., Agarwal, A.K., 1997. 11 beta-Hydroxysteroid dehydrogenase and the syndrome of apparent mineralocorticoid excess. Endocr Rev 18, 135-156.

Whitworth, J.A., Williamson, P.M., Mangos, G., Kelly, J.J., 2005. Cardiovascular consequences of cortisol excess. Vasc Health Risk Manag 1, 291-299.

Wilcox, C.S., 2002. Reactive oxygen species: roles in blood pressure and kidney function. Curr Hypertens Rep 4, 160-166.

Wilcox, C.S., Pearlman, A., 2008. Chemistry and antihypertensive effects of tempol and other nitroxides. Pharmacol Rev 60, 418-469.

Williams, G.H., 2005. Aldosterone biosynthesis, regulation, and classical mechanism of action. Heart Fail Rev 10, 7-13.

Williams, J.M., Pollock, J.S., Pollock, D.M., 2004. Arterial pressure response to the antioxidant tempol and ETB receptor blockade in rats on a high-salt diet. Hypertension 44, 770-775.

Williams, J.S., Williams, G.H., 2003. 50th anniversary of aldosterone. J Clin Endocrinol Metab 88, 2364-2372.

Williams, T.A., Mulatero, P., Filigheddu, F., Troffa, C., Milan, A., Argiolas, G., Parpaglia, P.P., Veglio, F., Glorioso, N., 2005. Role of HSD11B2 polymorphisms in essential hypertension and the diuretic response to thiazides. Kidney Int 67, 631-637.

Wilson, R.C., Dave-Sharma, S., Wei, J.Q., Obeyesekere, V.R., Li, K., Ferrari, P., Krozowski, Z.S., Shackleton, C.H., Bradlow, L., Wiens, T., New, M.I., 1998. A genetic defect resulting in mild low-renin hypertension. Proc Natl Acad Sci U S A 95, 10200-10205.

Wintermantel, T.M., Berger, S., Greiner, E.F., Schutz, G., 2005. Evaluation of steroid receptor function by gene targeting in mice. J Steroid Biochem Mol Biol 93, 107-112.

Wolf, G., 2002. Glucocorticoids in adipocytes stimulate visceral obesity. Nutr Rev 60, 148-151.

Xu, H., Bian, X., Watts, S.W., Hlavacova, A., 2005. Activation of vascular BK channel by tempol in DOCA-salt hypertensive rats. Hypertension 46, 1154-1162.

Yang, C.L., Angell, J., Mitchell, R., Ellison, D.H., 2003. WNK kinases regulate thiazide-sensitive Na-Cl cotransport. J Clin Invest 111, 1039-1045.

Yang, C.L., Zhu, X., Wang, Z., Subramanya, A.R., Ellison, D.H., 2005. Mechanisms of WNK1 and WNK4 interaction in the regulation of thiazide-sensitive NaCl cotransport. J Clin Invest 115, 1379-1387.

Yaron, Y., McAdara, J.K., Lynch, M., Hughes, E., Gasson, J.C., 2001. Identification of novel functional regions important for the activity of HOXB7 in mammalian cells. J Immunol 166, 5058-5067.

Yau, J.L., Noble, J., Kenyon, C.J., Hibberd, C., Kotelevtsev, Y., Mullins, J.J., Seckl, J.R., 2001. Lack of tissue glucocorticoid reactivation in 11beta - hydroxysteroid dehydrogenase type 1 knockout mice ameliorates age-related learning impairments. Proc Natl Acad Sci U S A 98, 4716-4721.

Ye, W., Zhang, H., Hillas, E., Kohan, D.E., Miller, R.L., Nelson, R.D., Honeggar, M., Yang, T., 2006. Expression and function of COX isoforms in renal medulla: evidence for regulation of salt sensitivity and blood pressure. Am J Physiol Renal Physiol 290, F542-549.

Yoshida, S., Hashimoto, T., Kihara, M., Imai, N., Yasuzaki, H., Nomura, K., Kiuchi, Y., Tamura, K., Ishigami, T., Hirawa, N., Toya, Y., Kitamura, H., Umemura, S., 2009. Urinary oxidative stress markers closely reflect the efficacy of candesartan treatment for diabetic nephropathy. Nephron Exp Nephrol 111, e20-30.

Young, D.B., 1985. Analysis of long-term potassium regulation. Endocr Rev 6, 24-44.

Young, M.J., Lam, E.Y., Rickard, A.J., 2007. Mineralocorticoid receptor activation and cardiac fibrosis. Clin Sci (Lond) 112, 467-475.

Yu, J., Carroll, T.J., McMahon, A.P., 2002. Sonic hedgehog regulates proliferation and differentiation of mesenchymal cells in the mouse metanephric kidney. Development 129, 5301-5312.

Zhang, Q., Piston, D.W., Goodman, R.H., 2002. Regulation of corepressor function by nuclear NADH. Science 295, 1895-1897.

Zhang, Y., Jang, R., Mori, T.A., Croft, K.D., Schyvens, C.G., McKenzie, K.U., Whitworth, J.A., 2003. The anti-oxidant Tempol reverses and partially prevents adrenocorticotrophic hormone-induced hypertension in the rat. J Hypertens 21, 1513-1518.

Zharkikh, L., Zhu, X., Stricklett, P.K., Kohan, D.E., Chipman, G., Breton, S., Brown, D., Nelson, R.D., 2002. Renal principal cell-specific expression of green fluorescent protein in transgenic mice. Am J Physiol Renal Physiol 283, F1351-1364.

Abstracts, Publications and Grant Awards

Published Abstracts

Craigie, E., Mullins, J.J., Bailey, M.A. "Chronic ENaC Blockade Rescues Na+ Induced High Blood Pressure in 11β-Hydroxysteroid Dehydrogenase Type 2 Heterozygote Mice."
J Physiol (2009) **Proc Physiol Soc 15** C29**.**

Craigie, E., Bailey, M.A. "11β-hydroxysteroid Dehydrogenase Type 2 Heterozygous Mice Display Blunted Naturesis, Increased Blood Pressure and Impaired ENaC Regulation on a High Sodium Diet."
J Physiol (2008) **Proc Physiol Soc 11** C37.

Craigie, E., Mullins, J.J., Bailey, M.A. "11β-hydroxysteroid Dehydrogenase Type 2 Heterozygous Mice Have Impaired Sodium Excretion and Salt-Sensitive Blood Pressure."
Presented as an oral presentation at the Endocrine Society Annual Meeting, San Francisco, June 2008 (OR48-1).

Craigie, E., Bailey, M.A. "11β-hydroxysteroid Dehydrogenase Type 2 Heterozygous Mice Display Increased Blood Pressure and Blunted Natriuresis in Response to a High Sodium Diet."
Presented as an oral presentation at the Scottish Society for Experimental Medicine Annual Meeting, Dundee, May 2008.

Review Article

Craigie, E., Bailey, M.A., Mullins, J.J. (2008). "Glucocorticoids and Mineralocorticoids." Chapter 1, pp 3-38 IN Cardiovascular Hormone Systems: from molecular mechanisms to novel therapeutics. Editor M. Bader. Wiley-Blackwell.

Journal Publication

Craigie, E., Bailey, M.A., Livingstone, D.E.W., Kotelevtsev, Y.V., Al-Dujaili, E.A.S., Kenyon, C.J., Mullins, J.J. (2011). "*Hsd11b2* Haploinsufficiency in Mice Causes Salt Sensitivity of Blood Pressure". Hypertension, 57, 515 - 520 (see Appendix 2 full publication).

Grant Awards

June 2009	Awarded travel grant for Physiological Society Main Meeting in Dublin, ROI (£459 from Physiological Society)
May 2009	Awarded University of Edinburgh Small Project Grant (£1500)
July 2008	Awarded travel grant for Physiological Society Main Meeting in Cambridge, UK (£400 from Physiological Society)
June 2008	Awarded travel grant for Endocrinology Society Annual Meeting in San Francisco, USA ($500 from Endocrinology Society)

David Brownstein DVM DACVP
Reader in Pathology
Room W3.06
Queen's Medical Research Institute
47 Little France Crescent
Edinburgh EH16 4TJ
Tel:+44-131-242-6730
e-mail: d.brownstein@ed.ac.uk

NECROPSY REPORT

Investigator: Eilidh Craigie
Date of necropsy: 14/10/08
Path#: DB229/08
Subject: chimeric male (129/B6)
History: Proven breeder developed scrotal fistula ? Second chimera to develop one.

Gross findings. Circular 1.5 mm penetrating ulcer of skin ventral midline 2 mm anterior to penis. Surrounding skin indurated.

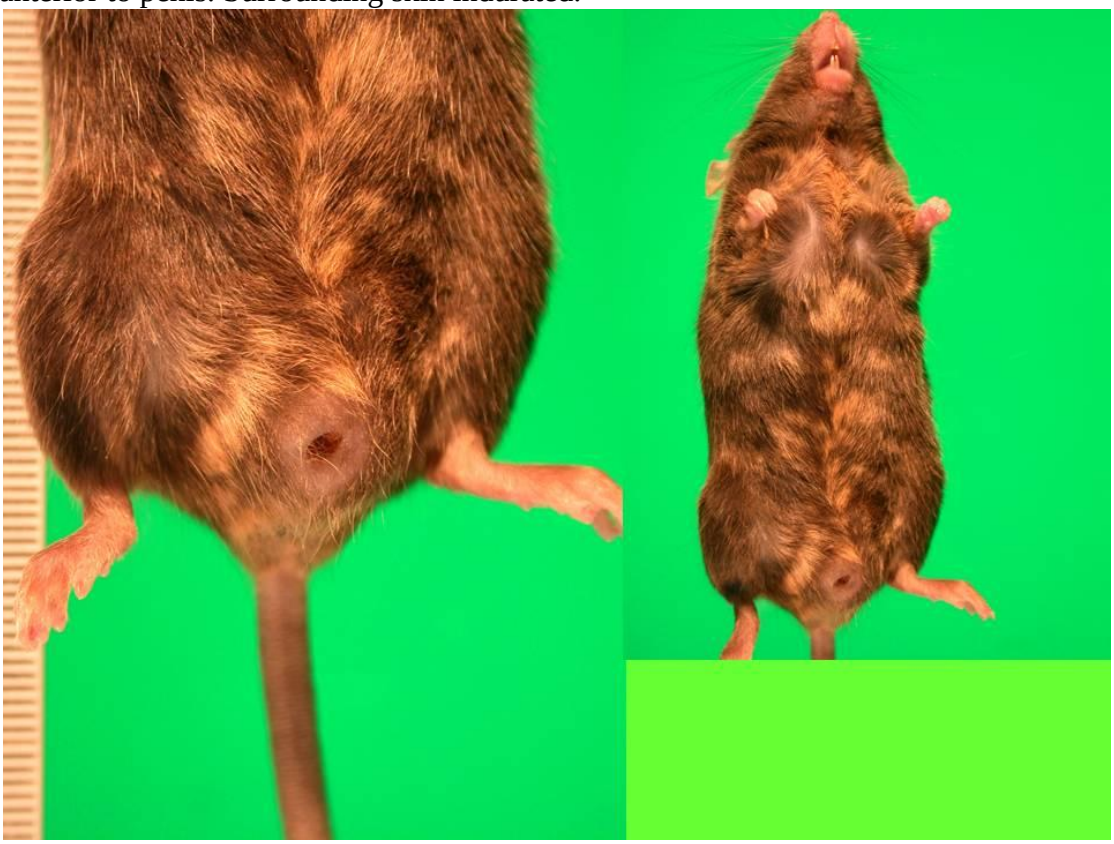

Underlying preputial gland swollen, irregular shape, cystic with inspissated pus. Fistulous tract communicating with skin ulcer.

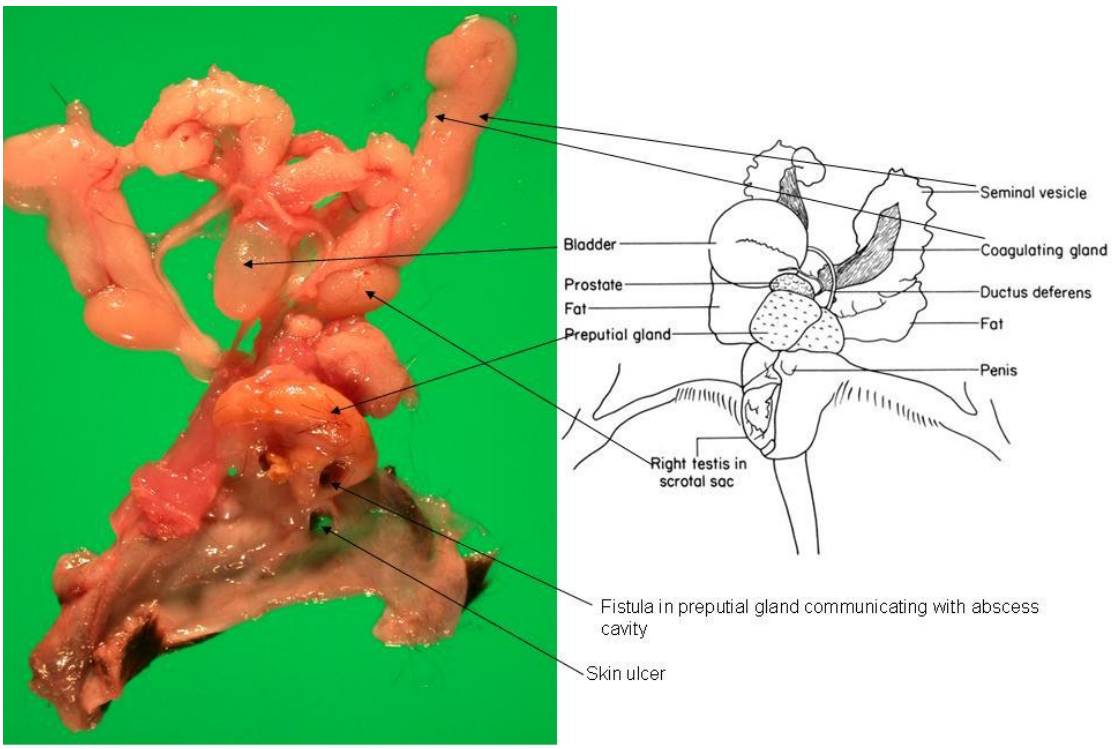

Diagnosis:
Preputial gland, abscess with skin fistula

Comments. This is a common condition of male mice with both environmental and genetic elements.

David Brownstein